

# THE NEW "DYNAMIC BEHAVIOR OF LIQUIDS IN MOVING CONTAINERS"

Franklin T. Dodge  
Southwest Research Institute  
San Antonio, Texas





# PREFACE

Southwest Research Institute has worked in “sloshing” since before the start of the US space program. Because of the wide-ranging nature of this work, NASA in the mid-1960s requested Dr. Norm Abramson, who was then Director of SwRI’s Department of Mechanical Sciences and the leader of the sloshing group, to organize the preparation of a monograph that would capture pretty much all that was then known about sloshing and related subjects. A team of experts from SwRI, NASA, and other organizations wrote the individual chapters, under the direction of an Advisory Committee composed of Dr. Abramson, Dr. Douglas Michel of NASA-OAST, Dr. George Brooks of NASA-Langley, and Dr. Helmut Bauer of Georgia Tech. The monograph was published in 1966 as **NASA SP-106 “The Dynamic Behavior of Liquids in Moving Containers”**. It proved to be extremely popular, and the print run of several thousand copies was rapidly distributed. Demand for it continued through the years, so it was re-issued several times with minor corrections. Unfortunately, NASA SP-106 is now out of print.

NASA SP-106 contains a lot of information, although the information is not always presented in a way that makes it easy to understand. In addition, many of the numerical results are presented as graphs and tables derived from approximate analytical methods (because of the limitations of 1960’s-era computers), and these results are now available in more accurate form. Furthermore, progress in sloshing and related technology has continued to advance since the mid-1960s, especially in low-gravity fluid mechanics and “fluid management”. For these reasons, it seemed to me that an update and revision of SP-106 would still be valuable to the sloshing community, and so I have prepared the present monograph.

This update does not cover all the subjects included in NASA SP-106. Some topics were omitted because they discuss marginally-related material accessible elsewhere (e.g., the principles of similitude as applied to scale models) or the material is quite specialized or does not now appear to be as important as it was in 1966 (e.g., vertical excitation of tanks). Other topics, such as structural dynamics, are still important but are omitted because they are covered extensively elsewhere. The update focuses primarily on the topics discussed in the SP-106’s **Chapter 2: Lateral Sloshing in Moving Containers**, **Chapter 3: Nonlinear Effects in Lateral Sloshing**, **Chapter 4: Damping of Liquid Motions and Lateral Sloshing**, **Chapter 6: Analytical Representation of Lateral Sloshing by Equivalent Mechanical Models**, **Chapter 7: Vehicle Stability and Control** (but greatly condensed) and **Chapter 11: Liquid Propellant Behavior at Low and Zero G** (greatly expanded with much new material on sloshing and propellant management devices). A new chapter is included on **Liquid Motions in a Spinning Tank** because of the importance of this subject to spacecraft stability. The chapters have been re-ordered to make the presentation more consistent. All the chapters contain new material from research and references that have become available since NASA SP-106 was written. Wherever the original material is retained, the original references were consulted to prevent propagation of errors in the update. Some of the lengthy mathematical presentations used to derive numerical results in Chapter 2 of NASA SP-106 (which is Chapter 1 of the update) are not included in the update, because equivalent results are now readily available from computer codes. In all cases, basic derivations have been clarified, and there is more emphasis throughout on physical interpretation of the results and on equivalent mechanical models.

The update emphasizes, just as NASA SP-106 does, literature and results of interest to spacecraft applications. Thus, the extensive literature on tanker trucks, ships, and other applications is not included except when some of the results are of interest to spacecraft. The Russian-language literature is also not covered thoroughly, primarily because of difficulties in obtaining English translations, even though this literature contains a lot of valuable material.

This update is complete in itself. When a graph or figure contained in NASA SP-106 was needed, it was redrawn, and generally, the new graphs are based on re-computed theoretical results or on the experimental results given in the cited references, so as to eliminate any errors in the original graphs. In addition, many new figures and graphs are included. Unfortunately, the photographs in NASA SP-106 are no longer available and so could not be included. In the update, text printed in a smaller type size indicates that the material is supplementary to the main text.

For historical completeness, a listing of all the references cited in NASA SP-106 (even those not used in the update) is contained in an Appendix.

## **SLOSH Computer Code**

Many of the linear, lateral slosh results presented in the update were computed from the computer program **SLOSH**. This program predicts the equivalent mechanical model and natural frequencies of linear sloshing for any axisymmetric tank. It is written in the Visual Basic language and contains on-screen instructions. The program runs on a PC using any version of Microsoft Windows. The basic theory is described in the Appendix to Chapter 3. **SLOSH** is available on request.

## **SP-106 Authors**

The authors of NASA SP-106 and their affiliations at the time it was issued are listed below.

H. NORMAN ABRAMSON, Southwest Research Institute  
HELMUT F. BAUER, Georgia Institute of Technology  
GEORGE W. BROOKS, NASA-Langley Research Center  
WEN-HWA CHU, Southwest Research Institute  
JOHN F. DALZELL, Southwest Research Institute  
FRANKLIN T. DODGE, Southwest Research Institute  
DANIEL D. KANA, Southwest Research Institute  
WILLIAM C. REYNOLDS, Stanford University  
HUGH M. SATTERLEE, Lockheed Missiles & Space Co.  
SANDOR SILVERMAN, Southwest Research Institute

# TABLE OF CONTENTS

	PAGE
<b>LATERAL SLOSHING IN MOVING CONTAINERS.....</b>	<b>1</b>
1.1 INTRODUCTION .....	1
1.2 MATHEMATICAL BACKGROUND.....	2
1.3 SOLUTION OF EQUATIONS FOR A RECTANGULAR TANK .....	5
1.4 CIRCULAR CYLINDRICAL TANK .....	14
1.5 SECTOR-ANNULAR CYLINDRICAL TANK.....	14
1.6 HORIZONTAL CYLINDRICAL TANK.....	16
1.7 SPHERICAL TANK.....	17
1.8 SPHEROIDAL TANK .....	18
1.9 TOROIDAL TANK.....	19
1.10 SOME PRACTICAL IMPLICATIONS .....	20
1.11 VERTICAL SLOSHING.....	20
1.12 CONCLUDING REMARKS .....	21
1.13 REFERENCES.....	21
APPENDIX: LINEAR SLOSHING ANALYSIS BY FINITE ELEMENT STRUCTURAL CODES .....	23
<b>DAMPING OF LATERAL SLOSHING .....</b>	<b>25</b>
2.1 INTRODUCTION .....	25
2.2 VISCOUS DAMPING FOR TANKS OF VARIOUS SHAPES .....	26
2.3 SLOSH DAMPING BY RING BAFFLES .....	29
2.4 DAMPING BY MOVABLE AND FLOATING BAFFLE DEVICES.....	35
2.5 DAMPING BY NON-RING BAFFLES.....	37
2.6 DAMPING BY PERFORATED BULKHEADS.....	37
2.7 REFERENCES.....	39
<b>MECHANICAL MODELS OF SLOSHING .....</b>	<b>43</b>
3.1 INTRODUCTION .....	43
3.2 ANALYTICAL DERIVATION OF MODEL PARAMETERS .....	43
3.3 INCLUSION OF DAMPING .....	49
3.4 MECHANICAL MODEL PARAMETERS FROM THE SLOSH CODE.....	51
3.5 EXPERIMENTAL DERIVATION OF MODEL PARAMETERS .....	51
3.6 NONLINEAR MECHANICAL MODELS.....	55
3.7 REFERENCES.....	59
APPENDIX: <i>SLOSH</i> CODE THEORY AND NUMERICS .....	60
<b>FLUID MANAGEMENT IN MICROGRAVITY .....</b>	<b>65</b>
4.1 HYDROSTATICS AND HYDRODYNAMICS IN ZERO OR MICROGRAVITY .....	65
4.2 THERMODYNAMICS OF CAPILLARY SYSTEMS .....	70
4.3 AXISYMMETRIC INTERFACE SHAPE.....	73
4.4 STABILITY OF ZERO-G INTERFACES.....	77
4.5 LOW-G SLOSHING IN AXISYMMETRIC TANKS.....	82
4.6 FLUID MANAGEMENT CONSIDERATIONS IN LOW GRAVITY.....	93
4.7 PROPELLANT MANAGEMENT AND LIQUID ACQUISITION DEVICES.....	97
4.8 PMD CONSIDERATIONS FOR CRYOGENIC LIQUIDS.....	108
4.9 REFERENCES.....	111
<b>NONLINEAR EFFECTS IN LATERAL SLOSHING.....</b>	<b>111</b>
5.1 INTRODUCTION .....	117
5.2 NONLINEAR EFFECTS ARISING FROM TANK SHAPE .....	118
5.3 THEORY OF LARGE AMPLITUDE MOTIONS .....	119
5.4 ROTARY SLOSHING .....	125
5.5 COMMENTS ON THE SUCCESSIVE APPROXIMATION METHOD.....	128
5.6 REFERENCES.....	129

<b>LIQUID MOTIONS IN A SPINNING TANK .....</b>	<b>131</b>
6.1 INTRODUCTION .....	131
6.2 LIQUID MOTIONS IN A SLOWLY SPINNING AXISYMMETRIC TANK .....	133
6.3 TANKS OFF THE SPIN AXIS – EXACT THEORY .....	136
6.4 TANKS LOCATED OFF THE SPIN AXIS – APPROXIMATE THEORY .....	139
6.5 ENERGY DISSIPATION .....	146
6.6 STABILITY OF A ROTATING INTERFACE IN ZERO-G.....	150
6.7 REFERENCES.....	151
APPENDIX: ANALYTICAL ENERGY DISSIPATION ESTIMATE.....	153
<b>SPACECRAFT STABILITY AND CONTROL .....</b>	<b>157</b>
7.1 INTRODUCTION .....	157
7.2 SIMPLIFIED EQUATIONS OF MOTION.....	157
7.2 STABILITY ANALYSIS .....	163
7.3 TYPICAL CONCLUSIONS OF STABILITY ANALYSES .....	165
7.4 REFERENCES.....	166
<b>NASA SP-106 REFERENCES BY CHAPTER .....</b>	<b>167</b>
1. INTRODUCTION .....	167
2. LATERAL SLOSHING IN MOVING CONTAINERS .....	168
3. NONLINEAR EFFECTS IN LATERAL SLOSHING.....	170
4. DAMPING OF LIQUID MOTIONS AND LATERAL SLOSHING.....	171
5. SIMULATION AND EXPERIMENTAL TECHNIQUES .....	173
6. ANALYTICAL REPRESENTATION OF LATERAL SLOSHING BY EQUIVALENT MECHANICAL MODELS .....	175
7. VEHICLE STABILITY AND CONTROL .....	176
8. VERTICAL EXCITATION OF PROPELLANT TANKS .....	177
9. INTERACTION BETWEEN LIQUID PROPELLANTS AND THE ELASTIC CONTAINER .....	179
10. SPECIAL TOPICS .....	181
11. LIQUID PROPELLANT BEHAVIOR AT LOW AND ZERO G.....	182
APPENDIX. PHYSICAL PROPERTIES OF SELECTED LIQUIDS.....	185
<b>TABLE A-1 .....</b>	<b>187</b>
PHYSICAL PROPERTIES OF SOME PROPELLANTS AND MODEL LIQUIDS .....	187
<b>AUTHOR INDEX.....</b>	<b>189</b>
<b>SUBJECT INDEX.....</b>	<b>193</b>

# LATERAL SLOSHING IN MOVING CONTAINERS

This chapter is a revision of Chapter 2 of SP-106; the original authors were SANDOR SILVERMAN and H. NORMAN ABRAMSON.

## 1.1 Introduction

By *lateral* sloshing is meant the standing wave formed on the surface of a liquid when a tank partially filled with liquid is oscillated. *Figure 1.1* shows such a wave schematically. The standing wave moves up one side of the tank and down the other; then the up half-wave moves down and the down half-wave moves up, and so on. The wave motion has a natural frequency which depends on (a) the tank shape and (b) the acceleration of gravity (in a laboratory) or the axial acceleration of the tank (for a missile under thrust).

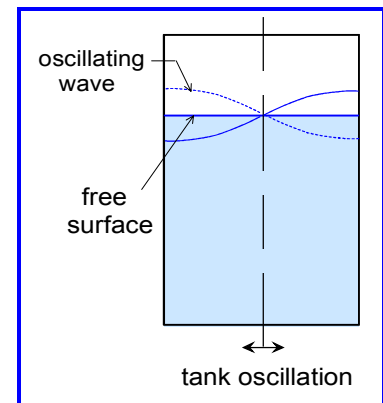


Figure 1.1. Schematic illustration of a slosh wave

### Equivalent mechanical models of sloshing

The main dynamical effect of lateral sloshing is a horizontal oscillation of the liquid center of mass relative to the tank. This effect can be equally well represented by an equivalent mechanical model. *Figure 1.2* illustrates two versions of such a model. In the model on the left, a pendulum represents the oscillation of the liquid c.m., while in the model on the right, a mass on a spring represents it. (These kinds of models will be discussed in detail in Chapter 3.) Both models give the same forces and torques, but the pendulum model has the advantage that its natural frequency  $(g/L)^{0.5}$  varies with changes in the  $g$  acceleration exactly as does the sloshing frequency of the liquid. The spring-mass model has to change its spring constant  $K$  when there is a change in  $g$ .

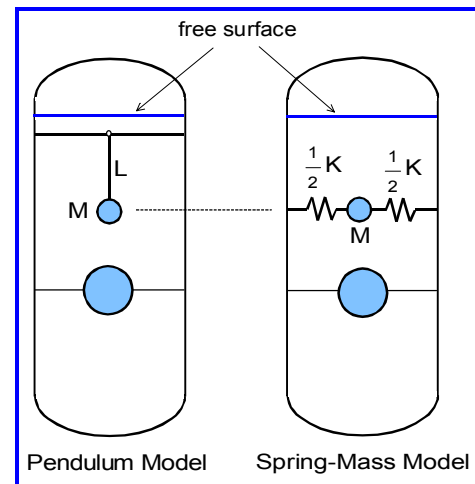


Figure 1.2. Mechanical models of sloshing

Both models show that a horizontal or *lateral* motion of the tank causes the liquid to slosh (i.e., causes the pendulum or sprung mass of the model to oscillate relative to the tank). They also show that an *axial* (vertical) oscillation of the tank does not generally set the liquid into motion.

To be more precise, when the frequency of an axial oscillation is very close to one-half the slosh natural frequency, the liquid surface becomes unstable and a slosh wave is excited parametrically. The pendulum model displays this same kind of instability. Since the forcing frequency has to be almost exactly one-half the slosh natural frequency to create the instability, “vertical” sloshing does not occur much in applications. Vertical sloshing is discussed briefly at the end of this chapter.

The various sloshing discussions given in this chapter can be understood more easily by keeping in mind the mechanical models shown in *Figure 1.2* and picturing how such a mechanical model would respond to various kinds of tank motions.

### Higher order sloshing responses

*Figure 1.1* shows a slosh wave that has one peak and one valley (which is actually only one half of a complete standing wave). This is the *fundamental antisymmetric* wave, and it has the lowest natural frequency. Waves with two or more peaks or valleys with higher natural frequencies can also occur. The mechanical model shown in *Figure 1.2* can represent these higher order waves by incorporating an additional pendulum or sprung-mass for each mode. The magnitudes of the pendulum or sprung mass for these modes are very small compared to the fundamental mode and, thus, higher order modes are usually of little concern. But for non-axisymmetric tanks, there is a fundamental mode for each of the principal axes of the cross-section, and the masses of these modes can all be comparable; if they are, a pendulum or sprung-mass is needed for each mode.

### SLOSH computer code

The basic theory of linear sloshing for several example tank shapes are reviewed in this chapter. The examples can be used to obtain a quick estimate of sloshing frequencies or forces. More detailed results can be obtained from the PC-based **SLOSH** computer code, which can determine the characteristics of sloshing in any axisymmetric tank shape. The **SLOSH** code is discussed in the Appendix to Chapter 3.

## 1.2 Mathematical Background

To explain the basic theory most clearly, the mathematical details of lateral sloshing are discussed for a rigid tank and an ideal liquid having no viscosity. These assumptions allow classical potential flow theory to be used. The wave motion is also assumed to be *linear*. Linear motions or linear responses mean different things in different contexts, but here it means that the amplitude of the wave and of the liquid motion is linearly proportional to the amplitude of the imposed tank motion, and the natural frequency of the slosh wave is not a function of the wave amplitude. The generalized linear theory is discussed more completely in FOX AND KUTTLER [1983]. Nonlinear corrections to the linear theory are discussed in Chapter 5.

For simplicity, the motion of the tank is assumed to be harmonic, which means that it varies with time as  $\exp(i\Omega t)$  where  $\Omega$  is the frequency of the motion. More complicated time-dependent motions of the tank can be considered by the use of Fourier series or Fourier integrals. But complicated and impulsive tank motions can best be handled by using the equivalent mechanical models discussed in Chapter 3.

### Basic differential equations and boundary conditions

Generally, we are interested in axisymmetric tanks for space applications but the basic differential equations and boundary conditions for lateral sloshing are most clearly expressed in a Cartesian  $x, y, z$  coordinate system, as shown in *Figure 1.3*. This is therefore the coordinate system used in this section. For a general case, the tank has a translational oscillation along the  $x$  and  $y$  axes, pitch and yaw oscillations

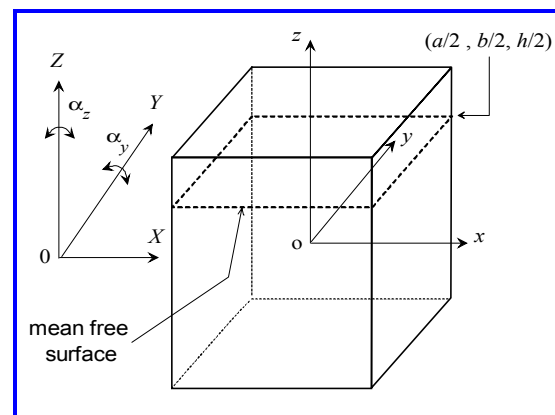


Figure 1.3 Coordinate system for the derivation of basic slosh equation

about the  $x$  and  $y$  axes, and a roll oscillation about the  $z$  axis. For clarity, *Figure 1.3* shows only one angular oscillation  $\alpha_y$  and a roll excitation  $\alpha_z$ . The  $x,y,z$  coordinate system is fixed to and moves with the tank, whereas the inertial  $X,Y,Z$  coordinate system is stationary.

### Velocity potential $\Phi$

Since the liquid is inviscid and the motion is assumed to be without vorticity, the slosh velocity distribution can be derived from a *velocity potential*  $\Phi$ . The  $x,y,z$  components of the velocity  $u,v,w$  components are computed from the spatial derivative of the potential:

$$u = \frac{\partial\Phi}{\partial x} \quad v = \frac{\partial\Phi}{\partial y} \quad w = \frac{\partial\Phi}{\partial z} \quad (1.1)$$

The basic differential equation that a velocity potential must satisfy everywhere in the liquid volume is the condition of liquid incompressibility, which is given by:

$$\frac{\partial u}{\partial x} + \frac{\partial v}{\partial y} + \frac{\partial w}{\partial z} = 0 \quad \text{or} \quad \frac{\partial^2\Phi}{\partial x^2} + \frac{\partial^2\Phi}{\partial y^2} + \frac{\partial^2\Phi}{\partial z^2} = 0 \quad \text{or} \quad \nabla^2\Phi = 0 \quad (1.2)$$

The last form of this equation is written in vector notation and so applies to any coordinate system.

### Equations of motion

For a potential flow that does not contain vorticity, the fluid dynamics equations of motion can be integrated directly to give the unsteady form of Bernoulli's equation:

$$\frac{\partial\Phi}{\partial t} + \frac{p}{\rho} + gz + \frac{1}{2}(u^2 + v^2 + w^2) = f(t) \quad (1.3)$$

where  $p$  is the fluid pressure,  $\rho$  is the fluid density, and  $g$  is the effective gravity directed in the negative  $z$  direction (which is equal to gravity in a laboratory but is the negative of the value of the axial acceleration for a space vehicle).

The velocities  $u,v,w$  are assumed to be so small that squared and higher power terms of them can be neglected in comparison to linear terms; that is, the equations are *linearized*. Since only the derivative of the potential has a physical meaning [for example, look at Eq. (1.1)], constants or even functions of time can be added to the definition of  $\Phi$  whenever it is convenient. This allows the constant of integration  $f(t)$  in Eq. (1.3) to be absorbed into the definition of  $\Phi$ . The linearized form of Eq. (1.3) is thus:

$$\frac{\partial\Phi}{\partial t} + \frac{p}{\rho} + gz = 0 \quad (1.4)$$

### Boundary conditions at the free surface

Any mathematical function that is a solution of Eq. (1.2) must be specialized to satisfy the boundary conditions at the tank walls and free surface. Equation (1.4) is used to derive one of the boundary condition at the free surface. The surface is free to move, so if the gas density is negligibly small compared to the liquid, the pressure at the surface is equal to the static pressure  $p_o$  of the gas above it. Hence, for the liquid at the free surface, the unsteady Bernoulli's equation written is:

$$\frac{\partial\Phi(x,y,z,t)}{\partial t} + g\delta(x,y,t) = -\frac{p_o}{\rho} \quad \text{for } z = h/2 \quad (1.5)$$

Here,  $\delta(x,y,t)$  is the small displacement of the free surface above the undisturbed level  $z = h/2$ . If the equations were not linearized, Eq. (1.5) would have to be evaluated at the actual displaced location  $z = h/2 + \delta$  of the surface rather than at the equilibrium location  $z = h/2$ . The difference between the two conditions ( $z = h/2$  and  $z = h/2 + \delta$ ) turns out to be a higher order term in  $\delta$  and so can be neglected (this will be proved when nonlinear analyses are considered in Chapter 5).

When  $g$  is small, the effects of surface tension have to be considered in Eq. (1.5). The gas pressure is still  $p_0$ , but there is a difference in pressure between the liquid at the surface and the gas on the other side of the surface, which depends on surface tension and the curvature of the surface. This kind of “low- $g$ ” sloshing will be discussed in Chapter 4.

Equation (1.5) is the “dynamic” condition at the free surface. A “kinematic” condition is needed to relate the surface displacement  $\delta$  to the vertical component of the liquid velocity at the surface. In a linearized form, this condition is simply:

$$\frac{\partial \delta}{\partial t} = w = \frac{\partial \Phi}{\partial z} \quad \text{for } z = h/2 \quad (1.6)$$

Equations (1.5) and (1.6) can be combined into a single condition written entirely in terms of  $\Phi$  (or  $\delta$ ) by differentiating Eq. (1.5) with respect to  $t$ , differentiating Eq. (1.6) with respect to  $z$ , and combining the two equations to eliminate  $\delta$  (or  $\Phi$ ). The result is:

$$\frac{\partial^2 \Phi}{\partial t^2} + g \frac{\partial \Phi}{\partial z} = 0 \quad \text{for } z = h/2 \quad (1.7)$$

Eventually, the time derivative of  $\Phi$  will involve the natural frequencies of the sloshing. Thus, Eq. (1.7) shows that these frequencies are directly related to the imposed gravitational field, as was mentioned earlier.

### Boundary conditions at the tank walls

Because viscosity and viscous stresses have been assumed to be negligibly small, the only condition that can be imposed at a wall of the tank is that the liquid velocity perpendicular to the plane of the wall has to be equal to the velocity  $V_n$  of the tank wall perpendicular to itself (where  $n$  stands for the normal or perpendicular direction). The usual “no-slip” condition cannot be imposed, and in general, the solutions will allow slipping in a direction parallel to the wall.

If the tank were stationary, the boundary condition at the wall would therefore just be that the component of the liquid velocity perpendicular to the wall is zero. This condition leads to a standard type of boundary value problem. Here, however, the tank is assumed to be oscillating back and forth, and this leads to a non-standard boundary value problem. As we will see by some examples given below, this non-standard boundary value problem can be solved by the use of Fourier series.

For some kinds of tank motion, the non-standard problem can be transformed into the standard type by the mathematical trick of expressing the liquid motion in two parts: a rigid body-like motion that is identical to the tank motion, and a motion of the liquid relative to the rigid body motion. This transformation is the same as the transformation used in dynamics to express the motion of a particle relative to a moving coordinate system. The transformation is written in terms of the velocity potential as  $\Phi = \phi_c + \phi$  where  $\phi_c$  is the potential for the rigid body motion of the tank. The boundary condition for  $\Phi$  at a tank wall then reduces to  $\partial \phi_c / \partial n = V_n$  and  $\partial \phi / \partial n = 0$ . Unfortunately, this trick cannot be used for rotational tank motions since the velocity potential  $\phi_c$  of the tank motion would have a non-zero value of vorticity.

Since the sloshing problem is linear, a series of individual problems can be considered, one for each type of tank motion of interest, and the results added to get the

velocity potential for the entire motion. Hence, various kinds of simple tank motion will be considered in turn.

**Horizontal motion parallel to the  $x$  axis.** For this case, the tank displacement is expressed as  $X(t) = -iX_o \exp(i\Omega t)$ . This choice makes the real displacement equal to  $X_o \sin \Omega t$ . The velocity components of the tank walls are  $v = w = 0$  and  $u = iX_o \Omega \exp(i\Omega t)$ . Thus, the boundary conditions at the wetted surfaces of the tank are expressed as:

$$\mathbf{n} \cdot \nabla \Phi = iX_o \Omega e^{i\Omega t} \quad \text{at wetted surfaces} \quad (1.8)$$

where  $\mathbf{n}$  is the unit vector normal to the wetted surface. (As an example, for a vertical wall perpendicular to the  $y$ -axis,  $\mathbf{n} \cdot \nabla \Phi$  reduces to  $\partial \Phi / \partial x$  and Eq. (1.8) merely states that the  $x$ -velocity of the liquid at the wall must equal the imposed  $x$ -velocity of the tank.)

**Pitching about the  $y$  axis.** For this case, the angular oscillation of the tank walls is expressed as  $\alpha_y(t) = -i\alpha_o \exp(i\Omega t)$ . The displacement of any point on a tank wall normal to the tank wall is proportional to the axial distance of the point from the pitch axis:  $X(t) = z\alpha_o \exp(i\Omega t)$ . There are also  $z$ -displacements of points on the bottom of the tank, which are proportional to the  $x$  distance of a point from the pitch axis, or  $Z(t) = -x\alpha_o \exp(i\Omega t)$ . These conditions can be combined into a single, vector boundary condition at the wetted surfaces which is expressed as:

$$\mathbf{n} \cdot \nabla \Phi = (ze_x - xe_z)\alpha_o \Omega e^{i\Omega t} \quad (1.9)$$

where  $e_x$  is the unit vector in the  $x$ -direction and  $e_z$  is the unit vector in the  $z$ -direction.

**Rolling about the  $z$  axis.** If the tank has internal walls or is not axisymmetric, roll oscillations  $\alpha_z = -i\gamma_o \exp(i\Omega t)$  about the  $z$  axis will cause the liquid to oscillate and create slosh waves. Generally, rolling is more important for an airplane than for a missile or spacecraft, but it is considered here for completeness. The appropriate vector boundary condition at the wetted walls is:

$$\mathbf{n} \cdot \nabla \Phi = (xe_y - ye_x)\gamma_o \Omega e^{i\Omega t} \quad (1.10)$$

For an axisymmetric tank without any internal walls, a roll motion of the tank will “slip” around the liquid without producing any liquid motion, because an inviscid liquid cannot sustain a shear stress between the walls and the liquid. For a real liquid with viscosity, a roll motion will cause some liquid motion in a thin boundary layer near the walls, but this motion will create little if any wave motion on the free surface.

### 1.3 Solution of Equations for a Rectangular Tank

A rectangular tank “fits” the  $x,y,z$  coordinate system shown in *Figure 1.3* and since the solutions of Eq. (1.2) are familiar trigonometric sines and cosines, it is used as a detailed example to show how the boundary conditions determine the sloshing motions [GRAHAM, ET AL, 1952]. Initially, the tank is considered to be stationary, and the solutions for this case are conventionally called the “eigenfunctions” of the problem.

#### Eigenfunctions of $\nabla^2 \Phi = 0$

The potential solutions of interest are assumed to be harmonic in time,  $\exp(i\omega t)$ . For much of this discussion, the time dependence of  $\Phi$  can be ignored, but when time derivatives are needed they are included by multiplying the potential by  $i\omega$ . The  $\Phi(x,y,z)$  eigenfunctions are found by the method of separation of variables, in which  $\Phi(x,y,z)$  is assumed to be the product of three individual functions  $\xi(x)$ ,  $\psi(y)$ , and  $\zeta(z)$  of the

coordinates. This assumption is inserted into Eq. (1.2) and the entire equation is divided by  $\Phi = \xi\psi\zeta$  to give:

$$\frac{1}{\xi} \frac{d^2\xi}{dx^2} + \frac{1}{\psi} \frac{d^2\psi}{dy^2} + \frac{1}{\zeta} \frac{d^2\zeta}{dz^2} = 0 \quad (1.11)$$

Since  $\xi$  is only a function of  $x$ ,  $\psi$  is only a function of  $y$ , and  $\zeta$  is only a function of  $z$ , each of the ratios in Eq. (1.11) must be independent of any coordinate and so must be equal to a constant. The form of the solution depends on whether the constant is assumed to be a positive or a negative number. To begin, both signs are assumed. The first set of eigenfunctions, for negative constants for  $\xi$  and  $\psi$  and positive for  $\zeta$ , is thus given by:

$$\frac{1}{\xi} \frac{d^2\xi}{dx^2} = -\lambda^2 \quad \Rightarrow \quad \xi(x) = A \sin \lambda x + B \cos \lambda x \quad (1.12a)$$

$$\frac{1}{\psi} \frac{d^2\psi}{dy^2} = -\beta^2 \quad \Rightarrow \quad \psi(y) = C \sin \beta y + D \cos \beta y \quad (1.12b)$$

$$\frac{1}{\zeta} \frac{d^2\zeta}{dz^2} = \lambda^2 + \beta^2 \quad \Rightarrow \quad \zeta(z) = E \sinh \sqrt{\lambda^2 + \beta^2} z + F \cosh \sqrt{\lambda^2 + \beta^2} z \quad (1.12c)$$

where  $\lambda$  and  $\beta$  are constants. The second set is obtained by changing the signs:

$$\frac{1}{\xi} \frac{d^2\xi}{dx^2} = \lambda^2 \quad \Rightarrow \quad \xi(x) = A \sinh \lambda x + B \cosh \lambda x \quad (1.13a)$$

$$\frac{1}{\psi} \frac{d^2\psi}{dy^2} = \beta^2 \quad \Rightarrow \quad \psi(y) = C \sinh \beta y + D \cosh \beta y \quad (1.13b)$$

$$\frac{1}{\zeta} \frac{d^2\zeta}{dz^2} = -(\lambda^2 + \beta^2) \quad \Rightarrow \quad \zeta(z) = E \sin \sqrt{\lambda^2 + \beta^2} z + F \cos \sqrt{\lambda^2 + \beta^2} z \quad (1.13c)$$

Obviously, there are also other possibilities obtained by mixing positive and negative constants in other ways. The simple solution:

$$\Phi((x, y, z)) = Gx + Hy + Kz + Lxy + Mxz + Nyz \quad (1.14)$$

is yet another possibility. All these solutions will be needed to satisfy the boundary conditions for particular cases.

## Eigenvalues

Some values of the constants  $\lambda$  and  $\beta$  naturally satisfy the boundary conditions of this standard boundary value problem. These values are called *eigenvalues*. The natural frequencies of the problem, in this case the sloshing frequencies, are determined by the eigenvalues. Since the natural frequencies will be needed subsequently, they are computed before considering the solutions for cases when the tank is in motion.

**Conditions at walls.** As shown in Figure 1.3, the tank walls are at  $x = \pm a/2$  and  $y = \pm b/2$ .

The unit normal vectors are  $e_x = \pm 1$ ,  $e_y = 0$  for the two walls perpendicular to the  $x$  axis, and  $e_x = 0$ ,  $e_y = \pm 1$  for the two walls perpendicular to the  $y$  axis. Thus, the wall boundary conditions become  $\partial\Phi/\partial x = 0$  for  $x = \pm a/2$  and  $\partial\Phi/\partial y = 0$  for  $y = \pm b/2$ . By studying the various possibilities presented by Eqs. (1.12), (1.13), and (1.14), it can be seen that Eqs. (1.12) can be made to satisfy these conditions, and Eqs. (1.13) and (1.14) cannot (short of making all the integration constants identically equal to zero). The relevant possibilities for making  $\partial\Phi/\partial x = 0$  for  $x = \pm a/2$  are:

$$A = 0 \text{ and } \lambda = 2n\pi/a \text{ or } B = 0 \text{ and } \lambda = (2n-1)\pi/a \quad n = 1, 2, 3, 4, \dots \quad (1.15a)$$

Likewise, the relevant possibilities for making  $\partial\Phi/\partial y = 0$  for  $y = \pm b/2$  are:

$$C = 0 \text{ and } \beta = 2n\pi/b \text{ or } D = 0 \text{ and } \beta = (2n-1)\pi/b \quad n = 1, 2, 3, 4, \dots \quad (1.15b)$$

These give several choices for the sum  $(\lambda^2 + \beta^2)^{0.5}$ , namely  $2n\pi/a$ ,  $2n\pi/b$ ,  $(2n-1)\pi/a$ ,  $(2n-1)\pi/b$ ,  $[(2n\pi/a)^2 + (2n\pi/b)^2]^{0.5}$ ,  $[(2n\pi/a)^2 + (2n-1)^2\pi^2/b^2]^{0.5}$ , and so on.

The requirement that  $\partial\Phi/\partial z = 0$  for  $z = -h/2$  at the tank bottom is satisfied for all values of  $\lambda$  and  $\beta$  by choosing:

$$E = F \tanh\left[\sqrt{\lambda^2 + \beta^2} (h/2)\right] \quad (1.15c)$$

in Eq. (1.12c).

Considering first two dimensional waves, the combinations of eigenvalues and eigenfunctions lead to the following possibilities for the potential  $\Phi = \xi\psi\zeta$ :

$$\Phi_1(x, z) = (AF) \cos[2n\pi(x/a)] \{ \cosh[2n\pi(z/a)] + \tanh[n\pi(h/a)] \sinh[2n\pi(z/a)] \} \quad (1.16a)$$

$$\Phi_2(x, z) = (BF) \sin[(2n-1)\pi(x/a)] \times \{ \cosh[(2n-1)\pi(z/a)] + \tanh[2(n-1)\pi(h/a)] \sinh[(2n-1)\pi(z/a)] \} \quad (1.16b)$$

$$\Phi_3(y, z) = (CF) \cos[2n\pi(y/b)] \{ \cosh[2n\pi(z/b)] + \tanh[n\pi(b)] \sinh[2n\pi(z/b)] \} \quad (1.16c)$$

$$\Phi_4(y, z) = (DF) \sin[(2n-1)\pi(y/b)] \times \{ \cosh[(2n-1)\pi(z/b)] + \tanh[2(n-1)\pi(h/b)] \sinh[(2n-1)\pi(z/b)] \} \quad (1.16d)$$

There are also three dimensional waves of various kinds, of which the following is just one possibility:

$$\Phi_5(x, y, z) = (BDF) \sin[(2n-1)\pi(x/a)] \sin[(2m-1)\pi(y/b)] \times \{ \cosh[\pi\gamma(z/a)] + \tanh[\pi\gamma(h/2a)] \sinh[\pi\gamma(z/a)] \} \quad (1.17)$$

where  $\gamma = (2n-1)^2 + (2m-1)^2(a/b)^2$ .

**Conditions at the free surface.** The boundary condition at the free surface is given by Eq. (1.7). The time derivative  $\partial^2\Phi/\partial t^2$  in this equation is replaced by the equivalent term  $-\omega^2\Phi \exp(i\omega t)$ , and the factor  $\exp(i\omega t)$  which multiplies both terms in Eq. (1.7) is canceled out. Thus, as an example, the solution represented by  $\Phi_2$  when it is inserted into Eq. (1.7) and  $z$  set equal to  $h/2$  gives the algebraic requirement that:

$$-\omega^2 BF \sin[\kappa(x/a)] \{ \cosh[\kappa(h/2a)] + \tanh[\kappa(h/2a)] \sinh[\kappa(h/2a)] \} + g(\kappa/a) BF \sin[\kappa(x/a)] \{ \sinh[\kappa(h/2a)] + \tanh[\kappa(h/2a)] \cosh[\kappa(h/2a)] \} = 0 \quad (1.18)$$

where  $\kappa = \pi(2n-1)$ .

**Natural frequencies.** For this example, the natural frequencies are determined by the roots of Eq. (1.18). After canceling out the common  $\sin$  term and the constant  $BF$  in Eq. (1.18), and simplifying the hyperbolic terms by the use of various hyperbolic identities, the solution  $\omega$  for the natural frequencies for these two-dimensional waves is found to be:

$$\omega_n^2 = \pi(2n-1) \left( \frac{g}{a} \right) \tanh \left[ \pi(2n-1) \left( \frac{h}{a} \right) \right] \quad (1.19a)$$

## 1. LATERAL SLOSHING IN MOVING CONTAINERS

where the subscript  $n$  indicates that  $\omega$  depends on the mode number  $n$ . The frequency decreases as the depth  $h$  decreases or the tank width  $a$  increases. The  $n = 1$  mode has the lowest of all natural frequencies.

**Slosh wave shape.** With this solution for  $\Phi_2$ , the slosh wave shape is found from Eq. (1.6) to be:

$$\delta(x,t) = -\frac{2BF_i}{a\omega_n} (2n-1) \sinh\left[\pi(2n-1)\left(\frac{h}{a}\right)\right] \sin\left[\pi(2n-1)\left(\frac{x}{a}\right)\right] \quad (1.19b)$$

When  $n = 1$ , the wave has zero amplitude at  $x = 0$ , a positive peak at one wall, and a negative peak at the other wall; this is the *fundamental antisymmetric* wave. For  $n > 1$ , there are intermediate peaks, and the number of peaks increases with  $n$ . Figure 1.4 shows a sketch of the first three modes and the relative shift of the liquid center-of-mass for each mode. The c.m. shift for the fundamental mode  $n = 1$  is substantially greater than that of the other modes for the same maximum wave amplitude. Since the c.m. oscillation is the source of the slosh-induced forces and torques, the  $n = 1$  wave produces a much greater force and torque than any other mode.

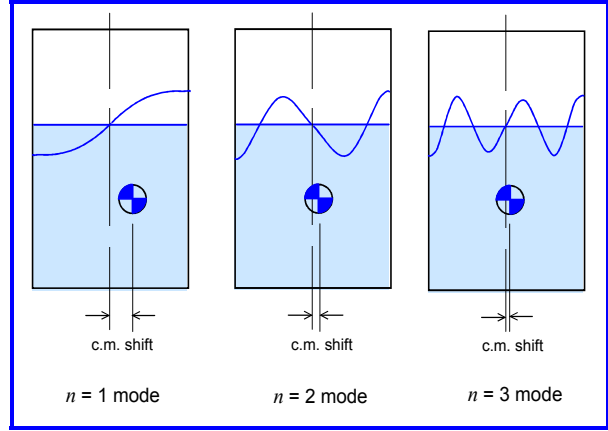


Figure 1.4. Slosh wave shapes for first three antisymmetrical  $x$ -modes of a rectangular tank.

**Symmetrical modes.** The symmetrical slosh modes are found similarly by starting with  $\Phi_1$  rather than  $\Phi_2$ . The symmetric mode natural frequencies, which are all higher than the corresponding antisymmetrical mode frequencies, are given by the relation:

$$\omega_m^2 = 2m\pi(g/a) \tanh[2\pi m(h/a)] \quad (1.20)$$

The first few symmetrical wave shapes are shown in Figure 1.5. Since there is no lateral shift of the liquid c.m. for any of these modes, they produce no lateral forces or torques.

**2-D “y”-modes.** The natural frequencies of the two dimensional “y” antisymmetric and symmetric modes (when occur when the tank has a translational oscillation along the  $y$ -axis) are determined by the same process, starting with  $\Phi_3$  and  $\Phi_4$ . The results are the same as the corresponding  $x$ -mode results with the width  $a$  replaced by the width  $b$ .

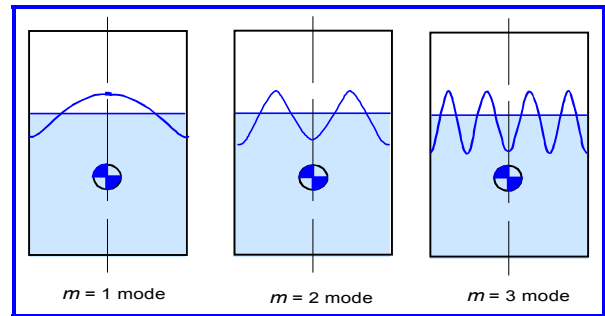


Figure 1.5. Slosh wave shapes for first three symmetrical  $x$ -modes for a rectangular tank.

**Three dimensional modes.** The natural frequencies of the modes that vary with both  $x$  and  $y$  can be determined by a similar process, starting with  $\Phi_5$ . The result is given by:

$$\omega_{m,n}^2 = \left\{ \left[ \gamma_n^2 + \eta_m^2 \left( \frac{a}{b} \right)^2 \right] \left( \frac{g}{a} \right) \right\} \tanh \left\{ \left[ \gamma_n^2 + \eta_m^2 \left( \frac{a}{b} \right)^2 \right] \left[ \frac{h}{a} \right] \right\} \quad (1.21)$$

where  $\gamma_n$  is either  $2\pi n$  or  $2\pi(n - 0.5)$  depending on whether the three dimensional wave is symmetrical or antisymmetrical in the  $x$ -direction, and  $\eta_m$  is likewise  $2\pi m$  or  $2\pi(m - 0.5)$ . The wave shapes are a combination of the two-dimensional  $x$ - and  $y$ -mode shapes.

### Forced motion - oscillatory translation of the tank

The free (eigenfunction) slosh modes are the basis for constructing a solution when the tank is forced to oscillate. For a first example, the tank is assume to oscillate along the  $x$  axis. For a rectangular tank, the boundary condition Eq. (1.8) therefore reduces to:

$$\frac{\partial \Phi}{\partial x} = \Omega X_o e^{i\Omega t} \quad \text{for } x = \pm a/2; \quad \frac{\partial \Phi}{\partial y} = 0 \quad \text{for } y = \pm b/2 \quad (1.22)$$

The free surface and bottom boundary conditions are the same as for free oscillations.

Oscillating the tank in the  $x$ -direction creates  $x$ -antisymmetrical waves, so the forced motion solution involves a series of the  $\Phi_2$  sloshing modes. Since these modes satisfy the condition that  $\partial \Phi / \partial x = 0$  for  $x = \pm a/2$  rather than the conditions given by Eq. (1.22), it is necessary to add on the  $x$ -varying part of the potential given by the simple solution Eq. (1.14). Altogether, the trial solution is assumed to be:

$$\Phi = \left\{ A_o x + \sum_{n=1}^{\infty} A_n \sin \left[ \lambda_n \frac{x}{a} \right] \left[ \cosh \left[ \lambda_n \frac{z}{a} \right] + \tanh \left[ \lambda_n \frac{h}{2a} \right] \sinh \left[ \lambda_n \frac{z}{a} \right] \right] \right\} e^{i\Omega t} \quad (1.23)$$

For compactness, the symbol  $\lambda_n$  is used for  $(2n - 1)\pi$  in Eq. (1.23) and the product of the integration constants  $BF$  of  $\Phi_2$  has been replaced by another constant  $A_n$ , where the subscript  $n$  indicates that the constant depends on the mode in question.

Note that  $\partial \Phi / \partial y \equiv 0$  identically and that  $\partial \Phi / \partial z = 0$  at the bottom of the tank  $z = -h/2$ . So if  $A_o$  is chosen to be equal to  $\Omega X_o$ , the potential  $\Phi$  will satisfy all the wall boundary conditions. The requirements for satisfying the free surface condition are now investigated. Substituting  $\Phi$  into the free surface condition Eq. (1.7) gives:

$$\begin{aligned} -\Omega^2 \left\{ \Omega X_o x + \sum_{n=1}^{\infty} A_n \sin \left( \lambda_n \frac{x}{a} \right) \left[ \cosh \left( \lambda_n \frac{h}{a} \right) + \tanh \left( \lambda_n \frac{h}{2a} \right) \sinh \left( \lambda_n \frac{h}{a} \right) \right] \right\} + \\ g \left\{ \sum_{n=1}^{\infty} A_n \left( \frac{\lambda_n}{a} \right) \sin \left( \lambda_n \frac{x}{a} \right) \left[ \sinh \left( \lambda_n \frac{h}{a} \right) + \tanh \left( \lambda_n \frac{h}{2a} \right) \cosh \left( \lambda_n \frac{h}{a} \right) \right] \right\} = 0 \end{aligned} \quad (1.24)$$

This equation in effect specifies the integration constants  $A_n$  in terms of  $X_o$ . But to determine them explicitly, the  $x$  in the first term of Eq. (1.24) has to be written as a Fourier series of  $\sin(\lambda_n x/a)$  terms (which is possible because the  $\sin(\lambda_n x/a)$  terms are orthogonal over the interval  $-a/2 < x < a/2$ ). This process gives:

$$x = \sum_{n=1}^{\infty} \left( \frac{2a^2}{\lambda_n^2} \right) (-1)^{n-1} \sin(\lambda_n x/a) \quad (1.25)$$

By replacing the  $x$  term in Eq. (1.24) with this series, terms can be grouped with respect to each  $\sin(\lambda_n x/a)$ , which allows each  $A_n$  to be solved for one at a time (again because the  $\sin$  terms are orthogonal). After some algebra and the substitution of Eq. (1.19a) for the natural frequencies, the final expression for the velocity potential is found to be:

$$\Phi(x, z, t) = -Ae^{i\Omega t} \left\{ x + \sum_{n=1}^{\infty} \frac{4a(-1)^{n-1}}{\pi^2(2n-1)^2} \left( \frac{\Omega^2}{\omega_n^2 - \Omega^2} \right) \sin \left[ (2n-1)\pi \frac{x}{a} \right] \times \frac{\cosh \left[ (2n-1)\pi(z/a + h/2a) \right]}{\cosh \left[ (2n-1)\pi(h/a) \right]} \right\} \quad (1.26)$$

**Forces and torques.** The slosh characteristics of most interest in applications are the natural frequencies and the forces and torques exerted on the tank by the sloshing liquid. The forces and torques are determined by integrating the *unsteady* part of the liquid pressure  $p$  over the tank wall area. Equation (1.3) (linearized) shows how to determine this pressure in terms of the velocity potential. The differential component of the  $x$ -force is  $dF_x = p(dA_x)$ , where  $dA_x$  is the differential element of wall area normal to the  $x$ -axis. The  $x$ -component of the force,  $F_x$ , is therefore found by integration:

$$F_x = \int_{-h/2}^{h/2+\Delta} \int_{-b/2}^{b/2} p|_{x=a/2} dydz - \int_{-h/2}^{h/2-\Delta} \int_{-b/2}^{b/2} p|_{x=-a/2} dydz = -2\rho b \int_{-h/2}^{h/2} \frac{\partial \Phi}{\partial t} \Big|_{x=a/2} dz \quad (1.27)$$

Equation (1.27) has been linearized with respect to both the unsteady pressure and the wave amplitude  $\Delta = \delta(x = \pm a/2)$  at the wall, and advantage has been taken of the anti-symmetry properties of  $\Phi$  to combine the integrals over each wall. Substituting the expression for  $\Phi$  from Eq. (1.26) and performing the integration gives:

$$\frac{F_{xo}}{-i\Omega^2 X_o m_{liq}} = 1 + 8 \frac{a}{h} \sum_{n=1}^N \frac{\tanh \left[ (2n-1)\pi h/a \right]}{(2n-1)^3 \pi^3} \frac{\Omega^2}{\omega_n^2 - \Omega^2} \quad (1.28)$$

Here  $F_{xo}$  is the amplitude of the oscillating force, and  $m_{liq} = \rho abh$  is the mass of liquid in the tank.

According to Eq. (1.28), the force exerted on the tank becomes indefinitely large when the excitation frequency  $\Omega$  equals any of the slosh natural frequencies  $\omega_n$ . This is because all viscous effects and other sources of damping have been neglected; these effects will be discussed in the next chapter. Because of the  $(2n-1)^3$  term in the denominator of Eq. (1.28), the magnitude of the resonant force *decreases* as the order of the slosh mode *increases*. For that reason, when damping is included, only the first mode or perhaps the first two modes create substantial forces. Other characteristics to note include:

- For low excitation frequencies (i.e.,  $\Omega \rightarrow 0$ ), the summation in Eq. (1.28)  $\rightarrow 0$ , and the force is just the product of the liquid mass and the tank acceleration; i.e., the liquid responds as if were frozen.
- For high excitation frequencies (i.e.,  $\Omega \gg \omega_n$ ), the summation is independent of  $\Omega$ , and the force is again like a rigid body, with a mass  $m_{liq} [1 - 8(a/h\pi^3) \tanh(\pi h/a)]$  that

is somewhat less than the liquid mass; this implies that some of the liquid (near the free surface) does not move with the tank.

- The  $z$  and  $y$  components of the force are zero.

Next, the torque  $M$  exerted on the tank is computed. This torque acts about the  $y$ -axis and is caused by the pressure acting on the  $x$ -walls and the bottom of the tank. With the  $y$  axis through the center of mass of the liquid, the differential element of torque is  $dM_y = -z(pdA_x) - x(pdA_z)$ . Thus the total torque is given by:

$$M_y = -2 \int_{-h/2}^{h/2+\Delta} \int_{-b/2}^{b/2} z p|_{x=a/2} dy dz - \int_{-a/2}^{a/2} \int_{-b/2}^{b/2} x p|_{z=-h/2} dy dx \quad (1.29a)$$

Linearizing and combining terms give:

$$M_y = 2b \int_{-h/2}^{h/2} z \frac{\partial \Phi}{\partial t} \Big|_{x=a/2} dz - 2b \int_{-a/2}^{a/2} x \frac{\partial \Phi}{\partial t} \Big|_{z=-h/2} dx \quad (1.29b)$$

After performing the indicated integrations, simplifying the result with various algebraic and hyperbolic transformations<sup>1</sup>, and rearranging the results to make for easy comparisons with the force, it is found that the torque is given by:

$$\frac{M_{yo}}{-i\Omega^2 X_o m_{liq} h} = \frac{1}{12} (a/h)^2 + 8(a/h) \sum_{n=1}^{\infty} \frac{\tanh[(2n-1)(\pi h/a)]}{(2n-1)^3 \pi^3} \times \left[ \frac{1}{2} - \frac{2(a/h) \tanh[(2n-1)(\pi h/2a)]}{(2n-1)\pi} + \frac{g}{h\omega_n^2} \right] \frac{\Omega^2}{\omega_n^2 - \Omega^2} \quad (1.30)$$

The  $g$ -term in the brackets on the right represents the gravitational torque of the oscillating center of mass of the liquid. When Eq. (1.30) is compared to Eq. (1.27), we can conclude that the terms that represent the oscillating masses in Eq. (1.27) are multiplied by factors that have dimensions of length.

There is a rigid-body torque even in the limit of small excitation frequencies (when the resonating terms disappear). For a true rigid body, there is no torque about the center of mass for a translational acceleration. However, here the lack of a “top” for the liquid pressure to act on and counterbalance the pressure on the tank bottom creates a liquid torque. The magnitude of this rigid-body torque is small.

### Forced motion - pitching of the tank about the $y$ axis

For the next example, the tank is assumed to pitch about the  $y$  axis. The boundary conditions at the wall are given by Eq. (1.9); for a rectangular tank, they reduce to:

$$\frac{\partial \Phi}{\partial x} = \alpha_o \Omega z e^{i\Omega t} \quad \text{for } x = \pm a/2; \quad \frac{\partial \Phi}{\partial z} = -\alpha_o \Omega x e^{i\Omega t} \quad \text{for } z = -h/2 \quad (1.31)$$

These conditions cause more than a little complexity in the expression for the potential because, as was discussed earlier, no single potential can be made to satisfy them both. In fact, in addition to the forms of the potential given previously, all of which satisfy the condition that the velocity is zero at the tank bottom, several other kinds of solutions of the basic differential equation, Eq. (1.2), are needed. For example, a potential is needed

<sup>1</sup> For example, the relation:  $1/\sinh \zeta = 1/\tanh \zeta - \tanh(\zeta/2)$  has been used.

that can be used to expand  $z$  into a Fourier series to satisfy the first part of Eq. (1.31). A suitable potential is:

$$\Phi(x, z) = \sum_{n=1}^{\infty} A_n \sin[(2n-1)\pi z/h] \sinh[(2n-1)\pi x/h] \quad (1.32)$$

The fact that Eq. (1.32) satisfies Eq. (1.2) can be verified by direct substitution. This potential, however, introduces a complication because  $\partial\Phi/\partial z$  at the free surface now involves  $\sinh$  terms in the variable  $x$ , whereas the other potentials used so far involve only  $\sin$  terms in the variable  $x$ . This means that a Fourier series expansion is needed to satisfy the free surface condition as well as the boundary conditions at the walls and bottom. The algebra gets fairly messy although it is straightforward. The final result is:

$$\begin{aligned} \Phi(x, z, t) = \alpha_o h^2 \Omega e^{i\Omega t} & \left\{ \sum_{n=1}^{\infty} \frac{4(-1)^n}{(2n-1)^3 \pi^3} \left( \frac{\sin[(2n-1)\pi z/h] \sinh[(2n-1)\pi x/h]}{\cosh[(2n-1)\pi a/2h]} \right. \right. \\ & \left. \left. + \frac{(a/h)^2 \sin[(2n-1)\pi x/a] \cosh[(2n-1)\pi(z/a - h/2a)]}{\sinh[(2n-1)\pi h/a]} \right) + \right. \\ & \left. \sum_{n=1}^{\infty} \frac{4(a/h)(-1)^n}{(2n-1)^2 \pi^2} \frac{\Omega^2}{\omega_n^2 - \Omega^2} \left( \frac{1}{2} - \frac{2(a/h) \tanh[(2n-1)\pi h/2a]}{(2n-1)\pi} + \frac{g}{h\omega_n^2} \right) \times \right. \\ & \left. \frac{\sin[(2n-1)\pi x/a] \cosh[(2n-1)\pi(z/a + h/2a)]}{\cosh[(2n-1)\pi h/a]} \right\} \quad (1.33) \end{aligned}$$

The first summation in this expression does not have a resonant component and hence it represents a liquid oscillation about the  $y$ -axis analogous to a rigid body.

**Forces and torques.** Proceeding as before to integrate the liquid pressure distribution on the walls and bottom, the  $x$ -component of the force exerted on the tank is found to be:

$$\begin{aligned} \frac{F_{xo}}{-i\Omega^2 m_{liq} h \alpha_o} = & \left\{ \frac{1}{12} \left( \frac{a}{h} \right)^2 + 8 \left( \frac{a}{h} \right) \sum_{n=1}^{\infty} \frac{\tanh[(2n-1)\pi h/a]}{(2n-1)^3 \pi^3} \left( \frac{1}{2} - \frac{\tanh[(2n-1)\pi h/2a]}{(2n-1)\pi h/2a} \right. \right. \\ & \left. \left. + \frac{g}{h\omega_n^2} \left( \frac{\Omega^2}{\omega_n^2 - \Omega^2} \right) \right) \right\} \quad (1.34) \end{aligned}$$

Equation (1.34) shows that the *force* for a pitching oscillation is the same as the *torque* for a lateral oscillation [Eq. (1.30)] when the amplitude  $X_o$  of the translation is replaced by  $h\alpha_o$ . The torque exerted on the tank is given by:

$$\begin{aligned} \frac{M_{yo}}{i m_{liq} h^3 \alpha_o \Omega^2} = & \left\{ \frac{I_y}{m_{liq} h^2} + 16 \left( \frac{a}{h} \right) \sum_{n=1}^{\infty} \frac{\tanh[(2n-1)\pi h/a]}{(2n-1)^3 \pi^3} \left( \frac{g}{h\omega_n^2} \right) \left( \frac{1}{2} + \frac{g}{h\omega_n^2} + \right. \right. \\ & \left. \left. \frac{\tanh[(2n-1)\pi h/2a]}{(2n-1)\pi h/2a} \right) + 8 \left( \frac{a}{h} \right) \sum_{n=1}^{\infty} \frac{\tanh[(2n-1)\pi h/a]}{(2n-1)^3 \pi^3} \left( \frac{g}{h\omega_n^2} \right) \left( \frac{1}{2} + \frac{g}{h\omega_n^2} + \right. \right. \end{aligned} \quad (\text{cont'd})$$

$$\frac{\tanh[(2n-1)\pi h/2a]}{[(2n-1)\pi h/2a]} \left\{ \frac{\Omega^2}{\omega_n^2 - \Omega^2} + \frac{1}{12} \left( \frac{a}{h} \right)^2 \left( \frac{g}{h\Omega^2} \right) \right\} \quad (1.35)$$

where the moment of inertia  $I_y$  in this expression is given by:

$$I_y = I_{Sy} \left\{ 1 - \frac{4}{1 + (h/a)^2} + \frac{768a/h}{\pi^5 [1 + (h/a)^2]} \sum_{n=1}^{\infty} \frac{\tanh[(2n-1)\pi h/2a]}{(2n-1)^5} \right\} \quad (1.36)$$

Here  $I_{Sy}$  is the  $y$ -moment of inertia of the frozen liquid about the liquid center of mass. A number of terms have been combined or rearranged to derive Eq. (1.35)<sup>2</sup>.

### Forced motion - rolling about the $z$ axis

As a final example, rolling about the  $z$ -axis is considered. A roll oscillation creates a three-dimensional motion, and waves are excited in both the  $x$  and  $y$  directions. Potentials of the form given by Eq. (1.18) are therefore needed as well as other potentials to satisfy the boundary conditions, which are given by Eq. (1.10). The total potential and the torque about the  $z$ -axis can be derived by analogous methods as those used for pitching about the  $y$ -axis (there are no net forces), but for brevity only the final results are given here.

$$\begin{aligned} \frac{\Phi(x, y, z, t)}{\gamma_o \Omega b^2} = e^{i\Omega t} & \left\{ \sum_{n=1}^{\infty} \frac{4(-1)^n}{(2n-1)^3 \pi^3} \left( \frac{\sin[(2n-1)\pi y/b] \sinh[(2n-1)\pi x/b]}{\cosh[(2n-1)\pi a/2b]} - \right. \right. \\ & \left. \frac{(a/b)^2 \sin[(2n-1)\pi x/a] \sinh[(2n-1)\pi y/a]}{\cosh[(2n-1)\pi b/2a]} \right) + \sum_{m=1}^{\infty} \sum_{n=1}^{\infty} (-1)^{m+n} \left( \frac{\Omega^2}{\omega_{mn}^2 - \Omega^2} \right) \times \\ & \left. \frac{16(a/b) \left[ (2n-1)^2 - (a/b)^2 (2m-1)^2 \right] \operatorname{sech} \left[ \sqrt{(2n-1)^2 + (a/b)^2 (2m-1)^2} (\pi b/a) \right]}{(2n-1)^2 (2m-1)^2 \pi^2 \left[ (2n-1)^2 + (a/b)^2 (2m-1)^2 \right]} \right\} \times \\ & \sin[(2n-1)\pi x/a] \sin[(2m-1)\pi y/b] \cosh \left[ \sqrt{(2n-1)^2 + (a/b)^2 (2m-1)^2} (\pi a/b) (z + h/2) \right] \end{aligned} \quad (1.37)$$

The natural frequencies  $\omega_{mn}$  depend on both the  $x$  and the  $y$  dimensions of the tank:

$$\omega_{mn} = \frac{\pi g}{a} \sqrt{A_{mn}} \tanh[A_{mn}(\pi h/a)] \quad (1.38)$$

where  $A_{mn} = (2n-1)^2 + (a/b)^2 (2m-1)^2$ . The  $z$ -torque is given by:

$$\begin{aligned} \frac{M_{zo}}{i m_{liq} h^3 \gamma_o \Omega^2} = & \left\{ - \left[ \frac{a^2 + b^2}{12h^2} \right] + \sum_{n=1}^{\infty} \frac{32}{(2n-1)^5 \pi^5} \left( \frac{a^3}{bh^2} \tanh \left[ (2n-1) \frac{\pi b}{2a} \right] + \right. \right. \\ & \left. \frac{b^3}{ah^2} \tanh \left[ (2n-1) \frac{\pi a}{2b} \right] \right) + \sum_{n=1}^{\infty} \sum_{m=1}^{\infty} \left( \frac{\omega_{mn} h}{g} \right) \frac{64 B_{mn}^2}{\pi^8 A_{mn}^2 (2m-1)^4 (2n-1)^4} \frac{\Omega^2}{\omega_{mn}^2 - \Omega^2} \left. \right\} \end{aligned} \quad (1.39)$$

where  $B_{mn} = (2n-1)^2 - (a/b)^2 (2m-1)^2$ .

### Basic theory summary

These examples for a rectangular tank demonstrate how a velocity potential is derived for a specific tank shape and excitation. The analysis is similar for other tank shapes, but the potential functions are no longer **sines** and **cosines**.

<sup>2</sup> For example, the identity:  $1/12 = 8 \sum [\pi(2n-1)]^{-4}$  has been used.

## 1.4 Circular Cylindrical Tank

The circular cylindrical tank is used in many applications because its shape can be packaged neatly into a missile or spacecraft. Some sample results are presented below. More complete sloshing characteristics can be obtained from **SLOSH** code.

### Potential and Eigenvalues

The derivation of the sloshing velocity potential for a cylindrical tank follows that given in Sections 1.2 and 1.3 [BAUER, 1964]. The main difference is that the **sines** and **cosines** used there are replaced by **Bessel** functions  $J_1(r)$  of the first kind, since these are the relevant solutions of Eq. (1.2) in cylindrical coordinates. Typical eigensolutions and eigenvalues are:

$$\Phi_{mn}(r, z) = J_1\left(\frac{\lambda_{mn}r}{a}\right) \cos(m\theta) \frac{\cosh[\lambda_{mn}(z/a + h/2a)]}{\cosh[\lambda_n h/a]} \quad (1.40)$$

$$\omega_{mn}^2 = \frac{g\lambda_{mn}}{a} \tanh\left(\frac{\lambda_{mn}h}{a}\right)$$

where  $r$  and  $\theta$  are the radial and angular coordinates,  $a$  is the tank radius, and  $\lambda_{mn}$  is a root of the eigenvalue equation  $dJ_1(\lambda r/a)/dr = 0$  for  $r = a$ .

### Antisymmetric modes

When  $m = 1$  in Eq. (1.40), the potential varies in the angular coordinate as  $\cos\theta$ , so that the wave is “up” over half the circumference and “down” over the other half, similar to the waves shown previously in *Figure 1.4*. When  $m > 1$ , the wave shape has several “ups” and “downs” around the circumference. But only the  $m = 1$  modes create a net force or torque on the tank, and they are the modes created by lateral or pitching motions of the tank. The  $m = 1$  modes are therefore the main ones of interest. The values of  $\lambda_{mn}$  for  $m = 1$  are denoted by  $\xi_n$ . Numerical values of  $\xi_n$  are:

$$\xi_1 = 1.841 \quad \xi_2 = 5.331 \quad \xi_3 = 8.536 \dots \quad \xi_{n+1} \rightarrow \xi_n + \pi \quad (1.41)$$

The shape of an antisymmetric free surface wave is proportional to  $J_1(\xi_n r/a)$ , and for  $n = 1$ , it is similar to the fundamental **sine** wave shown in *Figure 1.4*. For  $n > 1$ , the shape resembles a corresponding higher order **sine** wave but the peaks and valleys are more and more concentrated near the tank wall as  $n$  increases.

### Forces and torques

The forces and torques for various tank excitations can be computed from the velocity potential just as for the rectangular tank discussed above. But they are more easily computed by an equivalent mechanical model, and thus will be discussed in Chapter 3.

## 1.5 Sector-Annular Cylindrical Tank

The most general kind of cylindrical tank is a sector of an annular tank; all the other kinds of cylindrical tanks – including the right cylinder discussed in Section 1.4 – are special cases of it [BAUER, 1964]. *Figure 1.6* shows a cross section

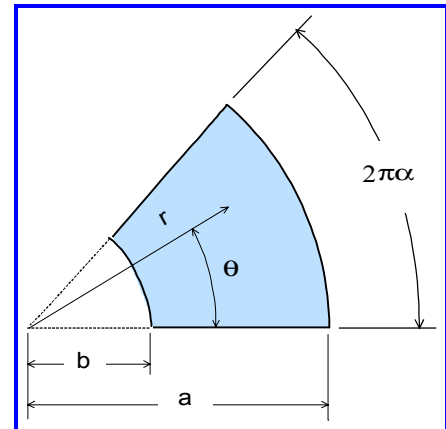


Figure 1.6. Annular sector tank cross section

through this general tank shape. The  $z$  or axial dimension is directed out of the paper. The width of the sector is specified by an angular fraction  $\alpha$  of a complete circle. The radius of the annulus is given by  $b$  and the radius of the tank is given by  $a$ . The coordinate system is cylindrical, with coordinates  $r, \theta, z$ .

The eigensolutions of Eq. (1.2) for this tank geometry again involve Bessel functions [BAUER, 1964]. Since the region of interest is not a complete circle, Bessel functions of fractional orders are needed, and since the liquid region may not extend all the way to  $r = 0$  Bessel functions  $Y(r)$  of the second kind are also needed to satisfy the boundary conditions at  $r = b$  and  $r = a$ . The algebra is complicated, but the velocity potential eigensolutions are given by:

$$\Phi_{mn}(r, \phi, z) = \cos\left[\frac{m\theta}{2\alpha}\right] \frac{\cosh[\lambda_{mn}(z/a + h/2a)]}{\cosh(\lambda_{mn}h/a)} \chi(\lambda_{mn}r/a) \quad (1.41a)$$

The  $\chi$  function in Eq. (1.41a) is defined in terms of Bessel functions as:

$$\chi(\lambda_{mn}r/a) = J_{m/2\alpha}\left(\frac{\lambda_{mn}r}{a}\right) Y'_{m/2\alpha}(\lambda_{mn}) - J'_{m/2\alpha}(\lambda_{mn}) Y_{m/2\alpha}\left(\frac{\lambda_{mn}h}{a}\right) \quad (1.41b)$$

where the prime indicates a differentiation with respect to  $r$ . The eigenvalues  $\lambda_{mn}$  are the roots of the equation:

$$J'_{m/2\alpha}(\lambda) Y'_{m/2\alpha}(\lambda b/a) - J'_{m/2\alpha}(\lambda b/a) Y'_{m/2\alpha}(\lambda) = 0 \quad (1.41c)$$

which arises from the simultaneous satisfaction of  $\partial\phi/dr$  at  $r = b$  and  $r = a$ . The natural frequencies are:

$$\omega_{mn}^2 = \frac{g\lambda_{mn}}{a} \tanh\left(\frac{\lambda_{mn}h}{a}\right) \quad (1.41d)$$

For a quarter sector tank ( $\alpha = 0.5, b = 0$ ), the first few roots are:  $\lambda_{00} = 3.832, \lambda_{01} = 7.016, \lambda_{02} = 10.173, \lambda_{10} = 3.054, \lambda_{11} = 6.706,$  and  $\lambda_{12} = 9.969$ .

### Slosh modes

For a *sector* tank ( $\alpha < 1, b = 0$  in Figure 1.6), slosh modes can be excited by lateral, pitching, and roll motions of the tank. As shown schematically in Figure 1.7, there are two general kinds of important modes, one kind of which has up and down motions aligned with the radius, and the other of which has up and down motions in the circumferential direction. The mode that has the lowest natural frequency depends upon whether the radial or the circumferential extent of the tank is the greater.

For an *annular* tank (i.e.,  $\alpha = 1, b > 0$ ), the antisymmetric modes resemble the antisymmetric mode in a cylindrical tank with the middle part of the wave near the tank axis missing. These modes can be excited by tank translation or pitching, and they create

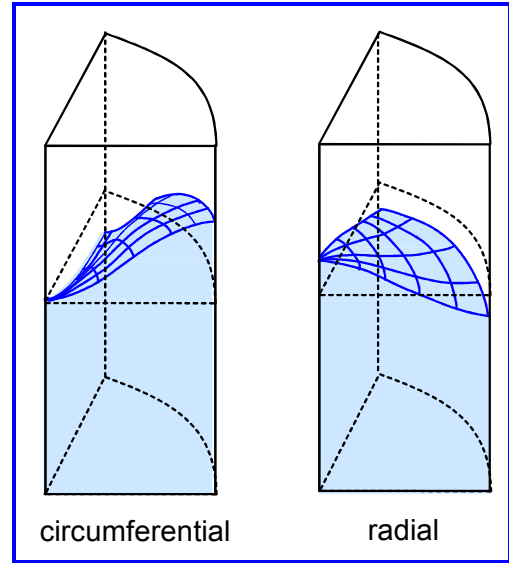


Figure 1.7. Slosh modes for a quarter-sector cylindrical tank

1. LATERAL SLOSHING IN MOVING CONTAINERS

a net force or torque on the tank. Since an annular tank is axisymmetric, the details of the sloshing can be computed by the SLOSH code.

**Forces and torques**

The analytical expressions for the forces and torques are quite complicated and are not given here. For a sector tank, a finite element computer code can be used to compute them, as is discussed later in the Appendix to this Chapter. For an annular tank, the SLOSH code can be used to derive the parameters of an equivalent mechanical model.

**1.6 Horizontal Cylindrical Tank**

Gasoline tanker trucks and some missiles use tanks that are essentially horizontal cylinders. As shown in Figure 1.8, sloshing modes can be created along the long axis of the cylinder or along the transverse axis. The lowest natural frequency corresponds to the mode directed along the longest axis (unless the depth  $h$  is very small, in which case transverse modes can have the lowest frequency even if  $L > 2a$ ).

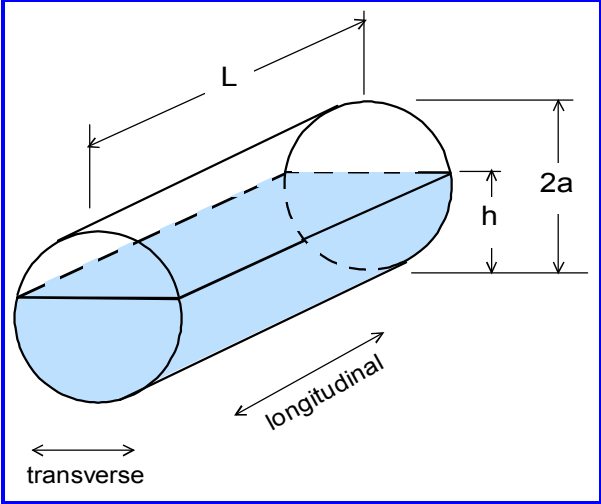


Figure 1.8. Schematic of a horizontal cylinder

An important point to note is that when  $L/2a \gg 1$  the longitudinal slosh modes, which are standing waves, are susceptible to a transformation to traveling waves similar to hydraulic jumps or bores, because standing waves are unstable for such a long, shallow geometry. (Note that this instability is not a nonlinear phenomenon; the characteristics of the traveling waves can in fact be computed accurately by a linear analysis.) To a good approximation, the speed of the traveling wave is such that the travel time of the wave front across the tank length and back is the same as the period of the standing wave. However, the forces exerted on the tank ends are not harmonic in time, but are impulsive, rising to a large value when the wave strikes the wall and then decreasing nearly to zero after the wave front is reflected. The shape of a horizontal cylinder does not fit neatly into any standard coordinate system, so the potential cannot be derived by the separation of variables method used in the previous analyses. Instead, an energy minimization principle and the calculus of variations have been used to derive some limited results

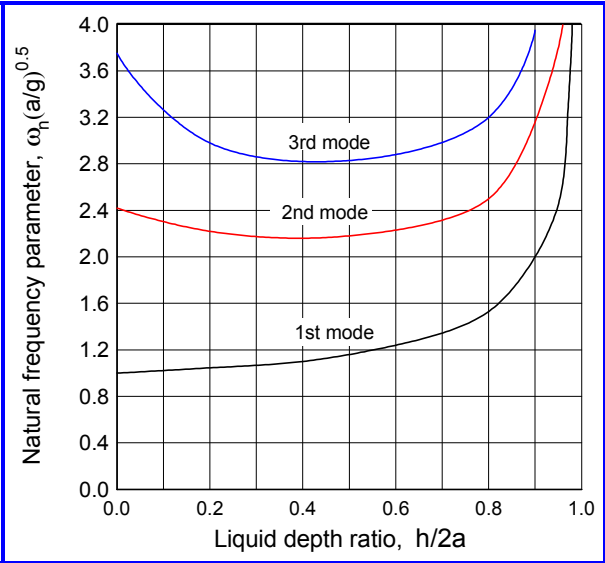


Figure 1.9. Natural frequency parameter of the transverse modes for a horizontal cylinder

for the transverse slosh modes [BUDIANSKY, 1960; MCCARTHY AND STEPHENS, 1960].

**Natural frequencies**

Figure 1.9 shows the nondimensional natural frequency of the three lowest frequency transverse modes, and Figure 1.10 shows the frequencies for the longitudinal modes, as a function of the liquid depth ratio,  $h/2a$ . (The dimensional frequency  $\omega_n$  in the plots has units of rad/sec.) The transverse mode frequencies were calculated from the theory described above. The longitudinal mode frequencies, however, are simply curves faired through experimental data, since there are no theoretical results available for these modes.

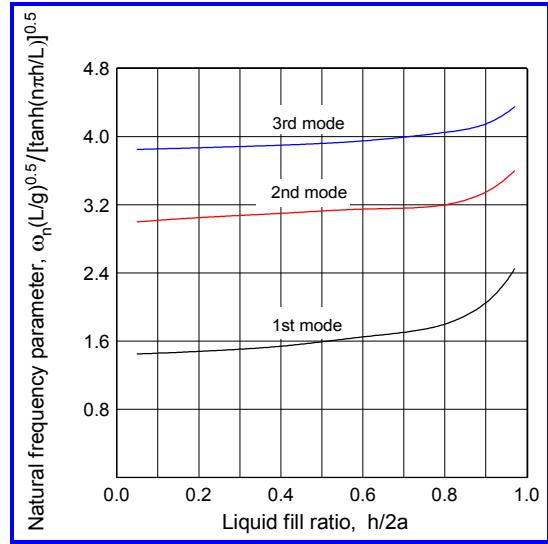


Figure 1.10. Natural frequency parameter for the longitudinal modes of a horizontal cylinder

**Approximate methods**

If the liquid depth is not too shallow or too full, the slosh characteristics can be computed by an approximate procedure. The horizontal cylindrical tank is replaced by a rectangular tank that has the same length  $2b_r = L$  as the cylinder, a width  $2a_r$  equal to the width of the actual free surface, and a liquid depth  $2h_r$  chosen such that the liquid volume of the rectangular tank is the same as the cylindrical tank. For example, for a half-full cylindrical tank, the rectangular tank values are  $a_r = a$  and  $2h_r = \pi a/4$ . From the results given in Section 1.3 by Eq. (1.20a), with these substitutions, the natural frequency parameter for the first transverse mode is predicted to be:

$$\omega_1 \sqrt{a/g} = \left[ \pi \tanh(\pi^2/16) \right]^{0.5} = 1.3 \tag{1.42}$$

This value is only slightly different from the value of 1.2 shown in Figure 1.9.

**Forces and torques**

The forces and torques can be computed from equivalent mechanical models.

**1.7 Spherical Tank**

Because of their high volume-to weight ratio, spherical tanks are often used in satellites and sometimes in launch vehicles.

**Natural frequencies**

Figure 1.11 shows the predicted natural frequency for the first two antisymmetric modes, where  $R_o$  is the sphere radius and  $h$  is the liquid depth, measured from the

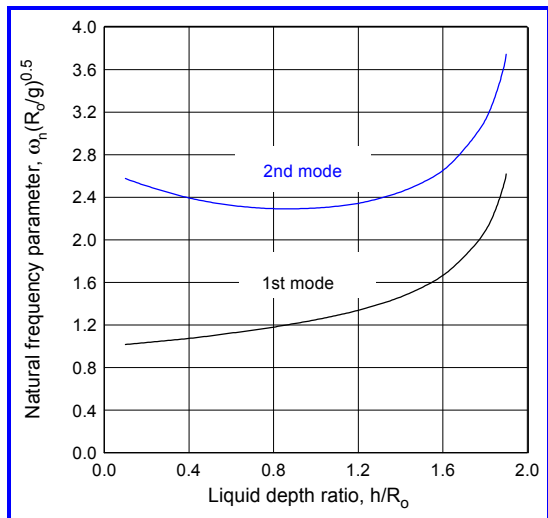


Figure 1.11. Natural frequency parameter for a spherical tank;  $\omega_n$  is in units of rad/sec

bottom of the tank. The initial 1960's era analytical predictions for spherical tanks were made only for certain fill levels, as a result of the need to use numerical methods and the limitations of 1960's computers [BUDIANSKY, 1960; RILEY AND TREMBATH, 1961; EHRLICH, ET AL, 1961; LAWRENCE, ET AL, 1958; STOFAN AND ARMSTEAD, 1962; CHU, 1964; RATTAYA, 1965]. The results shown in *Figure 1.11* are, however, based on the SLOSH code which can predict the slosh characteristics for a spherical tank regardless of fill level.

The natural frequencies become large for high fill levels, because the free surface diameter becomes small. For low fill levels, the free surface diameter also becomes small, which should increase  $\omega_n$ , but the small depth tends to decrease  $\omega_n$  [see Eq. (1.19a)]. The result is that the natural frequency asymptotes to a non-zero value as the tank fill level approaches zero.

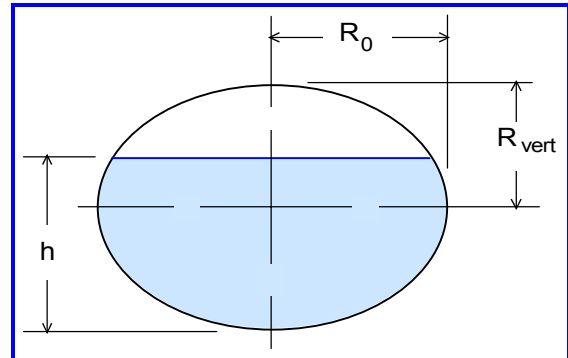


Figure 1.12. Schematic of a spheroidal tank

### Forces and torques

The SLOSH code can be used to compute the mechanical model parameters from which the forces and torques can be computed. It should be noted that an angular oscillation of a spherical tank does not excite sloshing of an ideal liquid, because the tank motion is tangential to the tank wall-liquid interface so the tank merely “slides” around the liquid.

## 1.8 Spheroidal Tank

Spheroidal (ellipsoidal) tanks are also commonly used in spacecraft. They can either be oblate, in which the short axis is the axis of symmetry, or prolate, in which the longer axis is the axis of symmetry. *Figure 1.12* shows the geometry of an oblate spheroidal tank. The cross-section of the tank looking down along the vertical axis is a circle. There are two other ways a spheroid can be oriented with respect to gravity; these other configurations are not axisymmetric and will not be considered here

### Natural frequencies

The slosh natural frequencies for a spheroidal tank are plotted in *Figure 1.13*, for an oblate tank shape  $R_{vert} = R_0/2$  (roughly the tank shape shown in *Figure 1.12*) and for a prolate shape  $R_{vert} = 2R_0$  [RATTAYA, 1965, BAUER AND EIDEL, 1989]. The previous results for a

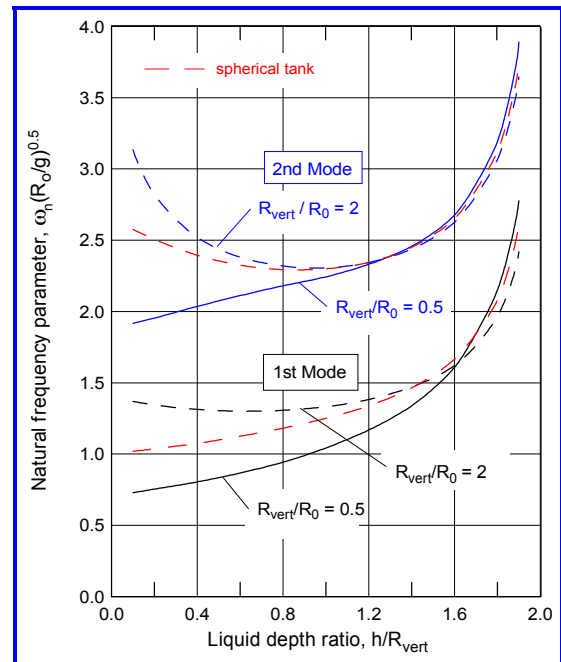


Figure 1.13. Natural frequency parameter for a spheroidal tank:  $\omega_n$  is in units of rad/sec

spherical tank are also repeated for comparison. Roughly the same trends with liquid depth are apparent as was noted for a spherical tank. Furthermore, the natural frequencies for spheres and spheroids are all nearly equal when the tanks are over half full. The SLOSH code can be used to compute any specific case.

### Forces and torques - spheroids

The forces and torques exerted on a spheroidal tank by sloshing liquid can best be computed by an equivalent mechanical model. The SLOSH code can be used to derive the appropriate model parameters.

## 1.9 Toroidal Tank

Toroidal tanks have been proposed for some launch vehicles and spacecraft because they can be fitted around engines or other tanks. Toroidal tanks are also used as “suppression pools” in some boiling-water nuclear reactors to condense the steam released in a postulated loss of coolant accident. Initially, only empirical data or approximate analyses were available for toroidal tanks [McCARTY, LEONARD, AND WALTON, 1960; SUMNER, 1963]. Modern computational methods such as the SLOSH code allow the sloshing characteristics for toroidal tanks to be predicted accurately.

### Natural frequencies

Figure 1.14 shows the configuration of a toroidal tank and the definition of the two radii  $R_o$  and  $R_i$  that describe its geometry. The figure also illustrates schematically the form of the two lowest frequency slosh modes. For the lowest frequency mode, the liquid in half the tank (on the right in Figure 1.14) moves upward and the liquid in the opposite half moves downward alternately. For the second lowest frequency mode, the liquid motion is similar in both halves of the tank. Both of these modes vary as  $\cos\theta$  around the tank circumference and therefore produce net forces and torques. For some radius ratios, the second mode in fact causes the larger forces. There is also a tendency for the two modes to interact.

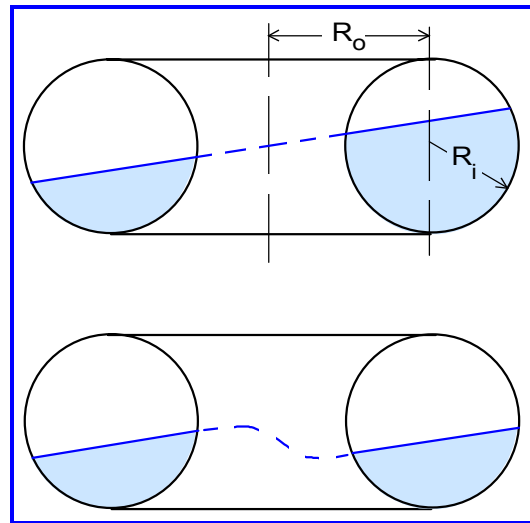


Figure 1.14. Illustration of first and second sloshing modes of a toroidal tank

There are other modes when the tank is oriented on its side such that the  $R_o$  axis is vertical. These modes also produce net forces and torques. The tank is not axisymmetric for this configuration and is generally not used in applications. For that reason, the modes are not discussed here; results for specific designs are given in McCARTY, LEONARD, AND WALTON [1960].

The nondimensional natural frequencies of the two modes illustrated in Figure 1.14 are shown in Figure 1.15 as a function of the liquid depth ratio  $h/2R_i$ . In general, the natural frequencies decrease when the liquid depth decreases, and an increase in the major radius  $R_o$ , for a constant minor radius  $R_i$ , also causes a decrease in the natural frequencies.

## Approximate methods

To compute the slosh characteristics, a toroidal tank can be approximated as an annular cylindrical tank, using the results described earlier. The inner and outer radii of the annular tank are chosen to be the radii to the inner and outer edges of the free surface, and the liquid depth is chosen to duplicate the actual liquid volume. The computer program **SLOSH** is capable of making exact computations for a toroidal tank so there is no need to use this approximate method.

## Forces and torques

The forces and torques exerted on a toroidal tank by sloshing liquid can best be computed by an equivalent mechanical model. The **SLOSH** code can be used to derive the appropriate model parameters.

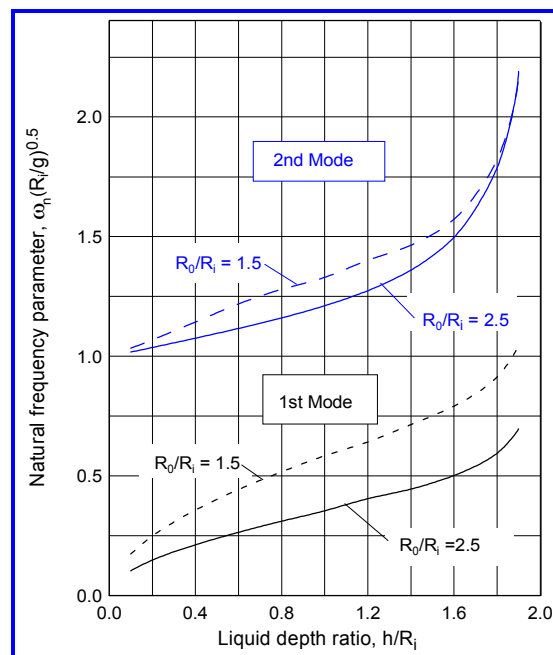


**Figure 1.15.** Natural frequency parameter for a toroidal tank;  $\omega_n$  is in units of rad./sec

## 1.10 Some Practical Implications

Several methods have been developed to minimize the dynamical effects of liquid sloshing in space vehicles. Baffles of various configurations have been devised to increase the natural viscous damping and decrease the magnitude of the slosh forces and torques; these are discussed in Chapter 2. If a shift in the range of the sloshing frequencies is desired, baffles are relatively ineffective and a better method is to divide the tank into subtanks or compartments, although it should be noted that for a cylindrical tank, compartmentation into sectors raises the fundamental slosh frequency and lowers the second frequency, so the two modes become less separated in frequency. Radial compartmentation is moreover not as effective as ring baffles in reducing the amplitude of the slosh forces and torques.

## 1.11 Vertical Sloshing<sup>3</sup>

Propellant tanks are subjected to vibrations along the thrust or g-vector in some applications, rather than transverse to it as shown in *Figure 1.1*. The resulting sloshing is called *vertical sloshing* and is due to a parametric instability since waves are not excited directly by vibration normal to the free surface.

If the excitation acceleration is large enough to exceed the thrust acceleration, the surface will throw off drops and sprays, and the drops as they fall back and impact the free surface can also set up sloshing by a complicated interaction [YARYMOVYCH, 1959; KANA, 1966]. Furthermore, small bubbles can become entrained in the bulk of the liquid, and the vertical vibration can tend to make the bubbles coalesce into one or more large bubbles; the large bubbles lower the effective speed of sound in the

<sup>3</sup> This section is a very brief summary of Chapter 8 *Vertical Excitation of Propellant Tanks* of SP-106; the original author was FRANKLIN T. DODGE of SwRI.

liquid to the point that extremely large acoustic or resonant motions of the liquid occur [BAIRD, 1963; KANA AND DODGE, 1966].

Vertical excitation is equivalent to a time-varying axial thrust acceleration, so Eq. (1.5), which was written for a steady axial acceleration, is replaced by.

$$\frac{\partial \phi}{\partial z} + (g - X_o \omega^2 \cos \omega t) \delta = 0 \quad (1.43)$$

where  $X_o$  is the amplitude of the vertical vibration and  $\omega$  its frequency. Now, as before, the velocity potential is assumed to be written as a series of the normal slosh modes with the integration constants denoted by  $A_m(t)$ . Proceeding just as before, it is found that the integration constants must be chosen to satisfy the following differential equation with non-constant coefficients:

$$\frac{d^2 A_m}{dt^2} + \xi_m(h) |g - X_o \omega^2 \cos \omega t| A_m = 0 \quad (1.44)$$

where  $\xi_m(h)$  depends on the tank shape. Equation (1.44) is a form of Mathieu's equation that has stable ( $A_m = 0$ ) or unstable solutions ( $A_m > 0$ ), depending on the values of  $X_o$  and  $\omega$ . These solutions are computed by assuming a harmonic series for  $A_m$ , starting with a frequency of  $\omega/2$  and continuing with frequency increases of  $\omega/2$  [DODGE, ET AL, 1965; MILES, 1984; POZRIKIDIS AND YON, 1998]. The solution shows that slosh is most easily created when the excitation frequency is close to twice the natural frequency of the fundamental axisymmetric mode; this is the 1/2-subharmonic response. The amplitude of the mode depends on the damping, and there is no motion unless  $X_o$  is sufficiently large [DODGE, ET AL, 1965]. The solution also shows that sloshing can be created when the excitation is near the natural frequency (the harmonic response), or near 2/3 the natural frequency (the 3/2 superharmonic response), or near 1/2 the natural frequency (the 2-superharmonic), and so on, but the excitation amplitude for a real liquid has to be quite large to create a noticeable slosh amplitude for these modes because of the viscous damping.

## 1.12 Concluding Remarks

There is a great deal of experimental and theoretical information for lateral sloshing in tanks of many different shapes. This chapter has emphasized theoretical information. The corresponding experimental results generally validate the theory so long as the wave amplitude is not too large. This restriction on "not too large" implies that the frequency of the tank excitation does not coincide exactly with one of the natural frequencies of the sloshing. When the excitation frequency does coincide with a natural frequency, the wave amplitude is set either by damping (which is discussed in Chapter 2) or by non-linear effects (which are discussed in Chapter 5). For practical purposes, the linear theory can still be used even for resonance conditions if the damping is not too small.

## 1.13 References

- BAUER, H. F., 1964, *Fluid Oscillations in the Containers of a Space Vehicle and Their Influence on Stability*, NASA TR R-187.
- BAUER, H. F., AND EIDEL, W., 1989, *Liquid Oscillations in a Prolate Spheroidal Container*, **Ingenieur-Archiv**, **59**, pp. 371-381.

- BUDIANSKY, B., 1960, *Sloshing of Liquids in Circular Canals and Spherical Tanks*, **J. Aerospace Sciences**, **27**, pp. 161-173.
- EHRlich, L. W., RILEY, J. D., STRANGE, W. G., AND TROESCH, B. A., 1961, *Finite-Difference Techniques for a Boundary Value Problem with an Eigenvalue in a Boundary Condition*, **J. Soc. Indust. Applied Math.**, **9**, pp. 149-164.
- DODGE, F. T., KANA, D. D., AND ABRAMSON, H. N., 1965, *Liquid Surface Oscillations in Longitudinally Excited Rigid Cylinders*, **AIAA Journal**, **3**, pp. 685-695.
- DODGE, F. T., AND KANA, D. D., 1966, *Bubble Behavior in Liquids Contained in Vertically Vibrated Tanks*, **AIAA J. Spacecraft and Rockets**, **3**, pp. 760-763.
- FOX, D. W., AND KUTTLER, J. R., 1983, *Sloshing Frequencies*, **J. Applied Mathematics and Physics**, **34**, pp. 668-696.
- GRAHAM, E. W., AND RODRIQUEZ, A. M., 1952, *The Characteristics of Fuel Motion which Affect Airplane Dynamics*, **ASME J. Applied Mechanics**, **19**, pp. 381-388.
- KANA, D. D., 1966, *An Experimental Study of Liquid Surface Oscillations in Longitudinally Excited Compartmented Cylindrical and Spherical Tanks*, NASA CR-545.
- LAWRENCE, H. R., WANG, C. J., AND REDDY, R. B., 1958, *Variational Solution of Fuel Sloshing Modes*, **Jet Propulsion**, **28**, pp. 729-736.
- MILES, J., 1984, *Parametrically Excited Solitary Waves*, **J. Fluid Mechanics**, **148**, pp. 451-460.
- MCCARTY, J. L., LEONARD, H. W., AND WALTON, W. C., 1960, *Experimental Investigation of the Natural Frequencies of Liquids in Toroidal Tanks*, NASA TN D-531.
- MCCARTY, J. L., AND STEPHENS, D. G., 1960, *Investigation of the Natural Frequencies of Fluids in Spherical and Cylindrical Tanks*, NASA TN D-252.
- POZRIKIDIS, C., AND YON, S. A., 1998, *Numerical Simulation of Parametric Instability in Two and Three Dimensional Fluid Interfaces*, **Proc., 4th Microgravity Fluid Physics and Transport Conference**, pp. 300-393.
- RATTAYA, J. V., 1965, *Sloshing of Liquids in Axisymmetric Ellipsoidal Tanks*, AIAA Paper 65-114.
- RILEY, J. D., AND TREMBATH, N. W., 1961, *Sloshing of Liquids in Spherical Tanks*, **J. Aerospace Sciences**, **28**, pp. 245-246.
- STOFAN, A. J., AND ARMSTEAD, A. L., 1962, *Analytical and Experimental Investigation of Forces and Frequencies Resulting from Liquid Sloshing in a Spherical Tank*, NASA TN D-1281.
- SUMNER, I. E., 1963, *Preliminary Experimental Investigation of Frequencies and Forces Resulting from Liquid Sloshing in Toroidal Tanks*, NASA TN D-1709.
- YARYMOVYCH, M. I., 1959, *Forced Large Amplitude Surface Waves*, D. Eng. Sci. Thesis, Columbia University.

## Appendix Linear Sloshing Analysis by Finite Element Structural Codes

G. C. EVERSTINE has shown in “Structural Analogies for Scalar Field Problems” (**Int. J. Numerical Methods in Engrg.**, 17, March 1981, pp. 471-476) that the equations of elasticity solved by conventional finite element *structural* codes can be adapted to other classical problems of mathematical physics, including sloshing, by a suitable choice of the elastic constants. The main results of this paper are summarized briefly here.

The  $x$ -component of the equations of elasticity can be written in the following form:

$$\left(\frac{\lambda+2\mu}{\mu}\right)\frac{\partial^2 u}{\partial x^2} + \frac{\partial^2 u}{\partial y^2} + \frac{\partial^2 u}{\partial z^2} + \left(\frac{\lambda+\mu}{\mu}\right)\left(\frac{\partial^2 v}{\partial x\partial y} + \frac{\partial^2 w}{\partial x\partial z}\right) + \frac{1}{\mu}F_x = \frac{\rho}{\mu}\left(\frac{\partial^2 u}{\partial t^2}\right) \quad (\text{A.1})$$

where  $u$ ,  $v$ ,  $w$  are the displacements in the  $x$ ,  $y$ ,  $z$  coordinate directions,  $\lambda$  and  $\mu$  are the Lamé elastic constants,  $F_x$  is the  $x$ -component of the body force per unit volume,  $\rho$  is the mass density, and  $t$  is the time. On the other hand, the governing equation for the velocity potential  $\Phi$  of sloshing is:

$$\frac{\partial^2 \Phi}{\partial x^2} + \frac{\partial^2 \Phi}{\partial y^2} + \frac{\partial^2 \Phi}{\partial z^2} = 0 \quad (\text{A.2})$$

A finite element code structural code can be made to solve Eq. (A.2) by: (1) identifying  $u$  with  $\Phi$ , (2) suppressing the  $v$  and  $w$  displacements, (3) artificially making  $\lambda$  equal to  $-\mu$ , and (4) setting  $F_x$  and  $\rho$  equal to zero. (In fact, this choice for  $\lambda$  makes the elastic modulus  $E$  and the Poisson's ratio  $\nu$  infinitely large. However, all that needs to be accomplished is to make  $E$  and  $\nu$  very large.)

The boundary conditions must also be chosen by analogy to the sloshing boundary conditions. A generalized boundary condition such as:

$$a_1 \frac{\partial u}{\partial n} + a_2 u + a_3 \frac{\partial u}{\partial t} + a_4 \frac{\partial^2 u}{\partial t^2} + a_5 = 0 \quad (\text{A.3})$$

can be applied in a structural problem. Since  $\partial u/\partial n$  is equal to  $T/\mu$ , where  $T$  is the force per unit area acting on a surface element, an analogous force must be applied to each surface element of the sloshing problem. For example, at a stationary wall of the tank where  $\partial\Phi/\partial n = 0$ , it is necessary to set  $T = 0$ , which implies that  $a_1 = 0$ , and  $a_2 = a_3 = a_4 = a_5 = 0$ . At the free surface, the boundary condition for the potential is:

$$\frac{1}{g} \frac{\partial^2 \Phi}{\partial t^2} + \frac{\partial \Phi}{\partial n} = 0 \quad (\text{A.4})$$

which means that  $a_1 = 1$ ,  $a_2 = a_3 = a_5 = 0$ , and  $a_4 = 1/g$ . This requirement can be met by applying a fictitious mass to each free surface element, whose magnitude is  $\mu/g$ .

All the other kinds of sloshing boundary conditions can also be simulated in a finite element structural code by suitable choices for the  $a$  parameters of Eq. (A.3) and by picking the surface force correspondingly.



# DAMPING OF LATERAL SLOSHING

This chapter is a revision of Chapter 4 of the same title of SP-106; the original authors were SANDOR SILVERMAN and H. NORMAN ABRAMSON.

## 2.1 Introduction

The term *damping* describes the fact that energy is always dissipated by the sloshing of a real liquid. The energy dissipation occurs at the walls and free surface as a result of viscous boundary layers and in the liquid interior as a result of viscous stresses. For small tanks, the boundary layer dissipation dominates, while for large tanks, the dissipation in the liquid interior may be the larger contribution.

For free oscillations of a liquid in a stationary tank, there is no energy input and the amplitude of successive slosh oscillations decreases because of energy dissipation. The decrease is characterized by the *logarithmic decrement*  $\Delta$ , defined as:

$$\Delta = \ln \left( \frac{\text{peak amplitude of oscillation}}{\text{peak amplitude of oscillation one cycle later}} \right) \quad (2.1)$$

It is also common to characterize the damping either by the damping ratio  $\gamma$ , which is defined by the relation  $\gamma = \Delta/2\pi$ , or by the percentage of critical damping (critical damping is defined as  $\gamma = 1$ ), which is 100 times  $\gamma$ . For a linear system, the damping ratio can be computed as the fractional part of the mechanical energy  $E$  dissipated into heat over one cycle of the oscillation:

$$\gamma = \frac{|dE/dt|}{2\omega E} \quad (2.2)$$

where  $\omega$  is the oscillation frequency and  $dE/dt$  is the time average of the energy dissipation rate. Equation (2.1) is a useful way to interpret experiments, and Eq. (2.2) is a useful way to compute the damping from fluid dynamics analyses.

When damping is included, the analytical models described in Chapter 1 would no longer predict that the wave amplitude and forces and torques are indefinitely large when the forcing frequency  $\Omega$  is near the resonance frequency  $\omega_n$ . To include the damping, the usual procedure is to determine the damping by a separate analysis or test and insert it in the inviscid relations by analogy to a linear vibrating system, instead of re-doing the fluid dynamics analysis for a viscous liquid. With this procedure, the inviscid force prediction for a rectangular tank, for example, which is given by Eq. (1.28), is:

$$\frac{F_{xo}}{-i\Omega^2 X_o m_{liq}} = 1 + 8 \frac{a}{h} \sum_{n=1}^N \frac{\tanh[(2n-1)\pi h/a]}{(2n-1)^3 \pi^3} \frac{\Omega^2}{\omega_n^2 - \Omega^2 + 2i\gamma_n \Omega \omega_n} \quad (2.3)$$

where  $\gamma_n$  is the damping ratio of the  $n^{\text{th}}$  mode. The real part of the expression is the actual force. The force is now not infinitely large when  $\Omega = \omega_n$ .

### Slosh damping experiments

Slosh damping is generally determined experimentally by the use of scale model tanks (although modern free-surface CFD codes are also capable of computing damping). Several different experiment methods can be used, as described below.

**Wave amplitude decay.** For this method, the tank is oscillated at the resonant frequency until steady state is reached and then the oscillation is stopped quickly. The rate of decay of the free surface displacement at some convenient location is monitored. The logarithmic decay of successive wave heights is calculated from Eq. (2.1). This method can only be used for the fundamental slosh mode, because other modes usually decay faster than the fundamental and the fundamental mode thereafter dominates the wave shape.

**Slosh force amplitude response.** For this method, the amplitude of the force exerted on the tank is measured by a load cell as a function of excitation frequency  $\Omega$  over a range of frequencies around the modal resonant frequency. Or, alternatively, the wave amplitude can be measured. The force or wave amplitude is plotted against  $\Omega$  as shown in Figure 2.1, and the half-power bandwidth technique [SCANLAN AND ROSENBAUM, 1960] is used to compute the damping by the relation:

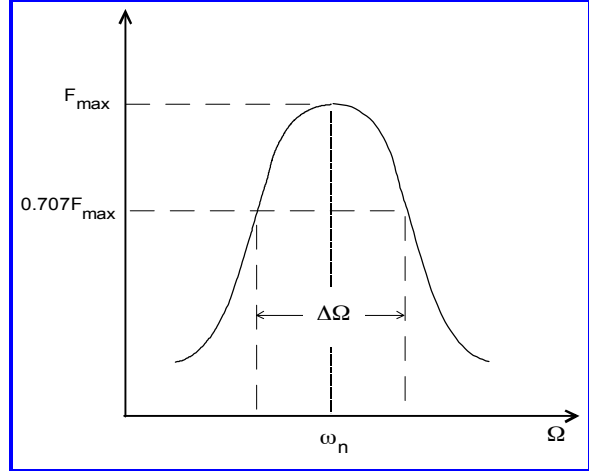


Figure 2.1. Typical force amplitude response curve

$$\gamma_n = \frac{1}{2} \frac{\Delta\Omega}{\omega_n} \tag{2.4}$$

where  $\Delta\Omega$  is the difference between the two excitation frequencies at which the force or wave amplitude is equal to  $1/\sqrt{2}$  times the maximum amplitude.

Equation (2.4) holds strictly only for a linear oscillator composed of a mass, spring, and dashpot. The slosh model, as shown in Chapter 3, contains a linear oscillator and an additional *fixed* mass that translates with the tank. The force due to the fixed mass causes the force to be slightly too large with respect to a linear oscillator for frequencies  $\Omega > \omega_n$  compared to the force for  $\Omega < \omega_n$ . The error is negligible if  $\gamma < 0.1$  or so, which encompasses nearly all the cases of interest.

**Anchor force decay.** This method is a variation of the wave amplitude decay method. The tank is attached to a load cell and the decay of the force is measured after the tank motion is stopped quickly.

**Cautions.** The relationship among the damping factors calculated by the various experimental methods is not easily determined unless the wave motion is linear, in which case they all give essentially the same answer. Caution is especially required when measuring the slosh damping in a tank that is not axisymmetric, because the apparent damping may then depend on the direction in which the tank is excited, the direction in which the force is measured, and the technique used to measure the damping.

## 2.2 Viscous Damping for Tanks of Various Shapes

Sloshing in a tank that does not contain an anti-slosh device is damped by viscous stresses. Although in principle the stresses can be determined theoretically, most of the available results have been obtained experimentally. The various experimental results are discussed below. All the damping correlation pertain to the fundamental slosh mode.

Since the damping is due solely to viscous effects (at least when surface tension effects are small), dimensionless analysis shows that it is a function only of tank shape, fill level, and a dimensionless parameter  $Re$  analogous to an inverse Reynolds Number:

$$Re_1 = \frac{\nu}{\sqrt{gL^3}} \quad \text{or} \quad Re_2 = \frac{\nu}{L^2 \omega_n} \quad (2.5)$$

where  $\nu$  is the kinematic viscosity of the liquid and  $L$  is a characteristic dimension of the tank such as the diameter. The first form of  $Re$  given in Eq. (2.5) is the one used in most correlations; it assumes that the characteristic slosh velocity is  $(gL)^{0.5}$ . Since the acceleration  $g$  appears in the denominator of  $Re_1$ , correlations that employ it are not useful for low gravity conditions when  $g \approx 0$ . The second form of  $Re$ , which uses a characteristic velocity of  $L\omega_n$ , is applicable to high and low gravity conditions and is thus used for the low-gravity slosh damping correlations discussed in Chapter 4.

Many of the available damping correlations were derived from scale-model tests. Tests of small tanks exactly duplicate the damping coefficients of large tanks if the model scale and full scale values of  $Re_1$  are the same. Generally, however, the model scale  $Re_1$  is larger than the full scale  $Re_1$  because of the smaller value of the model  $L$ . Even then, if both the laboratory and full-scale  $Re_1$  are sufficiently small, the damping values will be comparable. Otherwise, the relative contributions of boundary layer and bulk liquid viscous dissipation will be different. For that reason, there may be some errors when the scale-model-derived correlations are extrapolated to full-scale.

The SLOSH computer code incorporates the damping correlations described below as a function of tank shape, fill level, and liquid properties.

### Circular cylindrical tank

Circular cylindrical tanks are widely used in launch vehicles and spacecraft, so they have been the subject of many studies. There are some small differences between the correlations from these studies as the result of the different methods used to measure damping. Two of the more complete investigations are summarized here.

MIKISHEV AND DOROZHKIN [1961] proposed the following correlation from their tests:

$$\gamma = 0.79\sqrt{Re_1} \left[ 1 + \frac{0.318}{\sinh(1.84 h/R)} \left( 1 + \frac{1-h/R}{\cosh(1.84 h/R)} \right) \right] \quad (2.6a)$$

The tank radius  $R$  is used as the characteristic dimension in the definition of the  $Re_1$  parameter, and  $h$  is the liquid depth. For  $h > 2R$ , the correlation reduces to:

$$\gamma = 0.79\sqrt{Re_1} \quad (2.6b)$$

A similarly extensive but independent study [STEPHENS, ET AL, 1962] found a slightly different correlation:

$$\gamma = 0.83\sqrt{Re_1} \left[ \tanh(1.84 h/R) \left( 1 + 2 \frac{1-h/R}{\cosh(3.68 h/R)} \right) \right] \quad (2.7a)$$

When the liquid depth is large, Eq. (2.7a) reduces to:

$$\gamma = 0.83\sqrt{Re_1} \quad (2.7b)$$

The actual numerical differences between Eqs. (2.6) and (2.7) are quite small.

**Linear sloshing limitation.** By testing at various slosh amplitudes, these investigators found that the damping is independent of the wave amplitude – as the correlations assume – so long as the slosh amplitude at the wall is no greater than about  $0.1R$ .

**Draining effects.** When liquid is draining from a tank, the slosh damping increases slightly [LINDHOLM, ET AL, 1962].

**Cylindrical tank - spherical dome**

For a cylindrical tank with a spherical bottom, the damping increases significantly when the liquid level is in or slightly above the dome [MIKISHEV AND DOROZHKIN, 1961]. The damping can be computed by applying the correction factor shown in Figure 2.2 to the damping correlation Eq. (2.6a):

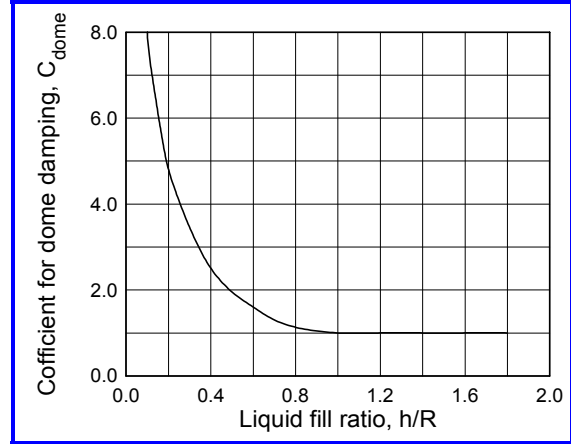


**Figure 2.2.** Viscous damping correction coefficient for a cylindrical tank with a spherical dome

$$\gamma = C_{dome} \left( 0.79 \sqrt{Re_1} \right) \left[ 1 + \frac{0.318}{\sinh(1.84 h/R)} \left( 1 + \frac{1-h/R}{\cosh(1.84 h/R)} \right) \right] \quad (2.8)$$

**Spherical tank**

Slosh damping for spherical tanks has been investigated experimentally by SUMNER AND STOFAN [1963]; MIKISHEV AND DOROZHKIN [1961]; and STOFAN AND ARMSTEAD [1962]. The recommended correlations depend on the liquid depth and are given by:

$$\gamma = 0.79 \sqrt{Re_1} (R/h) \quad \text{for } 0.1R \leq h \leq R \quad (2.9a)$$

$$\gamma = 0.79 \sqrt{Re_1} [1 + 0.46(2 - h/R)] / [1.46(2 - h/R)] \quad \text{for } h \geq R \quad (2.9b)$$

There is somewhat more discrepancy between these studies than for the cylindrical tank studies, primarily because of the different methods used to measure the damping.

Figure 2.3 shows a plot of Eqs. (2.9). The damping is a minimum for tanks that are half full. The damping is very large for nearly empty and nearly full tanks, since the mass of liquid that participates in the wave motion (which is always less than the liquid mass) decreases more rapidly for nearly empty or full tanks than the viscous energy dissipation does; hence, the damping coefficient [which from Eq. (2.2) is proportional to the ratio of the energy dissipation rate to the kinetic energy of the sloshing mass] becomes large.

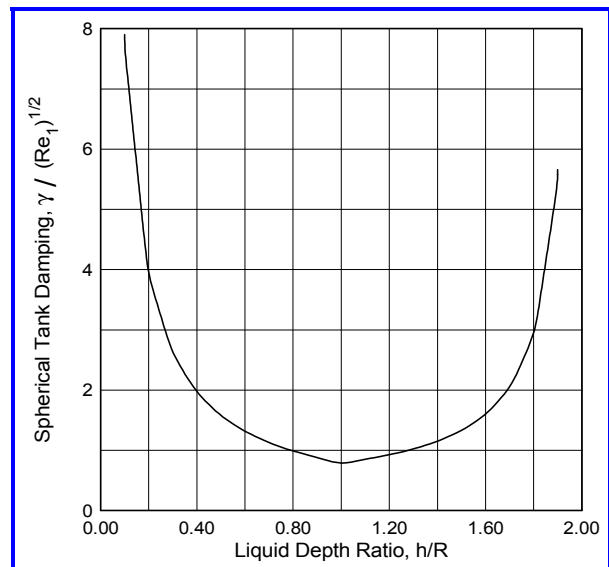


**Figure 2.3.** Viscous damping for a spherical tank

### Oblate spheroidal tank

Slosh damping for oblate spheroidal tanks has also been measured [STEPHENS, ET AL, 1961]. The results are shown in *Figure 2.4* for a tank having a ratio of horizontal diameter to vertical diameter equal to 1.33. The plot shows the ratio for the spheroid damping to the damping of a sphere; thus, the plot and Eqs. (2.9) allow the damping to be computed as a function of tank size and fill level.

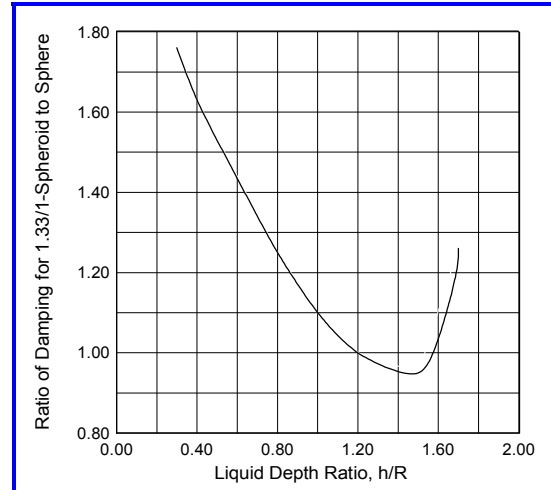


**Figure 2.4.** Viscous damping for a spheroidal tank; ratio of horiz. to vert. diam = 1.33

### Horizontal toroidal tanks

Toroidal tanks have a shape advantage for some applications. A limited amount of damping results are available for a scale-model size horizontal toroidal tank for both the 1st and 2nd slosh modes [SUMNER, 1963]. *Figure 1.14* of Chapter 1 illustrates the two slosh modes of interest and defines the minor radius  $r$  (the damping tends to be independent of the major radius of the tank). *Figure 2.5* shows the damping correlations. In the tests, the minor radius was held constant at 6.35 cm, and the ratio of the major to minor radius was varied from about 1.5 to about 3.5. The liquid was acetylene tetrabromide ( $\nu = 0.033 \text{ cm}^2/\text{sec}$ ). Damping for other liquids can be scaled from these results using the  $Re_1$  parameter defined by Eq. (2.5).

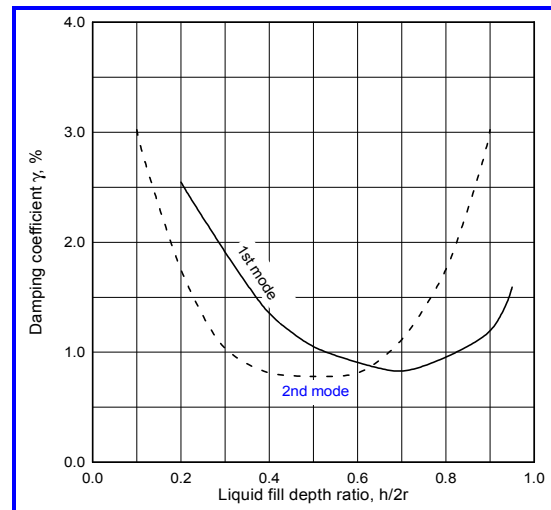


**Figure 2.5.** Damping of 1st and 2nd slosh modes for a horizontal toroidal tank.

## 2.3 Slosh Damping by Ring Baffles

Damping caused solely by viscous effects is quite small for even a moderately large tank, with  $\gamma$  generally being equal to 0.01 or less when the tank diameter is 1 meter or so. A missile or spacecraft's attitude control system usually requires  $\gamma$  to be considerably larger than 0.01 for stable flight. Consequently, some method of increasing the damping is required. For axisymmetric tanks, a common method is to attach a series of *ring baffles* to the tank walls. The baffles provide a substantial degree of damping when the free surface is near one of the baffles. The spacing between the baffles is chosen so that the minimum damping exceeds the damping requirements, regardless of fill level.

A ring baffle has the shape of a flat ring, with the outer edge of the ring attached to the tank wall (sometimes with a small gap between the ring and the wall). The plane of the ring may be perpendicular to the tank axis, which is the common arrangement, or it may be sloped up or down, and the inner edge of the ring may have a lip of some sort for structural reasons, although anything that reduces the sharpness of the inner edge

generally reduces the effectiveness of the baffle [COLE AND GAMBUCCI, 1961]. Perforating the baffles can be used to save weight, and both an increase in damping and saving in weight can be obtained by making the baffle flexible (discussed below).

### Ring baffle damping in a cylindrical tank - theory

The damping provided by a ring baffle is analyzed by analogy to the drag that a flat plate exerts on an oscillatory flow [MILES, 1958; BAUER, 1962]. As shown in *Figure 2.6*, the liquid is assumed to oscillate in the fundamental slosh mode, and the direction of the flow is assumed to be normal to the ring. Other assumptions include: (1) the linearized potential flow theory described in Chapter 1 is sufficiently accurate to predict the flow and slosh frequency; and (2) the local flow in the vicinity of the ring is not affected by the free surface or the tank bottom. These assumptions require that the baffle occupy only a small percentage of the tank cross section and not be too near the surface of the bottom. The damping is determined from *Eq. (2.2)*, by computing the mechanical energy and rate of energy dissipation.

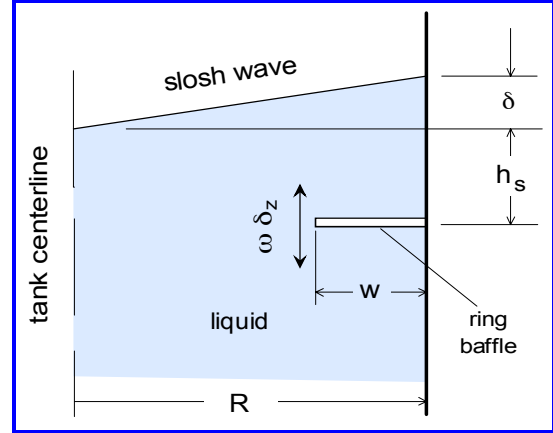


Figure 2.6. Schematic of ring baffle

**Mechanical energy.** The total slosh energy needed for *Eq. (2.2)* is the sum of the instantaneous kinetic and potential energies, but it is also equal to the *maximum* value of the kinetic energy. The kinetic energy can be computed from the velocity potentials given in Chapter 1 or from the equivalent mechanical model of sloshing (discussed in Chapter 3) which is the method used here. As shown in Chapter 3, a typical slosh mechanical model is a mass-spring oscillator, so the maximum kinetic energy is:

$$E = \frac{1}{2} m_s \omega^2 X_{max}^2 \quad (2.10a)$$

where  $m_s$  is the mass of the oscillator and  $X_{max}$  is its peak oscillatory amplitude.  $X_{max}$  is linearly related to the slosh wave amplitude,  $\delta$ , because when the free surface translates upward, the oscillator mass translates horizontally in proportion; thus,  $X_{max} = \Gamma \delta$ , where  $\Gamma$  is a number that depends on the tank shape. *Equation (2.10a)* can therefore be written as:

$$E = \frac{1}{2} m_s \Gamma^2 \omega^2 \delta^2 \quad (2.10b)$$

**Energy dissipation.** For a baffle oriented normal to the flow, energy is dissipated mostly by pressure drag. The instantaneous *drag force* is equal to one-half the product of (a) liquid density  $\rho$ , (b) square of the velocity at the plate location, (c) drag coefficient  $C_D$ , and (d) total area of the plate  $A_b$ . The instantaneous *energy dissipation rate* is the product of the drag force and the velocity. The instantaneous energy dissipation rate then has to be time averaged over one slosh cycle and spatially averaged around the tank circumference for use in *Eq. (2.2)*. The averaging gives:

$$\frac{dE}{dt} = \frac{1}{2} \rho \left( \frac{4}{3\pi} \right) C_\theta C_D A_b (\omega \delta_z)^3 \quad (2.11)$$

Here,  $\delta_z$  is the amplitude of the liquid motion at the baffle location where, as shown in *Figure 2.6*, the liquid velocity is  $\omega\delta_z \sin\omega t$ .  $\delta_z$  is related to the wave height  $\delta$  by a function that depends on depth below the surface; this function can be derived from the velocity potentials discussed in Chapter 1 and is represented here symbolically as  $\delta_z = f_d\delta$ . The factor  $(4/3\pi)$  in Eq. (2.11) is the result of time averaging the absolute value of  $(\sin\omega t)^3$ . The term  $C_\theta$  is similarly the spatial average of the absolute value of the cube of the slosh wave height around the baffle circumference; if the tank is a cylinder, the circumferential variation is  $\cos\theta$ , and if the baffle extends all the way around the tank circumference,  $C_\theta = (4/3\pi)$ . Otherwise  $C_\theta$  has some other numerical value.

**General damping coefficient.** Putting Eqs. (2.10b) and (2.11) into Eq. (2.2) gives the general relation for the damping coefficient  $\gamma$  of a plate that dissipates energy by drag:

$$\gamma_{drag} = \frac{(4/3\pi)C_D C_\theta A_b f_d^3 \delta}{2(m_s/\rho)\Gamma^2} \quad (2.12)$$

When  $C_D$  is constant (independent of slosh frequency or amplitude), it can be seen that the damping coefficient is proportional to the slosh wave amplitude. Generally, however,  $C_D$  is not constant but depends on the characteristics of the oscillating flow.

**Drag coefficient.** The drag coefficient for a plate in an oscillating liquid flow, which is needed for Eq. (2.12), is correlated by the expression [KEULEGAN AND CARPENTER, 1956]:

$$C_D = 15/\sqrt{UT/w} \quad \text{when } UT/w < 20 \quad (2.13)$$

where  $w$  is the plate width,  $U = \omega\delta f_d$  is the amplitude of the oscillating velocity, and  $T = 2\pi/\omega$  is the period of the oscillation<sup>4</sup>. Equation (2.13) was developed from tests of a plate in an oscillating flow for which  $U$  did not vary along the length of the plate. For a ring baffle in a tank, however,  $U$  varies around the circumference; the circumferential variation is accounted for by basing  $C_D$  on the reasonable assumption that the effective velocity is half the maximum velocity of  $\omega\delta f_d$ . The area  $A_b$  blocked by the baffle is characterized by  $C_1 A$  where  $A$  is the tank cross-sectional area and  $C_1$  is the ratio of the baffle area to the tank cross-sectional area.

**Ring baffle  $\gamma$ .** When all these relations are put in Eq. (2.12), the damping coefficient for a ring baffle in a cylindrical case is predicted to be:

$$\gamma = \frac{15(4/3\pi)^2 C_1 A f_d^{2.5} \sqrt{\delta w}}{2\sqrt{\pi}(m_s/\rho)\Gamma^2} \quad (2.14)$$

For the specific case when the liquid depth  $h$  is considerably greater than the tank radius ( $h/R > 2$ ), the following values can be used in Eq. (2.14):

$$m_s = 0.456(\rho AR) \quad C_1 = \frac{w}{R} \left( 2 - \frac{w}{R} \right) \quad w \approx \frac{1}{2} RC_1 \quad \Gamma = 0.649 \quad f_d = e^{-1.84h_s/R} \quad (2.15)$$

Putting these relations into Eq. (2.14) and combining the terms gives the result that:

$$\gamma = 2.83e^{-4.6(h_s/R)} C_1^{3/2} (\delta/R)^{1/2} \quad \text{cylindrical tank} \quad (2.16)$$

The exponential term in Eq. (2.16) implies that  $\gamma$  decreases with the depth  $h_s$  that the baffle is submerged below the free surface. In contrast to viscous damping, the damping

<sup>4</sup>  $C_D$  is constant and equal to 2 when the period parameter  $UT/w$  is greater than 100; for sloshing, however,  $UT/w < 20$  is the relevant value.

## 2. DAMPING OF LATERAL SLOSHING

provided by a ring baffle is nonlinear; that is,  $\gamma$  does depend on the amplitude of the sloshing.

*Figure 2.7* compares Eq. (2.16) to the results of damping measurements for a cylindrical tank as a function of submergence depth  $h_s$  and wave amplitude  $\delta$ . The data were obtained by a variety of methods (force on the baffle, force to drive the tank, amplitude of slosh wave, decay of slosh wave, decay of tank anchor force) indicated by the different symbols. The scatter in the data is primarily the result of the different measurement techniques. When the baffle is not too near the liquid surface, the theory compares reasonably well to the test results over the range of wave heights tested. When the baffle is near the surface, theory and test do not compare so well, for reasons discussed below.

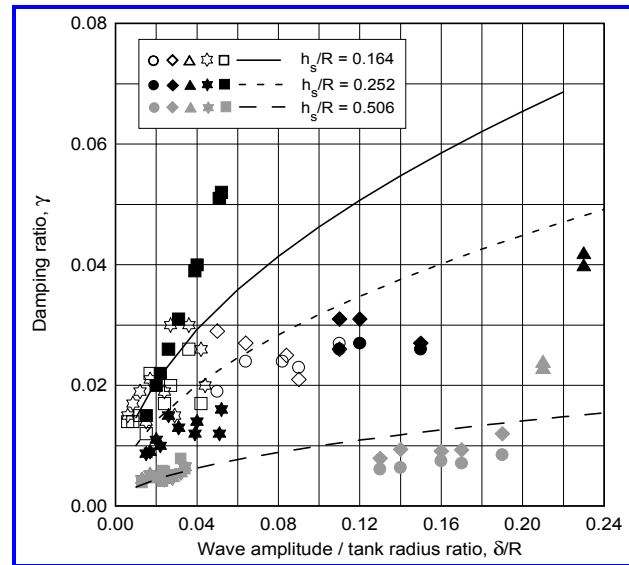


**Figure 2.7.** Damping of a ring baffle in a cylindrical tank; baffle area blockage = 23.5% [O'NEILL, 1960]

### Ring baffle - near free-surface effects

When the submergence depth of the baffle is less than the slosh amplitude, the baffle is uncovered during part of the slosh cycle and the damping is generally less than the predictions of Eq. (2.16). Predicted and measured damping values for a baffle near the liquid surface are shown in *Figure 2.8*, as a function of baffle submergence depth for a specific tank oscillation amplitude and an oscillation frequency equal to the slosh resonance. The plot shows that the measured damping for slightly submerged baffles is greater than the theory predicts [computed by using the measured slosh amplitude in Eq. (2.16)], while for baffles almost at the liquid surface, the measured damping is slightly less than the prediction. This complicated damping dependency on submergence is caused partly by the splashing of the slosh wave (which increases the damping), partly by the change in slosh natural frequency when the liquid surface intersects the baffle, and partly by the uncovering of the baffle during some or all of the wave cycle. An approximate correction for baffles near the free surface is available [BAUER, 1962]. However, in most applications, some *minimum* value of damping is

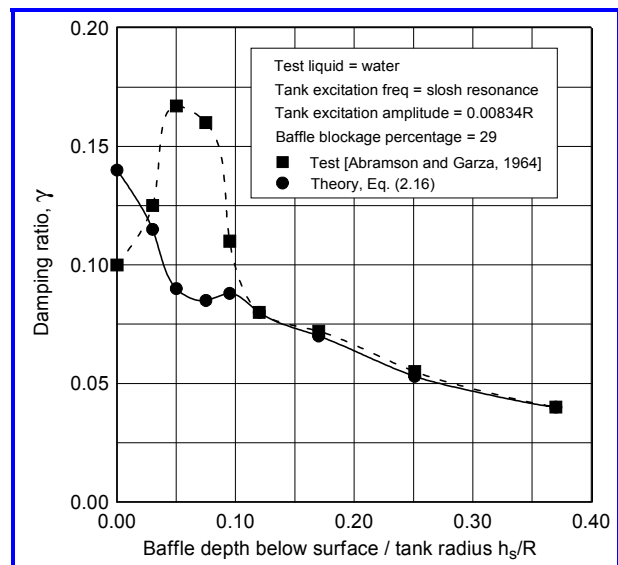


**Figure 2.8.** Comparison of ring baffle damping theory and tests as a function of submergence depth ratio,  $h_s/R$

required, and this minimum occurs when the baffle is relatively deeply submerged, so the correction is not usually necessary.

Of more importance is the fact that a ring baffle is able to provide some damping even when it is slightly *above* the free surface. Predicting this damping rigorously is a complicated problem, but the damping can be estimated approximately by the following simple procedure. When the baffle is above the free surface by a distance equal to or greater than the slosh amplitude, the slosh wave does not intersect the baffle and there is no damping. As the liquid level is dropped, the full baffle damping is approached. The damping for baffles located above the free surface can thus be estimated by linearly decreasing  $\gamma$  from the value predicted by Eq. (2.16) for  $h_s = 0$ , to a value of  $\gamma = 0$  when the height above the free surface is, say, conservatively 0.8 times the slosh amplitude  $\delta$ .

**Ring baffle - design value of slosh amplitude**

In most applications, the spacecraft stability analysis specifies the required *minimum* value of damping as a function of tank fill level. A system of ring baffle must be designed to meet the requirements. But the damping  $\gamma$  depends on the slosh amplitude  $\delta$  and  $\delta$  depends on  $\gamma$ . The question is: What value of  $\delta$  should be used to design the baffles? The answer is a classical trade study in which various slosh amplitudes are assumed, and a baffle width and a distribution of baffles along the tank axis are computed to satisfy the damping requirements. The design having the minimum weight (or some other criterion) is then chosen. Such a trade study invariably indicates that the total weight of baffles decreases when the slosh amplitude increases. The problem thus reduces to what is the largest slosh amplitude that can be assumed reasonably. Now, a slosh wave starts to become noticeably nonlinear and splashes, rotates, etc., when the amplitude exceeds about ten percent of the tank diameter. Consequently, the largest feasible slosh amplitude that can be assumed reasonably is  $0.2R$  (unless nonlinear effects can be analyzed). With a value of  $\delta = 0.2R$ , Eq. (2.16) reduces to:

$$\gamma = 1.27e^{-4.6(h_s/R)}C_1^{3/2} \tag{2.16a}$$

This relation allows the baffle width (i.e., blockage ratio  $C_1$ ) and baffle spacing to be chosen to meet the specified minimum damping requirement. *Figure 2.9* shows such a design schematically. The plot on the left of this figure shows the predicted damping as a function of the free surface location. The baffle spacing includes an allowance for the damping provided by a baffle slightly above the free surface. As can be seen, the *minimum* damping occurs when the free surface is slightly below (by  $0.8\delta$ ) the nearest baffle.

**Ring baffles - effect on slosh frequency**

When the free surface is at or slightly above a ring baffle, the slosh resonant frequency is altered from the “bare tank” value [SILVEIRA, ET AL, 1961]. The resonant frequency can be up to 15% higher than the bare tank value

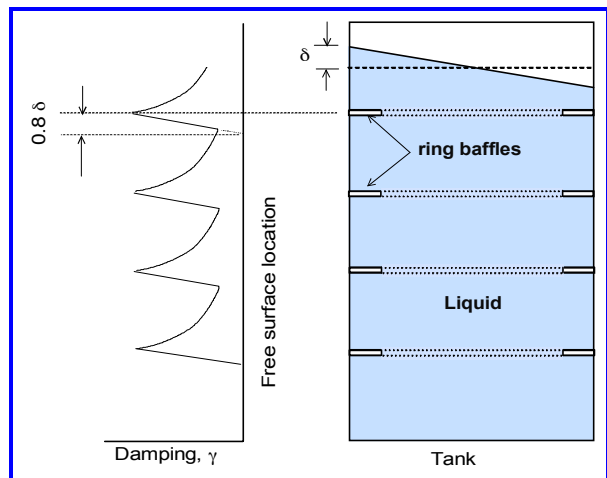


**Figure 2.9.** Ring baffle system design to meet a minimum required damping specification

when the baffle intersects the surface (partly caused by the apparent reduction in the free surface diameter), and up to 10% lower than the bare tank value when the free surface is about one baffle width above the baffle. When the baffle is submerged by two or more baffle widths, the resonant frequency is unaffected by the presence of the baffle. The minimum damping generally occurs, however, when the baffle nearest the free surface is submerged by more than one baffle width. The change in resonant frequency is small enough for this condition that it is usually not of any consequence.

### Ring baffle - spherical and spheroidal tanks

Ring baffles can also be used for tank shapes other than cylinders, such as spheres. The general theory [Eq. (2.14)] applies to any tank shape, so the damping can be predicted by substituting a depth function  $f_d$  and slosh mass that are specific to the tank shape. More simply, a reasonable estimate can be obtained from the cylindrical tank result by using an equivalent cylindrical-tank submergence depth  $h_s$  such that the liquid volume above the baffle is the same for the equivalent cylindrical tank as for the actual tank. Experimental data for several kinds of tanks and baffle designs confirm this simple approximation [STEPHENS, ET AL, 1961, ABRAMSON, ET AL, 1963, and SUMNER, 1964].

### Ring baffle - effects of baffle flexibility

Ring baffles are commonly designed as elastic plates and they are relatively rigid under the action of the slosh loads<sup>5</sup>. Rigid baffles may represent a significant percentage of the tank weight. The damping-to-weight efficiency of the baffle system can be improved by reducing the baffle weight, but to do so implies that the thickness of the baffle would be reduced and the baffle would consequently be flexible. Thus, flexible baffles have been evaluated by several investigators [SCHWIND, ET AL, 1968; STEPHENS, 1966; STEPHENS AND SCHOLL, 1967; GARZA AND DODGE, 1967; BUGG, 1970].

The results of these studies are summarized in *Figure 2.10*, in which the measured damping of a flexible baffle is compared to the measured damping of a similar rigid baffle of the same area. The comparisons are a function of two parameters: the *period parameter P* and the *flexibility parameter F*. The period parameter was introduced previously in the discussion of rigid ring baffles; it is the ratio of the amplitude of the liquid motion to the baffle width, and is defined for a cylindrical tank in which the liquid depth is greater than the tank radius by the following relation:

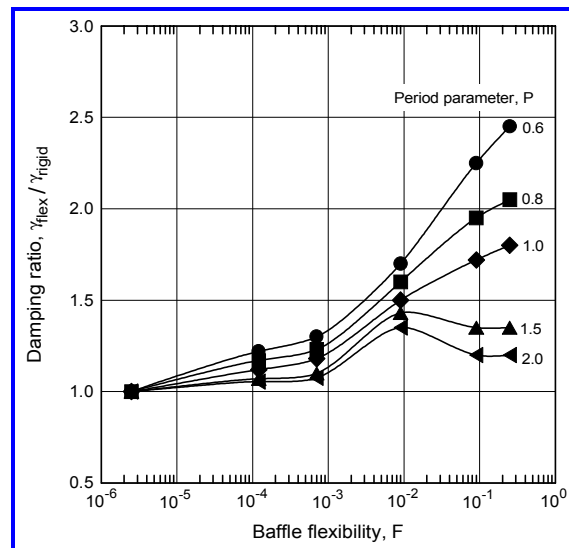


**Figure 2.10.** Damping as a function of flexibility  $F$  and period parameter  $P$  [STEPHENS & SCHOLL, 1967]

<sup>5</sup> The subject of slosh loads is discussed in NASA SP-8009, *Propellant Slosh Loads*. For a rigid ring baffle, the amplitude of the oscillating pressure exerted on the baffle is given by:

$$p(r, \theta) = 2\rho\omega^2\delta_w \cos\theta \sqrt{1 - [(R-r)/R]^2} e^{-1.84h_s/R}$$

where as before  $\omega$  is the slosh frequency and  $h_s$  is the baffle submergence depth [GARZA, 1966].

$$P = 2\pi \left( \frac{\delta}{w} \right) e^{-1.84h_s/R} \quad (2.17)$$

The flexibility parameter is proportional to the ratio of the elastic deflection of the baffle to the baffle width, for a period parameter of unity. It is defined by the relation:

$$F = 0.04 \left( \frac{\rho g R}{E} \right) \left( \frac{w}{R} \right)^5 \left( \frac{R}{b} \right) \quad (2.18)$$

where  $E$  is the elastic modulus of the baffle material and  $b$  is the baffle thickness. The actual flexibility of a baffle may be somewhat less than predicted by Eq. (2.18) because Eq. (2.18) ignores membrane tension and stiffness. However, it is apparent from Figure 2.10 that  $P$  and  $F$  are sufficient to correlate the relative damping of a variety of baffle designs.

From the results shown in Figure 2.10, it is concluded that the damping from a flexible baffle is never less than the damping of a rigid baffle. And as the baffle becomes more flexible ( $F$  increases), the relative damping increases and reaches a maximum which depends upon the value of the period parameter. Consequently, flexible baffles can allow a substantial improvement in baffle efficiency to be obtained.

Flexible baffle materials include plastics such as mylar and thin gauge metals such as aluminum and stainless steel. Other studies have investigated the use of flexible baffles for cryogenic liquids [DODGE, 1970; BASS, 1972]. Although flexible baffles might “stiffen” considerably at cryogenic temperatures, they are still light weight. Thus, the full damping improvement indicated in Figure 2.10 might not be obtained for cryogenic liquids. However, the baffle efficiency would still be improved because of the light weight design. The structural design of baffles for cryogenic applications is discussed in DODGE [1970].

### Ring Baffles - effects of holes

The weight of a ring baffle can be reduced by perforating it with small holes. The oscillating flow through the holes is an additional source of damping (which will be discussed below in conjunction with tank partitions) but this increase is partially offset by the decrease in the effective solid baffle area [ABRAMSON, ET AL, 1964]. The net effect is that the damping for a slightly submerged ring baffle is decreased while for a deeper submergence, the damping is about the same as for a non-perforated baffle.

## 2.4 Damping by Movable and Floating Baffle Devices

A large variety of devices that either float or are attached to the liquid free surface have been evaluated for their slosh effectiveness

### Floating lids, mats, and cans

Rigid lids that cover some fraction of the free surface and float up or down as the liquid level changes have been found to be reasonably good dampers when the coverage is 85% or more of the tank diameter [ABRAMSON AND RANSLEBEN, 1961]. Floating porous mats that greatly increase viscous effects at the surface have also been evaluated [EULITZ, 1958]. Because lids and covers can “hang up” on the internal hardware of the tank, these devices have not proved to be practical for spacecraft.

Arrays of light-weight cans have been proposed as a type of floating anti-slosh device that would not be subject to hanging up on the tank structure. Tests have shown,

however, that the damping is appreciable only when the cans are packed closely to increase their drag, and the weight is somewhat more than an equivalent ring baffle [ABRAMSON AND RANSLEBEN, 1960]. Floating cans have, however, been used in race car fuel tanks.

### Membranes and flexible diaphragms

Flexible diaphragms and positive expulsion devices that provide an impermeable barrier between the liquid and the gas in a tank are employed in tanks when there is a need to transfer liquid in a low gravity environment or when a high flow rate is desired without pumps. The membrane or flexible metal diaphragm is attached around the periphery to the tank wall. It is sized to be large enough to contain the initial liquid loading when it is in the fully extended orientation and to expel nearly all the liquid when it is near the tank bottom. As shown schematically in *Figure 2.11*, the constrained free surface at intermediate fill levels is of a complex, crinkled shape<sup>6</sup>. Because of the geometric constraints, a flexible diaphragm is most commonly (but not exclusively) a practical design only for spherical or oblate spheroidal tanks.

Diaphragms provide a substantial level of slosh damping as a result of the combination of viscoelastic flexing of the diaphragm (primarily) and the increased viscous effects at the liquid-diaphragm interface (secondary) [STOFAN AND PAVLI, 1962; STOFAN AND SUMNER, 1963; DODGE AND KANA, 1987]. A typical damping coefficient is  $\gamma = 0.1$ . A diaphragm also increases the slosh natural frequency because of the constraints imposed on the free surface shape. The effective mass of liquid participating in the sloshing is slightly smaller than for a tank of the same shape and fill level without a diaphragm [DODGE AND KANA, 1987]. Higher order slosh modes tend to be suppressed.

Since the damping depends primarily on the viscoelastic flexing of the diaphragm, it should be predictable in principle by a finite element structural analysis. The main difficulty is calculating the static interface shape, which is a calculus of variations problem. It would also be necessary to predict the slosh natural frequency. When these quantities are known, the damping coefficient can be computed from *Eq. (2.2)*. But if a full scale prototype tank is available, a better method of determining the damping is by laboratory testing. Generally, *subscale* testing, while not impossible, is difficult because of the conflicting simulation requirements imposed by liquid viscosity and diaphragm viscoelasticity.

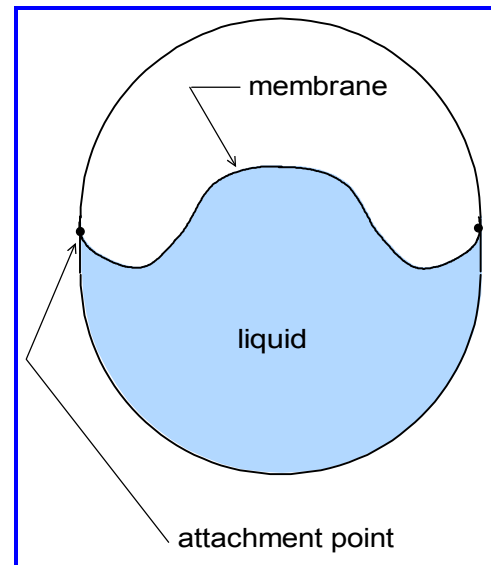


**Figure 2.11.** Schematic of bladdered tank.

<sup>6</sup> The shape of the liquid-diaphragm surface is determined by several constraints. First, the area of the surface must be equal to the area of the membrane. Second, the total potential energy of the system must be minimized. The potential energy is composed of the gravitational potential energy of the liquid and the strain energy of the bladder. Generally, the bladder strain energy is negligible compared to the gravitational potential energy. This implies that the equilibrium configuration of the liquid volume is as “low” in the tank as is possible considering the constraint that the liquid surface area (i.e., the membrane area) is fixed.

As was mentioned above, diaphragms can be used to hold liquid in a desired position over the tank exit for low gravity applications. For the *Tracking and Data Relay Satellite* (TDRS), a diaphragm was even used to hold liquid against the *top* of the tank (i.e., the tank was inverted compared to [Figure 2.11](#)) during periods of thrusting and high gravity. The static equilibrium position of the liquid for this tank was asymmetrical, and the liquid was located primarily on one side of the tank centerline, since this configuration minimized the total static potential energy [DODGE AND KANA, 1987].

## 2.5 Damping by Non-Ring Baffles

Other types of baffles than rings are also used to damp sloshing. In some cases, the baffle design is constrained by the internal structure of the tank, such that ring baffles are not feasible. In other cases, such as for low-gravity applications, the baffle design may serve a dual purpose of damping the slosh and ensuring that some minimum fraction of the liquid is always positioned over the tank outlet. [Figure 2.12](#) shows two such non-ring baffle arrangements, a *vane* arrangement on the left, and a *cruciform* arrangement on the right. The vanes are a typical low-gravity design.

These kinds of baffle designs provide less damping than a ring baffle of the same total area, as various tests have shown [STEPHENS, ET AL, 1961; SILVEIRA, ET AL, 1961; ABRAMSON, ET AL, 1963]. In the absence of test data for a new design, the damping can be estimated from the general ring baffle theory by identifying the appropriate blocked area and depth function.

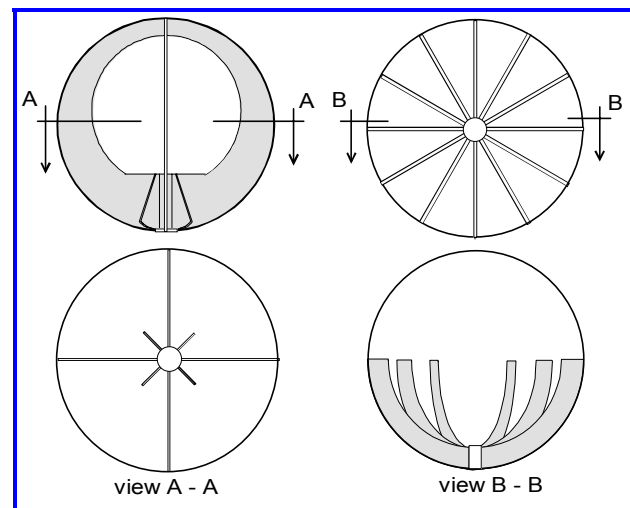


**Figure 2.12.** Schematics of typical vane and cruciform type slosh baffles

## 2.6 Damping by Perforated Bulkheads

Some missile tanks are divided into compartments by bulkheads or septums. Examples of compartmentation include the X-33 vehicle, in which the cylindrical-like LOX and LH2 tanks are divided into quarter sectors by bulkheads aligned with the tank axis, and the X-34 vehicle, in which the horizontal cylindrical-like LOX and RP tanks are divided into several smaller cylindrical-like compartments by bulkheads aligned normal to the tank axis. Compartmenting a tank increases the structural stiffness, shifts the slosh resonant frequencies to a higher range, and diminishes the slosh forces. The weight of the bulkheads is fairly large, so it is common practice to perforate them to reduce weight.

There is no simple answer to the question of how much of the area of the bulkhead can be removed by the perforations or how big the holes can be and still make the tank appear to be divided into isolated compartments with respect to the slosh dynamics. If the only purpose of the bulkheads is to increase tank stiffness, the fractional area of holes can be as large as desired consistent with the desired stiffness. But if the compartments are also meant to change the slosh dynamics, a rule-of-thumb is that the total area of the perforations cannot exceed 10% of the area; if the open area is a bigger percentage, the

liquid tends to slosh back and forth between the compartments and the slosh natural frequency tends to approach the value of an uncompartmented tank. In either case, holes in the bulkheads increase the viscous slosh damping, sometimes to  $\gamma = 0.1$  [ABRAMSON AND GARZA, 1965]. This additional damping is caused by irreversible pressure losses when the liquid flows back and forth through the holes. The magnitude of the additional damping is best determined by experimentation. However, the relatively simple analysis outlined below can be used to obtain a preliminary estimate of the damping.

The analysis is based on an application of Eq. (2.2). Consequently, both the energy dissipation rate and the total energy of the sloshing must be computed. The energy dissipation, which is due to the flow losses as the liquid oscillates back and forth through the hole, is computed by analogy to the energy dissipated by the flow through an orifice in a pipe. Thus, a proportionate fraction of the bulkhead area has to be assigned to each hole, and this bulkhead area is assumed to be analogous to the pipe cross sectional area. The pressure loss across the hole (i.e., the fraction of the pressure drop that is not recovered on the downstream side) is given by:

$$\Delta P_{loss} = \frac{1}{2} \rho U^2 \alpha \left[ 1 - \left( \frac{C_c A_{hole}}{A_{plate}} \right)^2 \right] \quad (2.19)$$

where  $\alpha$  is the irreversible loss coefficient [BLEVINS, 1984],  $C_c$  is the discharge coefficient for the hole,  $A_{hole}$  is the area of the hole,  $A_{plate}$  is the area of the plate or bulkhead associated with the hole, and  $U$  is the liquid velocity through the hole. Values of  $\alpha$  for turbulent flow for a circular hole are shown in Table 2.1 as a function of the area ratio  $A_{hole}/A_{plate}$ . The discharge coefficient also depends on the area ratio and the shape of the hole, but for this approximate analysis a value of  $C_c = 0.6$  can be assumed.

The velocity  $U$  depends on the slosh wave height and frequency and the location and depth of the hole relative to both the free surface and the wave nodal line. The geometric factors are lumped together, just as for a ring baffle, into a function  $f_d$  of the depth and angular coordinate; the wave height and frequency are treated explicitly. Hence, the velocity is given by the relation:

$$U = \delta f_d \omega \sin \omega t \quad (2.20)$$

The energy dissipation rate of the flow through the hole is the product of the pressure loss  $\Delta P_{loss}$  and the volumetric liquid flow rate  $V$  back and forth through the hole. There are several ways to estimate this oscillating liquid volume. For example, it could be estimated as the product of the hole area and the amplitude of the liquid oscillation at the hole location, which can be computed in terms of the wave amplitude and the depth function  $f_d$ . Another method is simply to base  $V$  on a fraction of the volume of the sloshing mass of the equivalent mechanical model; the fraction is determined by the location of the hole below the free surface (to account for the decrease in the oscillations with depth) and the fraction of the bulkhead area open to the oscillating liquid. This latter method is the one assumed here. Hence, the liquid volume that oscillates through

**Table 2.1** Loss coefficient as a function of area ratio

	Hole-to-Pipe Area Ratio							
	0.04	0.09	0.16	0.25	0.36	0.49	0.64	0.81
Loss coefficient, $\alpha$	0.93	0.89	0.82	0.74	0.63	0.53	0.38	0.22

the hole is given by:

$$V = \frac{m_{slosh}}{\rho} \left( \frac{A_{hole}}{A_{plate}} \right) f_d \quad (2.21)$$

The amplitude  $\omega V$  of the oscillating volume flow rate is the product of  $V$  and the oscillation frequency  $\omega$ .

The instantaneous energy dissipation varies with time roughly as  $(\sin\omega t)^3$ , so the time-average energy dissipation rate is:

$$\frac{dE}{dt} = \frac{1}{4} \rho \omega (\delta \omega f_d)^2 \left[ 1 - \left( \frac{C_c A_{hole}}{A_{plate}} \right)^2 \right] \left( \frac{m_{slosh}}{\rho} \left( \frac{A_{hole}}{A_{plate}} \right) f_d \right) \quad (2.21)$$

As before, the total energy of the motion is  $0.5 m_{slosh} \omega^2 \Gamma^2 \delta^2$ . Thus, the damping coefficient is given by:

$$\gamma_{hole} = \frac{f_d^3}{4\Gamma^2} \left( \frac{A_{hole}}{A_{plate}} \right) \left[ 1 - \left( \frac{C_c A_{hole}}{A_{plate}} \right)^2 \right] \quad (2.22)$$

The ratio  $A_{hole}/A_{plate}$  is now interpreted as the fractional area of the plate that is open. For this approximation, the damping estimate does not depend on the slosh amplitude. Experiments show, nonetheless, that there is usually a small dependency on both slosh amplitude and  $Re_1$  for most perforated anti-slosh devices [ABRAMSON AND GARZA, 1965]. Alternative methods of computing  $dE/dt$ , such as the first method mentioned above, might predict an amplitude dependence. However, Eq. (2.22) is sufficient to estimate the gross magnitude of the damping provided by holes in a plate or structure.

## 2.7 References

- ABRAMSON, H. N., AND RANSLEBEN, G. E., 1960, *Simulation of Fuel Sloshing in Missile Tanks by Use of Small Models*, **ARS Journal**, **30**, pp. 603-612.
- ABRAMSON, H. N., AND RANSLEBEN, G. E., 1961, *Some Studies of a Floating Lid Type Device for Suppression of Liquid Sloshing in Rigid Cylindrical Tanks*, Report TR-10, Contract DA-23-072-ORD-1251, Southwest Research Institute.
- ABRAMSON, H. N., CHU, W.-H., AND GARZA, L. R., 1963, *Liquid Sloshing in Spherical Tanks*, **AIAA Journal**, **2**, pp. 384-389.
- ABRAMSON, H. N., AND GARZA, L. R., 1964, *Some Measurements of the Effects of Ring Baffles in Cylindrical Tanks*, **AIAA J. Spacecraft and Rockets**, **1**, pp. 560-562.
- ABRAMSON, H. N., AND GARZA, L. R., 1965, *Some Measurements of Liquid Frequencies and Damping in Compartmented Cylindrical Tanks*, **AIAA J. Spacecraft and Rockets**, **2**, pp. 453-455.
- BASS, R. L., 1972, *Stress Corrosion and Fatigue Testing of Flexible Baffle Materials*, Final Report, SwRI Project 02-3243.
- BAUER, H. F., 1962, *The Damping Factor Provided by Flat Annular Ring Baffles for Free Surface Oscillations*, Report MTP-AERO-62-81, NASA-MSFC.

- BLEVINS, R. D. 1984, **Applied Fluid Dynamics Handbook**, Section 6.5.3, Van Nostrand Reinhold Co., New York.
- BUGG, F., 1973, *Evaluation of Flexible Ring Baffles for Damping Liquid Oscillations*, NASA TM X-64730.
- COLE, H. A., AND GAMBUCCI, B. J., 1961, *Measured Two Dimensional Damping Effectiveness of Fuel Sloshing Baffles Applied to Ring Baffles in Cylindrical Tanks*, NASA TN D-694.
- DODGE, F. T., 1970, *Engineering Study of Flexible Baffles for Slosh Suppression*, Final Report, SwRI Project 02-2842, Contract NAS1-10074.
- DODGE, F. T., AND KANA, D. D., 1987, *Dynamics of Sloshing in Upright and Inverted Bladdered Tanks*, **ASME J. Fluids Engineering**, **109**, pp. 58-63.
- EULITZ, W., 1958, *A Can-type Device Derived from Basic Slosh Studies*, ABMA Report DSD-TR-4-58 (available from DDC, AD-203348).
- GARZA, L. R., 1966, *A Comparison of Theoretical and Experimental Pressures and Forces Acting on a Ring Baffle Under Sloshing Conditions*, NASA CR-385.
- GARZA, L. R., AND DODGE, F. T., 1967, *A Comparison of Flexible and Rigid Ring Baffles for Slosh Suppression*, **AIAA J. Spacecraft and Rockets**, **6**, pp. 805-806.
- KEULEGAN, G. H., AND PARKINSON, L. H., 1956, *Forces on Cylinders and Plates in an Oscillating Fluid*, National Bureau of Standards Report 4821.
- LINDHOLM, U. S., KANA, D. D., CHU, W.-H., AND ABRAMSON, H. N., 1962, *Research in Liquid Dynamics in Missile Fuel Tanks*, Quarterly Report 7, Contract NASw-2, Southwest Research Institute.
- MIKISHEV, G. N., AND DOROZHKIN, N. Y., 1961, *An Experimental Investigation of Free Oscillations of a Liquid in Containers*, **Izv. Akad., Nauk SSSR, Otd. Tekh., Nauk, Mekh. I Mashinostr**, **4**, pp. 48-83
- MILES, J. W., 1958, *Ring Damping of Free Surface Oscillations in a Circular Tank*, **ASME J. Applied Mechanics**, **25**, pp. 274-276.
- O'NEILL, J. P., 1960, *Final Report on an Experimental Investigation of Sloshing*, Space Technology Laboratory Report STL/TR-59-0000-09960.
- SCANLAN, R. H., AND ROSENBAUM, R., 1960, **Introduction to the Study of Aircraft Vibration and Flutter**, Macmillan Co., New York.
- SCHWIND, R., SCOTTI, R., and SKOGH, J., 1966, *Analysis of Flexible Baffles for Damping Tank Sloshing*, AIAA Paper 66-97.
- SILVEIRA, M. A., STEPHENS, D. G., AND LEONARD, H. W., 1961, *Damping of Liquid Oscillations in Cylindrical Tanks with Various Baffles*, NASA TN D-715.
- STEPHENS, D. G., LEONARD, H. W., AND SILVEIRA, M. A., 1961, *An Experimental Investigation of the Damping of Liquid Oscillations in an Oblate Spheroidal Tank With and Without Baffles*, NASA TN D-808.
- STEPHENS, D. G., LEONARD, H. W., AND PERRY, T. W., 1962, *Investigation of the Damping of Liquids in Right-Circular Cylindrical Tanks*, NASA TN D-1367.

- STEPHENS, D. G., 1966, *Flexible Baffles for Slosh Damping*, **AIAA J. Spacecraft and Rockets**, **3**, pp. 765-766.
- STEPHENS, D. G., AND SCHOLL, H. F., 1967, *Effectiveness of Flexible and Ring Baffles for Damping Liquid Oscillations in Large Scale Cylindrical Tanks*, NASA TN D-3878.
- STOFAN, A. J., AND ARMSTEAD, A. L., 1962, *Analytical and Experimental Investigation of Forces and Frequencies Resulting from Liquid Sloshing in Spherical Tanks*, NASA TN D-1281.
- STOFAN, A. J., AND PAVLI, A. J., 1962, *Experimental Damping of Liquid Oscillations in a Spherical Tank by Positive-Expulsion Bags and Diaphragms*, NASA TN D-1311.
- STOFAN, A. J., AND SUMNER, I. E., 1963, *Experimental Investigation of the Slosh-Damping Effectiveness of Positive-Expulsion Bags and Diaphragms in Spherical Tanks*, NASA TN D-1712.
- SUMNER, I. E., 1963, *Preliminary Experimental Investigation of Frequencies and Forces Resulting from Liquid Sloshing in Toroidal Tanks*, NASA TN D-1709.
- SUMNER, I. E., AND STOFAN, A. J., 1963, *An Experimental Investigation of Viscous Damping of Liquid Sloshing in Spherical Tanks*, NASA TN D-1991.
- SUMNER, I. E., 1964, *Experimental Investigation of Slosh-Suppression Effectiveness of Annular-Ring Baffles in Spherical Tanks*, NASA TN D-2519.



# MECHANICAL MODELS OF SLOSHING

This chapter is a revision of Chapter 6 of SP-106 entitled “Analytical Representation of Lateral Sloshing by Equivalent Mechanical Models”; the original author was FRANKLIN T. DODGE.

## 3.1 Introduction

Lateral sloshing was described analytically and experimentally in the previous two chapters. Sloshing can have a significant influence on the stability of a space vehicle because the slosh forces and torques interact with the control system through a feedback loop. For the purposes of incorporating the dynamic effects of sloshing in the spacecraft control and stability analysis, it is convenient to replace the liquid conceptually by an equivalent linear mechanical system. The equations of motion of oscillating point masses and rigid bodies are included more easily in the analysis than are the equations of fluid dynamics; even with super computers, coupling the equations of motion of a flexible space vehicle to the equations of motion of a continuous liquid is too computationally demanding for ordinary design analyses.

When liquid completely fills a capped container, theory shows that the liquid can be replaced dynamically by an equivalent *rigid* body [ZHUKOVSKII, 1964]. But when the liquid surface is free to move, the resultant sloshing has one or more natural frequencies, so the equivalent mechanical model cannot be a rigid body. Theory shows, however, that the dynamic effects can still be represented by a mechanical model but the model must now contain some masses that are free to oscillate [OKHOTSIMSKII, 1960]. It is not surprising that the dynamic effects of *linear* sloshing can be represented by another *linear* dynamical system. It *is* perhaps surprising that the parameters of the mechanical model depend only on the tank shape and the liquid properties, and not on the type of excitation imposed on the tank – so long as the tank walls are rigid. (But it is usually accurate enough to use the mechanical model even for tanks with flexible elastic walls.)

One of the main benefits of a mechanical model is that damping can be included easily by adding linear viscous dashpots to the model. Another advantage is that the *form* of the model does not depend on the tank shape or fill level.

## 3.2 Analytical Derivation of Model Parameters

*Figure 3.1* illustrates the kind of mechanical models discussed in this chapter. Most of the discussion will pertain to the pendulum form of the model for the reason that the natural frequency of the pendulum  $(g/L)^{0.5}$  automatically adjusts to changes in the axial acceleration  $g$  (or gravity level) just as the liquid natural frequencies do, whereas for the spring-mass model, the

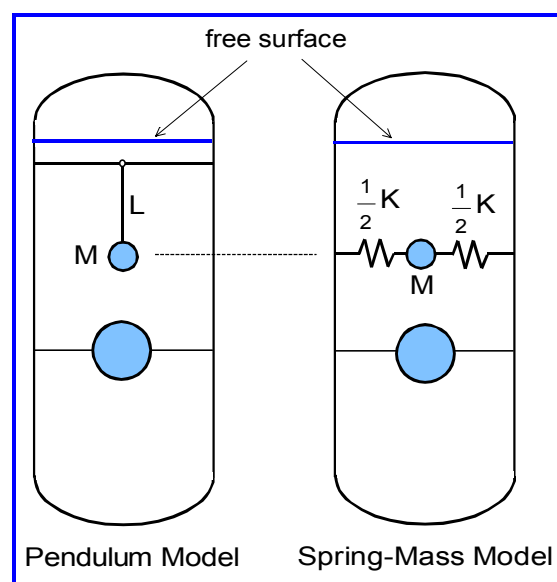


Figure 3.1. Mechanical models of sloshing

### 3. MECHANICAL MODELS OF SLOSHING

value of the spring constant  $K$  must be altered whenever  $g$  changes. The transformation between the pendulum model and the spring-mass model is straightforward. The spring-mass is located at the same elevation as the pendulum mass (not at the pendulum hinge elevation), the mass is attached to the tank walls through a spring having a spring constant  $K = mg/L$  that gives the same natural frequency as the pendulum, and the pendulum angular dashpot (which is not shown in *Figure 3.1*) is changed to a linear dashpot.

#### Equations of motion for the mechanical model

The equations of motion of the model are derived below for the spring-mass form of model because the derivation is a little bit more straightforward than for the pendulum form. Damping is neglected initially so that a direct comparison can be made with the slosh forces and torques given analytically in Chapter 1.

*Figure 3.2* shows the model and the symbols used in the analysis. The derivation of the model equations given below is independent of tank shape and fill level. The system of springs, masses, etc., is supposed to “fit” inside the actual tank and replace the liquid. For clarity, only two spring-masses are shown, but there is in fact one spring-mass for each slosh mode. The spring masses do not have a moment of inertia, so any needed moment of inertia  $I_0$  is assigned to the rigidly-attached mass  $m_0$ . The center of mass of the system is at the same height above the bottom of the tank as the liquid, and the locations  $H_n$  of the masses are referenced to the center of mass. The width of the tank is  $2a$ . Gravity  $g$  or an equivalent thrust-induced acceleration acts along the axis of the tank. The tank is excited by a small time-varying linear displacement  $X_0$  and angular rotation  $\alpha_0$  about an axis through the center of mass. The spring masses deflect a distance  $x_n$  relative to the tank walls as a result of the tank motion.

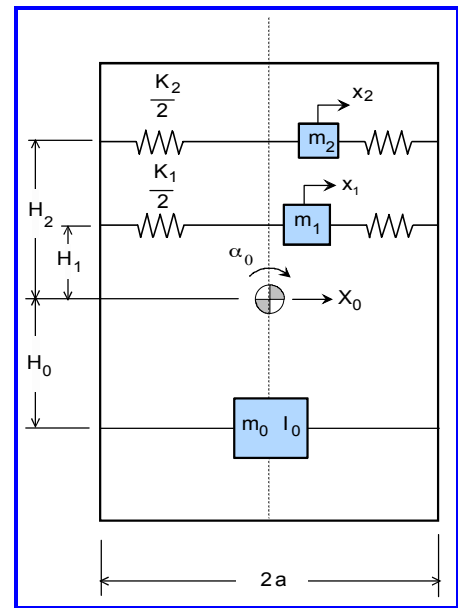


**Figure 3.2.** Schematic of equivalent mechanical model for lateral sloshing

**Static properties.** To preserve the static properties of the liquid, the sum of all the masses must be the same as the liquid mass  $m_{liq}$ , and the center of mass of the model must be at the same elevation as the liquid. These constraints are expressed analytically by:

$$m_0 + \sum m_n = m_{liq} \quad (3.1)$$

$$m_0 H_0 + \sum m_n H_n = 0 \quad (3.2)$$

**Dynamic properties.** Equations (3.1) and (3.2) are not sufficient to fix the values of the model parameters. To do that, the model must also duplicate the sloshing forces, torques, and natural frequencies. Duplication of the natural frequencies requires:

$$K_n / m_n = \omega_n^2 \quad (3.3)$$

where  $\omega_n$  is the slosh natural frequency of the  $n^{\text{th}}$  mode. This is a first relation that shows how the spring constant and spring-mass must be chosen; however, the model forces and torques have to be examined to develop other relations.

The net force exerted on the tank in the  $+X_0$  direction is given by the reversed inertia forces of the moving masses:

$$-F = m_0(\ddot{x}_0 - H_0\ddot{\alpha}_0) + \sum m_n(\ddot{X}_0 + H_n\ddot{\alpha}_0 + \ddot{x}_n) \quad (3.4a)$$

where  $\sin(\alpha_o)$  has been replaced by  $\alpha_o$  because of the small-amplitude assumption and the superscript dots indicate differentiation with respect to time<sup>7</sup>. Equation (3.4a) can be simplified by inserting Eq. (3.2) into it to give:

$$-F = m_0\ddot{X}_0 + \sum m_n(\ddot{X}_0 + \ddot{x}_n) \quad (3.4b)$$

Likewise, the net torque exerted on the tank is given by:

$$-M = (I_0 + m_0H_0)\ddot{\alpha}_0 + \sum m_n h_n(\ddot{x}_n + H_n\ddot{\alpha}_0) - g \sum m_n x_n \quad (3.5)$$

where the last term is the torque caused by the offset of each spring-mass from the tank centerline. (Some terms have already been cancelled out of this equation.) The equation of motion for each of the spring-masses is expressed as:

$$m_n(\ddot{X}_0 + \ddot{x}_n + H_n\ddot{\alpha}_0) + K_n x_n - m_n g \alpha_0 = 0 \quad (3.6)$$

Just as was done in Chapter 1, the tank accelerations are assumed to be oscillatory at frequency  $\Omega$ . The components of the tank motion are therefore given by  $-X_0 \exp(i\Omega t)$  and  $-i\alpha_o \exp(i\Omega t)$ , and Eq. (3.6) can be expressed as:

$$x_n = -\frac{i\Omega^2 X_0}{\omega_n^2 - \Omega^2} - \left( \frac{H_n + g/\Omega^2}{\omega_n^2 - \Omega^2} \right) i\Omega^2 \alpha_0 \quad (3.7)$$

where Eq. (3.3) has also been used to eliminate  $K_n$ . With these equations, the amplitudes of the force and torque on the tank can be expressed analytically as:

$$\frac{F_{amp}}{i\Omega^2 m_{liq}} = - \left[ 1 + \sum \frac{m_n}{m_{liq}} \left( \frac{\Omega^2}{\omega_n^2 - \Omega^2} \right) \right] X_0 - \alpha_0 \sum \frac{m_n}{m_{liq}} \left( \frac{H_n \Omega^2 + g}{\omega_n^2 - \Omega^2} \right) \quad (3.8)$$

$$\begin{aligned} \frac{M_{amp}}{i\Omega^2} = & -\alpha_0 \left[ I_0 + m_0 H_0^2 + \sum m_n H_n^2 + m_{liq} \sum \frac{m_n}{m_{liq}} \left( \frac{H_n^2 \Omega^2 + 2H_n g + g h^2 / \omega_n^2}{\omega_n^2 - \Omega^2} \right) \right] \\ & - m_{liq} X_0 \sum \frac{m_n}{m_{liq}} \left( \frac{H_n \Omega^2 + g}{\omega_n^2 - \Omega^2} \right) \end{aligned} \quad (3.9)$$

**Exceptions.** For a tank without an axis of symmetry such as a tank with a rectangular cross section, the specific slosh mode excited depends on the direction of the tank acceleration. There can be two or more sets of modes with comparable frequencies and slosh masses. The total model mass will therefore be greater than the total mass of liquid, in apparent

<sup>7</sup> There is also a net gravitational force or weight from the masses exerted in the lateral as well as in the axial direction, because of the tilting of the tank. This force is counterbalanced by the force (not shown in the figure) that supports the tank, which for a space vehicle is the lateral component of the thrust; the vertical component of the thrust supports the weight of the tank.

contradiction to Eq. (3.1). However, the total mass set in motion will never exceed the total mass of liquid. An example of this exception is discussed later.

### Rectangular tank

Since the slosh forces and torques were derived in detail in Chapter 1 only for a rectangular parallelepiped tank, that tank shape will be used as an example to demonstrate how model parameters such as  $m_n$ ,  $K_n$ , and  $H_n$  are determined as a function of tank shape and fill level. We will consider only the two-dimensional slosh modes that are excited by a translation of the tank in the  $x$ -direction or an angular rotation about the  $y$  axis, as indicated in Figure 3.2.

The lateral force exerted on the tank by the sloshing liquid for a horizontal excitation of the tank parallel to the  $x$ -axis is given by Eq. (1.28), which is reproduced below:

$$\frac{F_{xo}}{-\Omega^2 X_o m_{liq}} = 1 + 8 \frac{a}{h} \sum_{n=1}^N \frac{\tanh[(2n-1)\pi h/a]}{(2n-1)^3 \pi^3} \frac{\Omega^2}{\omega_n^2 - \Omega^2} \quad (1.28)$$

By comparing Eq. (1.28) to the expression for the force created by an  $x$ -translation of the model [Eq. (3.8)] it can be seen that the slosh force will be duplicated by the model if the model masses are chosen to be equal to:

$$m_n = m_{liq} \left\{ 8 \left( \frac{a}{h} \right) \frac{\tanh[(2n-1)\pi h/a]}{(2n-1)^3 \pi^3} \right\} \quad (3.10)$$

The slosh natural frequencies are given by Eq. (1.19a) (reproduced below):

$$\omega_n^2 = (2n-1)\pi(g/a) \tanh[\pi(2n-1)(h/a)] \quad (1.19a)$$

Hence, the spring constants of the model must be chosen as:

$$K_n = m_{liq} \left\{ 8 \left( \frac{g}{h} \right) \frac{\tanh^2[(2n-1)\pi h/a]}{(2n-1)^2 \pi^2} \right\} \quad (3.11)$$

The slosh force for a  $y$ -rotational acceleration about the axis through the center of mass is given by Eq. (1.34), which is reproduced below:

$$\frac{-F_{xo}}{m_{liq} \alpha_o \Omega^2 h} = \left\{ \frac{1}{12} \left( \frac{a}{h} \right)^2 + 8 \left( \frac{a}{h} \right) \sum_{n=1}^{\infty} \frac{\tanh[(2n-1)\pi h/a]}{(2n-1)^3 \pi^3} \left( \frac{1}{2} - \frac{\tanh[(2n-1)\pi h/2a]}{(2n-1)\pi h/2a} + \frac{g}{h \omega_n^2} \left( \frac{\Omega^2}{\omega_n^2 - \Omega^2} \right) \right) \right\} \quad (1.34)$$

To allow easy comparison to the model force comparison, the slosh force expression is re-written in a slightly different by using the following identities:

$$\frac{1}{\omega_n^2 - \Omega^2} = 1 + \frac{\Omega^2}{\omega_n^2 - \Omega^2} \quad \text{and} \quad 8 \sum \frac{\tanh[(2n-1)\pi h/a]}{\pi^3 (2n-1)^3} = \frac{1}{12} \frac{a}{h}$$

After rewriting Eq. (1.34) with these identities, it can be seen from Eq. (3.8) that duplication of the force caused by a  $y$ -rotation gives the same values for the model masses as Eq. (3.10) does, and the axial elevation of the masses must be chosen so that:

$$\frac{H_n}{h} = \frac{1}{2} - \frac{a}{2h} \frac{\tanh[(2n-1)\pi h/2a]}{(2n-1)\pi} \quad (3.12)$$

The slosh torque is given by Eqs. (1.30) for an  $x$ -translational excitation, and by Eqs. (1.35), and (1.36) for a  $y$ -rotational excitation. Comparing these relations to the model torque [Eq. (3.9)] gives (with the aid of some more identities) the same requirements for  $m_n$  and  $H_n$  that were found from the force duplication requirements. In addition, the total moment of inertia of the model must be chosen to satisfy:

$$I_0 + m_0 H_0^2 + \sum m_n H_n^2 = I_{Sy} \left\{ 1 - \frac{4}{1 + (h/a)^2} + \frac{768a/h}{1 + (h/a)^2} \sum_{n=1}^{\infty} \frac{\tanh[(2n-1)\pi h/2a]}{\pi^5 (2n-1)^5} \right\} \quad (3.13)$$

This equation in effect determines  $I_0$  since all the other model parameters are already determined. Generally,  $I_0$  is not a large contribution to the torque.

**Summary.** The expressions given above show that the model parameters do not depend on the amplitude or the frequency of a simple harmonic excitation of the tank. Since any periodic excitation can be represented by a Fourier series of harmonic terms, the model parameters are thus completely general and independent of the form of the tank excitation. Furthermore, the dependency of the model spring constant on  $g$  can be eliminated by switching to the pendulum form of the model. As was mentioned earlier, the transformation is accomplished by locating the pendulum hinge point for each slosh mass  $m_n$  at an elevation  $L_n + H_n$ , where  $L_n = (g/\omega_n)^{0.5}$  is the pendulum length.

The parameters for the pendulum model are summarized in Table 3.1. The axial locations  $H_n$  in the table give the positions of the pendulum *hinge* points. The table shows that the frequencies of the  $n > 1$  modes are considerably higher than the  $n = 1$  mode; for example, if  $h/a = 1$ , the pendulum lengths are  $L_1 = 0.317a$ ,  $L_2 = 0.106a$ , and  $L_3 = 0.064a$ . The slosh mass decreases dramatically for the higher modes; again for  $h/a = 1$ ,

**Table 3.1** Model Parameters for a Rectangular Tank

$m_{liq} = \rho ah = \text{mass per unit width}$

Parameter	Value
Slosh mass, $m_n$	$m_{liq} \left[ \frac{8a \tanh(2n-1)\pi h/a}{\pi^3 (2n-1)^3 h} \right]$
Pendulum length, $L_n$	$\frac{a}{\pi(2n-1)\tanh(2n-1)\pi h/a}$
Pendulum hinge location, $H_n$	$\frac{h}{2} - \frac{a}{(2n-1)\pi} \left[ \tanh(2n-1)\pi h/2a - \frac{1}{\sinh(2n-1)\pi h/a} \right]$
Rigidly attached mass, $m_o$	$m_{liq} - \sum m_n \approx m_{liq} \left[ 1 - \frac{8a \tanh(2n-1)\pi h/a}{\pi^3 (2n-1)^3 h} \right]$
Rigidly attached mass location, $H_o$	$\sum m_n (H_n - L_n) / m_o$
Rigidly attached mass moment of inertia, $I_o$	Eq. (1.36) - $m_o H_o^2 - \sum m_n (H_n - L_n)^2$

### 3. MECHANICAL MODELS OF SLOSHING

the masses are  $m_1 = 0.258m_{liq}$ ,  $m_2 = 0.0096m_{liq}$ , and  $m_3 = 0.0021m_{liq}$ . It can be concluded that only the first, lowest-frequency slosh mass usually needs to be considered.

#### Axisymmetric tanks

The parameters of the mechanical model for any *axisymmetric* tank can be computed from the SLOSH computer program (although the program gives results for only the two lowest-frequency slosh modes). For convenience, however, the model parameters for two common axisymmetric tanks – a cylinder and a sphere – are summarized here in tabular and graphical form below.

**Cylindrical tank.** *Table 3.2* and *Figure 3.3* summarize the pendulum model parameters for a cylindrical tank [BAUER, 1964]. The model moment of inertia is always only a fraction of the moment of inertia of the “frozen” liquid.

**Table 3.2** Model Parameters for a Cylindrical Tank

$$m_{liq} = (\pi/4)\rho d^2 h \quad \xi_1 = 1.841; \xi_2 = 5.329; \xi_3 = 8.531; \xi_n \approx \xi_{n-1} + \pi$$

Slosh mass, $m_n$	$m_{liq} \left[ \frac{d \tanh(2\xi_n h/d)}{\xi_n (\xi_n^2 - 1) h} \right]$
Pendulum length, $L_n$	$\frac{d}{2\xi_n \tanh(2\xi_n h/d)}$
Pendulum hinge location, $H_n$	$\frac{h}{2} - \frac{d}{2\xi_n} \left[ \tanh(\xi_n h/d) - \frac{1}{\sinh(2\xi_n h/d)} \right]$
Rigidly attached mass, $m_o$	$m_{liq} - \sum m_n \approx m_{liq} \left[ 1 - \frac{d \tanh(2\xi_n h/d)}{\xi_n (\xi_n^2 - 1) h} \right]$
Rigidly attached mass location, $H_o$	$\sum m_n (H_n - L_n) / m_o$
Rigidly attached mass moment of inertia, $I_o$	Figure 3.3

**Spherical tank.** The pendulum model parameters of the first mode for a spherical tank are

summarized in *Figure 3.4*, as computed by the SLOSH code. The value of  $I_o$  is zero, and the pendulum hinge points and the rigidly attached mass are all located at the center of the tank, because the model reflects the fact that an angular rotation of a spherical tank about an axis through its center does not cause any motion of an inviscid liquid. (That is, the tank just “slides” around the liquid.) Thus,  $I_o$ ,  $H_o$  and  $H_1$  are all equal to zero and are not shown in the figure. For low fill levels the slosh mass is nearly equal to the total liquid mass; that is, all the liquid participates in the sloshing. Furthermore, the

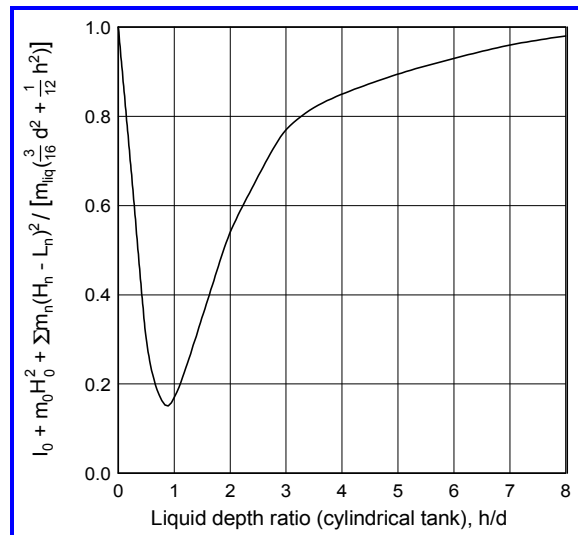


**Figure 3.3.** Ratio of model to frozen liquid moment of inertia for a cylindrical tank [BAUER, 1964]



### 3. MECHANICAL MODELS OF SLOSHING

to the translational motion and to the rotational motion of the model, but this has been verified experimentally [ABRAMSON, ET AL, 1961].

Figure 3.6 shows that the force predicted by the damped mechanical model (using a damping coefficient determined empirically by the methods discussed in Chapter 2) agrees well with experiments for the  $n = 1$  mode, thus validating the assumptions made in the model development. The  $n = 2$  mode resonance is more prominent in the tests than predicted by the model; this is primarily caused by the need to use the  $n = 1$  mode damping coefficient, for the  $n = 2$  mode since, as discussed in Chapter 2,  $\gamma_1$  is the only one that can be measured reliably in tests. Evidently the second mode damping was actually smaller than the first mode damping in these tests.

By following the same procedure, the torque predicted by the damped model can be written as:

$$\begin{aligned} \frac{M_{amp}}{i\Omega^2} = & -\alpha_0 \left[ I_0 + m_0 H_0^2 + \sum m_n H_n^2 + m_{liq} \sum \frac{m_n}{m_{liq}} \left( \frac{H_n^2 \Omega^2 + 2H_n g + gh^2 / \omega_n^2}{\omega_n^2 - \Omega^2 + 2i\gamma_n \omega_n \Omega} \right) \right] \\ & - m_{liq} X_0 \sum \frac{m_n}{m_{liq}} \left( \frac{H_n \Omega^2 + g}{\omega_n^2 - \Omega^2 + 2i\gamma_n \omega_n \Omega} \right) \end{aligned} \quad (3.17)$$

This result also agrees well with experimental results.

The damped slosh torque shows the same characteristics as the force for low and high frequencies. When the damping becomes very large, the model predicts that the torque asymptotically approaches:

$$M_{amp} = i\Omega^2 \alpha_0 \left[ I_0 + m_0 H_0^2 + \sum m_n H_n^2 \right] \quad (3.18)$$

(or with  $H_n$  replaced by  $H_n - L_n$  for the equivalent pendulum model). This expression represents the torque produced by an ideal inviscid liquid that fills a capped container. From the plot shown in Figure 3.3, it can be seen that the effective moment of inertia of this liquid mass is less than that of the equivalent rigidized or “frozen” liquid. But for large damping the effective moment of inertia should in fact be equal to that of the frozen liquid since the fluid’s resistance to shearing has theoretically become infinite. In other words,  $I_o$  must be changed to account for the damping. One way to do this is to modify the model by including a weightless disk with moment of inertia  $I_d$ , which is connected to the tank walls by means of a dashpot, and by replacing  $I_o$  with a moment of inertia equal to  $I_o - I_d$  [BAUER, 1964]. The magnitudes of  $I_d$  and the  $I_d$  dashpot are chosen to make the model’s effective rigid-body moment of inertia agree with experiments. These corrections are negligible for ordinary, realistic values of damping.

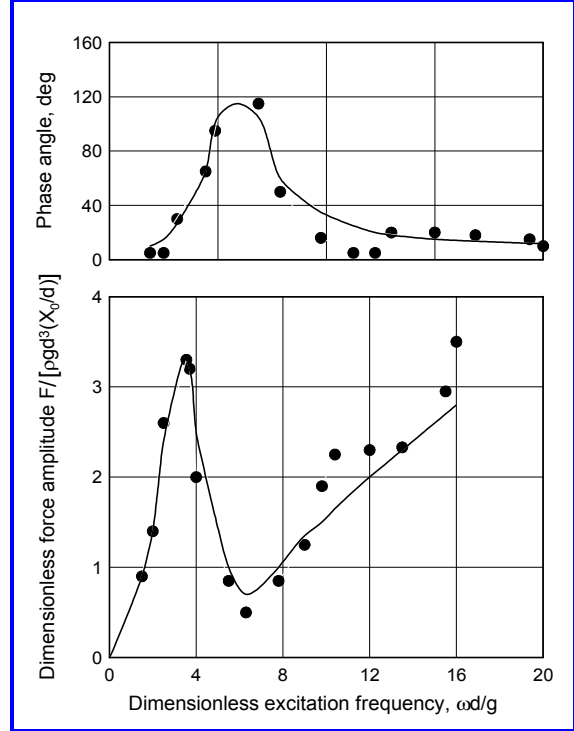


Figure 3.6. Comparison of mechanical model to cylindrical tank tests [ABRAMSON, ET AL, 1967]

### 3.4 Mechanical Model Parameters from the SLOSH Code

The **SLOSH** code can be used to predict the parameters of the first two slosh modes of a pendulum model for any axisymmetric tank shape, for any fill level. The damping is predicted from the correlations given in Chapter 2, and the code allows the use of ring baffles. The code also predicts the loads on a ring baffle and the pressures on the tank walls (outer and inner, as appropriate). The Appendix summarizes the theory upon which the code is based.

### 3.5 Experimental Derivation of Model Parameters

To determine the parameters of a mechanical model by the procedures described in Sections 3.2 and 3.3, a theoretical analysis of the sloshing is needed. In many cases, such an analysis is not possible (for example, a tank fitted with a flexible bladder that covers the liquid surface) or is not practical (for example, a cylindrical tank divided into irregularly shaped compartments). For those cases, the model must be developed from experimental measurements, generally using scale model tanks. The best procedure is to excite the tank into simple harmonic motion using both horizontal and pitching motions over a range of frequencies that encompasses the slosh natural frequencies, measure the resulting force and torque responses as a function of excitation frequency, and fit a model to the force and torque measurements [UNRUH, ET AL, 1986].

The test procedures can be simplified if the experimental apparatus allows the tank to be stopped quickly without introducing excessive electrical noise or structural ringing, and if the instrumentation is sufficient to resolve the maximum force and torque immediately after the tank is stopped [SUMNER, STOFAN, AND SHRAMO, 1964]. For example, if the tank excitation is a pure translation of amplitude  $X_0$  at a frequency  $\omega$  considerably below the slosh natural frequency  $\omega_1$ , the slosh mass can be computed by combining Eqs. (3.4a) and (3.6) to give:

$$m_1 = \frac{F_{max}}{X_0} \left( \frac{1}{\omega^2} - \frac{1}{\omega_1^2} \right) \quad (3.19a)$$

and the location of the slosh mass pendulum hinge point above the center of mass of the liquid can be computed as:

$$H_1 = \frac{M_{max}}{F_{max}} \quad (3.20a)$$

where  $F_{max}$  and  $M_{max}$  are the peak measured forces and torques just after quick stopping the tank. Generally, however, it is more accurate to conduct steady state sloshing tests to determine the complete force and torque response, if for no other reason than this allows the damping to be determined by the half power method.

**Examples.** The first example of the use of test data to develop a mechanical model is for a tank shape that is not axisymmetric. At one time, NASA considered using the liquid hydrogen tank of the *S-IVB stage* of the *SATURN V* “moon rocket” as an orbiting laboratory. The tank was subdivided into a series of irregular compartments, connected by doors, which would be used as laboratories after the liquid hydrogen had been expended. The configuration of the compartments is shown in *Figure 3.7* (looking down the tank axis). The irregularly-shaped compartments altered the sloshing characteristics of the S-IVB stage and also made the sloshing susceptible to roll excitation.

### 3. MECHANICAL MODELS OF SLOSHING

The slosh modes were determined by laboratory tests of a 1/14.8 scale model that used water as the model liquid [DODGE AND GARZA, 1969]. Tests were conducted with the doors between the compartments open and closed; the “doors open” configuration coupled the sloshing in each compartment, but it was found that the results did not differ greatly from the “doors closed” configuration, so most of the tests were conducted with the doors closed. Both translational and roll excitations were used. Load cells were used to measure the slosh force in the direction of excitation and the torque about an axis perpendicular to the direction of the translational excitation.

Only the translational excitation tests will be discussed. The slosh modes and natural frequencies were determined by oscillating the tank in translation at a series of angles  $\theta$  relative to a fixed direction (shown in the figure) over a range of frequencies. The modes were identified by noting the directions for which the maximum force was obtained for each compartment when only that compartment contained liquid. After the modes were identified, detailed steady state force and torque measurements were obtained over a frequency range that encompassed the slosh frequency. The damping was determined by the half-power method described in Chapter 2, using the force response plots as a basis.

*Figure 3.8* shows the model that was developed from the test results. The spring-mass form of the model is shown in the figure but a pendulum form is equally applicable. Note that the locations of the undisturbed slosh masses actually coincide with the center of mass of the compartment; they are shown displaced from this location only for the sake of clarity in depicting the number of slosh modes considered in the model. The small compartments shown to the right of Compartments 1 and 2 in *Figure 3.7* were not considered since their slosh masses were small and the slosh frequencies high.

The models for the rectangular Compartments 1 and 2 will be discussed as an example of the results. The directions of the two slosh modes for each compartment were at right angles to each other (i.e., one mode was aligned with  $\theta = 0^\circ$  and the other was

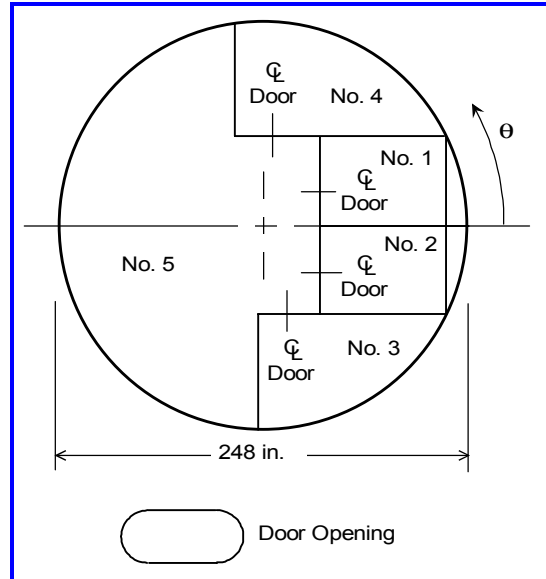


**Figure 3.7.** Schematic of compartmented S-IVB liquid hydrogen tank

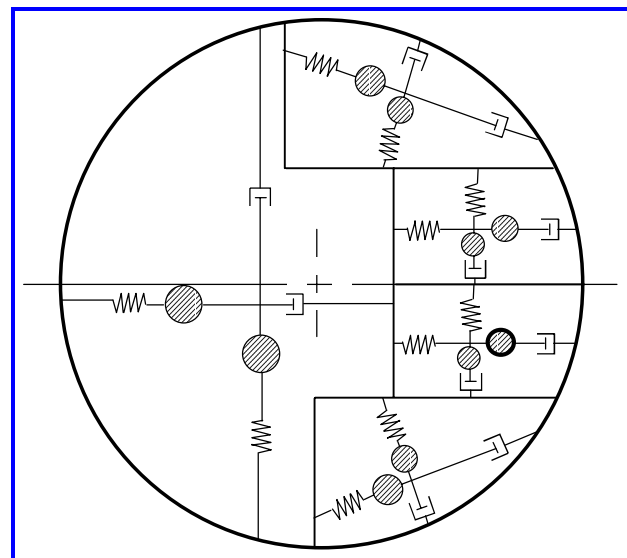


**Figure 3.8.** Equivalent mechanical model for the compartmented S-IVB stage.

aligned with  $\theta = 90^\circ$ ). When the excitation is directed along an arbitrary angle  $\theta$  (as shown in *Figure 3.7*), the forced response of the  $n^{\text{th}}$  slosh mode for, say, Compartment 1, can be expressed as:

$$m_n \ddot{x}_n + 2i\omega_n \gamma_n \dot{x}_n + k_n x_n = \ddot{X}_0 m_n \cos(\theta - \theta_n) \quad (3.21)$$

where  $x_n$  is the displacement of the slosh mass  $m_n$  along the line of action of the mode. From the general relations given previously, the force resolved in the direction of the excitation is given by:

$$F = m_0 \ddot{X}_0 + \sum m_n [\ddot{X}_0 + \ddot{x}_n \cos(\theta - \theta_n)] \quad (3.22)$$

where  $m_0$  is the rigidly attached mass for this compartment. Combining these two relations gives the result that the slosh force in the direction of the excitation is:

$$F = \ddot{X}_0 m_{liq} \left[ 1 + \sum_{n=1}^2 \frac{m_n}{m_{liq}} \left( \frac{(\omega/\omega_n)^2}{1 - (\omega/\omega_n)^2 + 2i\gamma_n (\omega/\omega_n)} \right) \cos^2(\theta - \theta_n) \right] \quad (3.23)$$

**Equation (3.23)** demonstrates that regardless of the direction of excitation, the effective mass that participates in the resonant part of the force is never larger than the total liquid mass, although the sum of the slosh masses of the model might indeed be larger than the liquid mass<sup>8</sup>. This confirms the remarks made earlier about the realism of the model.

The line of action of the two slosh modes in the wedge-shaped compartments (Compartments 3 and 4) were not quite perpendicular to each other, although they differed from perpendicularity by less than  $8^\circ$ . Thus, there was not a direction of excitation that excited only one of the modes. Whether this lack of perpendicularity was real or merely an artifact of small nonlinear effects was not clear in the experiments.

An example of the degree to which the model predicts the test results is shown in *Figure 3.9* for Compartment 5. For this compartment, there were two noticeable modes aligned with the  $\theta = 0^\circ$  direction and one mode aligned with the  $\theta = 90^\circ$  direction. (For clarity, only one  $\theta = 0^\circ$  mode was shown in *Figure 3.8*). The model-test comparison is reasonably close.

The force and torque amplitudes shown in *Figure 3.9* are for the 1/14.8 scale model, and they cannot be scaled directly to full size

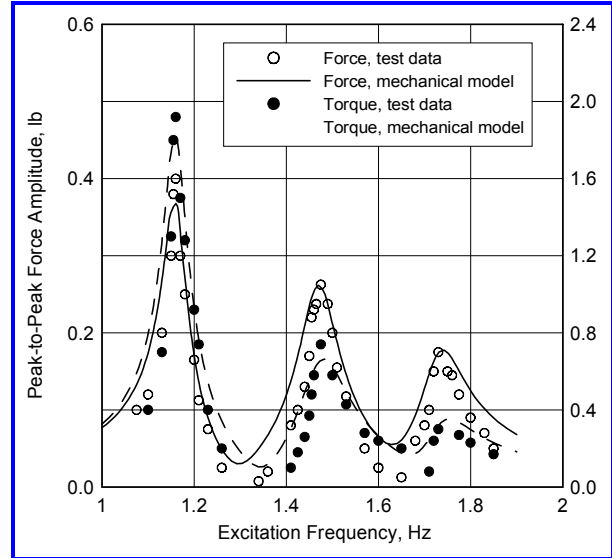


**Figure 3.9.** Model predictions for Compartment 5; half-full tank;  $\theta = 45^\circ$ ;  $X_0 = 0.0075$  inch.

<sup>8</sup> Let  $R_n$  represent the resonance factor for each mode. The resonant part of the force is then equal to  $m_1 R_1 [\cos(\theta - \theta_1)]^2 + m_2 R_2 [\cos(\theta - \theta_2)]^2$ . The worst case is when the natural frequencies of the modes are equal, so that  $R_1 = R_2$ . After expanding the cosine terms, the resonant part of the force is thus no bigger than  $R_1 [m_1 (\cos\theta)^2 + m_2 (\sin\theta)^2]$ . Even if  $m_1 = m_2 = m_{liq}$ , this term is no bigger than  $R_1 m_{liq}$ .

because the damping for the full size tank is considerably different than for the scale model tank. However, the model parameters, including the damping coefficient (using the  $Re$  parameter), can be scaled up and the full scale responses can be computed from the scaled up model.

Another example of a slosh model developed from test data is the model for the *Telemetry and Data Relay Satellite* (TDRS). To minimize shifting of the spacecraft center of mass as the propellants were depleted, TDRS utilized an over and under arrangement of tanks located on the centerline of the spacecraft. The liquid in each tank was held in place by a flexible bladder, as shown in *Figure 3.10*. The bladders also provided a positive method of expelling propellants from the tanks in low gravity. During thrusting conditions, the liquid configuration in the upper tank became unsymmetrical, with much of the liquid forming a pendulous “blob” on one side of the centerline, since this configuration has a smaller static potential energy than a symmetrical configuration. The inherent stiffness of the bladder was not enough to return the liquid to a symmetrical configuration during periods of low gravity, so a mechanical model for this tank had to be developed for an unsymmetrical configuration. A considerable amount of preliminary testing was needed to understand the sloshing in the upper tank [KANA, DODGE, ET AL, 1979, 1981, 1987].

Sloshing in the lower tank was fairly conventional although the bladder concentrated the slosh wave near the tank axis. A pendulum model was assumed but the pendulum hinge point had to be attached to the tank by a rotational spring to simulate the stiffness of the bladder. For this kind of model, the pendulum frequency is:

$$\omega_s = \left[ \frac{g}{L} + \frac{K_{bladder}}{m_{slosh} L^2} \right]^{0.5} \quad (3.24)$$

where  $L$  is the pendulum length,  $m_{slosh}$  is the slosh mass, and  $K_{bladder}$  is the effective torsional spring stiffness of the bladder. By conducting tests with two liquids of different density,  $m_{slosh}$  was actually varied in proportion to the different liquid densities, and different slosh natural frequencies were thereby measured for the different liquids. With two determinations of  $\omega_s$ , the model parameters  $m_{slosh}$ ,  $L$ , and  $K_{slosh}$  could all be determined from the force and frequency measurements.

Sloshing in the upper “upside down” tank was quite unconventional. If a translation excitation was applied along the long axis of the tank in the plane of *Figure 3.10*, an antisymmetrical wave was formed on the liquid bladder interface roughly like the one shown in *Figure 3.10*. If a translational excitation was applied in the direction normal to the plane of the tank shown in *Figure 3.10*, another, different slosh wave was formed in which the liquid blob tended to move in and of the plane of the figure. If the excitation was too large, the blob tended to rotate around the tank. Furthermore, if the tank was tilted to simulate an off-axis thrust direction, the entire blob “flopped” to a new

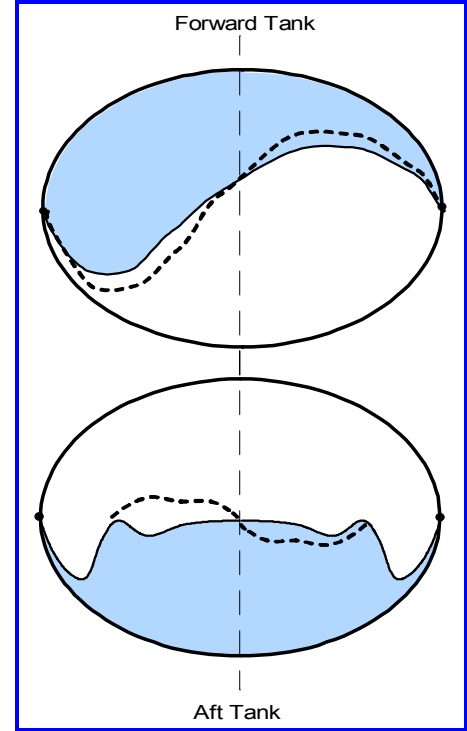


**Figure 3.10.** TDRS tank schematic

position when the tilt exceeded a critical magnitude (about  $20^\circ$ ). There were also other modes and stability considerations, but they are not discussed here.

After a lot of scoping tests, it was finally determined that an inverted pendulum was an acceptable

representation of the sloshing in the upper tank. The model is shown schematically in [Figure 3.11](#). The equilibrium position of the pendulum was tilted from the vertical at an angle equal to the critical tilt angle discussed above. The pendulum mass rested on a guiding surface through a spring and dashpot arrangement. This spring and dashpot

simulated the sloshing observed for an excitation direction parallel to the long axis of the tank (the mode illustrated in [Figure 3.10](#)).

The pendulum mass was also connected to another spring and dashpot that simulated the slosh observed for translational excitation perpendicular to the plane of [Figure 3.10](#). (The two slosh masses had different magnitudes but this feature is not depicted in [Figure 3.11](#).) The entire arrangement was attached to two slider blocks that rested on the guiding surface. The “stiction” between the sliders and the guiding surface prevented the mass-spring-dashpot combination from rotating around the tank except when the excitation exceeded some critical level (which determined the amount of stiction). The mechanical model represented the observed sloshing and stability characteristics very accurately.

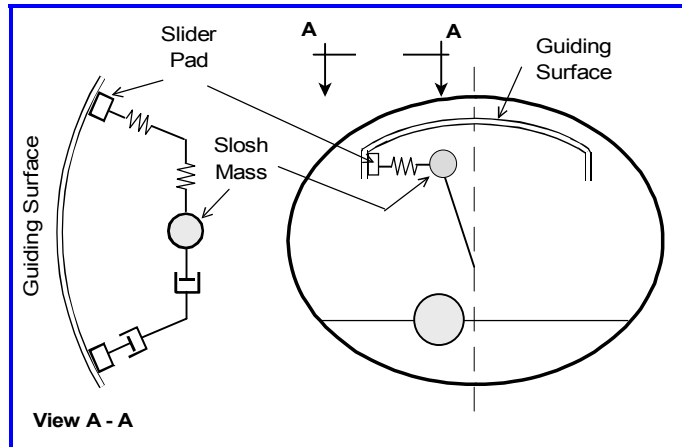


**Figure 3.11.** Equivalent mechanical model for TDRS forward tank.

### 3.6 Nonlinear Mechanical Models

Mechanical model analogies have also been developed for sloshing motions that have wave amplitudes large enough to make the linearized theory of Chapter 1 invalid. The theory of *nonlinear* sloshing is discussed in Chapter 5. There are many nonlinear phenomena of interest, ranging from an increase of slosh natural frequency with wave amplitude to the occurrence of very complicated nonplanar motions. The pendulum form of the mechanical model analogy for linear sloshing also possesses somewhat similar nonlinear characteristics when the pendulum amplitude is large. Several examples of nonlinear mechanical models are discussed below.

**Rotary slosh model.** When liquid in an axisymmetric tank is excited at a frequency very near the slosh natural frequency, the normal antisymmetric up-and-down planar-like slosh wave becomes unstable [BERLOT, 1959; HUTTON, 1964; ABRAMSON, ET AL, 1962; ABRAMSON, ET AL, 1966]. The form taken by the instability depends on the proximity of the excitation frequency to the natural frequency.

1. When the excitation frequency is significantly above or below the natural frequency, the normal antisymmetric planar motion of the surface occurs.
2. When the excitation frequency is just slightly greater than the natural frequency and the amplitude of the excitation motion is sufficiently large, the nodal line of the standing slosh wave rotates around the tank at about the same frequency as the

### 3. MECHANICAL MODELS OF SLOSHING

excitation; this rotational motion is superimposed on the normal antisymmetric wave. The liquid has a definite angular momentum which it acquires as a consequence of the nonlinear coupling between the wave motion parallel to the direction of excitation and that perpendicular to the plane of excitation.

- When the excitation is just below the frequencies for which rotational motion occurs, the slosh nodal line does not rotate steadily but instead first rotates in, say, the counterclockwise direction, then stops, and then rotates in the clockwise direction, then stops, and so on. This motion is called swirling.

A conical pendulum is known to have several similar instabilities, so several investigators have used a conical pendulum analogy to predict and understand the observed instabilities of sloshing. A conical pendulum (also called a spherical pendulum) is a pendulum that is free to swing in any plane.

Figure 3.12 shows a conical pendulum excited by a simple harmonic translation and defines the angles that specify the position of the pendulum with respect to the  $x, y, z$  axes. The length of the pendulum  $L$  is chosen so that the pendulum frequency  $\omega_1 = (g/L)^{0.5}$  is equal to the slosh natural frequency. The amplitude  $\epsilon$  of the excitation is scaled to the pendulum length  $L$ . The excitation is along the  $y$ -axis, so stable to-and-fro motion of the pendulum occurs in the  $y-z$  plane (i.e.,  $\beta = 0, \alpha = \gamma$ ). The stability of this motion is to be determined.

The equations of motion for the pendulum are derived by using the assumption that  $\sin(\alpha)$  can be approximated as  $\alpha - \alpha^3/6$  and  $\cos(\alpha) \approx 1 - \alpha^2/2$ , and similarly for the sines and cosines of the other angles. The governing equations for the pendulum are:

$$\left( \frac{d^2}{dt^2} + \frac{g}{L} \right) \alpha - \frac{g}{6L} \alpha^3 + \frac{1}{2} \left( \frac{d^2}{dt^2} + \frac{g}{L} \right) \alpha \beta^2 = \epsilon \omega^2 \cos \omega t \quad (3.25a)$$

$$\left( \frac{d^2}{dt^2} + \frac{g}{L} \right) \beta - \frac{g}{6L} \beta^3 + \frac{1}{2} \left( \frac{d^2}{dt^2} + \frac{g}{L} \right) \beta \alpha^2 = 0 \quad (3.25b)$$

The angle  $\gamma$  has been eliminated in these equations by using the trigonometric relation  $\sin^2 \gamma = \sin^2 \alpha + \sin^2 \beta$ .

The equations clearly have a solution  $\beta = 0$  that corresponds to planar but nonlinear motion. It can be shown that they also have a nonlinear solution in which the pendulum executes a rotation about the  $z$ -axis, and other solutions as well. These solutions represent stable solutions only for certain ranges of the parameters. The stability properties of the solutions can be found by introducing a small perturbation and determining the conditions for which the perturbations grow or decay in time. The results can be described in terms of a dimensionless frequency  $\mu = \epsilon^{-2/3} [(\omega^2 - \omega_1^2) / \omega_1^2]$ . FREED [1957] and MILES [1962] have shown that the motions and their stability depend on  $\mu$  as follows:

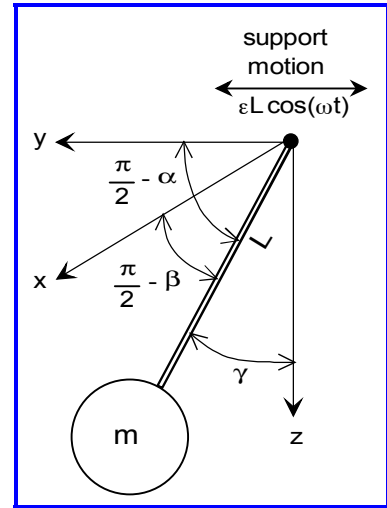


Figure 3.12. Conical pendulum analogy for rotary sloshing

1. Simple harmonic planar motion is stable in the frequency ranges  $\mu < -0.945$  and  $\mu > 0.757$ ; these solutions are analogous to the usual antisymmetric slosh wave with a fixed nodal line.
2. Simple harmonic nonplanar motion is stable in a frequency band just above the natural frequency  $0.154 < \mu < 0.757$ ; this solution is analogous to rotary sloshing in which the nodal line of the antisymmetric slosh wave rotates around the vertical axis of the tank.
3. Simple harmonic motions in which the plane of the pendulum motion oscillates are stable in a narrow frequency band around the natural frequency  $-0.945 < \mu < 0.154$ ; this solution corresponds to a to-and-fro swirling oscillation of the nodal line of the antisymmetric slosh wave about the vertical axis of the tank.

For frequencies such that  $\mu > 0.757$ , both planar and nonplanar (rotational) motions are stable. Which form of solution occurs (or which form of sloshing occurs) depends on whether there is any initial nonplanar motion (initial rotation of the liquid).

Figure 3.13 shows a comparison of the predictions of the model to experimental results [BERLOT, 1959]. The lower frequency boundary, above which the slosh wave nodal line oscillates to and fro, is predicted fairly well. However, the higher frequency boundary, which is the upper frequency for which a rotary slosh wave can occur even when there is no initial rotation, is only predicted well for small amplitude motions. Later experiments [ABRAMSON, ET AL, 1966] showed that the upper boundary is very sensitive to slight imperfections in the tank shape or excitation direction; when considerable care was taken to eliminate the imperfections, the experimental data was much closer to the conical pendulum predictions.

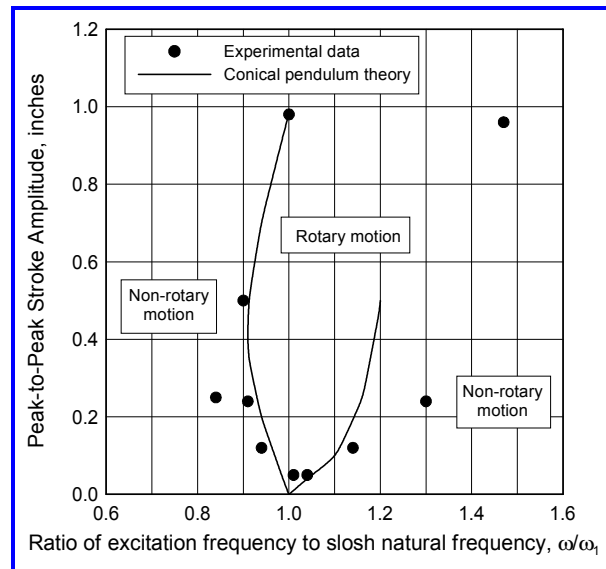


Figure 3.13. Comparison of experimental and conical pendulum boundaries for rotary sloshing.

KANA [1989] has shown that when the equations of the pendulum are solved without replacing the sines and cosines by the first few terms in their series expansions, the results agree well with experiments not only with respect to the regions of stability but also with respect to the force and moment magnitudes and phase angles. More complete analyses of the motions of type 3 above have revealed that they are essentially chaotic [MILES, 1984; KANA AND FOX, 1995].

**Large amplitude sloshing.** It is sometimes possible to develop a mechanical model for large amplitude sloshing by comparing the equations of motion of the hypothesized model to the force and torque expressions resulting from the relevant nonlinear slosh analysis or experiment. This procedure is similar to that described previously for linear sloshing. Since an analytical solution of the nonlinear equations of motion of sloshing is generally not available, the slosh forces and torques have to be predicted numerically by a computational fluid dynamics (CFD) simulation. The parameters of a hypothesized mechanical model are determined by a curve-fitting or other error minimization procedure but only for the tank fill levels and excitations conditions utilized in the CFD simulation. An example of this procedure is discussed below.

The CASSINI spacecraft mission has long periods of coasting in zero-g between intermittent firing of the course correction engines. During the coasting, the propellants in the tanks can easily accumulate in

### 3. MECHANICAL MODELS OF SLOSHING

locations that are not in contact with the tank outlets. If this were to occur, the engines could not be fired since there would be no propellant to feed them. Consequently, before each engine firing, small thrusters are fired to create a small gravity-like acceleration aligned with the vertical axis of the tanks to “settle” the propellants over the tank outlets; the thrusters are powered by hydrazine contained in a separate smaller tank that uses propellant management devices to ensure that hydrazine is available when needed. During the settling, the propellants move bodily in the tanks, and the resulting forces and torques needed to be accounted for in the control scheme. For that purpose, an equivalent mechanical model of the large amplitude motions was required.

The CASSINI tanks are spherical, so the torques exerted by the liquid about the center of the tank are negligibly small regardless of the amplitude of the motion. A CFD code was used to predict the propellant motion and the axial and lateral forces, for several fill levels (corresponding to the fill levels at the main course corrections) and thrust levels [DODGE AND GREEN, 1992; ENRIGHT AND WONG, 1994]. *Figure 3.14* illustrates typical liquid motions computed as a function of time, in a cross section through the center of the tank; the motions are three-dimensional, but because of symmetry, the motions in this cross section lie entirely in this plane. For clarity, only a few of the CFD velocity vectors are shown. A worst case initial condition was assumed in which the liquid was at the end of the tank opposite the outlet and slightly off center so that the liquid would roll around the tank when the settling acceleration was applied. (The initial configuration of the liquid does not conform to the correct zero-g surface tension configuration of a spherical gas bubble. In fact, at the time of the study, no CFD code could simulate the effects of surface tension accurately during a large amplitude motion. In any case, the liquid inertia forces are so large that surface tension forces are insignificant after a very brief time.)

*Figure 3.15* shows a model that was hypothesized to represent the sloshing dynamics. Since, as was shown by the CFD results, much of the liquid rotates during the settling, the effective moment of inertia of the rotating liquid tends to retard the settling. For that reason, the moving mass  $m_s$  (rather than the fixed mass) was assigned a moment of inertia  $I_s$ . The pendulum hinge point was connected to the tank by an angular dashpot  $C_s$  (not shown in the figure) to provide damping and to allow the liquid to settle.

The Equations of motion for the pendulum model are:

$$(m_s L_s^2 + I_s) \ddot{\theta} + C_s \dot{\theta} = a L_s \sin \theta \quad (3.26a)$$

$$F_{axial} = m_s (a - L_s \dot{\theta}^2 \cos \theta + L_s \ddot{\theta} \sin \theta) + m_0 a \quad (3.26b)$$

$$F_{transverse} = -m_s (L_s \ddot{\theta} \cos \theta - L_s \dot{\theta}^2 \sin \theta) \quad (3.26c)$$

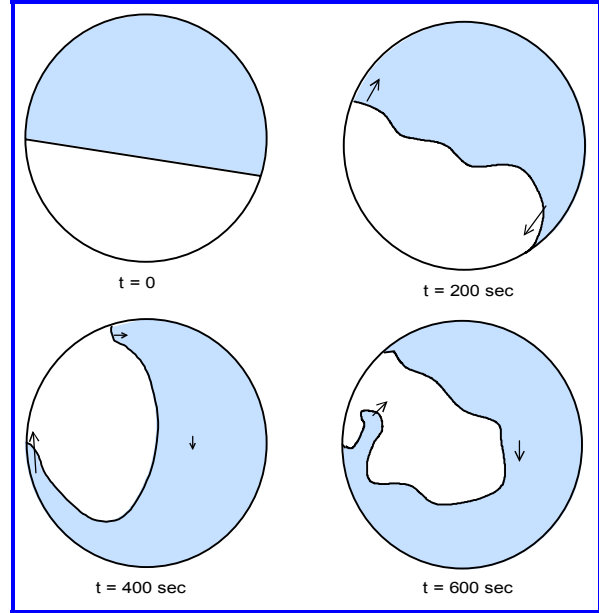


**Figure 3.14.** CFD simulation of liquid motion in a 60% full 1.56 m diameter spherical tank after a settling acceleration of  $3.27 \times 10^{-6} g_0$  is applied.

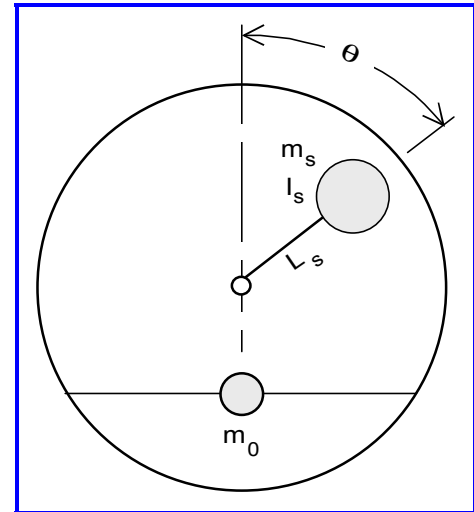


**Figure 3.15.** Hypothesized mechanical model of large amplitude sloshing.

where  $a$  is the applied settling acceleration. These equations were integrated numerically in time for each case. The pendulum angle  $\theta$  was assumed to correspond roughly to the space-average inclination of the liquid surface shown in *Figure 3.14*. The parameters of the model were determined by trial-and-error by comparing the model predictions to the CFD-computed forces and average inclination of the free surface, as a function of time, and adjusting the parameters until an acceptable correlation resulted. The pendulum mass was found to be very close to 100% of the total liquid mass except for nearly full tanks; thus the pendulum mass was somewhat larger than would be the case for the slosh mass of ordinary linear sloshing. *Figure 3.16*

compares the model to the CFD results. The mechanical model predicts the overall features of the CFD simulation and gives a reasonable estimate of the forces as a function of time, but there are some discrepancies. Better results could have been obtained by allowing the pendulum mass and pendulum length to be a function of angular position, but this complication would have negated the simplicity which is the main benefit of a mechanical model. There is no mathematical assurance in any case that a lumped parameter model can duplicate the computed nonlinear liquid motions.

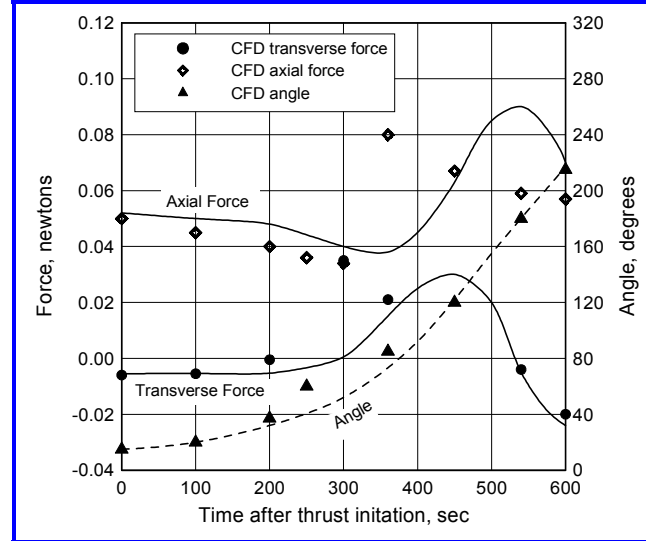


**Figure 3.16.** Comparison of mechanical model and CFD results for a 60% full nitrogen tetroxide tank

### 3.7 References

- ABRAMSON, H. N., CHU, W.-H., AND RANSLEBEN, G. E., Jr., 1961, *Representation of Fuel Sloshing in Cylindrical Tanks by an Equivalent Mechanical Model*, **ARS J.**, **31**, pp. 1697-1705.
- ABRAMSON, H. N., CHU, W.-H., GARZA, L. R., AND RANSLEBEN, G. E., Jr., 1962, *Some Studies of Liquid Rotation and Vortexing in Rocket Propellant Tanks*, NASA TN D-1212.
- ABRAMSON, H. N., CHU, W.-H., AND KANA, D. D., 1966, *Some Studies of Nonlinear Lateral Sloshing in Rigid Containers*, **Trans, ASME, J. Applied Mech.**, **33**, no. 4.
- BAUER, H. F., 1964, *Fluid Oscillations in the Containers of a Space Vehicle and Their Influence on Stability*. NASA TR-R-187.
- BERLOT, R. R., 1959, *Production of Rotation in a Confined Liquid Through Translational Motion of the Boundaries*, **Trans. ASME, J. Applied Mechanics**, **26**, pp. 513-516.
- DODGE, F. T., AND GARZA, L. R., 1969, *Equivalent Mechanical Model of Propellant Sloshing in the Workshop Configuration of the SATURN S-IVB*, Final Report, SwRI Project 02-2397, Contract NAS8-21478.
- DODGE, F. T., AND GREEN, S. T., 1992, *Propellant Motion Models for the CRAF/CASSINI Spacecraft*, Final Report, SwRI Project 04-4262, JPL Contract 959045.
- ENRIGHT, P. J., AND WONG, E. C., *Propellant Slosh Models for the CASSINI Spacecraft*, AIAA Paper 94-3730.
- FREED, L. E., 1957, *Stability of Motion of Conical Pendulums*, Report GM-45 3-437, Ramo Wooldridge Co.

- HUTTON, R. E., 1963, *An Investigation of Resonant, Nonlinear Nonplanar Free Surface Oscillations of a Fluid*, NASA TN D-1870.
- KANA, D. D., AND DODGE, F. T., 1979, *Preliminary Study of Liquid Slosh in the Tracking and Data Relay Satellite Hydrazine Tanks*, Final Report., SwRI Project 02-5887, Contract NAS5-25782.
- KANA, D. D., AND DODGE, F. T., 1981, *Study of Liquid Slosh in the Tracking and Data Relay Satellite Hydrazine Tanks*, Final Report, SwRI Project02-6539, Contract NAS-5-26482.
- KANA, D. D., DODGE, F. T., AND PITMAN, F. R., 1987, *Extended Study of Liquid Slosh in the Tracking and Data Relay Satellite Hydrazine Tanks*, Final Report, SwRI Project 06-1551, Contract 86HJ-WE-904850V
- KANA, D. D., 1989, *Validated Spherical Pendulum Model for Rotary Slosh*, **AIAA J. Spacecraft and Rockets**, **26**, pp. 188-195.
- KANA, D. D., AND FOX, D. J., 1995, *Distinguishing the Transition to Chaos in a Spherical Pendulum*, **Chaos**, **5**, pp. 298-310.
- LAWRENCE, H. R., WANG, C. J., AND REDDY, R. B., 1958, *Variational Solution of Fuel Sloshing Modes*, **Jet Propulsion**, **28**, pp. 729-736.
- LOMEN, D. O., 1965a, *Liquid Propellant Sloshing in Mobile Tanks of Arbitrary Shape*, NASA CR-222.
- LOMEN, D. O., 1965b, *Digital Analysis of Liquid Propellant Sloshing in Mobile Tanks with Rotational Symmetry*, NASA CR-230.
- MILES, J. W., 1984, *Stability of Forced Oscillations of a Spherical Pendulum*, **Quart. Appl. Mech.**, **20**, pp. 21-32.
- OKHOTSIMSKII, D., 1960, *Theory of the Motion of a Body with Cavities Partially Filled with a Liquid*, NASA TT F-33.
- SUMNER, I. E., STOFAN, A. J., AND SHRAMO, D. J., 1964, *Experimental Sloshing Characteristics and a Mechanical Analogy of Liquid Sloshing in a Scale-Model CENTAUR Liquid Oxygen Tank*, NASA TM X-999.
- UNRUH, J. F., KANA, D. D., DODGE, F. T., AND FEY, T. A., 1986, *Digital Data Analysis Techniques for Extraction of Slosh Model Parameters*, **AIAA J. Spacecraft and Rockets**, **23**, pp. 171-177.
- ZHUKOVSKII, N. E., 1936, *On the Motion of a Rigid Body Having Cavities Filled with a Homogeneous Liquid*, **Collected Works**, vol. 3.

## APPENDIX SLOSH code theory and numerics

The **SLOSH** code is a numerical implementation of the theory developed in NASA CR-222 and NASA CR-230 [LOMEN, 1965a, 1965b]. The code computes the parameters of the first two slosh modes for any axisymmetric tank shape and fill level, including tanks for which the free surface does not extend to the tank symmetry axis (e.g., a toroidal tank). The user describes the tank profile in the code by approximating it as a series of straight lines, circular arcs, and elliptical arcs. Damping is computed by one of the correlations described in Chapter 2; the user must choose a tank shape for which a damping correlation is available that best approximates the actual tank shape. Ring baffles are allowed. The output of the code includes the load on ring baffles and the slosh pressures on the tank walls (inner and outer, as appropriate.)

In the following development, the liquid volume of the axisymmetric tank is  $V$ . The free surface area is  $S_f$ . The height of the free surface above the tank bottom is  $H$ . The acceleration of gravity is  $g$ . The distance from the tank axis to the tank wall measured at the free surface elevation is  $a$ ; when the free surface intersects the tank centerline,  $a$  is also the radius to the tank wall at the free surface elevation.

The velocity potential of the sloshing is assumed to be of the form  $\Phi(r,z)\cos\theta$ , because only  $\cos\theta$  modes exert a net force or torque on the tank.  $\Phi$  is assumed to vary harmonically in time with frequency  $\omega$ . The natural frequencies  $\omega_n$  are computed by minimizing the following expression [LAWRENCE, ET AL, 1958]:

$$I(\Phi) = \iint_V \left\{ \left( \frac{\partial \Phi}{\partial r} \right)^2 + \left( \frac{\Phi}{r} \right)^2 + \left( \frac{\partial \Phi}{\partial z} \right)^2 \right\} r dr dz - \frac{\omega^2}{g} \int_{S_f} (\Phi)^2 r dr \quad (\text{A.1})$$

where the first (volume) integral is the sloshing kinetic energy and the second (area) integral is the sloshing gravitational potential energy<sup>9</sup>. The value of  $\omega$  that minimizes  $I(\Phi)$  (i.e., makes it equal to zero) therefore makes the amplitude of the potential energy equal to the amplitude of the kinetic energy, which it must be for any vibrating mechanical system without dissipation; this value of  $\omega$  is therefore the slosh natural frequency. The potentials used in Eq. (A.1) are solutions of the conservation of mass relation  $\nabla^2 \Phi = 0$ . To carry out the minimization numerically, the solutions are assumed to be “deep tank” and “shallow tank” functions and the potential is expressed as a series of these fundamental solutions:<sup>10</sup>

$$\Phi(r,z) = \sum_{n=1}^N C_n \phi_n(r,z) \quad (\text{A.2})$$

where:

$$\phi_n = R^{2n-1} \quad \text{for } n = 1, 2, \dots, M < N \quad (\text{shallow tank functions}) \quad (\text{A.3})$$

$$\phi_n = J_1(\beta_n r) e^{-\beta_n(H-z)} \quad \text{for } n = M + 1, \dots, N \quad (\text{deep tank functions}) \quad (\text{A.4})$$

Here,  $J_1$  are Bessel functions of the first kind of order one, and  $\beta_n = 1.841, 5.331, \dots$  are the roots of  $dJ_1(r)/dr = 0$ . Five terms of each kind (i.e.,  $M = 5, N = 10$ ) are sufficient for excellent convergence. Putting this series expansion for  $\Phi$  into the integrals and performing the minimization (with respect to the  $C_n$ ) gives a typical matrix eigenvalue problem. Nondimensional variables are used in the results below:  $R = r/a$ ;  $Z = z/a$ , and  $\Phi$  and  $\phi_n$  are nondimensional as well. The eigenvalue problem is written as:

$$\sum_{n=1}^{10} (A_{mn} - \lambda B_{mn}) C_n = 0 \quad m = 1, 2, 3, \dots, 10 \quad (\text{A.5})$$

where

<sup>9</sup> The gravitational potential energy is  $\rho g \iint \eta^2 dS_f$  but the wave height  $\eta$  is equal to  $[\partial \Phi / \partial t] / g = \omega \Phi / g$ , from the free surface boundary condition, with  $\Phi$  evaluated on the free surface.

<sup>10</sup> When the liquid depth is small compared to the tank diameter, the “shallow tank” potential is independent of the axial coordinate. When the liquid depth is large compared to the tank diameter, the “deep tank” potential does not depend on the bottom contour.

$$A_{mn} = \iiint_V \left[ \frac{\partial \phi_m}{\partial R} \frac{\partial \phi_n}{\partial R} + \frac{\phi_m \phi_n}{R^2} + \frac{\partial \phi_m}{\partial Z} \frac{\partial \phi_n}{\partial Z} \right] R dR dZ \quad (\text{A.6})$$

$$B_{mn} = \int_{S_f} \phi_m \phi_n R dR \quad (\text{A.7})$$

$$\lambda = a\omega^2/g \quad (\text{A.8})$$

The  $A_{mn}$  integral is taken over the volume of the liquid and the  $B_{mn}$  integral is taken over the free surface. As was mentioned earlier, the free surface does not have to extend all the way to the tank axis; for example, a toroidal tank or an annular tank is allowed, or whatever, so long as the shape is axisymmetric.

The  $n^{\text{th}}$  slosh mode potential is expressed in terms of the  $C_k$  obtained from the matrix eigenvalue solution for that mode:

$$\Phi^{(n)} = \sum_{k=1}^{10} C_k^{(n)} \phi_k(r, z) \quad (\text{A.9})$$

where the superscript  $\langle n \rangle$  indicates that the  $C_k$  for the  $n^{\text{th}}$  mode are selected.

The dimensional length of the pendulum for the  $n^{\text{th}}$  slosh mode is given by:

$$L_n = \frac{a}{\lambda_n} \quad (\text{A.10})$$

The slosh mass and pendulum hinge point are found by comparing the mechanical model force and torque to the slosh force and torque, which are computed from the pressure integrated over the tank walls. The pressure integrals are transformed using Green-like theorems so the computer code can use integrals that are already available from the eigenvalue problem. The intermediate steps are complicated and omitted here. The results are summarized below. The  $n^{\text{th}}$  slosh mass is given by:

$$M_n = M \gamma_n b_n^2 \lambda_n (H/a) \quad (\text{A.11})$$

where  $M$  is the liquid mass. The  $b_n$  parameter is defined as:

$$b_n = \frac{\pi}{V \gamma_n} \int R^2 \Phi^{(n)} dR = \frac{\pi}{V \gamma_n} \sum_{k=1}^N C_k^{(n)} R^2 \phi_k dR = \frac{\pi a^3}{V \gamma_n} \sum_{k=1}^{10} C_k^{(n)} B_{1k} \quad (\text{A.12})$$

The integral is taken over the free surface and uses the fact that  $\phi_1 = R$  to write the integral in terms of  $B_{1k}$ . The  $\gamma_n$  parameter is also given by an integral over the free surface:

$$\gamma_n = \frac{H}{V} \int \left( \Phi^{(n)} \right)^2 dR = \frac{\pi H a^2}{V} \sum_{k=1}^{10} \sum_{j=1}^{10} C_k^{(n)} C_j^{(n)} B_{kj} \quad (\text{A.13})$$

The dimensional height of the slosh mass pendulum hinge point above the bottom of the tank is given by:

$$H_n = -H + \frac{a}{\lambda_n} \left( 1 + 2 \frac{b_n}{h_n} \right) \quad (\text{A.14})$$

Here the  $h_n$  parameter is given by:

$$h_n = \frac{2a\pi}{HV\lambda_n} \int ZR\Phi^{(n)} dZ = \frac{2\pi a^4}{V\gamma_n\lambda_n H} \sum_{k=1}^{10} C_k^{(n)} \bar{h}_k \quad (\text{A.15})$$

where

$$\bar{h}_k = \int ZR\phi_k dZ \quad (\text{A.16})$$

and the integrals are evaluated over the wet wall (i.e.,  $R$  and  $Z$  on the wet wall).

The ratio of the slosh mass amplitude to the actual wave height amplitude at the tank wall is needed to compute the slosh pressure on the wall and other items of interest. It is computed in the computer program by equating the shift in the center of mass for the model to the shift in the center of mass for the liquid. For the sloshing liquid, the shift in the center of the mass for the  $n^{\text{th}}$  mode is determined by the wave height  $\eta_n = \eta_{0n} \Phi^{(n)} \cos\theta / [\Phi^{(n)}(a)]$  where  $\eta_{0n}$  is the wave height at the wall and  $\Phi^{(n)}(a)$  is the potential of the  $n^{\text{th}}$  mode evaluated at the free surface elevation at the wall. The dimensional  $x$ -direction shift in the liquid center of mass is therefore:

$$x_n = \frac{a^3}{V} \int_0^{2\pi} \int_0^a (R \cos\theta) \eta_0 \frac{\Phi^{(n)}}{\Phi^{(n)}(a)} \cos\theta (R d\theta) dR = \frac{\pi a^3 \eta_0}{V \Phi^{(n)}(a)} \int R^2 \Phi^{(n)} dR \quad (\text{A.17})$$

where the  $R$ -integral extends over the radial extent of the free surface. For the mechanical model, the  $x$ -direction shift in the center of mass is just the deflection  $x_n$  of the slosh mass times the ratio of the slosh mass to the total mass. Thus, the ratio of the wave amplitude to the slosh mass amplitude is:

$$\frac{\eta_{0n}}{x_n} = \frac{V \Phi^{(n)}(a)}{\pi a^3 \int R^2 \Phi^{(n)} dR} \left( \frac{m_n}{M} \right) \quad (\text{A.18})$$

The  $R$ -integral is equal to  $(V\gamma_n/\pi)b_n$  where  $\gamma_n$  and  $b_n$  are given above. Thus, after substituting in the relation for the slosh mass, the ratio of slosh wave amplitude to slosh mass amplitude can be written as:

$$\frac{\eta_{0n}}{x_n} = [\Phi^{(n)}(a)] b_n \lambda_n \frac{H}{a} \quad (\text{A.19})$$

Equation (A.19) is used in the code but the same result can be obtained by equating the dynamic forces exerted on the tank by the sloshing liquid and the slosh mass.

The pressure is equal to  $\rho A_0 [\partial \Phi_n / \partial t]$  where  $A_0$  is the amplitude of the potential. Given a slosh wave amplitude, the amplitude of the potential is equal to  $A_0 = g\eta_0/\omega_n \Phi_n(a)$ , from the free surface boundary condition. Hence the pressure exerted on the wall is equal to

### 3. MECHANICAL MODELS OF SLOSHING

---

$$p_n = \rho g \eta_{0n} \frac{\Phi_{wall}^{(n)}}{\Phi^{(n)}(a)} = \rho x_n \left( \frac{\eta_{0n}}{x_n} \right) \frac{\Phi_{wall}^{(n)}}{\Phi^{(n)}(a)} \quad (3.A20)$$

It might be noticed that  $\rho g \eta_0$  is the pressure on the wall at the free surface elevation, so the ratio of potentials in this expression merely indicates how the slosh pressure decays with depth.

Calculating the rigid body moment of inertia exactly is extremely complicated. The computer code approximates this moment of inertia by assuming it is the same as if the liquid were frozen, which is a geometric calculation.

The other parts of computer program are routines to obtain the input data that describe the tank shape, checking that the input is correct by drawing a picture of the tank on the screen as the input is given, and printing the computed results. Matrix manipulation subroutines are included as part of the program. Simpson's rule is used to perform the numerical integration.

# FLUID MANAGEMENT IN MICROGRAVITY

This chapter is a substantial revision and expansion of Chapter 10 “Liquid Propellant Behavior at Low and Zero-G” of NASA SP-106. The original authors were WILLIAM C. REYNOLDS and HUGH M. SATTERLEE.

## 4.1 Hydrostatics and Hydrodynamics in Zero or Microgravity

The previous chapters dealt with liquid motions for conditions when a large body force (gravitational or equivalent acceleration) acted on the liquid. When the body force becomes small – such as in the absence of gravity – other small forces come into play that affect the statics and dynamics of the liquid. The most important of these is usually the *surface tension* force at the free surface. Surface forces are sometimes called capillary forces, and surface phenomena are sometimes called capillarity. This chapter discusses the important effects of capillarity on fluid dynamics in low gravity.

**Meaning of the term zero-gravity.** A spacecraft would have to be billions of miles away from any massive body such as the earth to be in a location where all gravitational fields are absent. Most orbiting satellites and spacecraft are therefore not in a location of zero gravity (e.g., at a distance of 1000 miles above the earth, the gravitational acceleration is still 64% of earth’s surface  $g_0$ ). Nonetheless there are conditions where the dynamics of a liquid particle in a gravitational field can be treated as if the particle were in a zero-gravity field – which is the common meaning of the term *zero-g*. One example is a spacecraft in orbit around the earth. The acceleration  $a_V$  of the spacecraft in the direction toward the center of the earth is exactly equal to the acceleration of gravity  $g$  at the orbiting altitude. The force exerted on a particle of mass  $M$  in the vehicle can be expressed as the sum of two forces, the weight of the particle  $Mg$  and any other force  $F$ :

$$\mathbf{F} + M\mathbf{g} = M(\mathbf{a}_{\text{rel}} + \mathbf{a}_V) \quad \text{or} \quad \mathbf{F} = M\mathbf{a}_{\text{rel}}$$

where  $\mathbf{a}_{\text{rel}}$  is the relative acceleration. The force balance shows that the dynamics of the particle relative to the vehicle is identical to the dynamics of the particle in a zero-g environment, where the particle has no weight. For that reason, an apparent state of zero-g is also called a state of *weightlessness*.

The condition of weightless can be obtained for systems on earth by letting the system fall vertically downward, free of restraint, in a *drop tower*, or by containing the system in an airplane flying a *parabolic trajectory* such that the vertical acceleration of the airplane is equal to  $g_0$ , or by using some other method to cancel the gravitational body force such as magnetic effects [DODGE AND GARZA, 1972; SAWADA, ET AL, 1999]<sup>11</sup>.

For a spacecraft, the condition  $\mathbf{g} = \mathbf{a}_V$  is met exactly only at the center of mass of the vehicle and then only if there is no external drag on the vehicle. A vehicle in near earth orbit experiences a drag acceleration of the order of  $10^{-7}g_0$ . Furthermore, the earth’s gravitational acceleration varies across the radial width of the vehicle; in low earth orbit, this *gravity gradient* is of the order of  $10^{-7}g_0$  per meter. Consequently, for many space

<sup>11</sup> A solenoidal magnetic field is used to cancel the gravitational body force in a liquid that contains a colloidal dispersion of micron-size iron particles. The magnetic force is exerted only on the particles but the liquid clings to the particles. Small magnetic forces are introduced in transverse directions, so the zero-g simulation is not perfect.

missions, there is a residual effective gravity of about  $10^{-6}$  to  $10^{-8}g_0$  acting on systems within the spacecraft. For that reason, the environment in a spacecraft is generally referred to as a *micro-g* environment rather than as a *zero-g* environment.

### Surface tension and interface pressure jump

When a liquid has a free surface, the surface acts as if it were in a state of tension. The tension, which is the result of short-range molecular interactions, acts in the plane of the surface and is perpendicular to any line drawn in the surface. The force exerted per unit length of this line is called the *surface tension*, or more generally, the *interfacial tension*, and is denoted by the symbol  $\sigma$ .

Consider a section of a spherical free surface between a liquid and a gas, as shown in *Figure 4.1*. Since the interface has to be in equilibrium, the surface tension pulling on the interface has to be balanced by a pressure difference  $P_1 - P_0$  between the liquid and the gas pushing on the interface. The component of the surface tension force in the horizontal direction is  $\sigma[2R\pi\sin(\Delta\theta)]\sin(\Delta\theta)$ . The horizontal component of the pressure force is  $(P_1 - P_0)\pi[2R\sin(\Delta\theta)]^2$ . Since the two forces have to balance, the pressure difference has to be equal to:

$$P_1 - P_0 = \frac{2\sigma}{R} = \frac{4\sigma}{D} \quad (4.1)$$

where  $R$  is the radius of the spherical bubble and  $D$  its diameter. More generally, the interface curvature can vary from point to point, and the pressure difference is then:

$$P_1 - P_0 = \sigma \left( \frac{1}{r_1} + \frac{1}{r_2} \right) \quad (4.2)$$

where  $r_1$  and  $r_2$  are the principal radii of curvatures at the point. This relation forms the basis for the analysis of any hydrostatic interface in which capillary phenomena are important. *Equation (4.2)* is often called *Laplace's law*.

Surface tension is considered to be a thermodynamic property of the liquid and gas and is a function of temperature. The magnitude of surface tension decreases monotonically with temperature and becomes zero at the liquid's critical point temperature. The numerical value of  $\sigma$  is commonly cited for a liquid in contact with air but the same value applies with good accuracy for a liquid in contact with its vapor. During and shortly after the formation or destruction of new surface (for example, when the area of a surface increases during sloshing), the apparent surface tension can differ somewhat from the equilibrium value. This modified surface tension is called the *dynamic surface tension* [SCRIVEN, 1960]. Fortunately, dynamic effects are negligible for most liquids of interest in space applications.

**Contact angle.** Another important capillary property is the *contact angle*,  $\theta_c$ . The intersection of a liquid-gas interface with either a solid surface or another liquid forms three angles in a plane perpendicular to the three-phase line. The contact angle is a

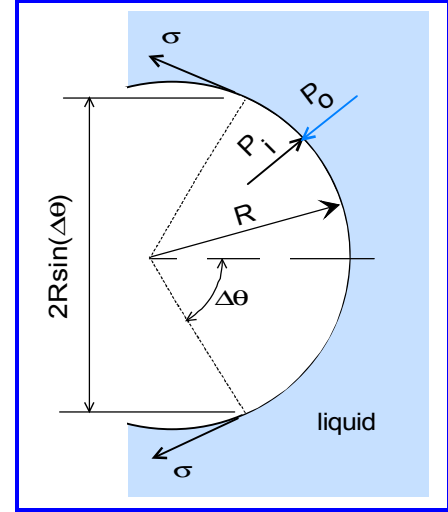


**Figure 4.1.** Pressure difference across a spherical liquid-gas interface

geometric description of the intersection. *Figure 4.2* shows several examples of such intersections. The contact angle is the angle measured within the liquid tangent to the liquid-gas interface at the contact line. The value of the contact angle is related to the relative magnitudes of microscopic adhesive and cohesive forces [BIKERMANN, 1958]. If the contact angle is less than  $90^\circ$ , the liquid is said to “wet” the solid; if the contact angle is greater than  $90^\circ$ , the liquid is said to be “non-wetting”; if the contact angle is exactly  $0^\circ$ , the liquid is said to be perfectly wetting. Both wetting and non-wetting liquids adhere to solid surfaces.

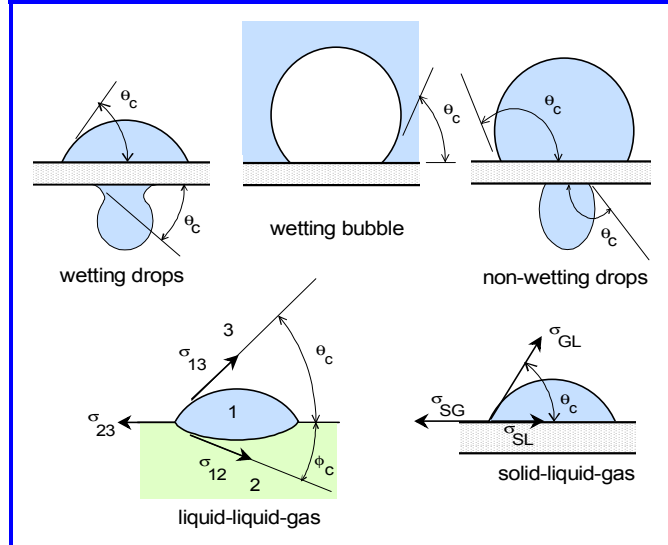


**Figure 4.2.** Various wetting and non-wetting contact angles.

Consider a liquid drop resting on the surface of another liquid, as shown in the bottom left illustration of *Figure 4.2*, with both liquids under a third liquid or gas. Subscripts are used to indicate the different surface tensions at the interfaces between each of the three fluids. Force equilibrium of the contact line requires:

$$\sigma_{23} = \sigma_{13} \cos \theta_c + \sigma_{12} \cos \phi_c \quad \text{and} \quad \sigma_{13} \sin \theta_c = \sigma_{12} \sin \phi_c \quad (4.3)$$

These relations among the various contact angles and surface tensions have been substantiated reasonably well by experiment.

Next, consider the intersection formed by a liquid, a gas, and a solid, as shown in the bottom right illustration of *Figure 4.2*. The condition of horizontal force equilibrium is satisfied by:

$$\sigma_{SG} = \sigma_{GL} \cos \theta_c + \sigma_{SL} \quad (4.4)$$

However, the condition of vertical equilibrium cannot be satisfied. Nevertheless, this picture of the interfacial force is commonly employed and justified on the basis of its analogy to Eq (4.3). Equation (4.4) is called Young’s equation. (There are obvious problems in measuring the surface tension between the gas and the solid and the liquid and the solid, but these tensions are conceptually similar to the surface tension between the gas and the liquid.) As is evident from Eqs. (4.3) and (4.4), the contact angle is a function of all three materials at the contact line, and in particular, it is *not* a property of only the gas and liquid.

Although surface tension does not change markedly when the interface is in motion, the contact angle may, and contact angle hysteresis and dynamic effects are common. If a little liquid is added to a drop on a solid surface, the area of the base of the drop does not change immediately but the drop merely changes shape and consequently the contact angle changes. After a period of growth, the base area suddenly expands in a jerky manner, and the contact angle obtains its previous value. The greatest angle measured during growth is termed the *advancing contact angle* and the smallest angle measured when liquid is removed is the *receding contact angle*. A similar effect is observed when the plate on which the drop is rested is tilted: the downhill angle is different than the uphill value. This *hysteresis* is also observed with a moving interface or even when the interface becomes contaminated with dust or other foreign materials. The angular amount of hysteresis is not large, and is practically non-existent for pure liquids on clean

surfaces [MICHAELS AND DEAN, 1961], including hydrocarbon propellants contained in clean metal tanks and liquids such as methanol that tend to clean tank walls. Conversely, water tends to exhibit a considerable amount of hysteresis, possibly because of the ease with which a water interface can be affected by contaminants [DODGE AND GARZA, 1967]. A contact line for which the contact angle remains reasonably constant during motion is called a *free contact line*; if the hysteresis is so large that the contact line does not appear to move when the surface moves, the contact line is similarly said to be *stuck*.

### Hydrostatic regimes

A simple estimate of the conditions for which surface tension is important can be obtained from the rise of liquid in a very small diameter (capillary) tube, as shown in *Figure 4.3*. The liquid is “sucked” up into the tube by the negative pressure created by surface tension. The pressure jump across the interface from Eq. (4.1) is  $P_\infty - P_2 = 2\sigma\cos\theta_c/r$ , assuming that the shape is approximately spherical with a radius of curvature of  $r/\cos\theta_c$ . The negative pressure balances the weight of the liquid column; that is,  $\rho gh = P_1 - P_2$ . Since  $P_1$  is equal to  $P_\infty$ , combining these two expressions gives:

$$h/r = 2\sigma/\rho gr^2 \quad (4.5)$$

The height of the column depends on  $\sigma$  and  $r$ . The dimensionless group  $\rho gr^2/\sigma$  (or sometimes  $\rho gd^2/\sigma$ ), in Eq. (4.5) is the *Bond number*,  $Bo$ ; it is a comparison of the relative magnitude of gravitational and capillary forces<sup>12</sup>.

The shape of an interface depends on the value of  $Bo$ . For  $Bo \gg 1$ , gravitational forces are dominant and the free surface is flat (except right at the wall where the contact angle condition must be satisfied) while for  $Bo \ll 1$ , capillary forces are dominant and the free surface will be highly curved (unless  $\theta_c = 90^\circ$  in which case it will be flat). For the special case  $Bo = 0$ , there are no gravitational forces and the shape is determined entirely by the contact angle.

An immediate application of these ideas is the positioning of liquid propellant in a space vehicle tank. Consider a cylindrical tank with a central tube as shown in *Figure 4.4*. By choosing the tube and tank radii properly, the propellant can be made to flow into the central tube when the vehicle enters zero-g. Neglecting the thickness of the tube wall and assuming  $\theta_c = 0^\circ$ , the pressures at the inner and outer interfaces are:

$$P_b = \frac{2\sigma}{r_i} - P_g \quad P_a = \frac{2\sigma}{r_o - r_i} - P_g \quad (4.6)$$

If  $P_b < P_a$ , liquid will flow into the inner tube. From Eq. (4.6), this happens when  $r_i < r_o/2$ . Equation (4.6) has been

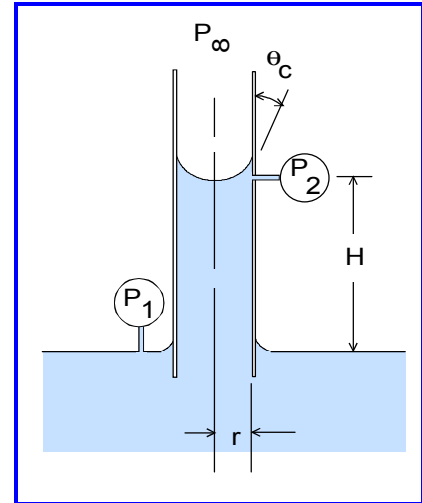


Figure 4.3. Capillary action in a tube

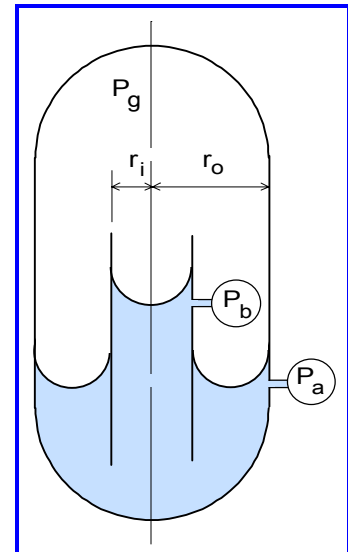


Figure 4.4. Parallel interfaces in a tank

<sup>12</sup> Named after *W. N. Bond*, who did research at least as early as 1928 on the effects of surface tension on the rise rate of bubbles in tubes.

confirmed experimentally by drop tower experiments [PETRASH AND OTTO, 1964].

### Hydrodynamic regimes

The motion of a liquid-gas system can be influenced by capillary forces, body forces, inertia forces, and viscous forces. In some cases, all but one or two of the forces are small and can be neglected, and analyzing the motion is considerably simplified. Whether or not this is possible depends on the value of the dimensionless numbers that separate the hydrodynamic behavior into regimes.

The relative importance of inertial and capillary forces is indicated by the ratio:

$$We = \frac{\text{inertia}}{\text{capillary}} = \frac{\rho V^2 L}{\sigma} \quad (4.7a)$$

This is the *Weber* number, where  $L$  is a characteristic length of the system and  $V$  is a characteristic velocity. If  $We \gg 1$ , inertia forces dominate the behavior.

The relative importance of inertia and gravity (body) forces is indicated by:

$$Fr = \frac{\text{inertia}}{\text{gravity}} = \frac{V^2}{gL} \quad (4.7b)$$

This is the *Froude* number. When  $Fr \gg 1$ , inertia forces are dominant compared to gravity forces. The Froude number is also equal to the ratio of the Weber number and the Bond number,  $Fr = We/Bo$ . The flow regimes determined by  $We$ ,  $Fr$ , and  $Bo$  are shown schematically in *Figure 4.5*. In each case, the importance of viscous effects must be determined separately (for example, from the Reynolds number).

**Response time estimates.** Related to these dimensionless numbers is the time for a given dynamic response to occur. As a specific example, we will consider the slosh natural frequency. Chapter 1 demonstrated that under high-g conditions the slosh frequency  $\omega_n$  can be expressed as:

$$\omega_n^2 (L/g) = A \quad \text{for } Bo = 1 \quad (4.8a)$$

where  $A$  is a constant that depends only on fill level and tank shape. The left hand side of this equation is a form of Froude number. When  $g$  becomes small, Eq. (4.8a) predicts that  $\omega_n$  approaches zero. But when  $g$  is small, the flow regime is not dominated by gravity, so the Froude number is not the relevant dimensionless parameter. Instead, the flow regimes depends on capillary and inertial forces, and the Weber number is the relevant dimensionless number. Since the characteristic velocity is still  $L\omega_n$ , the relevant dimensionless form of the low-g natural frequency is therefore expressed as:

$$\omega_n^2 (\rho L^3 / \sigma) = B \quad \text{for } Bo = 1 \quad (4.8b)$$

where  $B$  can depend on tank shape and fill level. Since Eq. (4.8b) does not depend on  $g$ ,  $\omega_n$  does not necessarily go to zero in zero-g.

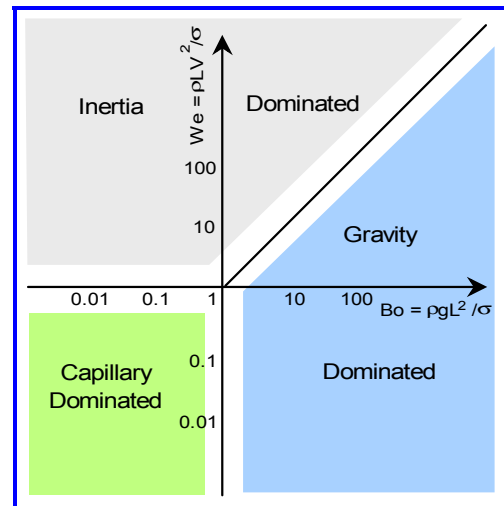


Figure 4.5. Hydrodynamic regimes

#### 4. FLUID MANAGEMENT IN MICROGRAVITY

Response times for other kinds of liquid motions can be estimated from the appropriate dimensionless numbers. The characteristic times are given by:

$$T = \sqrt{L/g} \quad \text{for the gravity - dominated regime} \quad (4.9a)$$

$$T = \sqrt{\rho L^3 / \sigma} \quad \text{for the capillary - dominated regime} \quad (4.9b)$$

These estimates are shown quantitatively in *Figure 4.6*. for a typical value of  $\sigma/\rho = 50 \text{ cm}^3/\text{sec}^2$ . The characteristic low-g time for a large tank can be several minutes in low-g.

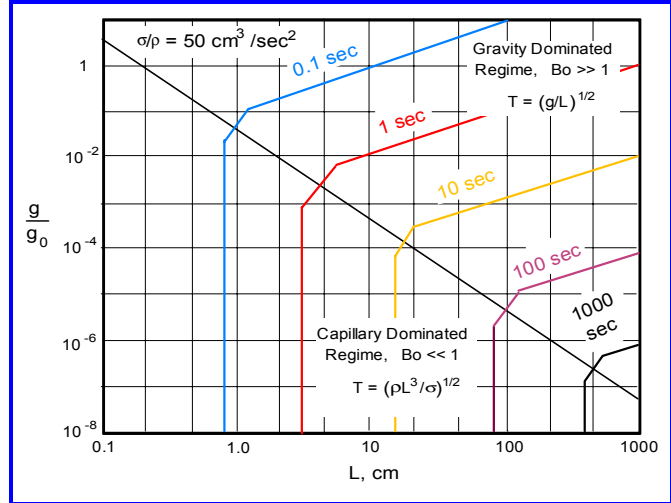


**Figure 4.6.** Hydrostatic regimes and characteristic response times

### 4.2 Thermodynamics of Capillary Systems

The thermodynamic relations that describe a capillary system are helpful in understanding the dynamics, equilibrium, and stability conditions of an interface in weightlessness [REYNOLDS, ET AL, 1964]. To derive these relations, we will consider the mechanical work done when a change is imposed on the interface area and the wetted area of a capillary system. The discussion is restricted to isothermal conditions; temperature effects are discussed in a later section.

Consider a section through the a liquid cylinder attached to two solid conical end pieces, as shown in *Figure 4.7*. We imagine that the cones are pulled apart a small distance  $\Delta x$ , while the

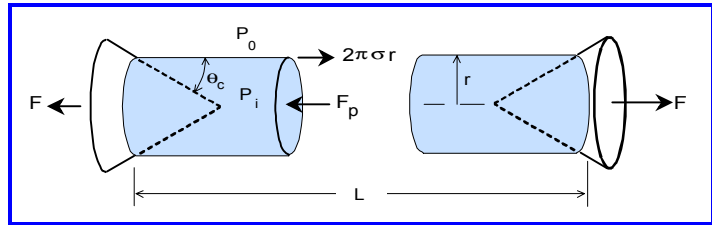


**Figure 4.7.** Computing the energy change in a capillary system

volume of liquid is kept constant and the shape remains cylindrical. The capillary pressure force  $F_p$  acting on the section is  $\pi r^2(P_i - P_0) = \pi r^2(\sigma/r) = \pi \sigma r$ . The surface tension force pulling on the section is  $2\pi \sigma r$ . Since these forces are not equal, an additional force  $F = 2\pi \sigma r - \pi \sigma r = \pi \sigma r$  has to be applied to maintain the initial separation. The work done when the cones are pulled apart is therefore  $(F + \Delta F)\Delta x \approx F\Delta x$ , after neglecting second order terms. The change in liquid volume (which is zero) is given by:

$$\Delta Vol = 2\pi r L \Delta r + \pi r^2 \Delta L - 2\pi \frac{r^2}{\tan \theta_c} \Delta r = 0 \quad \text{or} \quad \Delta L = -2\Delta r \left( \frac{L}{r} - \frac{1}{\tan \theta_c} \right) \quad (4.10a)$$

where  $\Delta r$  is positive when  $r$  decreases. From the geometry of the configuration, we find:

$$\Delta L = \Delta x + (2\Delta r / \tan \theta_c) \quad (4.10b)$$

The work done on the system can therefore be expressed as:

$$dW = F\Delta x = \pi\sigma r[\Delta L - (2\Delta r/\tan\theta_c)] \quad (4.10c)$$

The change in the area of the interface is  $\Delta A_i = 2\pi r\Delta L + 2\pi L\Delta r$ , and the change in the wetted area of the cone is  $\Delta A_{wet} = -4\pi r\Delta r/\sin\theta_c$ . By substituting Eq. (4.10a) into the expressions for these two areas, we find that  $\Delta A_i - \cos\theta_c\Delta A_{wet} = -2\pi L\Delta r$ . This last expression is also equal to  $\pi r\Delta L - 2\pi r\Delta r/\tan\theta_c$ . So, the work done on the system is:

$$\Delta W = \sigma(\Delta A_i - \cos\theta_c\Delta A_{wet}) \quad (4.11)$$

Equation (4.11) shows that work is done when there is a change of the interface areas.

The case of constant  $\theta_c$  is of the most interest. For that case, the *capillary area*  $A_c$  is defined as:

$$A_c = A_i - \cos\theta_c A_{wet} \quad (4.12)$$

Hence, the work depends on the change in the capillary area:

$$\Delta W = \sigma\Delta A_c \quad (4.13)$$

An energy balance on the system while the interface is being stretched gives:

$$\Delta U = \Delta Q + \Delta W \quad (4.14)$$

where  $\Delta U$  is the internal energy change of the system and  $\Delta Q$  is the heat transfer. Since the process is thermodynamically reversible,  $\Delta Q = T\Delta S$ , where  $\Delta S$  is the entropy change and  $T$  is the absolute temperature. Combining these relations with Eq. (4.11) gives:

$$T\Delta S = \Delta U - \sigma\Delta A_c \quad (4.15)$$

Now, consider a capillary system which reaches equilibrium with its environment without a work interaction, such as liquid in a tank in zero-g. Conservation of energy is simply  $\Delta U = \Delta Q$  and the second law of thermodynamics gives  $\Delta Q \leq T\Delta S$ , where  $T\Delta S$  is given by Eq. (4.15). Combining these relations gives:

$$\Delta A_c \leq 0 \quad (4.16)$$

This final result states the important conclusion that the equilibrium configuration in zero-g has the *minimum capillary area* of any possible configuration.

Figure 4.8 illustrates the conclusion derived from Eq. (4.16) for liquid in a cylindrical tank when  $\theta_c = 0^\circ$ . Both configurations have the same liquid volume. The configuration on the right has a hemispherical interface, and since  $\theta_c = 0^\circ$ , the radius of the hemisphere is the same as the tank radius. Thus, for this hemispherical interface configuration, the capillary area is equal to:

$$A_{c1} = A_i - \cos\theta_c A_{wet} = 2\pi R_0^2 - (\pi R_0^2 + 2\pi H R_0 + 2\pi R_0 R_0) = -\pi R_0^2 - 2\pi H R_0 \quad (4.17a)$$

The configuration on the left is similar to the normal high-g configuration. The interface is flat except for a negligibly-small region right at the wall where the surface curves upward to meet the contact angle condition. The liquid depth has increased by  $R_0/3$  for this configuration, compared to the hemispherical configuration, since the volumes are equal for both. The capillary area for the flat interface is:

$$A_{c2} = \pi R_0^2 - \left[ \pi R_0^2 + 2\pi H R_0 + 2\pi R_0 \left( \frac{1}{3} R_0 \right) \right] = -\frac{2}{3} \pi R_0^2 - 2\pi H R_0 \quad (4.17b)$$

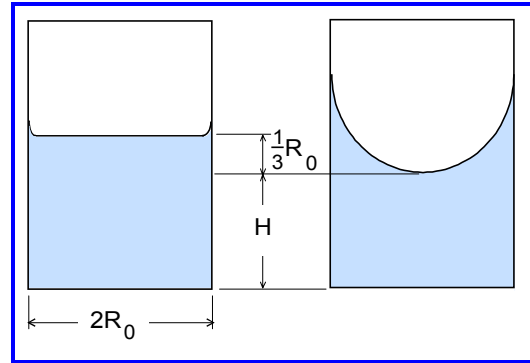


Figure 4.8. Two possible zero-g configurations of liquid in a cylindrical tank.

The capillary area for both configurations is negative, but the capillary area for the hemispherical interface is more negative; hence we can conclude that for  $\theta_c = 0^\circ$  the configuration with the spherical interface is the preferred one in zero-g. The preferred interface can be flat for some value of  $\theta_c$ ; for example, it would be flat in a cylindrical tank when  $\theta_c = 90^\circ$ .

The case when the gravitational force is not zero is analyzed similarly. The work done on a capillary system during a process when its center of mass is lifted by an amount  $\Delta h$  is  $\Delta W_g = Mg\Delta h$  where  $M$  is the liquid mass. By following the same procedure as before, it is found that the equilibrium configuration is such that:

$$\sigma\Delta A_c + Mg\Delta h \leq 0 \quad (4.18)$$

The term  $Mgh$  is the gravitational potential energy of the system. By analogy, the term  $\sigma A_c$  is called the capillary potential energy. Therefore, the equilibrium state is the state of *minimum total potential energy PE*, where:

$$PE = \sigma A_c + Mgh \quad (4.19)$$

This relation is the basis for determining low-g equilibrium capillary configurations as well as the stability of those configurations.

**Metastable configurations.** The previous thermodynamic analysis has proved that the stable equilibrium configuration of a capillary system in an isothermal zero-g environment is one for which the capillary potential energy  $PE = \sigma A_c$  has the smallest possible value. There may be, however, several other configurations for which the  $PE$  has a local minimum so that small perturbations also lead to an increase in the  $PE$ . All these states are metastable because for a sufficiently large disturbance the system will settle down in the configuration with the lowest of all values of  $PE$ . Nonetheless, the system may be trapped in one of the metastable states if there are no large disturbances.

**Non-isothermal conditions.** The preceding discussion considered only conditions for which the temperature of the capillary system was uniform. Since surface tension depends on temperature, additional phenomena need to be considered when the temperature is not the same throughout the system. Non-isothermal configurations will be discussed briefly later in this chapter.

#### Preferred configuration of drops and bubbles in zero-g

Consider a collection of bubbles in a zero-g liquid. Each bubble forms a sphere, because that is the configuration with the minimum  $A_c$  (and therefore minimum  $PE$ ) for each bubble. But if two or more bubbles collide with a sufficient velocity, the bubbles will coalesce into one larger bubble, because  $A_c$  of the combined bubble is less than the sum of the  $A_c$ 's of the individual bubbles. Thus, there is a tendency for all the bubbles to coalesce into one large bubble. We can conclude, therefore, that gas in a propellant tank in zero-g will tend to form one connected volume (a single ullage volume). Experiments have shown, however, that two or more large ullage bubbles can persist for considerable periods of time [DOMINICK AND DRISCOLL, 1993]. By the same reasoning, we can conclude that a collection of drops floating in the gas in a tank will tend to collect into one large connected body of liquid.

We can also show that a drop prefers to be attached to the wall of a tank, as was assumed in the illustrations shown previously in [Figure 4.2](#), rather than floating freely in the gas. The capillary area of the free drop is simply  $4\pi R^2$ , where  $R$  is the radius of the drop. The radius of the flattened spherical shape of the same drop attached to the wall is somewhat bigger than  $R$ . When we account for this change in radius and for the wetted

area of the wall under the wall-bound part of the drop, we find that the ratio of the two capillary areas is:

$$\frac{A_{c \text{ attached}}}{A_{c \text{ free}}} = \left[ \frac{1}{4} \left( 2 - 3\cos\theta_c + \cos^3\theta_c \right) \right]^{1/3} \quad (\text{drops}) \quad (4.20a)$$

This ratio is less than one for any value of  $\theta_c > 0^\circ$  and is equal to one for  $\theta_c = 0^\circ$  (for which the attached drop looks just like a free drop). Consequently, we can conclude that the drop attached to the wall is the preferred configuration because this configuration has the smaller capillary area.

For a gas bubble, we can make the same analysis with the same conclusion. For a bubble, it is more convenient, as shown in *Figure 4.2*, to define the capillary potential in terms of the *non-wetted* area. This change is allowed because a constant can always be added to the potential energy, since only changes in potential energy have meaning. If we add the product of the total wall area and the contact angle to the capillary potential area, and realize that the total area less the wetted area is the non-wet or *dry* area  $A_{dry}$ , we find that the capillary potential area is also equal to  $\sigma A_i + \sigma \cos\theta_c A_{dry}$ . Using this definition, analysis of the potential energies of a freely-floating bubble and the same bubble attached to the wall gives the ratio:

$$\frac{A_{c \text{ attached}}}{A_{c \text{ free}}} = \left[ \frac{1}{4} \left( 2 + 3\cos\theta_c - \cos^3\theta_c \right) \right]^{1/3} \quad (\text{bubbles}) \quad (4.20b)$$

This ratio is also always less than one.

To summarize, the preceding analyses prove that the most stable equilibrium configuration of liquid and gas in a tank has the liquid collected into a single mass, the gas collected into a single bubble, and both the liquid and the gas attached to the wall. Most of the illustrations in this chapter are drawn in accordance with these conclusions.

### 4.3 Axisymmetric Interface Shape

One of the fundamental problems of managing liquid in a tank in low gravity is to determine the shape and orientation of the liquid interface. Here, we will consider only axisymmetric tanks when the gravity vector is aligned with the axis of the tank. The shape of the equilibrium interface is then axisymmetric and can be derived from the preceding potential energy relations by expressing the capillary areas in terms of the coordinates. It is easier, however, to derive the governing differential equation directly from a force balance on the interface. Consider the infinitesimal annular ring cut from the interface shown in *Figure 4.9*. Surface tension pulls on the edges of the annular ring and the pressure difference between the gas and liquid pushes on it. The force balance in the vertical direction is:

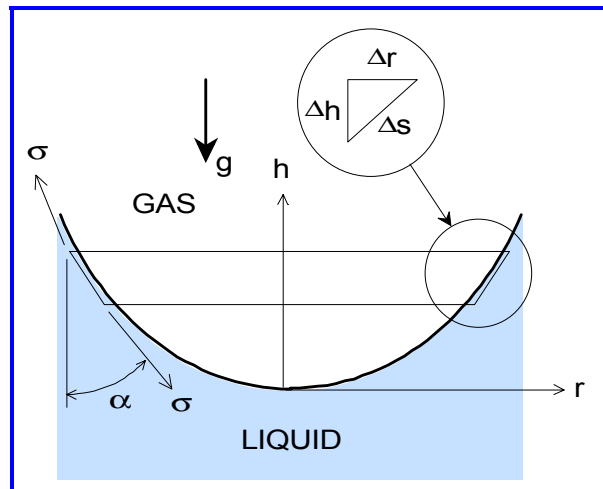


Figure 4.9. Force balance for an axisymmetric interface

$$-2\pi r\sigma \frac{\Delta h}{\Delta s} + 2\pi(r + \Delta r)\sigma \left[ \frac{\Delta h}{\Delta s} + \frac{d}{ds} \left( \frac{\Delta h}{\Delta s} \right) \Delta s \right] = (P_g - P_L)(2\pi r)\Delta r \quad (4.21a)$$

After combining terms and discarding second order infinitesimals, the force balance simplifies to:

$$\sigma \frac{d}{ds} \left( r \frac{dh}{ds} \right) = r(P_g - P_L) \frac{dr}{ds} \quad (4.21b)$$

As can be seen [Figure 4.9](#), the geometric condition  $(dh/ds)^2 + (dr/ds)^2 = 1$  also has to be satisfied in addition to the force balance.

The gas pressure in [Eq. \(4.21b\)](#) can reasonably be assumed to be constant but the liquid pressure  $P_L = P_{L0} - \rho gh$  is a function of elevation  $h$ , where  $P_{L0}$  is the (unknown) pressure just below the center  $r = 0$  of the interface. All these relations can be made dimensionless in terms of the tank characteristic length  $D$ , with the dimensionless symbols written as capital letters. We also need to define a dimensionless parameter  $\lambda$  based on the pressure  $P_{L0}$  by the relation  $\lambda = D(P_g - P_{L0})/\sigma$ , the value of which is unknown until the interface shape is determined. With these definitions, the shape of the interface is governed by the following two differential equations:

$$\frac{d}{dS} \left( R \frac{dH}{dS} \right) = R \frac{dR}{dS} (Bo + \lambda) \quad (4.22a)$$

$$\frac{dH}{dS} \frac{d^2 H}{dS^2} + \frac{dR}{dS} \frac{d^2 R}{dS^2} = 0 \quad (4.22b)$$

subject to the boundary conditions that:

$$R(0) = H(0) = \frac{dH(0)}{dS} = 0 \quad \text{and} \quad \frac{dR(0)}{dS} = 1 \quad (4.22c)$$

([Equation \(4.22b\)](#) was derived by differentiating the geometric condition  $(dh/ds)^2 + (dr/ds)^2 = 1$  with respect to  $s$ .) The Bond number  $Bo$  is here defined as  $\rho g D^2 / \sigma$ . (These equations can be expressed in terms of the radial coordinate  $r$  instead of arc length  $s$ , but doing so can cause difficulties if  $h$  is double valued for some values of  $r$ , which occurs when the interface is bent over in spheroidal tanks.)

[Equation \(4.22c\)](#) specifies four boundary conditions, which is appropriate for the two coupled second order differential equations given by [Eqs. \(4.22a\) and \(4.22b\)](#). However, the parameter  $\lambda$  in [Eq. \(4.22a\)](#) represents a fifth unknown, and in fact, there is a fifth boundary condition, namely that the interface slope  $\alpha$  at the tank wall has to correspond to the contact angle. In terms of the wall slope  $\alpha_w$  at the contact line, this condition is  $\theta_c = \alpha - \alpha_w$  (negative values of  $\alpha$  are used for convex interfaces). Furthermore, the axial location of the center of the interface  $h = 0$  is in effect a sixth unknown that must be chosen such that the liquid volume is equal to the prescribed volume. Although it is not difficult to integrate [Eqs. \(4.22a\) and \(4.22b\)](#) numerically, generally an iterative procedure is required to match the conditions imposed at the unknown elevation of the contact line at the wall.

An alternative method is to integrate the equations for a series of values of  $\lambda$ , which yield values of  $\alpha$  as byproducts, and cross plot the results [[REYNOLDS, ET AL, 1964](#)]. [Figures 4.10a](#) and [4.10b](#) show a set of such plots from which the parameters of a given interface can be determined. The sector volume  $V_s$  shown in [Figure 4.10a](#) is the volume

of revolution bounded by the interface and the plane of the contact line; likewise, the sector height  $H$  graphed in Figure 4.10b is the height of the sector volume from the center of the interface to the plane of the contact line.

Figure 4.11 illustrates how the plots can be used to determine the shape and location of the liquid interface for an example of a spherical tank. Assume that the Bond number has a value of two, the contact angle is  $20^\circ$ , and the tank is 33% full. After a few trial and error iterations that involve reading off values of the sector volume  $V_s$  and height  $H$  for assumed values of  $\alpha$ , we find that  $\beta = 100^\circ$ ,  $\alpha = 10^\circ$ ,  $H = 0.65R_0$ ,  $L = 1.17R_0$ , and  $R = 0.98R_0$ . Thus, for this fill level, the contact line is slightly above the center of the tank, and the middle of the interface is slightly below the center of the tank.

For axisymmetric tanks, approximate methods have been developed to predict the interface shape with good accuracy [SATTERLEE AND CHIN, 1965; CUTSHALL, ET AL, 1996]. These methods assume that the interface shape is an ellipsoid of revolution:

$$h = b \left[ 1 \pm \sqrt{1 - (r/a)^2} \right] \tag{4.23}$$

where, as before,  $h$  is the height of a point on the interface above the center of the interface;  $a$  is the semimajor axis of the ellipse;  $b$  is the semiminor axis; and the  $+$  sign is used for the upper half of the ellipse when the interface shape is bent over. To determine the  $a$  and  $b$  parameters of the ellipsoid, Eq. (4.23) is substituted into Eq. (4.22a) and evaluated at the contact line (for a non-bent over interface) or at  $r = a$  (for a bent over

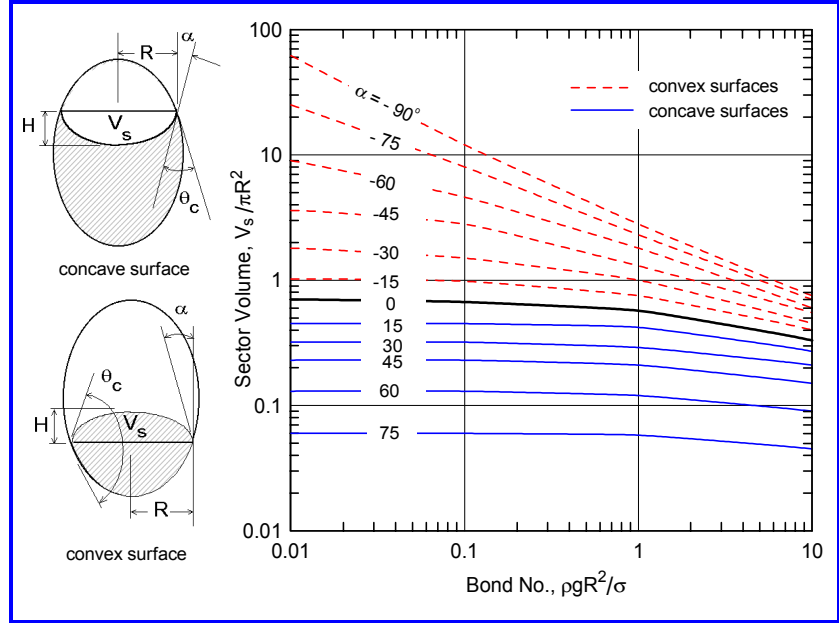


Figure 4.10a. Sector volume for axisymmetric interfaces

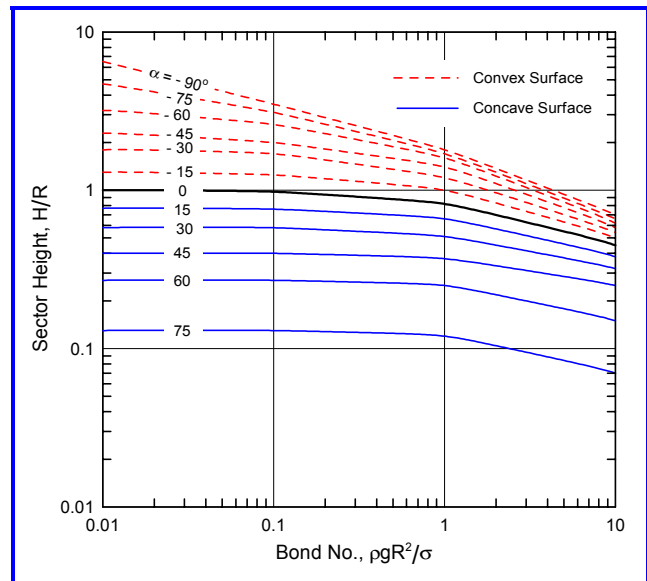


Figure 4.10b. Sector height for axisymmetric interfaces



## 4.4 Stability of Zero-G Interfaces

In zero-g, a liquid interface will hold its position and shape when the container is slowly inverted, because there are no external forces to cause the liquid to “fall”. The inversion may also be possible for some range of small but not exactly zero gravitational accelerations. The interface is said to be stable for this level of adverse acceleration; when the acceleration exceeds the critical value, the interface is unstable and the liquid will fall when the container is inverted. The magnitude of acceleration that must be imposed on the zero-g configuration to make the liquid in a tank “fall” to a position over the tank exit is important in space applications.

The concept of interface stability can be demonstrated with a mercury-in-glass thermometer. When the thermometer is held in any position, the interface is stable and the mercury does not run down the tube. But if the thermometer tube is too large, say, 3 cm in diameter, the mercury always falls when the thermometer is inverted. We expect, therefore, that there is a critical radius below which the interface is stable and above which it is unstable. Alternatively, for a given tube radius, there is a critical acceleration that can be imposed below which the interface is stable and above which it is unstable.

At first thought, we might attribute the support of the mercury in the upside down position to surface tension because the convex shape of the interface creates a force at the tube walls that opposes the weight of the liquid. However, a wetting liquid such as an alcohol-in-glass thermometer, which has a concave interface shape and for which surface tension exerts a force at the wall in the same direction as the weight, is also stable. In fact, it is the negative pressure (relative to atmospheric) at the top, closed end of the tube that supports the liquid weight in both cases. This can be demonstrated again by the common experience of sucking water into a drinking straw, capping one end of the straw with a finger, and turning the straw upside down. As long as the upper end of the straw is capped, the water remains in the straw. But when we uncap the straw, and release the negative pressure, the water runs out.

Interface stability can be analyzed in several ways. One can do a dynamic analysis of the liquid motion, and look for normal modes of oscillation that grow in amplitude with increasing time [CONCUS, 1963]. This method is difficult computationally, for although the problem might be linearized to investigate small perturbations, the domain in which the solution must be obtained is not simple. It is possible to show, however, that the stability limit obtained from the eigenvalue equation of the dynamic analysis is exactly the same as that obtained from the thermodynamic criterion discussed earlier, for which the marginal stability of the interface is determined statically [CONCUS, 1964]. The thermodynamic or static method is significantly easier analytically than the dynamic method and will therefore be used in the examples discussed below. The low-g sloshing analysis described later in this chapter will demonstrate that both methods give identical results.

### Axisymmetric interface example

To illustrate the thermodynamic criterion of marginal stability, we will carry out an analysis for the case of an axisymmetric interface in a cylindrical tank as shown in *Figure 4.13*. The contact angle is assumed to be equal to  $90^\circ$  so the zero-g equilibrium interface is flat. We want to determine the magnitude of an imposed gravitational acceleration  $g$

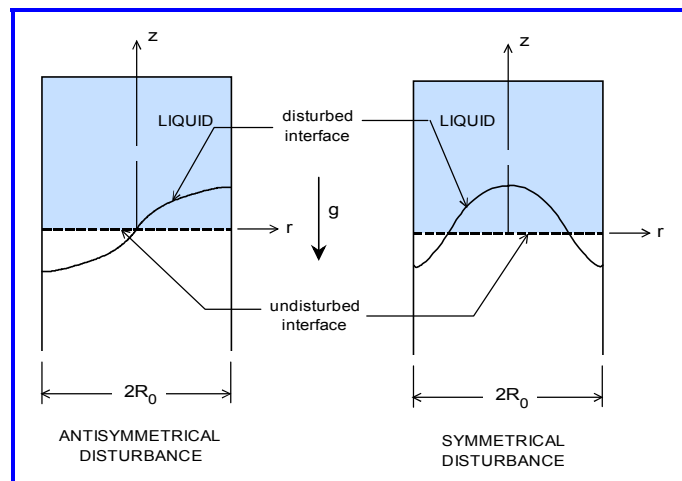


Figure 4.13. Stability of liquid in an inverted cylinder

that will de-stabilize the flat interface and cause the liquid to fall to the bottom of the tank. To use the thermodynamic criterion method, the area of the interface has to be computed for a small disturbance  $\delta z(r, \theta)$  of the flat interface, where  $\theta$  is the angular coordinate. The area  $A_i$  of the disturbed interface is given by:

$$A_i = \int_0^{R_0} \int_0^{2\pi} \sqrt{1 + \left(\frac{\partial \delta z}{\partial r}\right)^2} \sqrt{1 + \left(\frac{\partial \delta z}{r \partial \theta}\right)^2} r d\theta dr \quad (4.25)$$

Since  $\theta_c = 90^\circ$  for this example, the wetted area  $A_{wet}$  contribution to the capillary energy  $A_c$  in Eq. (4.19) falls out of the calculations. Further, since  $\delta z$  is a small perturbation, Eq. (4.25) can be simplified by retaining only the lowest order terms. The capillary potential energy is therefore:

$$PE_c \approx \sigma A_{i0} + \frac{\sigma}{2} \int_0^{R_0} \int_0^{2\pi} \left[ \left(\frac{\partial \delta z}{\partial r}\right)^2 + \left(\frac{\partial \delta z}{r \partial \theta}\right)^2 \right] r d\theta dr \quad (4.26a)$$

where  $A_{i0}$  is the area of the flat interface. The gravitational potential energy is given by:

$$PE_g = PE_0 - \frac{1}{2} \int_0^{R_0} \int_0^{2\pi} \rho g (\delta z)^2 r dr d\theta \quad (4.26b)$$

where  $PE_0$  is the potential energy of the initial flat interface configuration.

At the marginal stability limit, the total potential energy does not change when the interface is perturbed slightly. Consequently, by combining Eqs. (4.26a) and (4.26b), the condition of marginal stability is found as the solution of:

$$\delta PE = 0 = \frac{1}{2} \sigma \int_0^{R_0} \int_0^{2\pi} \left[ \left(\frac{\partial \delta z}{\partial r}\right)^2 + \left(\frac{\partial \delta z}{r \partial \theta}\right)^2 \right] r d\theta dr - \frac{1}{2} \int_0^{R_0} \int_0^{2\pi} \rho g (\delta z)^2 r dr d\theta \quad (4.27)$$

since  $\sigma A_{i0} = PE_0$  cancels out. A realistic or ‘‘acceptable’’ perturbation has to be assigned to Eq. (4.27). The perturbation must satisfy the condition that the liquid volume is the same for the perturbed configuration as for the equilibrium configuration. (Furthermore, although it is not absolutely necessary, the perturbation function should also satisfy the equations of motion of the liquid for best accuracy in predicting the value of the critical acceleration.)

For a first example, an antisymmetric instability is assumed, as shown in the left hand part of Figure 4.13. The antisymmetric perturbation that satisfies the condition of constant liquid volume and the equations of motion is  $\delta z = A J_1(\lambda r) \cos \theta$ , where  $J_1$  is the Bessel function of the first kind,  $\lambda$  is an eigenvalue such that  $dJ_1/dr = 0$  at  $r = R_0$  (which is required to make the liquid velocity at the wall zero perpendicular to the walls), and  $A$  is an arbitrary amplitude. With this definition of  $\delta z$ , the integrations in Eq. (4.27) can be performed, and we find that the critical acceleration  $g$  that makes  $\delta PE = 0$  is equal to:

$$g_{crit} = \lambda^2 \left( \frac{\sigma}{\rho R_0^2} \right) \quad \text{or} \quad Bo_{crit} = \lambda^2 \quad (4.28)$$

The smallest value of  $\lambda$  from  $dJ_1/dr = 0$  is 1.84 (which is the eigenvalue for normal high-g sloshing in a cylindrical tank), so the critical Bond number is  $Bo_{crit} = 1.84^2 = 3.386$ . Consequently, if we want to cause liquid in a zero-g environment to reorient or settle

over the tank exit, thrusters must be used to exert an acceleration along the tank axis at least equal in magnitude to  $g_{crit} = 3.386\sigma/\rho(R_0)^2$ .

As a second example, a symmetric perturbation is assumed. The appropriate perturbation function is  $\delta z = AJ_0(\lambda r)$ , where  $\lambda$  is now the root of  $dJ_0/dr = 0$ . Equation (4.27) again gives  $Bo_{crit} = \lambda^2$ , except that now  $\lambda^2 = 3.832^2 = 14.68$ . The symmetrical perturbation requires a considerably larger acceleration than the antisymmetrical one. Thus, the antisymmetrical instability should always occur in practice. That is, the acceleration required to make the interface unstable will correspond to the value appropriate for an antisymmetric perturbation. This is in fact a general result. The antisymmetric mode (sometimes called modal reorientation) always requires a smaller de-stabilizing acceleration than the symmetric mode (sometimes called quiescent reorientation) [STEPHENS, 1965].

As might be expected, the de-stabilizing acceleration depends on the contact angle. The case  $\theta_c = 0^\circ$  is somewhat more difficult analytically than the case  $\theta_c = 90^\circ$  because the equilibrium zero-g interface is highly curved. The symmetric instability for  $\theta_c = 0^\circ$  has been investigated experimentally, and the critical Bond number found to be 0.84 [MASICA, ET AL, 1964]. An approximate solution of the equations for the antisymmetric mode yields  $Bo_{crit} \approx 0.81$ , which is less than the experimental value found for the symmetric mode. Hence, the difference between the critical accelerations for the symmetric and antisymmetric instabilities is small. As a result, the drop tower experiments from which the symmetrical instability results were obtained had to be done very carefully to prevent the antisymmetric mode from occurring [MASICA, ET AL, 1965].

The difference between the critical accelerations for  $\theta_c = 90^\circ$  and  $\theta_c = 0^\circ$  is significantly large. Similar differences occur for other tank shapes. For example, for a two dimensional rectangular tank, the antisymmetric solution for  $\theta_c = 90^\circ$  is  $Bo_{crit} = 2.46$  while  $Bo_{crit} = 0.72$  for  $\theta_c = 90^\circ$  [CONCUS, 1963]. This is a general result; that is, the critical acceleration always has its largest possible value for a flat interface ( $\alpha = 0^\circ$ , in the nomenclature of Figures 4.10a and 4.11).

### Annular interface

Annular tanks are used in some booster designs. The computed stability of a flat interface in an annular tank can be determined in a manner similar to that used for the previous cylindrical tank example. Figure 4.14 shows the results [REYNOLDS, ET AL, 1964]. As can be seen, the critical Bond number for the ratio  $R_i/R_0 = 0$  (corresponding to a thin wire) is the same as that obtained above for a cylindrical tank. This suggests that a small-diameter standpipe in the center of a large tank would have little effect on the critical Bond number.

It is perhaps surprising that the critical acceleration decreases as

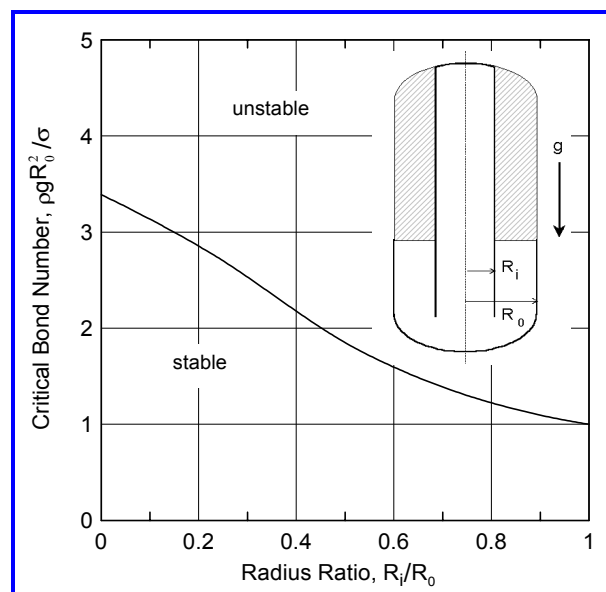


Figure 4.14. Stability of an annular interface:  $\theta_c = 90^\circ$

the width  $R_0 - R_i$  of the interface decreases (i.e., as the radius ratio increases toward one). However, the slosh frequency for an annular tank also decreases as the radius ratio increases, and the interface stability is related to the slosh frequency (which will be discussed in the next section).

### Neutrally stable zero-g interfaces

For some combinations of tank shape, liquid fill level, and contact angle, the zero-g equilibrium interface is neutrally stable. This means that any value of acceleration – regardless of how small – will cause the interface to become unstable, and the liquid will move bodily to the lowest position in the tank.

*Figure 4.15* shows graphically why the interface in a spherical tank, for example, is neutrally stable regardless of contact angle.

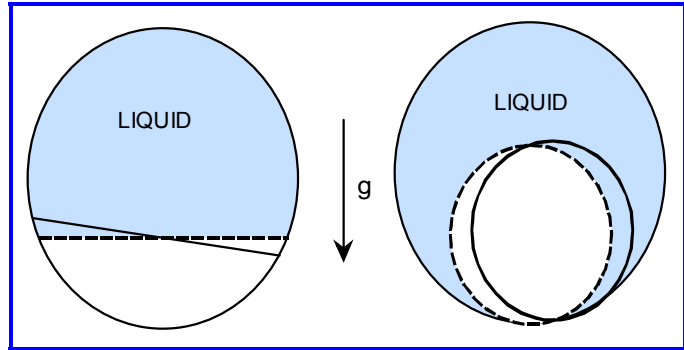


**Figure 4.15.** Interface stability for a spherical tank.

When an antisymmetric perturbation is imposed on the zero-g interface, the interface area does not change, and the capillary potential energy does not change either. However, the center of mass falls relative to the imposed acceleration, so the total potential energy decreases. Thus, the interface is unstable when any adverse acceleration is imposed. Zero-g interfaces in certain other tank shapes with curved walls are also neutrally stable [MYSHKIS, ET AL, 1987; ANTAR AND NUOTIO-ANTAR, 1993].

### General interface stability criteria

By making the governing equations dimensionless and examining the forms of the possible solutions, it has been found that the critical Bond number for interface stability in an axisymmetric tank can be related to (a) the radius of curvature  $R_w$  of the bounding walls at the contact point in the plane containing the tank axis and (b) the angle  $\alpha$  which the interface makes with the tank axis at the contact line. This relationship can be expressed nondimensionally in the form:

$$Bo_{crit} = f\left(\frac{R_0}{R_w \sin \theta_c}, \alpha\right) \quad (4.29)$$

Some of the conclusions that can be drawn from these analyses [MYSHKIS, ET AL, 1987; ANTAR AND NUOTIO-ANTAR, 1993] include:

1. An interface is unstable for all settling accelerations if the wall curvature is positive (concave with respect to the interface) and the parameter  $R_0/R_w \sin \theta_c$  is greater than +1; this includes a spherical tank as a special case.
2. When the walls are straight (e.g., cylinder or cone,  $R_w = \infty$ ), the critical acceleration depends only on the angle  $\alpha$  and is otherwise independent of the contact angle.
3. The maximum critical acceleration occurs when the interface is flat ( $\alpha = 90^\circ$ ).

These conclusions apply strictly only to cases when the liquid temperature is uniform. When there is a temperature gradient in the liquid, there is also a surface tension gradient (since surface tension decreases with temperature) and this can affect the stability of the

interface. For the example of a spherical tank, the capillary energy will be greatest when the interface is near the cooler end of the tank and smallest when the interface is near the hotter end. Thus, if the vapor bubble in zero-g is at the hot end of the tank, the critical de-stabilizing acceleration is greater than zero, because to move the bubble towards the cooler end requires an increase of the capillary energy, even though the gravitational potential energy decreases just as for the isothermal case [DODGE AND GREEN, 1992].

### Settling time estimates

When the bulk of the liquid in a tank has to be settled over the outlet, say, to start an engine, the imposed acceleration must not only be large enough to de-stabilize the interface but it must also be exerted for a long enough time period to move the liquid to the desired location. Surprisingly little work has been devoted to the settling time problem, so approximate estimates of the time are required in most cases.

Experiments have shown that the leading edge of a de-stabilized interface “falls” at a rate nearly equal to the imposed acceleration [MASICA, ET AL, 1965]. Thus, one estimate of the settling time is simply the time required for the liquid center of mass to fall freely from its original position to its new position in the settled configuration, multiplied by a factor of three or four to account for the fact that the liquid will initially overshoot its new equilibrium position before coming to rest. Another way to estimate the settling time is to combine the free fall time of the center of mass with the time required for ten or so slosh cycles of the liquid in the new settled configuration. The settling acceleration must be exerted for a time at least as long as the greater of these two estimates.

An efficient method of settling the liquid is to “pulse” the thrusters by firing them for a short duration (a fraction of a second) and then turning them off for a longer time period [HOCHSTEIN, 1989]. The ratio of firing time to off time is called the “duty cycle.” Duty cycles of one-tenth or so are used commonly. During the time between firings, the liquid continues to fall with nearly a constant velocity. The total time required for settling can be estimated approximately by assuming a constant settling acceleration equal to the time-average of the pulsed acceleration [DODGE AND GREEN, 1992]. One caution is that the time between thrusting firings must be short enough to prevent the liquid from forming a new zero-g interface before the next firing; otherwise, the liquid will tend to come to rest between firings, and the benefits of pulsing will be lost. The time for a zero-g interface to form is discussed below. Settling as a means of managing liquid in a tank in low-g is discussed in detail later in the chapter.

### Zero-g interface formation times

The time required for an interface to obtain its zero-g configuration after a step reduction in gravitational acceleration (e.g., after a settling thrust is turned off or when a test tank is released in a drop tower) is of interest for reasons discussed above. The formation time is sometimes called the *reorientation* time, although that term is also used for the time required for a liquid to settle in a tank after an acceleration is imposed.

SIEGERT, ET AL [1964, 1965] studied zero-g formation time  $t_s$  experimentally and correlated the experiment results in the form:

$$t_s = K \sqrt{\frac{\rho D^3}{\sigma}} \quad (4.30)$$

Values of the constant  $K$  are listed below for liquids having  $\theta_c \approx 0^\circ$  for several common tank shapes (for the annular tanks,  $D$  in Eq. (4.30) is  $R_0 - R_i$ ).

Cylindrical tank . . . . .	0.15
50% full spherical tank . . . . .	0.16
Annular tank:	
$R_i/R_0 = 0.25$ . . . . .	0.15
$R_i/R_0 = 0.50$ . . . . .	0.10
$R_i/R_0 = 0.75$ . . . . .	0.42

The capillary energy of the initial high-g configuration can be considerably in excess of the capillary energy of the final zero-g configuration, and the excess energy is transformed into sloshing kinetic energy. The estimates given by Eq. (4.30) do not include the time for the slosh waves to damp out, so an additional time of about five or six slosh wave periods should be added to these formation time estimates.

Correlations specifically for cylindrical tanks have been determined experimentally that are valid for any contact angle less than  $90^\circ$  [WEISLOGEL AND ROSS, 1990]. The results are summarized by the relation:

$$t_s = \frac{R_0^2}{\nu} \left( \frac{10^B \zeta^A + 0.01\alpha^2}{1 + \alpha^2} \right) \tag{4.31}$$

where  $\nu$  is the liquid kinematic viscosity, and the other parameters are defined as:

$$\alpha = \frac{1 - \sin \theta_c}{\cos \theta_c} \quad A = 0.28 + 2.2\alpha - 1.2\alpha^2 \quad B = 3.9A - 3.32 \quad \zeta = \nu \sqrt{\frac{\rho}{R_0 \sigma \alpha^2 \cos \theta_c}}$$

Equation (4.31) includes the time required to damp the slosh waves after the zero-g interface is formed.

### 4.5 Low-g Sloshing in Axisymmetric Tanks

In normal gravity, sloshing is controlled by the interaction of gravitational body forces and inertial forces. In reduced gravity, the gravitational body force is weak, but surface tension becomes important because it tends to restore the original configuration when a liquid interface moves. Hence, liquid in a container in zero-g may still have a non-zero sloshing natural frequency. Since the surface tension force is much smaller than the normal gravitational or thrust-induced body force, the low-g slosh frequency is generally much smaller than it is normal gravity.

Further, the fact that the surface tension restoring force is small implies that small motions of the container can lead to large motions of the liquid. As a result, zero-g sloshing tends to be of large amplitude, which makes the assumption of linearized motions employed in Chapters 1, 2, and 3 less realistic than for normal, high-g sloshing. When the wave amplitude is large, the liquid motion is dominated by inertia, as is indicated by the upper left hand quadrant of Figure 4.5, and hence, the natural frequency of sloshing is not so important in analyzing the motions as it is for high-g sloshing. Low-g motions in general thus have to be analyzed numerically, as for example, in NAVICKAS, ET AL [1986]. There are some instances, nonetheless, when the amplitude of the tank motion is itself small, such as during station keeping of an orbiting spacecraft. For these cases, knowledge of the low-g sloshing frequencies and dynamics is important.

#### General theory for an axisymmetric tank

The general theory for low-g sloshing given here is similar to the discussion in Chapter 1 for high-g sloshing. The tank shape and the equilibrium liquid configuration are assumed to be axisymmetric. The liquid motions are assumed to be small, so the equations can be

linearized with respect to the liquid velocity and surface wave amplitude. Viscous damping is neglected, so the liquid motion is derivable from a velocity potential  $\phi$ . In contrast to Chapter 1, only those slosh modes that vary as the cosine of the angular coordinate  $\theta$  are considered here, because, as was shown in Chapter 1, only these modes produce a net force or moment on the tank. Finally, only free, unforced slosh motions are analyzed in detail. The analysis of forced motion follows directly from the free slosh modes, but it is easier to compute the forced motion dynamics by an equivalent mechanical model. The geometry of low-g sloshing in an axisymmetric tank is shown in *Figure 4.16*. The analysis follows that given by DODGE, GREEN, and CRUSE [1991]. The main analytical difficulties arise from the boundary conditions at the curved free surface and at the contact line.

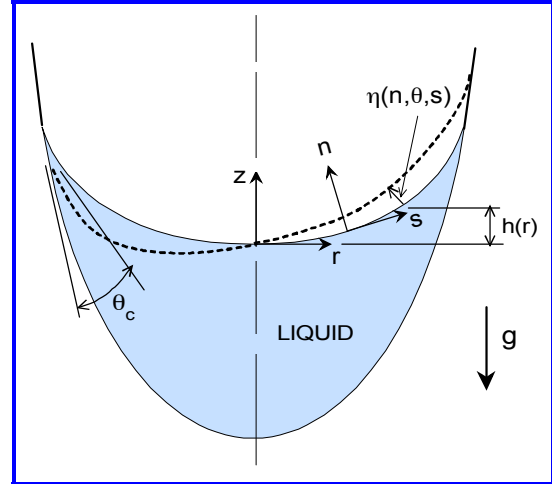


**Figure 4.16.** Schematic of low g sloshing in an axisymmetric tank

Since the equilibrium interface shape  $z = f(r)$  can be highly curved and even “bent over” the boundary conditions at the interface are best expressed in a surface normal coordinate system  $s, n, \theta$  where  $s$  is arc length measured from the tank centerline ( $s = 0$  corresponds to  $r = 0$ ),  $n$  is measured perpendicular to the interface, and  $\theta$  is the angular coordinate.

The potential must satisfy the Laplace equation (conservation of mass) within the liquid:

$$\nabla^2 \phi = 0 \quad \text{in the fluid volume, } V \quad (4.32)$$

**Boundary conditions.** Since the liquid cannot penetrate the tank walls, the component of the liquid velocity at the tank walls perpendicular to the walls must be zero:

$$\frac{\partial \phi}{\partial n} = 0 \quad (\text{or } \nabla \phi \cdot \mathbf{n} = 0 \text{ in vector notation}) \quad \text{on the walls, } W \quad (4.33)$$

The velocity of the free surface must equal the liquid velocity at the free surface:

$$\frac{\partial \eta}{\partial t} = \frac{\partial \phi}{\partial n} \quad \text{on the free surface, } F \quad (4.34)$$

where  $\eta$  is the slosh wave height measured in the  $n$  direction.

The liquid pressure  $p$  at the free surface is different from the gas pressure  $p_g$  above the free surface as a result of surface tension. The jump in pressure is given by  $p_g - p = 2\sigma \mathcal{H}$ , where  $\mathcal{H}$  is the mean curvature of the perturbed interface. In this linearized formulation, the mean curvature is the sum of the mean curvature  $\mathcal{H}_0$  of the equilibrium axisymmetric interface and the perturbation to the curvature caused by the slosh wave. A relation for  $\mathcal{H}$  in terms of the slosh wave amplitude can be derived from differential geometry:

$$2H = -\nabla \cdot \left( \frac{\nabla F}{|\nabla F|} \right)_{F=0}$$

where  $F(s, \theta, \eta) = 0$  is the equation of the perturbed free surface. After this relation is linearized with respect to  $\eta$ , we find that the instantaneous mean curvature is the sum of (a) the equilibrium mean curvature, (b) the deviation of the mean curvature for a constant value of wave height  $\eta$  over the surface and (c) the deviation caused by the variation of  $\eta$  over the surface:

$$2H = 2H_0 + \left( \frac{1}{r_1^2} + \frac{1}{r_2^2} \right) \eta + \nabla_s^2 \eta$$

where  $r_1$  and  $r_2$  are the principal radii of curvature of the equilibrium free surface shape, and  $\nabla_s$  is the Laplace operator expressed in the surface coordinates.  $H_0$ ,  $r_1$ , and  $r_2$  can all be expressed in terms of  $z = f(r)$  and its derivatives, where  $f(r)$  is the equilibrium free surface shape. When the pressure jump is expressed in terms of the time-varying mean curvature, the expression can be separated into a time-varying part and a time-invariant part. The time-invariant part represents the pressure jump for the equilibrium free surface shape, and so it cancels out. The final result is that the unsteady part of the pressure condition at the free surface, which is derived from the unsteady Bernoulli's equation just as for the high-g slosh theory discussed in Chapter 1, is:

$$\rho g \left( \frac{dr_e}{ds} \right) \eta - \sigma \left[ \left( \frac{d^2 z_e}{ds^2} \frac{dr_e}{ds} - \frac{d^2 r_e}{ds^2} \frac{dz_e}{ds} \right)^2 + \left( \frac{1}{r} \frac{dz_e}{ds} \right)^2 \right] \eta - \sigma \left[ \frac{1}{r_e} \frac{\partial}{\partial s} \left( r \frac{\partial \eta}{\partial s} \right) + \frac{1}{r_e^2} \frac{\partial^2 \eta}{\partial \theta^2} \right] = \rho \frac{\partial \phi}{\partial t} \quad (4.35)$$

where  $z_e$  and  $r_e$  are the coordinates of a point on the equilibrium free surface. (The terms that are squared in this equation are equal to  $r_1$  and  $r_2$ , respectively)

The wave shape must preserve the equilibrium contact angle<sup>13</sup>. Since the slope of the tank wall may change as the wave moves up the wall, determining the correct contact angle condition is an involved geometric problem. *Figure 4.17* shows how the derivation is accomplished analytically. The contact angle is expressed in terms of the unit normal vectors at the wall and the free surface:

$$\cos \theta_c = \mathbf{e}_w \cdot \mathbf{e}_n$$

The unit vector wall normal is  $\mathbf{e}_w = \cos \theta_c \mathbf{e}_n - \sin \theta_c \mathbf{e}_s$ . When the surface moves, the unit vectors change by a small amount  $\Delta \mathbf{e}_w$  and  $\Delta \mathbf{e}_n$ . The change in the  $\mathbf{e}_w$  vector is expressed in terms of the change in the angle  $\alpha_w$  of the

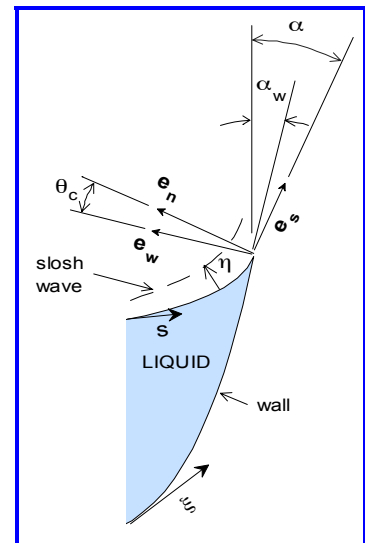


Figure 4.17. Motion near the contact line

<sup>13</sup> This requirement must also be met for high-g sloshing. But for high-g sloshing, the effect of contact angle is confined to a very small region near the wall, so the requirement can be ignored with little loss of accuracy, as was assumed implicitly in Chapter 1.

point on the wall in contact with the free surface when the free surface moves along the wall a distance  $\Delta\xi$ :

$$\Delta\mathbf{e}_w = -\Delta\xi \left( \frac{d\alpha_w}{d\xi} \right) (\cos\theta_c \mathbf{e}_s + \sin\theta_c \mathbf{e}_n)$$

Likewise, the change in the normal vector to the free surface is given by:

$$\Delta\mathbf{e}_n = -\left[ \Delta s \left( \frac{d\alpha}{ds} \right) + \left( \frac{\partial\eta}{\partial s} \right) \right] \mathbf{e}_s - \frac{1}{r} \left( \frac{\partial\eta}{\partial\theta} \right) \mathbf{e}_\theta$$

Also,  $\Delta s = \eta \cot\theta_c$  and  $\Delta\xi = \eta/\sin\theta_c$ . Therefore, when these relations are combined, the linearized form of the contact angle condition  $\cos\theta_c = (\mathbf{e}_w + \Delta\mathbf{e}_w) \cdot (\mathbf{e}_n + \Delta\mathbf{e}_n)$  reduces to:

$$\sin\theta_c \left( \frac{\partial\eta}{\partial s} \right) + \left[ \cos\theta_c \left( \frac{d\alpha}{ds} \right) - \frac{d\alpha_w}{d\xi} \right] \eta = 0 \quad \text{for } s = s_c \quad (4.36)$$

where  $s_c$  is the total arc length to the equilibrium free surface contact point at the wall, and  $\xi$  is the arc length coordinate measured along the tank wall. Equation (4.36) is satisfied identically when  $\theta_c = 0^\circ$ .

As was mentioned earlier, the contact line is *free* when the contact angle does not change as the liquid moves up and down; Eq. (4.36) applies only to this condition. For some liquids and tank wall materials, the contact angle changes noticeably [DODGE AND GARZA, 1968; DODGE, 1988; CONEY AND MASICA, 1969]; this phenomenon was discussed earlier in the chapter and was called contact angle hysteresis or dynamic contact angle. One way to include a changing contact angle in the analysis is to assume the change is proportional to the amplitude of the wave height at the wall. However, there are little or no data available on the value of the proportionality constant or how it varies with liquid properties and liquid velocity, except for the special case when the proportionality constant is extremely large; the contact line is then in effect pinned or *stuck* to the wall, so this condition is expressed as  $\eta = 0$  at the contact line.

Equations (4.32) - (4.36) define the low-g sloshing problem for an axisymmetric tank for the case when the contact line is free to move without restraint. We are interested in solutions corresponding to unforced sloshing, so the time derivatives in the equations can be replaced by  $i\omega_n$  where  $\omega_n$  is the slosh natural frequency.

### Methods of solution

Because of the analytical complications introduced by Eqs. (4.35) and (4.36), closed form solutions of the equations are not possible in general. The most prominent exception to this statement is a cylindrical tank with  $\theta_c = 90^\circ$  [e.g., REYNOLDS AND SATTERLEE, 1964]; the equilibrium interface is flat for this case so the  $r$  and  $s$  coordinates are identical;  $z_e = 0$ ; and Eq. (4.35) simplifies considerably. Furthermore, Eq. (4.36) reduces to  $\partial\eta/\partial r = 0$  at the wall, which is the same condition as  $\partial\phi/\partial r = 0$  imposed on the velocity potential. The solution is given in terms of Bessel functions just as for high-g sloshing; this solution will be discussed later in the section. But in most cases of interest, an approximate or numerical solution is the only possibility.

General purpose computational fluid dynamics codes with a free surface capability could be used to solve the low-g sloshing problem directly. But at this point in their development (end of 2000), such codes do not simulate the surface tension forces at the free surface accurately enough to make reliable predictions. They are, however, of great utility when the tank motion is large and the liquid motions are dominated by inertia rather than by surface tension. On the other hand, finite difference codes have been written specifically to solve Eqs. (4.32) - (4.36) for several kinds of tank shapes and they do give accurate predictions. Results from these computations will be summarized later

in the section. One limitation of CFD codes is that the contact angle cannot be exactly  $0^\circ$  because the computing cell then has two sides that lie on top of each other; thus, a small but not exactly zero contact angle (generally  $5^\circ$ ) must be used.

Another solution method is to construct the potential  $\phi$  in terms of functions  $\psi_i(r,z)\cos\theta$  that satisfy part of the problem [such as Eq. (4.32)]; the other equations are then satisfied in some approximate way. The success of this method depends on the choice of the functions  $\psi_i$  and how  $\phi$  is made to satisfy the remaining equations. Convergence to the true solution is more rapid and accurate when the remaining equations are satisfied in an overall, integral sense. For example, the previous set of differential equations can be shown to be the same as the set determined from a velocity potential and free surface slosh wave shape that minimize the following integral [DODGE, ET AL, 1991; CONCUS, ET AL, 1969]:

$$\begin{aligned}
 I(\Phi, H) = & \frac{1}{2}(1 + Bo)\Omega \iiint (\nabla\Phi \cdot \nabla\Phi) dV - (1 + Bo)\Omega^2 \iint_F (\Phi H) dA_F + \\
 & \frac{1}{2}\Omega \iint_F \left[ \left( \frac{\partial H}{\partial S} \right)^2 + \left( \frac{1}{R} \frac{\partial H}{\partial \theta} \right)^2 + \left( \frac{1}{\mathcal{R}_1^2} + \frac{1}{\mathcal{R}_2^2} \right) H^2 - Bo \left( \frac{dR}{dS} \right) H^2 \right] dA_F - \\
 & \frac{1}{2}\Omega \int_0^{2\pi} \left[ \frac{R}{\sin\theta_c} \left( \frac{d\alpha}{dS} \cos\theta_c - \frac{d\alpha_w}{d\xi} \right) H^2 \right]_{S=S_c} d\theta
 \end{aligned} \quad (4.37)$$

Equation (4.17) is written in dimensionless variables, and  $F$  is the equilibrium free surface and  $V$  is the liquid volume. The time dependence of the potential has been assumed to be  $\exp(i\omega t)$ . The dimensionless variables in this expression are defined as:

$$\begin{aligned}
 \Phi(R, \theta, Z) = \frac{\phi(r, \theta, z)}{\sqrt{(1 + Bo)(\sigma R_0 / \rho)}} \quad \Omega = \frac{\omega}{\sqrt{(1 + Bo)(\sigma R_0^3 / \rho)}} \quad H(S, \theta) = \frac{\eta(s, \theta)}{R_0} \\
 R = \frac{r}{R_0} \quad Z = \frac{z}{R_0} \quad S = \frac{s}{R_0} \quad \Xi = \frac{\xi}{R_0} \quad \mathcal{R}_1(S) = \frac{r_1(s)}{R_0} \quad \mathcal{R}_2(s) = \frac{r_2}{R_0}
 \end{aligned} \quad (4.38)$$

As usual,  $Bo = \rho g(R_0)^2 / \sigma$  and  $R_0$  is the characteristic dimension of the tank (e.g., radius).

The solution procedure starts by expressing the nondimensional potential in terms of a series of trial functions:

$$\Phi(R, \theta, Z) = \sum a_i \psi_i(r, z) \cos\theta \quad (4.39a)$$

where the  $a_i$  are numerical parameters to be determined. The wave amplitude  $H(S, \theta)$  can also be expressed in terms of the  $a_i$  and  $\psi_i$  by using Eq. (4.34):

$$H(S, \theta) = \sum a_i \frac{\partial \psi_i}{\partial N} \cos\theta \quad (4.39b)$$

or by using an expansion in terms of  $\psi_i$  and another set of parameters  $b_i$ . Convergence is more rapid when Eq. (4.39b) is used for  $H$  but sometimes the  $\psi_i$  are only known numerically, so the normal derivative of  $\psi_i$  may not be available. These expressions are substituted into the integrals, and the derivative of  $I(\Phi, H)$  with respect to each coefficient  $a_i$  is set equal to zero to minimize  $I(\Phi, H)$ . In that way, a set of  $K$  linear equations can be derived to determine the  $a_i$ , where  $K$  is the number of terms retained in the series of Eqs. (4.39). In matrix form, these equations are written as  $\{[M_1] - \Omega^2[M_2]\}[a] = 0$ , which is a

standard eigenvalue equation that can be solved for the dimensionless natural frequencies  $\Omega_n$  and eigenvectors  $a_i$  corresponding to each  $\Omega_n$ .

The more of Eqs. (4.32) - (4.36) that can be satisfied by the trial functions  $\psi_i$ , the better the convergence of the approximation to the true solution and the more that Eq. (4.37) can be simplified. The  $\psi_i$  should *always* be chosen to satisfy Eq. (4.32), perhaps only numerically, however. If in addition, they satisfy the wall boundary condition, Eq. (4.33), and the expression for  $\mathbf{H}$  given by Eq. (4.39b) is utilized, only a few terms in the integral have a value different than zero. The approximation then reduces to finding the  $a_i$  and  $\Omega$  that satisfy:

$$\int_0^{S_c} \sum_{i=1}^K a_i \left\{ \left[ Bo \left( \frac{dR}{dS} \right) - \frac{1}{R} \frac{\partial}{\partial S} \left( R \frac{\partial}{\partial S} \right) + \frac{1}{R^2} - \left( \frac{1}{\mathcal{R}_1^2} + \frac{1}{\mathcal{R}_2^2} \right) \right] \frac{\partial \psi_i}{\partial N} \right\} \frac{\partial \psi_j}{\partial S} R dS -$$

$$(1 + Bo) \Omega^2 \int_0^{S_c} \sum_{i=1}^K \psi_i \frac{\partial \psi_j}{\partial N} R dS +$$

$$\Omega^2 \frac{R_c}{\sin \theta_c} \sum_{i=1}^K a_i \left\{ \sin \theta_c \frac{\partial}{\partial S} \left( \frac{\partial \psi_i}{\partial N} \right) - \left[ \frac{d\alpha}{dS} \cos \theta_c - \frac{d\alpha_w}{d\xi} \right] \frac{\partial \psi_i}{\partial N} \right\} \left( \frac{\partial \psi_j}{\partial N} \right)_c = 0$$
(4.40)

for  $j = 1, 2, \dots, K$ , where the integral is evaluated on the equilibrium free surface. Integration with respect to  $\theta$  has already been performed. The subscript  $c$  means that a variable is to be evaluated at the equilibrium contact line. If  $\theta_c = 0^\circ$ , the last summation is equal to zero identically and can be ignored.

For a cylindrical tank and fill levels for which the equilibrium free surface intersects the tank walls rather than the top or bottom, the equilibrium free surface does not bend over on itself. Hence, a standard  $r, \theta, z$  coordinate system can be used since double-valued slosh wave functions cannot occur. For this liquid configuration, Eq. (4.40) can be simplified and rewritten as:

$$\int_0^{R_c} \sum_{i=1}^K a_i \left\{ Bo \frac{\partial \psi_i}{\partial N} - \frac{1}{R} \frac{\partial}{\partial R} \left[ \frac{R}{\left( \sqrt{1 + F_R^2} \right)^3} \frac{\partial \psi_i}{\partial N} \right] - \frac{1}{R^2 \sqrt{1 + F_R^2}} \frac{\partial \psi_i}{\partial N} \right\} \frac{\partial \psi_j}{\partial N} R dR -$$

$$(1 + Bo) \Omega^2 \int_0^{R_c} a_i \psi_i \frac{\partial \psi_j}{\partial N} R dR = 0$$
(4.40a)

where  $F(R)$  is the dimensionless equation of the equilibrium free surface and  $F_R$  is its derivative with respect to  $R$ . The normal derivative of  $\psi$  on the equilibrium free surface can be evaluated simply as  $\partial \psi / \partial Z - (F_R) \partial \psi / \partial R$ .

The general theory and many analytical approximations to the solutions of the governing differential equations are discussed at length in several text books [MYSHKIS, ET AL, 1987, ANTAR AND NUOTIO-ANTAR, 1993].

**Slosh forces and torques.** In high-g sloshing, an unsteady slosh force is caused by the liquid pressure acting on the wetted walls. In low-g, there is an additional force caused by the unbalanced surface tension force at the contact line, and the pressure force itself includes a component that is negligibly small for high-g conditions.

The unsteady pressure is given by the linearized Bernoulli's equation, Eq. (1.3), so the pressure contribution to the lateral slosh force is:

$$F_P = \int_0^{2\pi} \int_{-z_B}^{f_c + \eta_0 \cot \theta_c \sin \alpha} \left[ P_{L0} - \rho g z - \rho \frac{\partial \phi}{\partial t} \right]_{r=r_w} r_w \cos \theta dz d\theta \quad (4.41a)$$

Here,  $f_c$  is the equilibrium free surface height at the contact line;  $\eta_0 = \eta_c \cot \theta_c \sin \alpha$  is the vertical slosh height at the contact line, where  $\eta_c$  is the slosh height at  $\theta = 0^\circ$ ;  $r_w$  is the radial coordinate of the wall; and  $z = -z_B$  is the coordinate of the tank bottom at  $r = 0$ . As before,  $P_{L0}$  is the liquid pressure at the free surface at the axis of the tank. Integrating this expression and then linearizing gives:

$$F_P = [(P_{L0} - \rho g f_c) \pi r_w \cot \theta_c] \eta_c \sin \alpha - \pi \rho \int_{-z_B}^{f_c} \left( \frac{\partial \phi}{\partial t} \right)_{r=r_w} r_w dz \quad (4.41b)$$

The first term on the right term is caused by the pressure jump  $P_{L0} - \rho g f_c$  at the contact point. It is a function of the surface tension and the curvature of the equilibrium free surface.

During sloshing, the contact line is displaced and a net surface tension force is created that “pulls” on the wall. *Figure 4.18* shows how this force is computed. The surface tension force acting on an element  $\Delta s$  of the contact line is  $\sigma \Delta s$ , and the component of this force that lies in the plane of the wall is  $(\sigma \Delta s) \cos \theta_c$ . The line element  $\Delta s$  is tilted; the tilt depends on the slosh wave amplitude and how the amplitude varies with angular position. By computing the tilt in terms of the slosh wave amplitude, the  $x$ -component of the force is found to be given by the expression  $(\sigma \Delta s) \cos \theta_c (\Delta \eta \cot \theta_c / r_w \Delta \theta) \sin \theta$ . The element length  $\Delta s$  is equal to  $r_w \Delta \theta$  to the first order. Hence, the net contact line force in the  $x$ -direction is computed as:

$$F_S = -\sigma \cos \theta_c \cot \theta_c \int_0^{2\pi} \left( \frac{\partial \eta}{\partial \theta} \right)_{r=r_w} \sin \theta d\theta = (\pi \sigma \cos \theta_c \cot \theta_c) \eta_c \quad (4.41c)$$

The other components of the unsteady surface tension force at the wall integrate to zero. In dimensionless variables, the total lateral slosh force is therefore:

$$\frac{F_S}{\sigma R_0} = \pi \Omega (1 + Bo) \left\{ \int_{-Z_B}^{F_c} (\Phi)_{R=R_w} R_w dZ - \left[ \frac{(2\kappa_c \sin \alpha - \cos \theta_c) \cot \theta_c}{1 + Bo} \right] \left[ \left( \frac{\partial \Phi}{\partial N} \right)_{R=R_w} \right] \right\} \quad (4.42)$$

where  $\kappa_c$  is the dimensionless mean curvature of the equilibrium free surface at the contact line. The slosh torque can be computed in a similar way, as outlined in Chapter 1. *Equation (4.42)* shows clearly that there is a component of the force that depends on the slosh wave height directly, which is not negligible when  $Bo$  is small. Most investigators have apparently not recognized this fact, which makes their computations of the slosh force questionable, as well as the parameters of any equivalent mechanical model derived from the slosh force and torque.

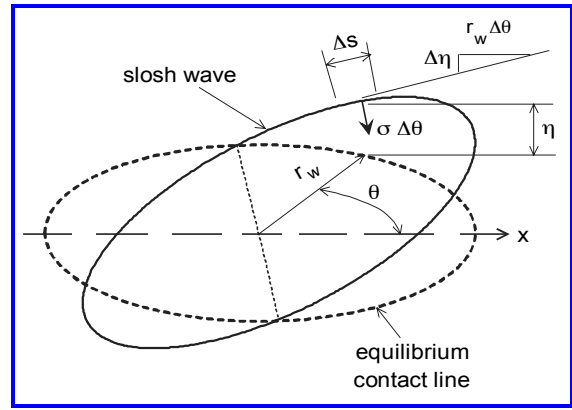


**Figure 4.18.** Unbalanced surface tension force of a moving contact line

### Equivalent mechanical model parameters

Just as for high-g sloshing, linear low-g sloshing can be represented by an equivalent mechanical model composed of, for example, a set of pendulums and a rigidly attached mass. In low-g, however, the pendulum or spring-mass must account for the effects of surface tension. The method used to determine the model parameters is discussed below.

From the previous development [Eq. (4.38)], we can conclude that the natural frequency of each slosh mode is expressible in the form:

$$\omega_n^2 = \Omega_n^2 \left[ \frac{g}{R_0} + \frac{\sigma}{\rho R_0^3} \right] \quad (4.43a)$$

where  $\Omega_n$  is the dimensionless eigenfrequency obtained from the solution of the low-g theory. The natural frequency  $\omega_{pend}$  of a pendulum that is attached to its pivot point by a torsional spring  $k_\theta$  is given by:

$$\omega_{pend}^2 = \frac{g}{L} + \frac{k_\theta}{mL^2} \quad (4.43b)$$

where  $L$  is the pendulum length and  $m$  is the pendulum mass. By comparing Eqs. (4.43a) and (4.43b), it is evident that such a pendulum will simulate the low-g slosh frequency if  $L$  and  $k_\theta$  are selected as:

$$L = \frac{R_0}{\Omega_n^2} \quad k_\theta = \frac{mgR_0}{\Omega_n^2 Bo} \quad (4.44)$$

for the  $n^{\text{th}}$  mode, The pendulum mass can be determined by comparing the model and slosh ratios of the amplitudes of the force  $F$  and the kinetic energy  $KE$ . For a harmonic motion at frequency  $\omega$ , the effective oscillating mass is equal to the ratio  $F^2/2KE\omega^2$ . For the pendulum, this ratio is  $m_n$ . For the sloshing liquid, the ratio can be found from the velocity potential. By equating the two ratios, the slosh mass of the model is found to be:

$$\frac{m_n}{\pi\rho R_0^3} = \frac{\left\{ \int_{-Z_B}^{F_c} (\Phi)_{R=R_w} R_w dZ - \left[ \frac{(2\kappa_c \sin \alpha - \cos \theta_c) \cot \theta_c}{1 + Bo} \right] \left( \frac{\partial \Phi}{\partial N} \right)_{R=R_w} \right\}^2}{\int_0^{S_c} \Phi \frac{\partial \Phi}{\partial N} R dS} \quad (4.45)$$

The pendulum attachment point is determined from the slosh torque expression. The torsional spring has to be attached to the tank walls by “sliders” so that for an angular displacement of the tank, only the component of the tank motion normal to the tank walls tends to rotate the spring.

### Cylindrical tank

Because a cylindrical tank is a relatively simple shape and is widely used in spacecraft applications, it has been the subject of several analytical and experimental investigations of low-g sloshing [SATTERLEE AND REYNOLDS, 1964; CONCUS, CRANE, AND SATTERLEE, 1967; DODGE AND GARZA, 1968; SALZMAN AND MASICA, 1969; BAUER AND EIDEL, 1990, among others]. Only SATTERLEE AND REYNOLDS [1964] considered contact angles other than  $0^\circ$ . All the predictions of the fundamental slosh frequency agree fairly well over the range of the common Bond numbers. The results of CONCUS, CRANE, AND SATTERLEE [1967], which were obtained by a finite difference computer code, cover the widest range

of  $Bo$ , so their results are summarized here. The results strictly apply only for the value of  $\theta_c = 5^\circ$  used in the numerical computations, but this is close enough to zero that the natural frequency predictions can be used for a zero degree contact angle.

**Natural frequency.** The dimensionless natural frequencies for the first two modes are shown as a function of Bond number in *Figure 4.19* for a tank with a liquid depth  $h > 3R_0$ . As can be seen, for  $Bo > 10$ , the predicted natural frequencies approach the high-g values given in Chapter 1. The first mode frequency is well correlated by the simple relation:

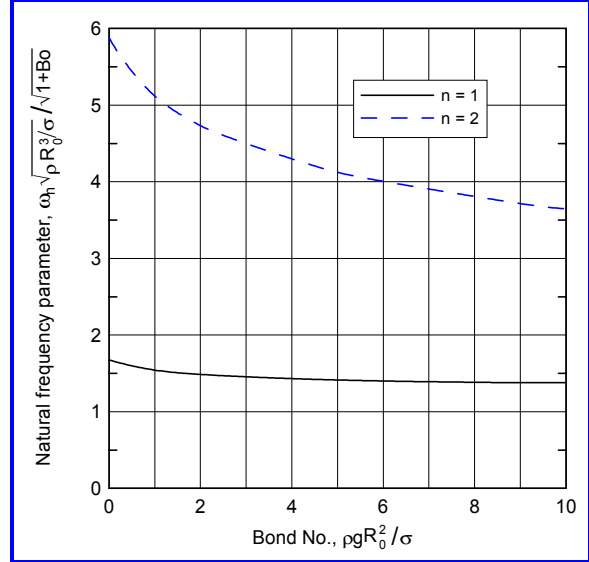


**Figure 4.19.** First and second slosh frequencies for a cylindrical tank for  $\theta_c \approx 0^\circ$ , with  $h/R_0 > 3$

$$\omega_1 = 1.61 \left[ \frac{\sigma}{\rho R_0^2} (1 + 0.798Bo) \right]^{1/2} \quad (4.46a)$$

For  $Bo \ll 1$ , the natural frequency is thus practically independent of  $Bo$  and approaches the value  $1.61\sigma/\rho(R_0)^2$ . When  $h < 3R_0$ , the natural frequencies can be computed approximately from the values shown in the figure or from Eq. (4.46a) by multiplying them by the depth factors from high g theory, namely the square root of  $\tanh(1.841h/R_0)$  for the first mode and the square root of  $\tanh(5.331h/R_0)$  for the second mode. The theoretical natural frequency predictions have been confirmed by numerous drop tower experiments [SALZMAN, ET AL, 1967; SALZMAN, ET AL, 1968; SALZMAN AND MASICA, 1969].

For  $\theta_c = 90^\circ$ , the frequency can be predicted exactly because the free surface is flat [REYNOLDS AND SATTERLEE, 1964]. The result is:

$$\omega_n^2 = \left[ n^2 \lambda_n^2 \frac{\sigma}{\rho R_0^3} + \frac{g}{R_0} \right] \lambda_n \tanh\left(\frac{\lambda_n h}{R_0}\right) \quad (4.46b)$$

where  $\lambda_n$  are the roots of  $dJ_1(r)/dr = 0$ , or  $\lambda_n = 1.841, 5.331, 8.536, \dots$ . When the acceleration  $g$  is reversed in direction with a magnitude such that  $Bo < -(\lambda_1)^2 = -3.386$ , the frequency is imaginary; this means that the interface becomes unstable when the imposed acceleration exceeds  $-3.386\rho(R_0)^2/\sigma$ . This is the same result for interface stability found previously by the thermodynamic stability method.

**Slosh mass.** With the exception of the results of DODGE AND GARZA [1968], the predicted slosh forces and the slosh masses of the mechanical model have apparently been computed in error, because of the neglect of the additional terms in Eq. (4.45). The predictions of DODGE AND GARZA [1968] were based on an approximate analytical method that converged well only for  $Bo > 5$ , but their analysis shows that the slosh mass decreases slightly as  $Bo$  decreases, and for  $Bo = 10$ , the mass is about 10% smaller than the high-g value.

### Spherical tanks

A spherical tank is also widely used in applications, so it has also been the subject of several low-g sloshing investigations [CONCUS, ET AL, 1969; DODGE AND GARZA, 1970; CONEY AND SALZMAN, 1971; DODGE, GREEN, AND CRUSE, 1991]. All the natural frequency predictions generally agreed within 10%, although the solution methods varied from finite difference computer programs to semi-analytical exact methods.

**Natural frequency.** The first and second mode natural frequencies are shown in *Figure 4.20*. The first mode frequency is zero for  $Bo \equiv 0$ ; this result is analogous to the fact that a liquid interface in a spherical tank is neutrally stable. The theoretical predictions as a function of  $Bo$  and  $\theta_c = 0^\circ$  have been confirmed by drop tower experiments [CONEY AND SALZMAN, 1971].

**Slosh mass.** Most investigators neglected the additional terms in the slosh force relation, Eq. (4.45), so their predictions of the slosh mass of an equivalent mechanical model are in error. The predictions of DODGE, GREEN, AND CRUSE [1991] are believed, however, to be correct. Their predictions are shown in *Table 4.1* in terms of the ratio of slosh mass  $m_1$  for the fundamental mode to the mass of liquid  $m_{liq}$  in the tank. Since the liquid does not have a fundamental slosh mode for  $Bo = 0$ , the tabulated results start with  $Bo = 1$ . As can be seen, the slosh masses for small  $Bo$  are considerably smaller than the masses for the  $Bo = \infty$  high-g limit.

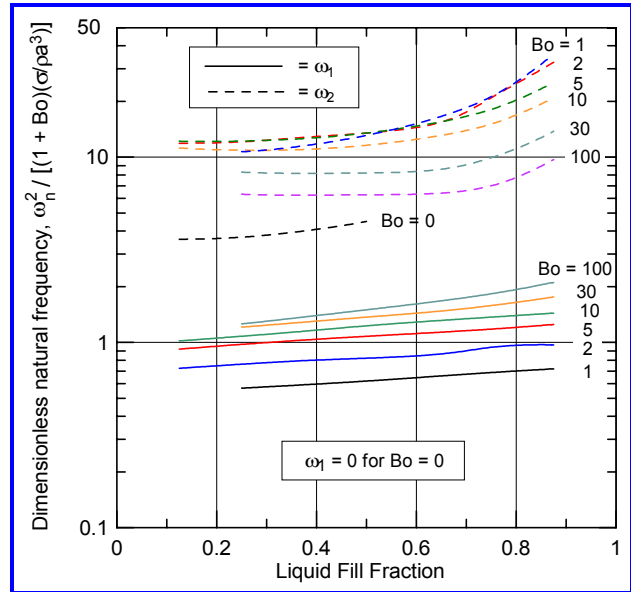


**Figure 4.20.** First and second mode slosh frequencies for a spherical tank, for  $\theta_c = 0^\circ$

**Table 4.1** Slosh mass ratio,  $m_1/m_{liq}$ , for a spherical tank with  $\theta_c = 0^\circ$

Fill Level, %	Bond Number		
	1	2	$\infty$
25	0.210	0.380	0.745
50	0.200	0.250	0.580
75	0.130	0.168	0.269

### Spheroidal tanks

Tanks that have an oblate spheroidal shape (i.e., a shape formed by rotating an ellipse around its minor axis) are used in some satellite designs, and the low-g sloshing in such tanks has therefore been the subject of analysis and testing by several investigators [CONCUS, ET AL, 1969; DODGE AND GARZA, 1970; CONEY AND SALZMAN, 1971].

**Natural frequency.** *Figure 4.21* shows the natural frequencies of the first two modes for an oblate spheroidal tank formed by an ellipse having a ratio of minor to major axis of 0.733 (eccentricity of 0.68). The curves for  $Bo = 0$  and  $Bo = 1$  do not cover the low fill fraction range, because the interface becomes annular for small  $Bo$  (*Figure 4.12*). The solution method also did not converge well for high fill levels. Frequencies for other minor to

major axis ratios are given in CONCUS, ET AL [1969]. The theoretical predictions have been validated by drop tower experiments [CONEY AND SALZMAN, 1971].

**Slosh mass.** There are no reliable predictions or measurements of the slosh force or slosh mass. By analogy with the spherical tank results given above, it is expected that the slosh mass under reduced gravity conditions will be somewhat less than for high-g conditions.

**Other axisymmetric tank shapes**

Some data on low-g slosh natural frequencies have been obtained for other axisymmetric tanks, for example, an annular cylinder tank [LABUS, 1969] and cylindrical tanks with inverted and upright hemispherical or ellipsoidal bottoms [DODGE AND GARZA, 1968; SALZMAN AND MASICA, 1969]. The data are limited in fill level range and Bond number and so are not summarized here. SNYDER [1999] discusses the general case.

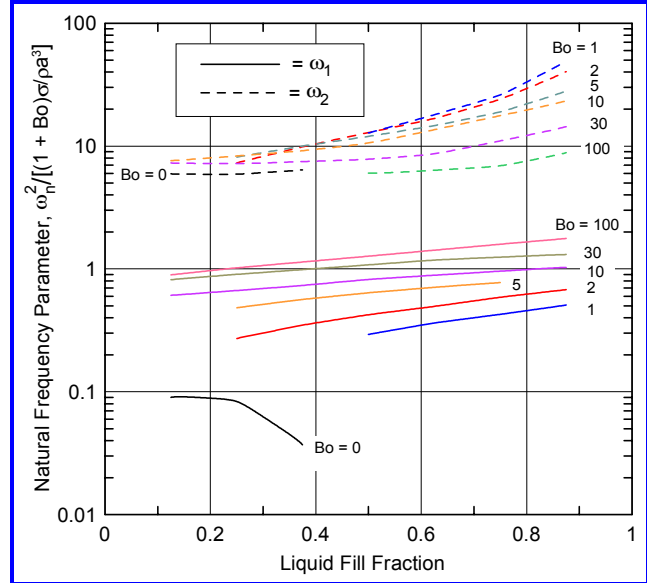


**Figure 4.21.** 1st and 2nd mode frequencies for an oblate spheroidal tank with an eccentricity of 0.68, for  $\theta_c = 0^\circ$

**Viscous slosh damping in low gravity**

Viscous damping of slosh waves in low-g is somewhat greater than it is in high-g because of the greater wetted area and presumably because of the smaller fraction of the liquid mass that participates in the sloshing. Damping correlations have been determined by a number of investigators [for example, CLARK AND STEPHENS, 1967; DODGE AND GARZA, 1968, 1970; SALZMAN AND MASICA, 1969] and predicted theoretically [for example, BAUER AND KOMATSU, [1998]. Most of the correlations and analyses apply only to slosh waves that have a *free* contact line; contact lines that are *stuck* increase the damping significantly [DODGE AND GARZA, 1968] VAN SCHOOR AND CRAWLEY 1995].

For *cylindrical tanks* with  $Bo > 5$  and liquid depths greater than the tank diameter, DODGE AND GARZA [1968] found that the damping ratio (fraction of critical damping) is correlated by an expression that involved both viscous and Bond number parameters:

$$\gamma = 0.97 \left( 1 + \frac{8.20}{Bo^{0.6}} \right) \sqrt{\frac{\nu}{\omega_1 R_0^2}} \quad Bo \geq 5 \tag{4.47a}$$

where  $\omega_1$  is the low-g slosh frequency. The second form  $Re_2$  of the inverse Reynolds number defined in Eq. (2.5) is used in this correlation. The numerical factor 0.97 corresponds to the correct high-g limit of 0.83 in Eq. (2.7b) when the high-g relation  $\omega_1 = (1.84g/R_0)^{0.5}$  is substituted into Eq. (4.47). Using drop tower tests, SALZMAN AND MASICA [1969] extended this correlation to  $Bo = 0$  and found that the damping was independent of  $Bo$  for  $Bo < 1$ ; their correlation is:

$$\gamma = 4.47 \sqrt{\frac{\nu}{\omega_1 R_0^2}} \quad 0 \leq Bo \leq 1 \quad (4.47b)$$

For  $Bo = 5$ , the numerical factor in Eq. (4.47a) is 4.0, so these two relations can be merged fairly smoothly in the region  $1 \leq Bo \leq 5$ . The damping increases somewhat as the depth decreases, just as for high-g sloshing.

A long duration experiment conducted in space aboard the Space Shuttle generally confirmed the drop tower data [VAN SCHOOR AND CRAWLEY, 1995]. The in-space data were obtained from force response data, rather than from free decay tests as was used in SALZMAN AND MASICA [1969] but were still within 10% of the drop tower data.

Damping data for *spherical* and *spheroidal* tanks are very sparse. The only extensive damping tests were acquired by DODGE AND GARZA [1970] and their tests were limited to  $Bo > 10$ . They found that the damping depended on both  $Bo$  and the inverse Reynolds number, just as for a cylindrical tank, but the data sets were not extensive enough to develop reliable correlations. For a spherical tank, the minimum damping occurred for a half full tank, which is also the case in the high-g limit, and the damping increased substantially for either smaller or larger fill levels.

## 4.6 Fluid Management Considerations in Low Gravity

Positioning liquid at a desired location in a spacecraft tank is not a straightforward task in low-gravity. During thrusting, the liquid location is determined by the acceleration-induced body forces, but in low-gravity, it is determined by the interaction of surface tension forces and body forces resulting from various small accelerations. If the liquid location were clearly dominated by surface forces, it would be relatively simple to make sure that the liquid is always positioned in a desired location. However, surface tension forces are so small for any reasonably size tank that random accelerations and vibrations make the location of the liquid practically indeterminate. Consequently, we cannot be sure, for example, that liquid will be over the tank outlet when it is desired to restart an engine or supply liquid to some process. Likewise, we cannot be sure that gas will cover the tank vent when it is desired to release gas to control tank pressure. Some means must therefore be employed to “manage” the liquid and gas in a spacecraft tank so that the liquid and gas are in the desired locations.

### Liquid settling and gas venting

As was discussed in Section 4.4, settling or “reorienting” liquid over the tank outlet by the use of small thrusters is one way to make sure that liquid is over the tank outlet and that gas covers the tank vent. Many space vehicles use settling to manage liquid in low g.

Settling thrusters have to be supplied with propellant by some method that works in low gravity. One common method is to use “cold gas” thrusters that eject pressurized gas from a separate tank. In some cases, the acceleration is too large for efficient settling; this might be the case, for example, when the primary purpose of the thrusters is for attitude control. The liquid then falls to the bottom of the tank at a high velocity and rebounds to form a geyser [SALZMAN AND MASICA, 1967; SALZMAN, ET AL, 1973] or else circulates within the tank for a long time. Generally, for best settling, the liquid leading edge velocity  $V_L$  (computed as if in free fall for the imposed acceleration) should be small enough to give a Weber number  $We = \rho R_0 (V_L)^2 / \sigma$  of about ten [GRAYSON, 2000].

If  $We > 10$ , pulsed settling should be used, in which the thrusters are alternately fired for a short period and then turned off for a longer period, for many cycles. The

time-average  $We$  can be made to be less than ten by this process, and considerably less propellant is needed to settle the liquid [HOCHSTEIN, 1989; PATAG, 1988]

Tests have shown that ring baffles in the tank drastically change the flow pattern during settling but have only a minor effect on the time required to collect the liquid over the tank outlet [SALZMAN, ET AL, 1973].

Gas sometimes has to be vented from a spacecraft tank to control tank pressure. Some of the passive methods described later in this chapter, which are used to ensure that liquid is located over the outlet, also enable the venting of liquid-free gas. When these passive methods are not available, liquid settling must be used. Other possibilities include placing non-wetting screens over the vent to allow gas to flow through but not liquid [SMITH, LI, AND CIMA, 1965]; dielectrophoresis; and high frequency acoustic waves that “push” liquid away from the vent and gas towards it. At present, these methods are experimental and have never been tested in an actual spacecraft application.

### Outflow and inflow phenomena

Resupply of liquids on orbit will be a key element of some future space operations. For that reason, the problems of low-g liquid inflow and outflow have been investigated by experiments and analyses. The results of these investigations suggest that flow rates will have to be considerably less than are commonly used in normal gravity.

**Outflow and suction dip.** When a tank is drained through a central outlet, a “dip” is formed in the interface at low liquid levels; the dip is caused by the lower pressure near the center resulting from the inward acceleration

of liquid toward the drain. *Figure 4.22* illustrates schematically this phenomenon of “suction dip” for both normal and low-g conditions, for a case when the outflow is driven by a pressure difference between the tank and the external receiver. For normal gravity conditions, the body forces are relatively large compared to the drop in dynamic pressure at the center, so the dip is relatively small. Under weightless conditions, however, only the surface tension force is available to smooth out the interface, and the dip becomes fairly large [NUSSEL, ET AL, 1965; BHUTA AND KOVAL, 1965]; hence, a significant volume of liquid may be left in the tank at the time when the dip uncovers the drain. For example, for a cylindrical tank with a flat bottom, drop tower experiments have shown that the amount of liquid left in the tank when gas is first ingested in the outlet is as much as 74% of a reference cylindrical volume having a depth equal to the tank diameter [ABDALLA AND BERENYI, 1969]. Even when the outflow was reduced to make  $We$  as small as unity, the residual liquid volume was about 20% of the reference volume. (Here,  $We = \rho Q^2 / \sigma (R_0)^3$  where  $Q$  is the volumetric outflow rate.)

Placing a small baffle above the drain can reduce the residual volume slightly; for example, for a disk having a radius equal to 0.485 of the tank radius and located one to two disk radii above the outlet, the residual volume for large outflow Weber numbers

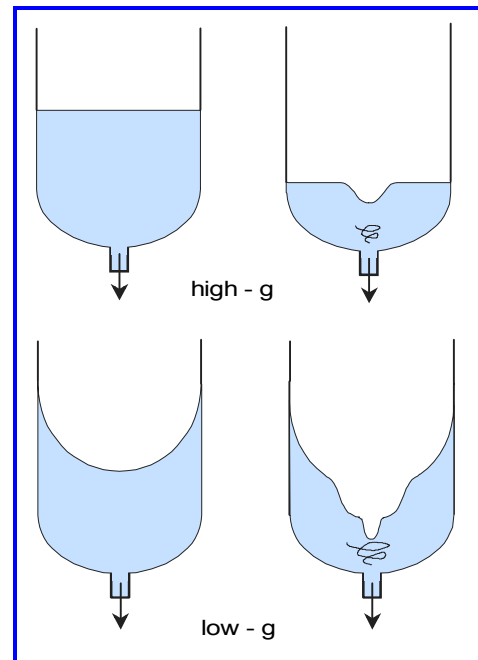


**Figure 4.22.** Interface shape during outflow in normal and low-g conditions

was found in the tests to be reduced from 74% to about 58% of the reference volume [BERENYI, 1970]. Larger disks were found to yield more improvement, but even when the disk radius was 98% of the tank radius the residual volume was still almost 35% of the reference volume for large Weber numbers. The residual volumes were somewhat lower when the tank bottom was hemispherical, since the interface shape then conformed more closely to the tank shape. Even so, small Weber numbers were required to make the residual volume small.

When the gravitational field is small but not exactly zero, another type of problem also becomes important, namely choking at the outlet. The choking is similar to choking of a compressible fluid at an orifice in a pipe. The velocity of the free surface waves here is analogous to the velocity of sound in the compressible flow case, and the Froude

number is analogous to the Mach number. *Figure 4.23* illustrates the choking phenomenon. When the flow velocity over the lip of the drain becomes critical (i.e., the Froude number is equal to unity), the flow rate cannot be increased further. Since the Froude number is  $V^2/gh_0$ , and the outflow rate  $Q$  is approximately  $V(\pi dh_0)$  where  $d$  is the diameter of the drain, the maximum or choked flow rate is about  $Q_{max} = \pi dh_0(gh_0)^{0.5}$ .

Similarly, if the outflow rate is fixed, the drain will become choked when the depth over the drain falls below  $(Q^2/\pi^2 d^2 g)^{1/3}$ . In low gravity, the critical depth  $h$  of the liquid in the tank can be rather large. Assuming that the rate at which the liquid level falls is slow compared to the liquid velocity over the drain, one-dimensional quasi-steady theory can be used to estimate the critical value of  $h$ . The gravity-driven velocity is equal to  $[2g(h-h_0)]^{0.5}$  and at the critical point this must be equal to  $(gh_0)^{0.5}$ . Thus, the critical depth  $h$  is 1.5 times  $h_0$ . These relations have been verified by experiments [GLUCK, ET AL, 1965]. The residual volume when the outlet becomes choked can be estimated from  $h$  and  $h_0$ .

**Drain vortex.** A vortex may form over the drain in low or normal gravity as a result of Coriolis and viscous effects or from rotary sloshing. The vortex accentuates the suction dip, especially in low gravity, as indicated schematically in *Figure 4.22*. Fortunately, simple cross-type baffles placed over the drain will prevent the formation of a vortex [KAMEL, 1964]. Even the disk-like baffle described previously, which was meant to diminish suction dip, is effective in eliminating the vortex. The radial length of the arms of a cross-type baffle should be at least twice the diameter of the drain, and the height of the arms should also be at least twice the drain diameter.

**Liquid inflow.** Re-filling tanks in reduced and zero-gravity is not without problems related to making sure that the inflowing liquid accumulates in a pool. Drop tower experiments have shown that the interface remains stable and the incoming jet of liquid remains in the vicinity of the interface when the Weber number is less than about 1.3 [SYMONS, ET AL, 1968; SYMONS, 1969]. The Weber number here is defined as  $\rho(R_i)^2(V_i)^2/2\sigma R_j$ , where  $R_i$  is the radius of the inlet,  $V_i$  is the velocity of the liquid in the inlet line, and  $R_j$  is the radius of the liquid jet at the liquid-vapor interface. When the Weber number exceeded 1.3 in the tests, the incoming jet formed a geyser that moved toward the other end of the tank, and only a small quantity of liquid was collected in the bottom of the tank, at least when

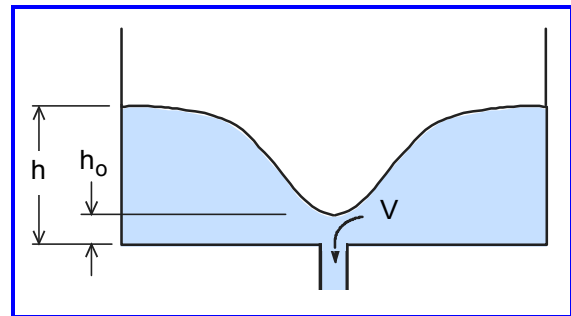


**Figure 4.23.** Simple model for estimating the onset of drain choking

the liquid depth in the tank was no greater than about ten inlet diameters. When the liquid depth exceeded about ten inlet diameters, the jet velocity could be increased somewhat. *Figure 4.24* (adapted from the photographs of SYMONS [1969]) illustrates these phenomena of stable and unstable inflow in zero-g. In these tests, the inlet jet spreading angle was less than  $10^\circ$ .

Similar inflow behavior has been observed in much longer duration tests conducted aboard the

Space Shuttle [DOMINICK AND DRISCOLL, 1993]. The tank was a sphere, and it contained a set of

screened channels to permit gas-free outflow (which had no effect on the inflow phenomenon discussed here). The inlet line was slightly off-center to accommodate the channel outflow manifold. A perforated baffle was placed over the inlet line to deflect the inlet jet. The inflow was supplied from a pressurized tank that used a positive displacement diaphragm to transfer liquid to the spherical tank at a measured rate. The

Weber number of the tests was varied from about 0.6 to 5.2. *Figure 4.25*

illustrates the main observations from the tests. The baffle deflected the inflow toward the walls, and a liquid film collected around the inlet and then climbed the walls. Eventually the liquid collected near the top vent, and a spherical bubble of gas was formed. As more liquid was collected, the diameter of the bubble decreased. Because of the off-center inlet and the fact that the bubble did not attach to the top of the tank, liquid eventually covered the vent line. At that point, the vent was closed, and the filling proceeded until the tank pressure became equal to the supply tank pressure. The fastest filling rate and maximum filling percentage occurred when the inlet Weber number was near the stability limit discussed in the previous section. Note that a cylindrical tank is better suited to low-g filling than a spherical tank since the interface does not bring liquid as quickly to the top.

Larger inflow rates have been shown to be feasible if the tank contains a set of vanes similar to those shown later in *Figure 4.31*. Final fill fractions of 95% or more were obtained routinely in these Space Shuttle experiments [DOMINICK AND TEGART, 1994]. In additions, the vanes were effective in allowing gas-only venting [CHATO, 1997].

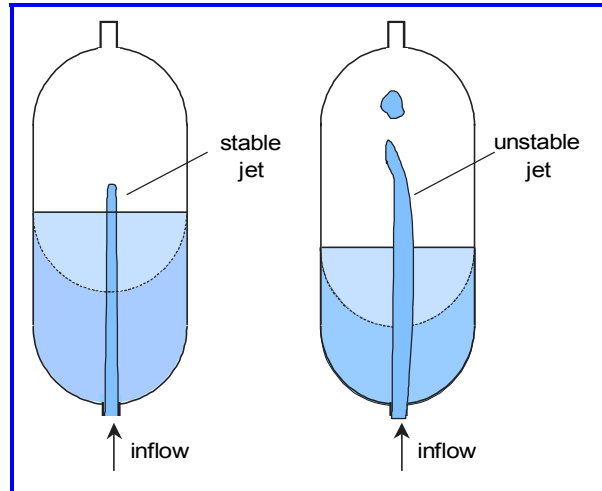


**Figure 4.24.** Stable and unstable inflow to a tank in zero gravity

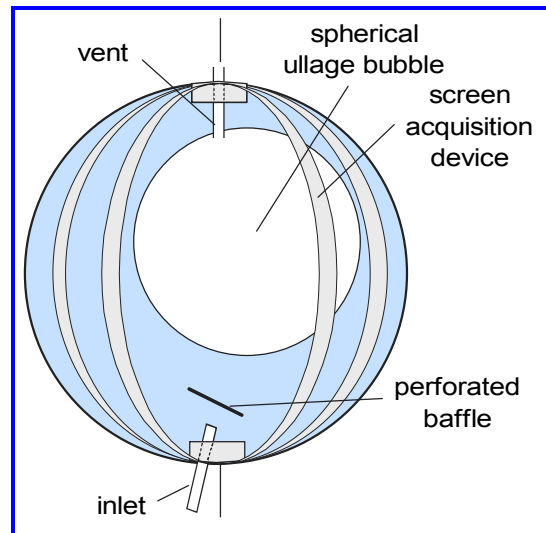


**Figure 4.25.** Typical results of in-space tank filling tests; fill volume about 70%

**Effects of cryogenic liquids.** The outflow and inflow tests discussed above were conducted with so-called “storable” liquids that have a vapor pressure which is much lower than the tank pressure. When the liquid is a cryogen, or any other liquid for which the vapor pressure is near the tank pressure, refilling a tank is more difficult because some part of the liquid flashes to vapor near the start of the refilling. The vapor generally has to be condensed or vented in some way to allow the filling to proceed efficiently [KRAMER, 1998]. Problems specific to cryogenic liquids will be discussed later in the chapter.

## 4.7 Propellant Management and Liquid Acquisition Devices

It is not always possible or weight-efficient to settle the liquid before initiating a liquid outflow. Instead, many spacecraft use passive *propellant management devices* (PMDs), which are also called *liquid acquisition devices* (LADs), to capture some part of the liquid and eliminate the possibility that random

accelerations and other disturbances will move the liquid away from the outlet.

Typically, the devices are made of fine mesh screens or perforated sheet metal. *Figure*

*4.26* shows how a simple fine-mesh screen PMD extending across the tank cross section can retain liquid over the outlet. When the liquid is subjected to an acceleration  $a$  that would make the liquid run toward the top of the tank, the strong capillary forces in the screen pores prevent the lower liquid from flowing out through the screen. Thus, this part of the liquid stays in contact with the tank outlet. However, when the liquid level is below the screen, even the lower liquid can move away from the bottom, so a series of such screens would be necessary for effective control at all liquid levels.

*Figure 4.27* shows a more sophisticated application of screens, which was used on the AGENA upper stage vehicle. The sump at the bottom of the tank was separated from the main propellant tank by a conical screen “trap”. The trap contained enough liquid to restart the engine, after which the thrust-induced acceleration settled the liquid over the trap, through the screens and into the outlet, and refilled the trap.

These two fine-mesh screen devices are examples of propellant management devices. The primary objective of a PMD is to keep the tank outlet covered with liquid whenever outflow is required. Secondary objectives might include controlling the center of mass of the liquid, minimizing sloshing, and allowing the venting of liquid-free gas.

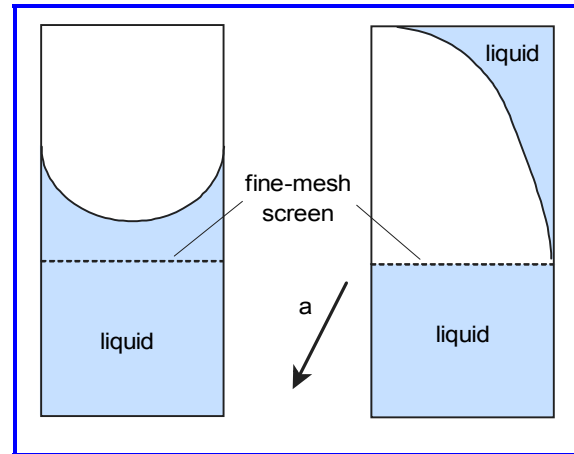


**Figure 4.26.** Screen baffle for low-g liquid control

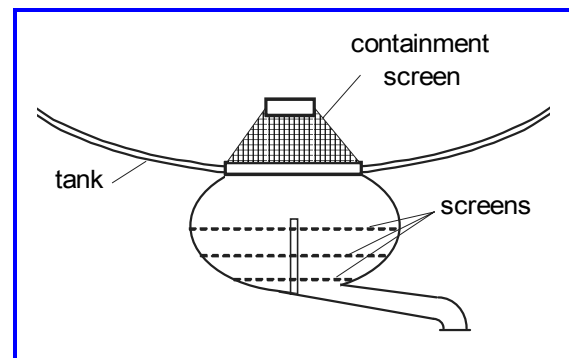


**Figure 4.27.** AGENA PMD sump and trap

### Type of propellant management devices

Propellant management devices use surface tension forces to maintain the liquid at a specific location. They can be classified into three general types described as follows [ROLLINS, ET AL, 1985]:

- Partial communication devices.** These devices hold only a fraction of the liquid over the outlet, and the remaining liquid is free. They are used when a space vehicle must maneuver considerably or when many small engine firings are needed. If the thrust acceleration is sufficient to settle the liquid, the PMD can be designed to be refillable and its volume can be made just large enough to provide gas-free propellant to start the engine each time (with a margin). *Figure 4.28* shows a schematic of an idealized refillable, partial communication PMD, composed of a trap whose walls are made of fine mesh screen and a vent pipe to allow gas to vent during refill when the trap is submerged in liquid. If the thrust acceleration is not sufficient to settle the liquid, the PMD volume must be large enough to provide gas-free liquid for all the operations. *Figure 4.29* shows a schematic of an idealized non-refillable PMD. Each successively lower volume of liquid is emptied in turn, with the exposed screen preventing the entrance of gas from the empty volume just above it. Because of their relatively small size, partial communication PMDs can be made stable (i.e., retain liquid) against large acceleration disturbances.

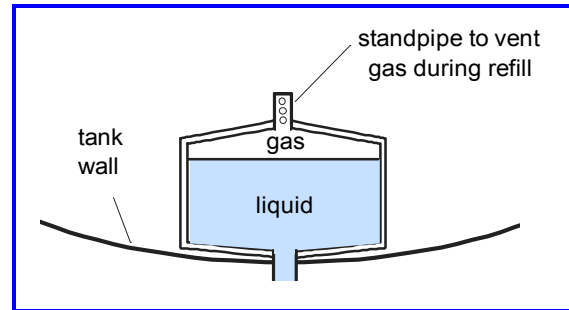


Figure 4.28. Schematic of idealized refillable PMD

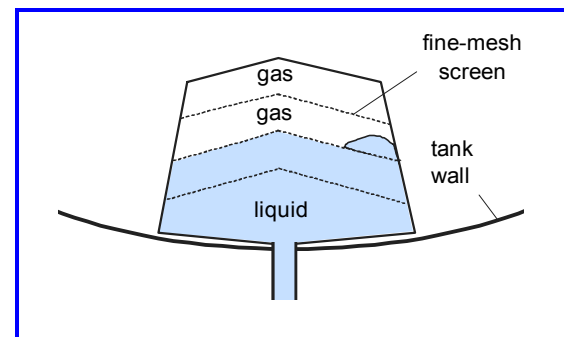


Figure 4.29. Schematic of non-refillable PMD

- Total communication devices.** These PMDs are designed to establish a flow path from the bulk liquid to the outlet at all times. Since, as was discussed earlier, the liquid tends to remain bound to the wall, common forms of total communication PMDs include flexible bladders that cover the free surface (discussed previously in Chapter 3) and flow channels or galleries near the wall. *Figure 4.30* illustrates a gallery PMD. The flow channels (galleries) are all connected to a manifold at the tank outlet. As long as at least one of the channels remains in contact with the bulk liquid, liquid will flow from the bulk into that

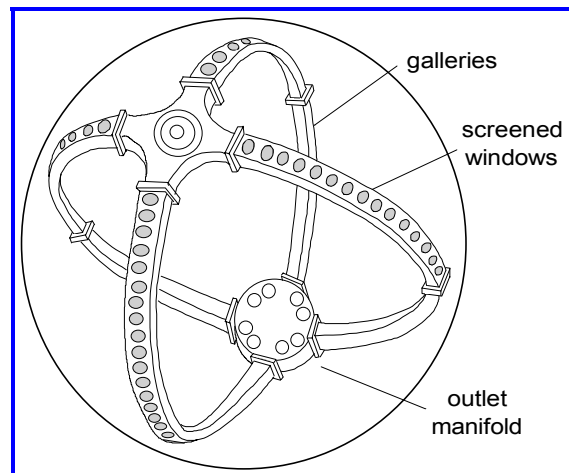


Figure 4.30. Example of gallery PMD

channel and thence to the outlet. Capillary forces prevent gas from being driven into the channels that are not in contact with bulk liquid. The figure shows channels made of sheet metal with small holes covered with a fine-mesh screen. Another common design employs channels of a square cross section, made of sheet metal on three sides and with a fine-mesh screen for the fourth side, usually the side nearest the wall. Because of their large size, total communication PMDs are only stable against moderate accelerations and will admit gas under large accelerations.

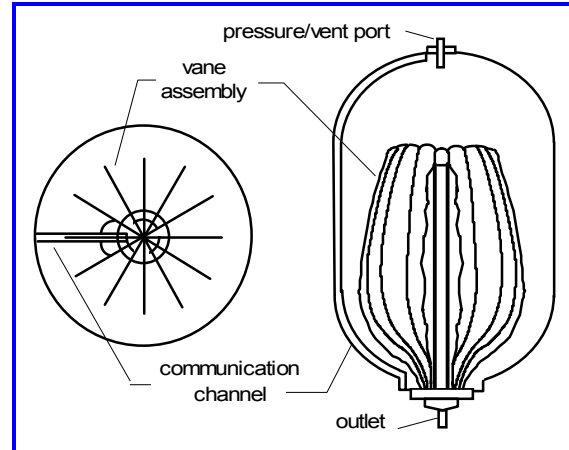


Figure 4.31. Example of a sponge PMD

Another type of total communication PMD uses vanes connected to a standpipe to maintain a path between the bulk liquid and the outlet. *Figure 4.31* illustrates a typical “sponge” PMD made of many such vanes [DOWDY, ET AL, 1976; JAEKLE, 1993]. By tapering the open area of the vanes, the liquid is “wicked” to the standpipe. Because the interfaces are large, the liquid position is relatively unstable, so vane PMDs are used only when disturbing accelerations are small, such as for deep space probes. Large thrusting accelerations do not create a problem, however, because the vanes will refill after the thrusting stops.

- **Total control devices.** These PMDs hold all the liquid over the outlet. They are effectively a non-refillable, partial control PMD that occupies the entire tank volume. Their main use is with vehicles where slosh control is a dominant concern.

Traps, galleries, vanes and sponges will be discussed in more detail later. Since most PMDs employ fine-mesh screens or perforated plates, the design principles of screens and plates are discussed first.

### Design characteristics of fine mesh screens and perforated plates

The most important PMD-related characteristics of a screen or perforated plate are that they (1) can withstand a pressure differential from the gas side to the liquid side and (2) can wick liquid from wet areas to dry areas.

- **Screen geometry.** The pressure and wicking characteristics of a screen depend on the geometry of the screen mesh. The screens used in space applications are usually either of the “plain” or “dutch” weaves.

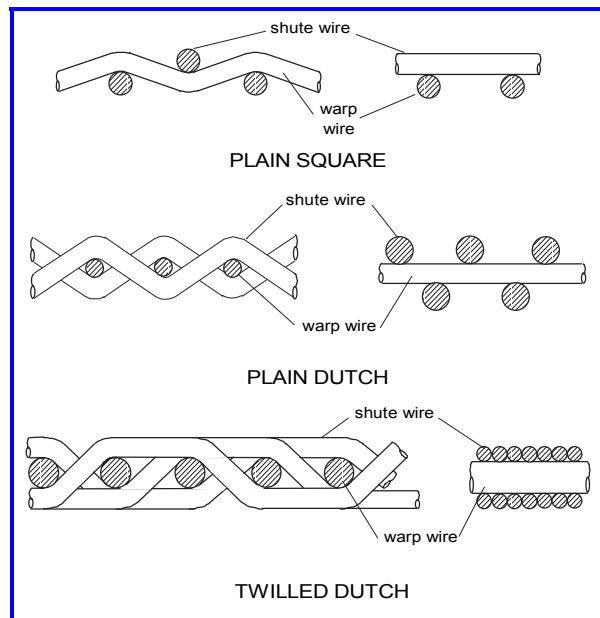


Figure 4.32. Cross sectional views of plain and dutch weave fine-mesh screens

Figure 4.32 shows the geometry of these weaves. Other details of the screen weaves will be summarized later.

A plain square weave is similar to an ordinary window screen weave; screens are available with weaves of up to 400 X 400 wires per inch, which has a pore size of 0.0015 inch (38 microns). Dutch and twilled dutch weaves use interwoven wires and have little open area. Plain dutch screens are available in weaves up to 50 X 250 wires per inch (pore size of 0.0022 inch = 56 microns). Twilled dutch screens are available up to 325 X 2400 wires per inch (pore size of 0.00002 inch = 5 microns)

**Bubble point pressure.** The maximum possible gas-to-liquid pressure differential that a screen or perforated plate can withstand is a function of its pore size and the liquid surface tension  $\sigma$ . This pressure is called the “bubble point pressure”  $P_{BP}$  and is given analytically by the expression:

$$P_{BP} = 4\sigma/D_{BP} \tag{4.48}$$

where  $D_{PB}$  is the *effective pore diameter*. It is assumed that the liquid wets the material so that the contact angle is  $0^\circ$ ; otherwise the expression must be multiplied by  $\cos\theta_c$ .

The bubble point pressure is measured with an apparatus similar to that shown schematically in Figure 4.33 [BLATT, 1970; DODGE AND BOWLES, 1984]. A sample of the screen is stretched over the open end of a box and submerged to a depth of 3/8 inch (0.95 cm) in a reservoir of a reference liquid (generally isopropyl alcohol, although any liquid that wets the screen can be used). The box is pressurized until an air bubble breaks through the screen. The bubble point is the breakthrough pressure, including the 3/8-inch hydrostatic head.

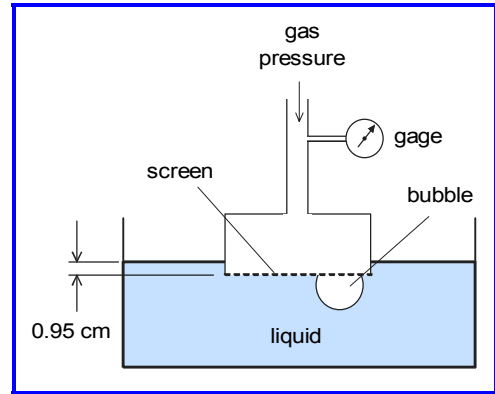


Figure 4.33. Bubble point test set up

The effective pore diameter is computed from the bubble point data by using Eq. (4.48). Bubble point data will be presented later. There is no corresponding “droplet point” pressure for a pressure difference from the reservoir to the gas.

**Wicking.** Wicking in a fine-mesh screens can be important both in obtaining and maintaining a filled PMD. High wicking rates may be undesirable for a refilling or filling application since the wicking liquid might seal the device before complete filling is obtained. Conversely, high wicking rates may be needed for heat pipe applications. For a cryogenic tank, wicking can be effective in preventing the drying out of screens by evaporation.

There are two important wicking-related phenomena: (1) the capillary suction pressure that drives the wicking, and (2) the friction-factor resistance of the screen to wicking. The suction pressure  $P_w$  is a fraction of the bubble point pressure:  $P_w = \Phi_w\sigma/D_{BP}$ , where  $\Phi_w$  is a screen characteristic. The wicking friction parameter  $C_w$  also depends on the screen weave. The wicking velocity is determined by analogy to laminar flow in a channel of height equal to  $B_s$ , the screen thickness; the velocity expression is:

$$V_w = \frac{\Phi_w B_s^2}{C_w L \mu_L} \left( \frac{\sigma}{D_{BP}} \right) \tag{4.49}$$

where  $L$  is the screen length in the wicking direction and  $\mu_L$  is the liquid viscosity. Data for  $\Phi_w$

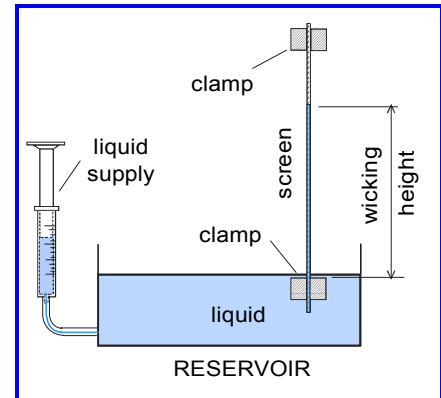


Figure 4.34. Test set up to measure wicking suction pressure

and  $C_w$  for various screen weaves will be presented later.

Figure 4.34 shows schematically how to measure the *wicking suction pressure* [DODGE AND BOWLES, 1984]. A sample of the dry screen is stretched between two clamps. One end of the screen is submerged in liquid (e.g., isopropyl alcohol) contained in a reservoir. (The screen is held in a vertical position by a support that is not shown in the schematic.) To start the test, liquid is added to the reservoir from the liquid supply until the lower clamp is just submerged. At that point, liquid will wick up the screen. If necessary, liquid is continuously added to ensure that the lower clamp remains submerged. The wicking height is measured when it has reached a maximum. (For liquids that evaporate easily, the measurements must be done rapidly.) Since the wicking suction pressure  $P_w$  at the wet-dry interface supports the hydrostatic head of the liquid in the screen, the suction pressure can be computed from the wicking height  $H_w$ :

$$P_0 - P_w = \frac{\Phi_w \sigma}{D_{BP}} = \rho_L g H_w$$

where  $P_0$  is atmospheric pressure. The measurements determine the factor  $\Phi_w$ ;

in effect, the wicking pore diameter is different than the bubble point pore diameter, unless  $\Phi_w = 4$ .

The wicking friction-factor resistance of a screen is measured by a modification of the apparatus used to measure the wicking suction pressure. Figure 4.35 shows the apparatus schematically. A sample of the dry screen is held between two clamps, just as for the suction pressure measurement, but for this test the screen is horizontal, with the end in the reservoir stretched over a knife edge to create a definite starting location for the wicking. To begin a test, liquid is added to the reservoir from the supply until the liquid surface is level with the knife edge. The location  $L(t)$  of the wicking interface is then measured as a function of time. (The screen is actually tilted very slightly, with the end in the reservoir below the exposed end, to prevent liquid from flowing along the screen by gravity.) The friction factor resistance of the screen is determined from the test data by using Eq. (4.49):

$$P_0 - P_w = C_w \mu_L \frac{L(dL/dt)}{B_s^2}$$

where inertial effects are ignored as being small compared to viscous effects. The dimensionless factor  $C_w$  accounts for the geometry of the screen weave and the fact that the effective open thickness of the screen is not  $B_s$ . By integrating this relation with respect to time, the wetted length of the screen is found to be:

$$L(t) = \left[ 2 \left( \frac{\Phi_w B_s^2}{D_{BP} C_w} \right) \left( \frac{\sigma t}{\mu_L} \right) \right]^{1/2}$$

The  $L$  vs.  $t$  best fit to the data is therefore a straight line when  $L$  is plotted against the square root of elapsed time. The  $C_w$  parameter is determined from the slope  $S$  of this plot by using the preceding relation:

$$C_w = \sqrt{\frac{2\Phi_w B_s^2}{D_{BP}} \left( \frac{\sigma}{\mu_L} \right)} (S)^{-1}$$

For some screen weaves, only the ratio  $C_w/\Phi_w$  has been measured, but this ratio is usually sufficient to compute wicking velocities and mass flow rates.

The wicking flow rate itself cannot be computed from Eq. (4.49) since the actual open area of the screen cross section is not known. However, the effective open thickness  $B_{fs}$  of the screen can be related conceptually to the actual screen thickness  $B_s$  by imagining it to be the width of an ordinary flow channel, so that:

$$B_{fs} = 3.464 B_s / \sqrt{C_w} \quad (4.50)$$

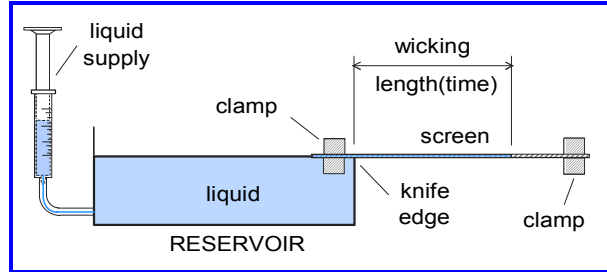


Figure 4.35. Test set up to measure wicking resistance

#### 4. FLUID MANAGEMENT IN MICROGRAVITY

The flow rate per unit width of the screen is estimated as  $V_w B_s$ .

**Cross flow pressure drop.** For most PMDs, liquid has to flow across the screen at some time. For that reason, the cross flow pressure drop  $\Delta P_f$  vs. flow velocity  $V_f$  relation has been measured for many types of screens and correlated to expressions of the form:

$$\Delta P_f = K_1 \frac{\mu_L B_s}{D_{BP}^2} V_f + K_2 \frac{\rho_L B_s}{D_{BP}} V_f^2 \quad (4.51)$$

where  $K_1$  is a laminar flow resistance and  $K_2$  is a turbulent or inertial flow resistance. The pore diameter for crossflow is not necessarily the same as the bubble point pore diameter, but  $K_1$  and  $K_2$ , which depend on the screen weave, account for this difference.

**Screen data summary.** Table 4.2 summarizes the data for commonly used square and twilled weave screens. The data comes from a variety of sources, which do not always agree<sup>14</sup>; when there was a discrepancy, either the data from BLATT [1970] or an average was used. Square weave screens do not wick (i.e.,  $\Phi_w = 0$ ), and the wicking characteristics of twilled dutch weave screens depend on whether the wicking is

**Table 4.2** Geometric data for selected square and twilled dutch weave screens

Screen Mesh	$D_{BP}$ , microns	$B_s$ , microns	$\Phi_w$	$C_w$	$C_w/\Phi_w$	$K_1$	$K_2$
20 X 20	860	-	0	-	-	$\approx 0$	$1.36 D_{BP}/B_s$
40 X 40	440	-	0	-	-	$\approx 0$	$3.16 D_{BP}/B_s$
50 X 50	280	-	0	-	-	$\approx 0$	$5.44 D_{BP}/B_s$
80 X 80	180	-	0	-	-	$\approx 0$	$4.77 D_{BP}/B_s$
100 X 100	140	-	0	-	-	$\approx 0$	$5.34 D_{BP}/B_s$
150 X 150	104	-	0	-	-	$\approx 0$	$2.90 D_{BP}/B_s$
200 X 200	74	-	0	-	-	$\approx 0$	$3.77 D_{BP}/B_s$
325 X 325	44	-	0	-	-	$\approx 0$	$0.62 D_{BP}/B_s$
400 X 400	38	-	0	-	-	$\approx 0$	$4.94 D_{BP}/B_s$
20 X 250	53	711	NA NA	NA NA	5610 $\perp$ 2805 $ $	17.3	6.80
30 X 250	49	673	NA	NA	40400 $\perp$	24.3	5.19
50 X 250	34	323	0.393 0.231	754 1058	1918 $\perp$ 4580 $ $	7.9	50.00
80 X 700	30	249	NA NA	NA NA	4920 $\perp$ 2376 $ $	45.5	7.25
150 X 700	23	178	NA	NA	NA	69.7	49.66
165 X 800	23	165	1.128 1.047	835 2580	740 $\perp$ 2466 $ $	9.42	63.18
200 X 600	19	140	NA NA	NA NA	1063 $\perp$ 2063 $ $	14.0	1.56
165 X 1400	19	152	NA NA	NA NA	6400 $\perp$ 3200 $ $	64.8	10.52
200 X 1400	14	147	0.225 0.318	3157 1444	14031 $\perp$ 4540 $ $	65.6	10.58

<sup>14</sup> ARMOUR AND CANNON, [1968]; BLATT, ET AL [1970]; SYMONS [1974]; BINGHAM AND TEGART [1977]; DODGE AND BOWLES [1984]; these references also use data from other older sources.

perpendicular to or parallel to the warp wires, as indicated by the  $\perp$  and  $|$  symbols in the table. Furthermore, for square weave screens, the laminar flow resistance  $K_1$  is negligibly small, and the  $K_2$  factor listed in the table includes the ratio  $D_{BP}/B_S$  so the cross flow pressure drop for a square weave screen is simply the listed numerical factor (e.g., 1.36 for a 20 X 20 mesh screen) times the liquid density and the square of the velocity; for this reason, the thickness of the square weave screens is not listed in the table.

**Perforated plates.** PMDs fabricated from plates containing a myriad of small diameter holes have some structural advantages compared to screens; for example, they can be fastened to the tank rather than welded. Special manufacturing procedures are needed, however, to make the diameter of the holes small enough to have a large bubble point. An alternative is to stack several plates, with the holes staggered from one plate to the next, so that only a small fraction of each hole is open [TEGART AND WRIGHT, 1983]; stacking the plates also allows a small gap to be maintained between the plates which might be effective in wicking, for otherwise a perforated plate does not wick liquid. The characteristics of perforated plates are mostly proprietary to the manufacturer. Hence, little or no data are available for use in the design of a PMD.

### Typical design considerations for PMD/LADs

The design of a spacecraft tank PMD or LAD requires that the designer evaluate the mission requirements to determine what kind of PMD is best. The design details are then explored and the failure mechanisms (leakage, gas ingestion, etc.) investigated. This last step is particularly important since many PMDs cannot be ground tested. Simplified design concepts for several types of PMD are discussed below.

**Refillable trap (“start basket”).** Suppose a spacecraft mission requires a few restarts of a small thruster for maneuvering or course corrections. If the thrusting duration is sufficient to settle the liquid each time, a refillable trap or start basket, such as the one shown in *Figure 4.36*, may be the best light weight and simple PMD. The trap volume must be big enough (with margin) to supply the thruster during the settling period, and the trap must be refillable to allow the thruster to be restarted the next time.

The mission specifications are summarized as follows:

- Hydrazine propellant:  $\rho_L = 0.036 \text{ lb/in}^3$  and  $\sigma = 60 \text{ dyne/in}$
- Thrust:  $F = 1 \text{ lb}$
- Mass of spacecraft:  $M_{sc} = 1200 \text{ lb}$
- Propellant flow rate:  $Q = 1.5 \text{ in}^3/\text{sec}$
- Minimum thruster duration:  $T_{min} = 150 \text{ sec}$
- Volume of tank:  $V_T = 14000 \text{ in}^3$ ; height of tank:  $H_T = 30 \text{ in}$
- Maximum lateral acceleration (occurs during launch):  $g_x = \pm 4 g_o$
- Maximum axial acceleration (occurs during launch):  $g_z = 2 g_o$
- Maximum flow pressure drop allowed for PMD:  $\Delta P_{max} = 2 \text{ psi}$

The tank is pressurized to allow the propellant to be fed by the pressure difference between the tank and the engine chamber.

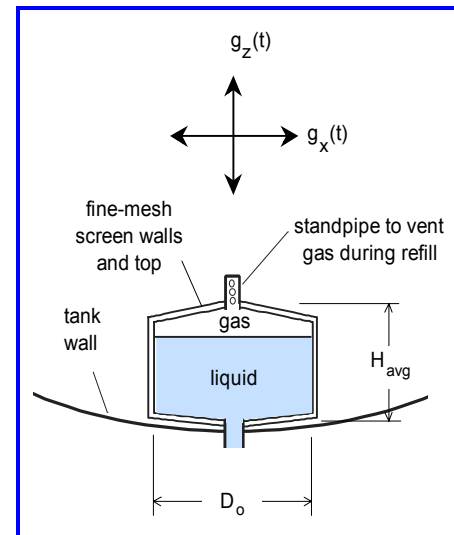


**Figure 4.36.** Schematic of a refillable trap PMD

#### 4. FLUID MANAGEMENT IN MICROGRAVITY

---

The trap volume is computed first. We need to know how much propellant the trap must supply before the liquid is settled and the covers the trap, so the settling time has to be estimated. The settling acceleration is  $F/M_{sc} = 1/1200 = 0.00083 g_o = 0.322 \text{ in/sec}^2$ . The time required for a liquid particle to fall freely from the top of the tank to the bottom is therefore  $(2 \times 30 \text{ in}/0.322 \text{ in/sec}^2)^{0.5} = 13.6 \text{ sec}$ . The time required to settle liquid over the trap is estimated conservatively as four times this free-fall time, or  $54.4 \text{ sec}$ . This is considerably less than the engine firing duration of  $150 \text{ sec}$ , so liquid should refill the trap after each firing. The required minimum volume of trap is therefore  $54.4 \text{ sec} \times Q = 81.6 \text{ in}^3$ . The first design equation is thus:

$$\frac{\pi}{4} D_o^2 H_{avg} = 81.6 \text{ in}^3 \quad (4.52a)$$

As a first trial, the trap diameter is estimated to be the same as the average height; thus,  $D_o = H_{avg} = 4.7 \text{ in}$ .

A screen mesh must now be selected that has an adequate bubble point. When the trap is full and  $g_z$  is oriented to make the liquid in the tank move away from the trap, the screens are exposed to gas on the outside and liquid on the inside. Hence, if the hydrostatic head caused by either the  $g_z$  or  $g_x$  accelerations exceeds the bubble point, the trap will admit gas and expel liquid. Considering first the  $g_x$  acceleration, the hydrostatic head across the trap is equal to  $\rho_L g_x D_o$ . Since the screens cannot support any pressure increase from the liquid to the gas, a pressure balance along a path from the outside gas, through the screen, horizontally along the liquid, and then back to the gas shows that the bubble point pressure at the low pressure side of the trap must be at least equal to the specified hydrostatic head. Thus, the second design equation for the trap is:

$$\Delta P_{BP} = \frac{4\sigma}{D_{BP}} = \rho_L g_x D_o = \left(0.036 \frac{\text{lb}}{\text{in}^3}\right)(4)(4.7 \text{ in}) = 0.68 \text{ psi} \quad (4.52b)$$

The surface tension of hydrazine is about  $60 \text{ dyne/cm} = 0.00034 \text{ lb/in}$ , so Eq. (4.52b) indicates that the bubble point diameter can be no larger than  $D_{BP} = 0.002 \text{ in} = 51 \text{ microns}$ . A fairly fine mesh screen will be needed, and it may not be practical to fabricate the trap. Nonetheless, from Table 4.2, a square mesh screen with either  $325 \times 325$  or  $400 \times 400$  wires per inch will provide the required bubble point with some margin. Next we should consider the hydrostatic head caused by the  $g_z$  acceleration. However, here the  $g_z$  head is not of concern, because it is smaller than the  $g_x$  head.

A square mesh screen is preferred since the trap must be refilled, and a twilled dutch screen might wick closed during the refilling and trap some gas. However, a twilled dutch screen could be used, if the top surface of the trap was made solid so that refilling would have to occur through the sides and bottom of the trap.

Next, the pressure drop across the trap must be checked. During the thrusting period after the propellant has settled, liquid flows across the trap into the outlet. The flow velocity depends on the screen area; neglecting the screens facing the bottom, the flow area is  $A = 86.7 \text{ in}^2$ . The liquid velocity  $V_{avg}$  across the screens is  $Q/A = 1.5 \text{ in}^3/\text{sec}/(86.7 \text{ in}^2) = 0.0173 \text{ in/sec}$ . For a  $325 \times 325$  mesh screen,  $K_2$  from Table 4.2 is  $0.62 D_{BP}/B_s$ , so the flow-through pressure drop of  $0.5 \rho K_2 B_s (V_{avg})^2/D_{BP}$  is equal to  $0.00036 \text{ psi}$ . This value is negligible compared to the 2 psi requirement. Hence the conceptual design satisfies the requirements.

Refilling can be aided by installing a small standpipe at the top of the trap to give gas a place to exit. The openings in the standpipe must be covered with a non-wicking screen, and the hydrostatic head caused by the  $g_z$  acceleration must not exceed the bubble point of this screen. If a standpipe is not used, the trap upper surface must be conical or some shape that will permit gas to collect and exit at a high point.

Other considerations may affect the trap design. For example, the maximum residual volume of propellant in the tank after the last restart may be specified, so the design should be checked to ensure that liquid in the trap and tank does not exceed the specified value at the point when the level in the tank just falls below the top of the trap. An anti-vortex baffle may also be required over the outlet.

**Galleries or channels.** As another example, consider a communication satellite that uses an arcjet thruster for its transfer orbit maneuver. The arcjet is activated several hundred times, each time creating an acceleration of the order of  $10^{-5}g_0$  for up to 30 minutes. The hydrazine propellant tank is a 21-in diameter cylinder with hemispherical ends, and the end-to-end length is 30 in. The time for a fluid particle to fall freely from one end of the tank to the other when the arcjet is thrusting is only about 2.5 minutes; liquid will settle over the outlet during the thrusting, but the settling acceleration is so low that the liquid could not penetrate the screens of a trap PMD to refill it. Hence, some other kind of PMD is required. A gallery or channel PMD is an option, as shown in *Figure 4.37*.

The propellant flow from the tank is driven by pressure. The tank is initially pressurized, but it is not repressurized as it is emptied. Thus, to ensure that the pressure does not decrease significantly as the tank empties, the tank volume ( $8330 \text{ in}^3$ ) is designed to be about three times the initial propellant volume ( $2747 \text{ in}^3$ ). The settled depth of the liquid at liftoff is thus only 11.4 in. Other specifications are listed below.

- maximum axial acceleration:  $g_z = 8g_0$  (during launch)
- maximum lateral acceleration:  $g_x = \pm 3.5g_0$  (during launch)
- Attitude control acceleration:  $g_x = \pm 0.00025g_0$  (from catalytic thrusters not fed from the hydrazine tank)
- propellant flow rate:  $Q = 0.137 \text{ in}^3/\text{sec}$
- maximum PMD pressure drop:  $\Delta P_{max} = 5 \text{ psi}$
- maximum propellant residual at end of mission: 1.5% of initial loading =  $41.2 \text{ in}^3$ .

At least one PMD channel has to remain in contact with the propellant at all times to ensure gas-free propellant to the arcjet, otherwise the tank pressure will drive gas into one or all of the channels. The exposed areas of the screens also must not dry out from evaporation. Since there is no assurance that liquid will be located in any

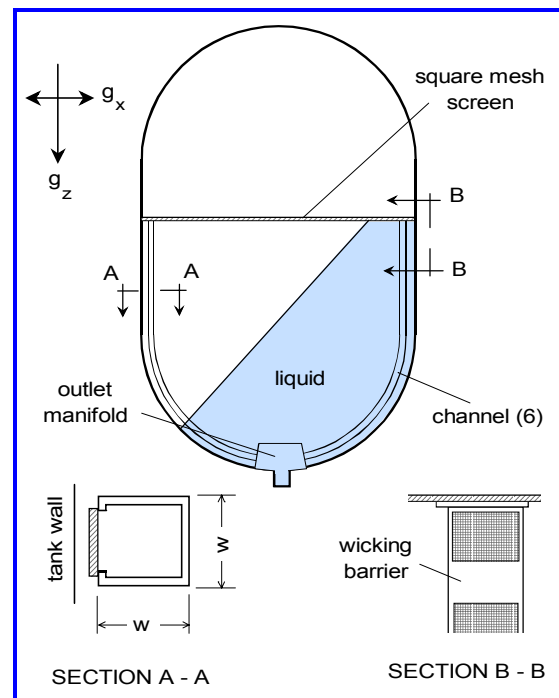


**Figure 4.37.** Schematic of channel PMD

predictable location in zero-g, the channels must be designed to accommodate any liquid location. One option is to make the channels extend from the bottom of the tank to the top, with the spacing of channels around the tank circumference small enough so that the tank liquid cannot “hide” between the channels. (The liquid tends to remain bound to the walls.) But during launch, the liquid depth is only 11.4 in above the outlet, so a channel that extends from the bottom to the top will be exposed to gas over the upper  $H = 18.6$  in of its axial length. For hydrazine, the hydrostatic head created by the  $8g_o$  launch acceleration in the exposed upper part is  $\rho_L g_z H = (0.036 \text{ lb/in}^3)(8g_o)(18.6 \text{ in}) = 5.36 \text{ psi}$ . At the top of the channel, there is thus a pressure difference of 5.36 psi exerted across the screen from the gas to the channel liquid. The screen bubble point must be 5.36 psi so as not to leak during launch. For hydrazine, this would require a pore diameter of about 0.00028 in (7 microns). The data in [Table 4.2](#) indicate that such a tight screen weave would be difficult to acquire. Consequently, an alternative concept is needed.

Since the maximum depth of settled liquid is only 11.4 in, the channel does not have to extend all the way to the top of the tank if some method is used to prevent liquid from being located at the top of the tank in zero-g. [Figure 4.37](#) shows one way to accomplish this. The channels terminate at a height slightly greater than the maximum settled depth of the propellant, and a *blocking* screen prevents the propellant from migrating to the upper end of the tank during zero-g. During launch, the combined effect of the axial and transverse accelerations causes the settled liquid to be inclined at  $30^\circ$  to the horizontal, so the highest edge of the liquid surface is 6.1 in above the settled depth. Therefore, the channels need to extend to a height of about  $11.4 + 6.1 = 17.5$  in above the tank bottom. The critical hydrostatic head is now only  $(0.036)(8g_o)(6.1) = 1.76 \text{ psi}$ . The corresponding pore diameter is 0.008 in (21 microns). A twilled dutch screen with a mesh of  $165 \times 1400$  or  $200 \times 600$  wires per inch should be adequate, considering the conservatism in the calculations.

In zero-g, the blocking screen must retain the liquid in the lower part of the tank. The contact line of the zero-g liquid interface on the walls is about 7.0 in above the settled liquid level. Since the blocking screen is 6.1 in above the settled level, the interface will therefore exert a very small pressure on the screen during the arcjet thrusting and the catalytic thruster firing. The blocking screen is likely to be dry in zero-g, but the interface pressure is so low that the “drop point” pressure of the screen, which is usually assumed to be zero, will exceed it, so the screen will not leak. Sloshing creates an additional impact pressure. An estimate of the low-g slosh amplitude is 4 in for the specified transverse impulsive acceleration of  $0.00025g_o$ . The slosh impact pressure is therefore no greater than about  $(0.036)(0.00025g_o)(4) = 0.0139 \text{ psi}$ . The blocking screen may leak very slightly during the transient sloshing intervals.

The blocking screen has to remain open to gas flow, so it should be made from a square mesh weave to prevent wicking. The channel screens must remain wet, however, so they should be made from twilled dutch screens to permit wicking. To assist in filling the channels initially, a small wicking barrier is used at the upper end of each channel, as shown in [Figure 4.37](#); this keeps the upper screen dry during the filling so that gas can be expelled.

The pressure drop from the bulk liquid to the channel during outflow is a maximum when the liquid volume is a minimum, since that corresponds to the minimum wet surface area of the channels. The settled depth for the minimum liquid volume of  $41.2 \text{ in}^3$  is about 1.2 in. For conservatism, all the outflow is assumed to pass through one channel, which considering the shape of the bottom of the tank therefore corresponds to

a wetted length of about 5 in. For this flow length, the screen flow area needed to ensure that the pressure drop does not exceed 5 psi gives a width of  $W = 0.006$  in, which is too small to be practical, so it is increased to 0.25 in. The channel cross section is thus  $0.25 \times 0.25$  in, with the wall facing the tank wall being a screen, as indicated in *Figure 4.37*. When the channel liquid flows toward the outlet, there is a pressure drop along the axis of the channel. Again, for maximum conservatism, it is assumed that all the arcjet flow occurs in one channel, and the liquid enters this channel at its very top. The computed pressure drop is less than 0.005 psi. This value is well within the specifications, and further it will not result in the bubble point being exceeded at the lower end. The spacing of the channels is determined by the requirement that the minimum liquid volume ( $41.2$  in<sup>3</sup>) cannot fit in between two adjacent channels. Assuming that the liquid is distributed along the cylindrical walls during the catalytic thruster firing (the critical condition), the minimum spacing corresponds to six equally spaced channels. If the channels are spaced in the tank such that the line of action of the catalytic thrusters does not bisect the open space between any two channels, four equally spaced channels is sufficient. The channels are interconnected over the tank outlet by a manifold which may contain a sponge to make sure it remains full of liquid. The manifold must be designed so that the maximum residual propellant volume specification is not violated. This implies that the manifold upper surface must be below the settled liquid depth (1.2 in) when the residual propellant volume is attained.

VAN DYKE [1998] has shown that the optimum screens (i.e., lightest weight) have the smallest value of the ratio of the  $\Delta P$  caused by the flow across the screen to the bubble point  $\Delta P_{BP}$  and that these screens have the coarsest mesh that can be made to satisfy the bubble point requirement. Methods of ground testing to confirm the performance of gallery and other types of PMDs are discussed by YEH AND BOND [1988]

**Vane PMD.** For satellites that thrust in any direction and for any duration, a combination of vanes and a refillable sponge may be the lightest and simplest PMD. *Figure 4.38* shows such a PMD. If the thrust direction is completely arbitrary, the vanes must extend all the way to the top of the tank.

Vanes pump propellant to the outlet or the sponge by trapping the liquid in the fillets between the vanes and the wall as a result of surface tension forces created by shaping the vanes near the tank wall such that the radius of curvature of the trapped liquid interface decreases near the outlet [JAEKLE, 1991]. (The figure shows the vanes immersed in liquid; the critical case is when the liquid pool is away from the outlet and only part of the vane is immersed in liquid.) The acceleration that results in the vanes leaking is determined by these radii of curvature.

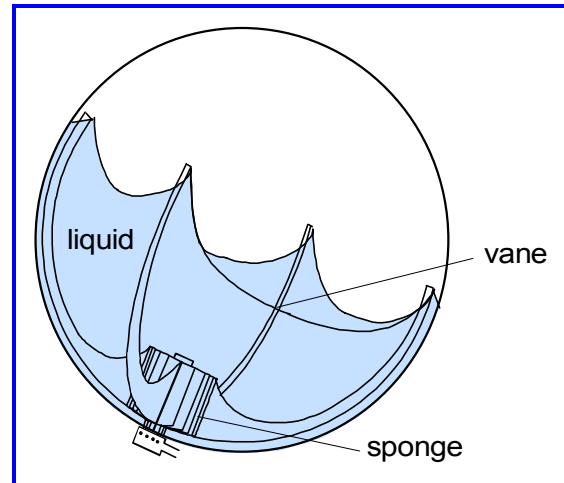


**Figure 4.38.** Vane and refillable sponge PMD

A vane PMD cannot provide high propellant flow rates or retain liquid when the disturbing accelerations are large [DREYER, ET AL., 1998]. If large accelerations occur only during launch, a vane PMD might still be useful by installing a blocking screen at the top of the vanes similar to that shown previously in *Figure 4.38*.

**Other PMD designs.** The PMD designs discussed above are only a small sample of the designs that have been used in spacecraft. PMDs are designed specifically for each mission. More complete details of the design and operation of propellant management devices are given in DOWDY, ET AL [1976], TEGART [1979]; DODGE [1992], PUROHIT, ET AL [1998], DEBRECENI AND LAY [1998], and TAM, ET AL [1998].

## 4.8 PMD Considerations for Cryogenic Liquids

Although much of the preceding discussions applies equally well to cryogenic liquids, cryogenics do introduce several new problems [FISHER, ET AL, 1991; SCHUSTER, ET AL, 1991; FRANK AND JAEKLE, 1996]. Not all the technology to solve these problems has advanced beyond drop-tower tests and analytic models [AYDELOTT, ET AL, 1985; BAILEY, 1991]. An example of a specific cryogenic problem is the fact that the vapor pressure of a cryogen is not greatly different from the tank pressure, which can easily lead to local boiling or vaporization of the liquid.

**Heat transfer and pressure control.** Heat transfer between a cryogenic tank and its surroundings is considerably different than for a storable liquid. While the mean temperature of the tank surface for a storable liquid can be controlled within the temperature range in which the liquid must be used, the tank outer surface for a cryogenic tank is at least 100°F above the desired temperature of even the warmest cryogen. This means that the tank must be well insulated to prevent excessive boiling of the cryogen and a subsequent pressure rise in the tank. Even with many layers of high performance insulation, however, heat can reach the liquid through the support system, the plumbing penetrations, and instrumentation lead wires.

It might be expected that, given the heat transfer rate, estimating the temperature and pressure rise rate would be straightforward, by assuming the liquid is at a uniform temperature and the vapor pressure is equal to the saturation pressure at the liquid temperature. However, the liquid temperature is generally far from uniform, and the liquid and the vapor do not reach thermal equilibrium instantaneously. The lack of temperature uniformity is caused by natural convection. Even in low gravity, buoyancy forces can be significant for large tanks. *Figure 4.39* illustrates the phenomenon of stratification for a case when the residual gravity is sufficient to settle the liquid. Many analyses of stratification have been conducted [e.g. BAILEY, ET AL, 1963; LEVY, ET AL, 1964; TELLEP AND HARPER, 1964; SCHWARTZ AND ADELBERG, 1965]. The thickness of the hotter layer on top grows with time as a result of the hotter buoyant fluid rising along the sides of the tank. These natural convection boundary layers are usually turbulent. A mass balance gives the following relation for the thickness of the stratified layer as a function of time:

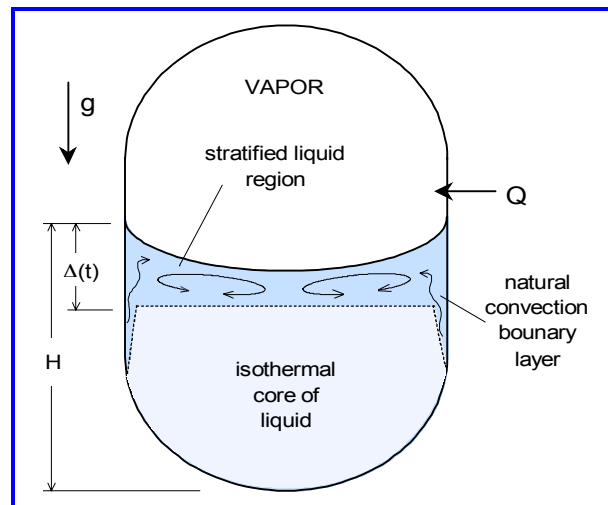


**Figure 4.39.** Cryogenic liquid stratification

$$\frac{\Delta(t)}{H} = 1 - \left[ 1 + 0.092 \frac{H}{R_0} \left( \frac{\mu_L t}{\rho_L H^2} \right) \frac{1}{Pr^{2/3}} \left( \frac{Gr}{1 + 0.443 Pr^{2/3}} \right)^{2/7} \right]^{-7} \quad (4.53)$$

where  $Pr = (\mu C_p/k)_L$  is the Prandtl number and  $Gr = g\beta_L(R_0)^2 Q(\rho_L/\mu_L)^2/k_L$  is the Grashof number based on the heat transfer rate  $Q$  per unit per unit wall area, with  $k_L$  being the liquid thermal conductivity and  $\beta_L$  the liquid thermal expansion coefficient. With this relation, the temperature of the stratified liquid can be estimated from the heat transfer rate across the tank walls into the liquid.

If the vapor and the liquid in the tank are in equilibrium, the pressure would be equal to the saturation pressure of the hot surface liquid. This pressure is considerably larger than it would be if the liquid was well mixed at a uniform temperature. Although the liquid and vapor are not likely to be in thermal equilibrium, especially if a non-condensable gas is mixed with the vapor to pressurize the tank, the tank pressure will nonetheless increase at a rate that is probably larger than for a mixed liquid. Consequently, a tank containing cryogenic liquid must be vented periodically. Mixing the liquid, with axial jets or otherwise, tends to breakup the stratification and thus reduce the need for frequent venting [BENTZ, ET AL, 1997]. This need to vent the tank gives rise to the same problem as if the liquid were storable, namely how to ensure gas is vented rather than the more valuable liquid, as was discussed previously.

For a cryogen, the possibility that liquid rather than gas may be vented has been used to advantage to develop an ingenious method of cooling the tank liquid with the vented fluid. One form of this *thermodynamic vent system* (TVS) is shown schematically in [Figure 4.40](#) [BAILEY, 1991]. A TVS operates by expanding some of the tank liquid through a Joule-Thomson expander connected between the tank and the vacuum of space; the process evaporates part of the liquid and the overall temperature of the expanded fluid

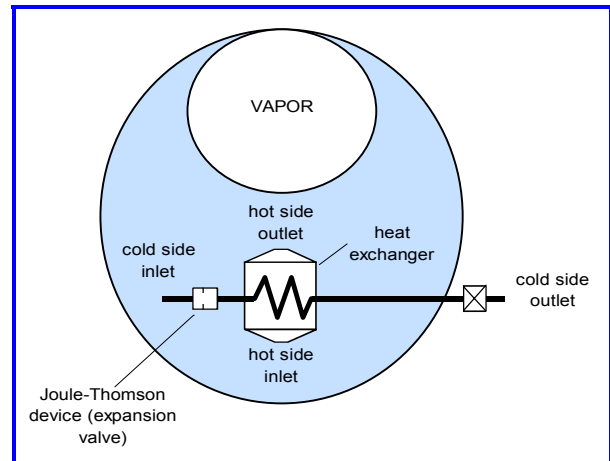


**Figure 4.40.** Schematic of thermodynamic vent for cryogenic liquids

decreases significantly. In the application shown in [Figure 4.40](#), the colder TVS fluid flows through a heat exchanger to cool the liquid bulk and then is vented. Alternatively, the colder fluid can be used to form a cold jacket around the tank (a *vapor cooled shield*). The venting fluid can also be used to augment the thrusting. A TVS works best if the entering fluid is liquid, so the TVS inlet is generally connected to the tank liquid acquisition device. Some designs employ a separate pump to mix the bulk liquid to prevent stratification [CADY AND OLSEN, 1996].

**Tank filling and liquid transfer.** Some future missions will require filling tanks with cryogen in space. It is difficult to fill a tank efficiently with a storable liquid in a low-gravity environment because of the gas venting problem, and it is even more difficult when the liquid is a cryogen because vaporization and boiling accentuates the venting problem. [Figures 4.41a](#) and [4.41b](#) illustrate two concepts for filling a tank with a cryogen, neither of which vents the receiver tank during the filling [CHATO, 1993].

For the no-vent filling process show in *Figure 4.41a*, the first step is to chilldown the transfer lines and the receiver tank using liquid from the supply tank. This clearly vaporizes some of the liquid. The process can be made more efficient by using a direct contact wall-mounted heat exchanger or by a charge-and-hold process in which liquid is sprayed into the receiver tank where it flashes to vapor and is allowed to reach thermal equilibrium with the tank walls. Eventually, the tank temperature is decreased to the point at which the filling can proceed. Part of the incoming liquid vaporizes, but the subsequent compression by additional liquid condenses most of it. The liquid is sprayed into the tank to enhance the condensation process and to “find” and condense the ullage vapor bubbles to maximize the fill level.

The ullage exchange process shown in *Figure 4.41b* is similar to the no-vent process except that the receiver tank is vented back to the supply tank during the filling. Both liquid and vapor may be vented.

Both processes require a liquid acquisition device in the supply tank to ensure that only liquid is transferred from the supply tank. The receiver tank may also contain a LAD but if so it should always remain full of liquid because refilling a LAD in low gravity is extremely difficult. It is clear that all these processes involve low-g two-phase mass and heat transfer, which are subjects of intense research.

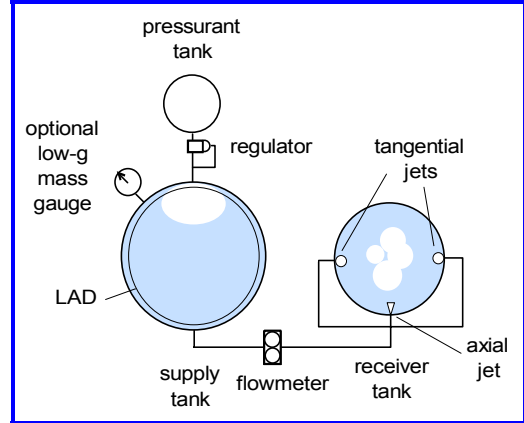


Figure 4.41a. No-vent fill process

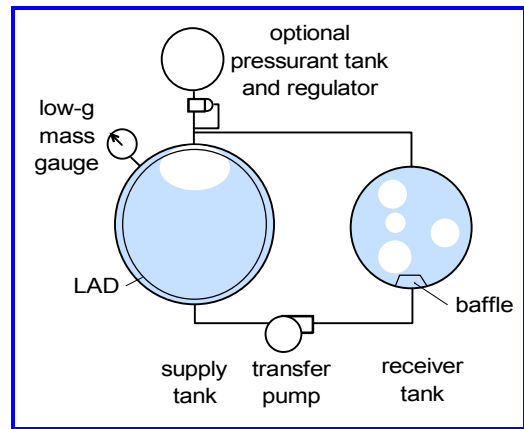


Figure 4.41b. Ullage exchange process

**Interaction of bubble point pressure and**

**vaporization from screens.** Both the wicking and bubble point pressures of a liquid acquisition device screen depend on capillary forces. When wicking and a pressure difference occur simultaneously, the total capillary potential of the screen is not available for either phenomena [DODGE AND BOWLES, 1984].

Experiments have shown that to a good approximation, the bubble point pressure decreases linearly with wicking velocity and that the bubble point is greater than zero even when the wicking rate is the maximum possible. These experimental observations are expressed by the relation:

$$\Delta P_{BP} = \frac{4\sigma}{D_{BP}} \left( 1 - K_{BP} \frac{V_w}{V_{w,max}} \right) \tag{4.54}$$

Here,  $V_{w,max}$  from Eq. (4.49) is the maximum possible wicking velocity for the screen,  $V_w$  is the actual wicking velocity, and  $K_{BP}$  is a numerical factor that depends on the screen weave. Data for  $K_{BP}$  are available for only a few twilled dutch screens (24 X 110 and 50 X 250 wires per inch), and for these screens  $K_{BP} \approx 0.5$ ; this value is probably applicable to other screen weaves as well. The actual wicking velocity  $V_w$  is determined by the evaporation rate from the screen.

Similarly, the maximum possible wicking suction pressure has been found to decrease linearly with the gas-to-liquid pressure differential  $\Delta P$  across the screen. To be

consistent with Eq. (4.54), the wicking suction pressure must be equal to its maximum value when the gas-to-liquid pressure is less than  $(1 - K_{BP})(4\sigma/D_{BP})$ . Thus:

$$\phi_{ws} = \phi_{ws,max} \left[ 1 - \frac{1}{K_{BP}} \left( \frac{\Delta P}{\Delta P_{max}} + K_{BP} - 1 \right) \right] \quad \text{for } \Delta P \geq (1 - K_{BP})\Delta P_{max} \quad (4.55a)$$

$$\phi_{ws} = \phi_{ws,max} \quad \text{for } \Delta P \leq (1 - K_{BP})\Delta P_{max} \quad (4.55b)$$

where  $\Delta P_{max} = 4\sigma/D_{BP}$ . To be conservative, one should probably assume that  $V_w = V_{w,max}$ ; in that case, the maximum bubble point pressure is  $4\sigma/D_{BP}(1-K_{BP}) \approx 2\sigma/D_{BP}$ .

**Cryogenic-specific failures of LADs and PMDs.** Propellant management devices such as channels, start baskets, and traps work by establishing a capillary barrier between the liquid in the device and the exterior gas. But when the liquid is a cryogen, gas can be generated within the device by local boiling as a result of heat transfer. A few vapor bubbles within the PMD are not likely to cause problems because the PMD screen will wick over any dry spots and prevent the entrance of large quantities of exterior gas. However, if most of the liquid in the PMD is vaporized, problems will occur. Various methods of eliminating vapor bubble from the inside of PMDs have been proposed, such as tapering the channel of a gallery PMD to force vapor bubbles to a specific location within the PMD where they might be vented; none of these methods have yet been tested. The most fail-safe method of eliminating vapor bubbles appears to be to re-condense them by cooling the PMD liquid with a thermodynamic vent system. At present, the lack of flight data and proved methods of ensuring the operation of channels, start baskets, and traps for cryogenic liquids have prevented the use of these types of PMD in cryogenic tanks of space vehicles. Other forms of PMD, such as vanes, do work well with cryogens.

**Other cryogenic considerations.** A phenomenon related to the stratification of a cryogenic liquid in a tank is *ullage pressure collapse*. As mentioned earlier, the pressure of the vapor in the ullage is equal to the saturation pressure of the hot liquid at the surface, assuming that sufficient time has elapsed for the vapor to be in thermal equilibrium with the liquid. If the liquid is suddenly mixed, say by sloshing or otherwise, the temperature of the surface liquid will suddenly decrease. As a result, the pressure of the ullage vapor will also suddenly decrease. This collapse of the ullage pressure can cause a problem if liquid outflow is being driven by the tank pressure, because the outflow will also suddenly decrease.

Because cryogens boil easily, two-phase flow is prevalent in flow lines. Two-phase flow in low-gravity is not yet well understood, but it is apparent that choking and transients such as water hammer might be problems. Furthermore, flow meters which are routinely used as a method of gauging the total flow from the tank to determine the fluid inventory, are considerably less accurate when the flow is two-phase.

## 4.9 References

- ABDALLA, K., AND BERENYI, S., 1969, *Vapor Ingestion Phenomenon in Weightlessness*, NASA TN D-5210.
- ANTAR, B., and NUOTIO-ANTAR, V., 1993: **Fundamentals of Low Gravity Fluid Dynamics and Heat Transfer**. CRC Press, Ann Arbor.
- ARMOUR, J., AND CANNON, J., 1968, *Fluid Flow Through Woven Screens*, **AICHE J.**, **14**, pp. 415-420.

#### 4. FLUID MANAGEMENT IN MICROGRAVITY

---

- AYDELOTT, J., CARNEY, M., AND HOCHSTEIN, J., 1985, *NASA Lewis Research Center Low-Gravity Fluid Management Technology Program*, NASA TM 87145.
- BAILEY, W., 1991, *What is the Future of Cryogenic Fluid Management Technology?*, AIAA Paper 91-3480.
- BAILEY, T., VANDEKOPPEL, R., SKARTVEDT, G., AND JEFFERSON, J., 1963, *Cryogenic Propellant Stratification Analysis and Test Data Correlation*, **AIAA J.**, **1**, pp. 1657-1658.
- BAUER, H., AND EIDEL, W., 1990, *Linear Liquid Oscillations in Cylindrical Container Under Low Gravity*, **Applied Microgravity Technology**, **II**, pp. 212-220.
- BAUER, H., AND KOMATSU, 1998, *Vibration of a Hydroelastic System Consisting of a Sector Shell and Viscous Liquid in Low Gravity*, **J. Fluids and Structures**, **12**, pp. 367-385.
- BINGHAM, R., AND TEGART, J., 1977, *Wicking in Fine Mesh Screens*, AIAA Paper 77-849.
- BENTZ, M., ALBAYYARI, J., KNOLL, R., HASAN, M., AND LIN, C., 1997, *Tank Pressure Control Experiment: Results of Three Space Flight Tests*, AIAA Paper 97-2816.
- BERENYI, S., AND ABDALLA, K., 1969, *The Liquid-Vapor Interface During Outflow in Weightlessness*, NASA TM X-1811.
- BERENYI, S., 1970, *Effect of Outlet Baffling on Liquid Residuals for Outflow from Cylinders in Weightlessness*, NASA TM X-2018.
- BIKERMAN, J., 1958, **Surface Chemistry**, Academic Press.
- BRAKKE, K., 1992, *The Surface Evolver*, **Experimental Mathematics**, **1**, pp. 141-165.
- BLATT, M., 1970 (editor), *Low Gravity Propellant Control Using Capillary Device in Large Scale Cryogenic Vehicles - Design Handbook*, General Dynamics Convair Report GDC-DDB70-006.
- BHUTA, P., AND KOVAL, L., 1965, *Sloshing of a Liquid in a Draining or Filling Tank Under Variable G Conditions*, **AFOSR Symposium on Fluid Mechanics and Heat Transfer Under Low Gravitational Conditions**, pp. 10-1 to 10-24.
- CADY, E., AND OLSEN, A., 1996, *Cryogen Storage and Propellant Feed System for the Integrated Solar Upper Stage (ISUS) Program*, AIAA Paper 96-3044.
- CARNEY, M., 1986, *Liquid-Vapor Interface Locations in a Spheroidal Container Under Low Gravity*, NASA TM 87147.
- CHATO, D., 1993, *Ground Testing for the No-Vent Fill of Cryogenic Tanks: Results of Tests for a 71 Cubic Foot Tank*, AIAA Paper 93-1967.
- CHATO, D., 1997, *Vented Tank Resupply Experiment – Flight Test Results*, AIAA Paper 97-2815.
- CLARK, L., AND STEPHENS, D., 1967, *Simulation and Scaling of Low-Gravity Slosh Frequencies and Damping*, **Proc., 2<sup>nd</sup> ASTM, IES, and AIAA Space Simulation Conference**, pp. 43-49.
- CONCUS, P., 1963, *Capillary Stability in an Inverted Rectangular Tank*, **Symposium on Physical and Biological Phenomena in a Weightless State**, **14**.

- CONCUS, P., 1964, *Capillary Stability in an Inverted Rectangular Channel for Free Surfaces with Curvature of Changing Sign*, **AIAA Journal**, **2**, p. 2229.
- CONCUS, P., CRANE, G., AND SATTERLEE, H., 1967, *Small Amplitude Lateral Sloshing in a Cylindrical Tank with a Hemispherical Bottom Under Low Gravitational Conditions*, NASA CR-54700.
- CONCUS, P., CRANE, G., AND SATTERLEE, H., 1969, *Small Amplitude Lateral Sloshing in Spheroidal Containers Under Low Gravitational Conditions*, NASA CR-72500.
- CONEY, T., AND MASICA, W., 1969, *Effect of Flow Rate on the Dynamic Contact Angle for Wetting Fluids*, NASA TN D-5115.
- CONEY, T., AND SALZMAN, J., 1971, *Lateral Sloshing in Oblate Spheroidal Tanks Under Reduced and Normal Gravity Conditions*, NASA TN D-6250.
- CUTSHALL, W., DODGE, F., GREEN, S., AND UNRUH, J., 1996, *Modeling Low-G Liquid Motions in Spacecraft Tanks*, SwRI Final Report, Project 04-9769.
- DEBRECENI, M., LAY, W., AND JAEKLE, D., 1998, *Design and Development of a PMD-Type Bipropellant Tank*, AIAA Paper 98-3200.
- DODGE, F., AND GARZA, L., 1967, *Experimental and Theoretical Studies of Liquid Sloshing at Simulated Low Gravity*, **Trans. ASME Journal of Applied Mechanics**, **34**, pp. 555-562.
- DODGE, F., AND GARZA, L., 1968, *Simulated Low-Gravity Sloshing in Spherical Tanks and Cylindrical Tanks with Inverted Ellipsoidal Bottoms*, Report No. 6, SwRI Project 02-1846, Contract NAS8-20290.
- DODGE, F., AND GARZA, L., 1970, *Simulated Low-Gravity Sloshing in Spherical, Ellipsoidal, and Cylindrical Tanks*, **AIAA J. Spacecraft and Rockets**, **7**, pp. 204-206.
- DODGE, F., AND GARZA, L., 1972, *Free-Surface Vibrations of a Magnetic Liquid*, **ASME Journal of Engineering for Industry**, **94**, pp. 103-108.
- DODGE, F., AND BOWLES, E., 1984, *Vapor Flow into a Capillary-Propellant Acquisition Device*, **AIAA J. of Spacecraft and Rockets**, **21**, pp. 267-273.
- DODGE, F., 1988, *The Spreading of Liquid Droplets on Solid Surfaces*, **J. Colloid and Interface Science**, **121**, pp. 154-160.
- DODGE, F., GREEN, S., AND CRUSE, M., 1991, *Analysis of Small Amplitude Low Gravity Sloshing in Axisymmetric Tanks*, **Microgravity Science and Technology**, **IV**, pp. 228-234.
- DODGE, F., 1992, *Preliminary Design of Channel and Vane PMDs for the IRIDIUM Spacecraft Hydrazine Tank*, SwRI Final Report Project 04-3155-021.
- DODGE, F., AND GREEN, S., 1992, *Propellant Motion Models for the CRAF/CASSINI Spacecraft*, Final Report, SwRI Project 04-4263, Contract JPL 959045.
- DOMINICK, S., AND DRISCOLL, S., 1993, *Fluid Acquisition and Resupply Experiment (FARE I) Flight Results*, AIAA Paper 93-2424.
- DOMINICK, S. AND TEGART, J., 1994, *Orbital Test Results of a Vaned Liquid Acquisition Device*, AIAA Paper 94-3027.

#### 4. FLUID MANAGEMENT IN MICROGRAVITY

---

- DOWDY, M., HISE, R., PETERSON, R., AND DEBROCK, S., 1976, *Surface Tension Propellant Control for Viking 75 Orbiter*, AIAA Paper 76-596.
- DRYER, M., ROSENDAHL, U., AND RATH, H., 1998, *Experimental Investigation on Flow Rate Limitations in Open Capillary Flow*, AIAA Paper 98-3165.
- FISHER, M., SCHMIDT, G., AND MARTIN, J., 1992, *Analysis of Cryogenic Propellant Behavior in Microgravity and Low Thrust Environments*, **Cryogenics**, **32**, pp. 230-235.
- FRANK, D., AND JAEKLE, D., 1986, *Cryogenic Fluid Management for Low-G Transfer*, **SPIE**, **619, Cryogenic Optical Systems and Instruments II**, pp. 21-28.
- GRAYSON, G., 2000, *A Computational Design Approach to Propellant Settling*, AIAA Paper 00-5151.
- HOCHSTEIN, J., 1989, *Computational Modeling of Steady and Pulsed Propellant Reorientation*, Presentation to Cryogenic Technology Advisory Group, NASA-Lewis.
- JAEKLE, D., 1991, *Propellant Management Device Conceptual Design and Analysis: Vanes*, AIAA Paper 91-2172.
- JAEKLE, D., 1993, *Propellant Management Device Conceptual Design and Analysis: Sponges*, AIAA Paper 93-1970.
- KAMEL, M., 1964, *The Effect of Swirl on the Flow of Liquids Through Bottom Outlets*, ASME Paper 64-WA/FE-37.
- KRAMER, E. (editor), 1998, *Cryogenic On-Orbit Liquid Depot-Storage, Acquisition and Transfer (COLD-SAT) Experiment Conceptual Design and Feasibility Study*, NASA Technical Paper 3523.
- LABUS, T., 1969, *Natural Frequency of Liquids in Annular Cylinders Under Low Gravitational Conditions*, NASA TN D-5412.
- LEVY, A., CHIN, J., DONALDSON, J., GALLAGHER, L., HARPER, E., HURD, S., AND SATTERLEE, H., 1964, *Analytical and Experimental Study of Liquid Orientation and Stratification in Standard and Reduced Gravity Fields*, Lockheed Missiles and Space Co. Report 2-05-64-1.
- NAVICKAS, J., CROSS, C., AND VAN WINKLE, D., 1986, *Propellant Tank Forces Resulting from Fluid Motion in a Low-Gravity Field*, **Symposium on Microgravity Fluid Mechanics, FED-Vol. 42**, ASME, pp. 69-73.
- NUSSLE, R., DERDUL, J., AND PETRASH, D., 1965, *Photographic Study of Propellant Outflow from a Cylindrical Tank During Weightlessness*, NASA TN D-2572.
- MASICA, W., AND SALZMAN, J., 1965, *An Experimental Investigation of the Dynamic Behavior of the Liquid-Vapor Interface Under Adverse Low-Gravitational Conditions*, **AFOSR Symposium on Fluid Mechanics and Heat Transfer Under Low Gravitational Conditions**, pp. 2-1 to 2-18.
- MICHAELS, A., AND DEAN, S., 1961, *Contact Angle Relationships of Silica Aquagel Surfaces*, Report, Chem. Engrg. Dept., M.I.T.
- MYSHKIS, A., BABSKII, V., KOPACHEVSKII, N., SLOBOZHANIN, L., AND TYUPTSOV, A., 1987, **Low-Gravity Fluid Mechanics**, Springer-Verlag.
- PATAG, A., 1988, *Pulsed Settling for Low-Gravity Liquid Propellant Reorientation*, M.Sc. Thesis, Washington University, St. Louis, MO.

- PETRASH, D., AND OTTO, E., 1964, *Controlling the Liquid-Vapor Interface Under Weightlessness*, **Astronautics & Aeronautics**, **2**, p. 56.
- PUROHIT, G., SMOLKO, J., ELLISON, J., AND JAEKLE, D., 1998, *Propellant Management Device Performance During an Off-Nominal Transfer Orbit Mission*, AIAA Paper 98-4033.
- REYNOLDS, W., SAAD, M., AND SATTERLEE, 1964, *Capillary Hydrostatics and Hydrodynamics at Low G*, Report LG-3, Stanford Univ. Mech. Engrg. Dept.
- ROLLINS, J., GROVE, R., AND JAEKLE, D., 1985, *Twenty-Three Years of Surface Tension Propellant Management System Design, Development, Manufacture, Test, and Operation*, AIAA Paper 85-1199.
- SALZMAN, J., LABUS, T., AND MASICA, W., 1967, *An Experimental Investigation of the Frequency and Viscous Damping of Liquids During Weightlessness*, NASA TN D-4132.
- SALZMAN, J., AND MASICA, W., 1967, *Experimental Investigation of Liquid-Propellant Reorientation*, NASA TN D-3789.
- SALZMAN, J., CONEY, T., AND MASICA, W., 1968, *Effects of Liquid Depth on Lateral Sloshing Under Weightless Conditions*, NASA TN D-4458.
- SALZMAN, J., AND MASICA, W., 1969, *Lateral Sloshing in Cylinders Under Low Gravitational Conditions*, NASA TN D-5058.
- SALZMAN, J. A., AND MASICA, W., 1973, *Low-Gravity Reorientation in a Scale-Model CENTAUR Liquid-Hydrogen Tank*, NASA TN D-7168.
- SATTERLEE, H., AND REYNOLDS, W., 1964, *The Dynamics of the Free Liquid Surface in Cylindrical Containers Under Strong Capillary and Weak Gravity Conditions*, Report LG-2, Stanford Univ. Mech. Engrg. Dept.
- SATTERLEE, H., AND CHIN, J., 1965, *Meniscus Shape Under Reduced Gravity Conditions*, **AFOSR Symposium on Fluid Mechanics and Heat Transfer Under Low Gravitational Conditions**, pp. 13-1 to 13-24.
- SAWADA, T., KIKURA, H., AND TANAHASHI, T., 1999, *Kinematic Characteristics of Magnetic Fluid Sloshing in a Rectangular Container Subject to Non-Uniform Magnetic Fields*, **Experiments in Fluids**, **26**, pp. 215-221.
- SCHUSTER, J., BASSETT, C., CHRISTENSEN, E., HONKONEN, S., MERINO, F., MUNKO, D., PIETRZYK, J., AND WOLLEN, M., 1991, *CENTAUR-Based Liquid Hydrogen Fluid Management Flight Experiments*, AIAA Paper 91-3539.
- SCHWARTZ, S., AND ADELBERG, M., 1965, *Some Thermal Aspects of a Contained Fluid in a Reduced-Gravity Environment*, **AFOSR Symposium on Fluid Mechanics and Heat Transfer Under Low Gravitational Conditions**, pp. 4-1 to 4-47.
- SCRIVEN, L., 1960, *Dynamics of a Fluid Interface*, **Chem. Eng. Sci.**, **12**, pp. 98-108.
- SIEGERT, C., PETRASH, D., AND OTTO, E., 1964, *Time Response of Liquid-Vapor Interface After Entering Weightlessness*, NASA TN D-2458.
- SIEGERT, C., PETRASH, D., AND OTTO, E., 1965, *Behavior of Liquid-Vapor Interface of Cryogenic Liquids During Weightlessness*, NASA TN D-2658.
- SNYDER, H., 1999, *Sloshing in Microgravity*, **Cryogenics**, **39**, pp. 1047-1055.

- SMITH, J., LI, Y., AND CIMA, R., 1965, *The Application of Hydrophilic and Hydrophobic Surfaces for Phase Separation in a Low-g Environment*, **AFOSR Symposium on Fluid Mechanics and Heat Transfer Under Low Gravitational Conditions**, pp. 16-1 to 16-19.
- STEPHENS, D., 1965, *Experimental Investigations of Liquid Impact in a Model Propellant Tank*, NASA TN D-2913.
- SYMONS, E., NUSSLE, R., AND ABDALLA, K., 1968, *Liquid Inflow to Initially Empty, Hemispherical Ended Cylinders During Weightlessness*, NASA TN D-4628.
- SYMONS, E., 1969, *Liquid Inflow to Partially Full, Hemispherical-Ended Cylinders During Weightlessness*, NASA TM X-1934.
- SYMONS, E., 1974, *Wicking of Liquids in Screens*, NASA TN D-7657.
- TAM, W., JAEKLE, D., AND FAROKHI, S., 1998, *Design and Manufacture of the HS 601 Block II Propellant Tank Assembly*, AIAA Paper 98-3199.
- TEGART, J., 1979, *Performance of a Capillary Propellant Management Device with Hydrazine*, AIAA Paper 79-1259.
- TEGART, J., AND WRIGHT, N., 1983, *Double Perforated Plate as a Capillary Barrier*, AIAA Paper 83-1379.
- TELLEP, D., AND HARPER, E., 1963, *Approximate Analysis of Propellant Stratification*, **AIAA J.**, **1**, pp. 1954-1956.
- VAN DYKE, M., 1998, *Identification of Influential Factors for Liquid Acquisition Device Designs*, AIAA Paper 98-3198.
- VAN SCHOOR, M., AND CRAWLEY, E., 1995, *Nonlinear Forced-Response Characteristics of Contained Fluids in Microgravity*, **AIAA J. Spacecraft and Rockets**, **32**, pp. 521-532.
- WEISLOGEL, M., AND ROSS, H., 1990, *Surface Reorientation and Settling in Cylinders Upon Step Reduction in Gravity*, **Microgravity Science and Technology**, **III**, pp. 24-32.
- YEH, T.-P., AND BOND, D. L., 1988, *Testing of Propellant Management Device for 3-Axis Geosynchronous Spacecraft*, **Proc., Institute of Environmental Sciences**, pp. 137-141.

# NONLINEAR EFFECTS IN LATERAL SLOSHING

This chapter is a shortened revision of Chapter 3 of the same title. The original authors were H. NORMAN ABRAMSON, WEN-HWA CHU, AND FRANKLIN T. DODGE.

## 5.1 Introduction

The preceding chapters presented the basic technology of lateral sloshing from the point of view of both theory and experiment for conditions when the slosh wave amplitude is so small that the wave responses are linear. In reality, nonlinear effects are always present, and they sometimes dominate the sloshing response. These nonlinear slosh effects can be described in terms of three classes: (a) those that arise primarily as a consequence of the shape of the tank and are apparent even for relatively small wave amplitudes; (b) those that arise primarily as a consequence of large wave amplitudes; and (c) those that involve essentially different forms of sloshing as a result of instabilities.

At the time when NASA SP-106 was published (1966), the most applicable and useful theoretical way to analyze the effects of nonlinearities on sloshing was the classical *perturbation method* [VAN DYKE, 1964] applied to the nonlinear equations that describe free surface waves, which are discussed in many texts and references [for example, STOKER, 1957; DEBNATH, 1994]. Nowadays, general purpose computational fluid dynamics computer codes having a free surface capability are usually employed to investigate nonlinear effects<sup>15</sup>. Perturbation methods are still valuable, however, because they clearly show how the solution varies with the parameters of the problem. But they are, however, applicable only over a limited range of wave amplitudes, as a result of convergence considerations. In this chapter the application of the perturbation method to free surface waves is described, both for historical reasons and because there are some kinds of sloshing (e.g., rotary) for which CFD codes are even now not generally applicable. The use of CFD codes, which is a subject unto itself, is not discussed here except in passing.

### Engineering estimates of maximum wave amplitudes

Sometimes all that is required is an estimate of the maximum wave amplitude expected during some part of a space mission. This would be the case, for example, when the maximum slosh load on a baffle or tank partition has to be estimated. There are relatively simple methods of obtaining these estimates.

When surface tension is negligible, the maximum downward acceleration exerted on a liquid particle at the free surface (which occurs just when the wave peaks in the upward direction) is  $g - \delta\omega^2$ , where  $g$  is the effective gravitational acceleration,  $\delta$  is the wave amplitude, and  $\omega$  is the slosh natural frequency [BRASLOW, 1968]. Since the maximum acceleration at the peak height always has to remain positive (for otherwise the fluid particle would tear off from the surface), the maximum wave height can therefore be no larger than  $\delta_{max} = g/\omega^2$ , and the maximum usually occurs at the tank walls. As an example, for a cylindrical tank with a liquid depth considerably greater than the tank diameter, the slosh natural frequency is  $(1.841g/R_0)^{0.5}$  so the maximum wave

<sup>15</sup> One example of this use of CFD codes was discussed in Section 3.6 with reference to propellant settling in the CASSINI spacecraft tanks.

amplitude can be no greater than  $R_0/1.841 \approx 0.54R_0$ , or roughly 25% of the tank diameter. In fact, splashing, breaking waves, and even rotary sloshing would probably occur for such a large amplitude. A somewhat better estimate, which can be used for ring baffle damping determinations, is that the maximum amplitude cannot be more than about 10% of the tank diameter, beyond which splashing and rotary sloshing will occur and add additional apparent damping to the sloshing.

## 5.2 Nonlinear Effects Arising from Tank Shape

**Compartmented cylindrical tanks.** Early experiments of sloshing in cylindrical tanks

divided into compartments failed to produce resonant frequency data that agreed satisfactorily with theory [ABRAMSON, ET AL, 1962, 1965]. The measured resonant frequencies were always lower than the theory predicted, sometimes substantially so, as shown in *Figure 5.1*. (The reasons why the measured frequencies were lower than the predicted ones will be explained theoretically in Section 5.3.) Later, more careful experiments showed that measurements and theory agreed when the amplitude of the tank oscillation was very small. But the tank oscillation amplitude had to be much smaller than experience had shown to be necessary to obtain satisfactory agreement for uncompartmented cylindrical tanks.

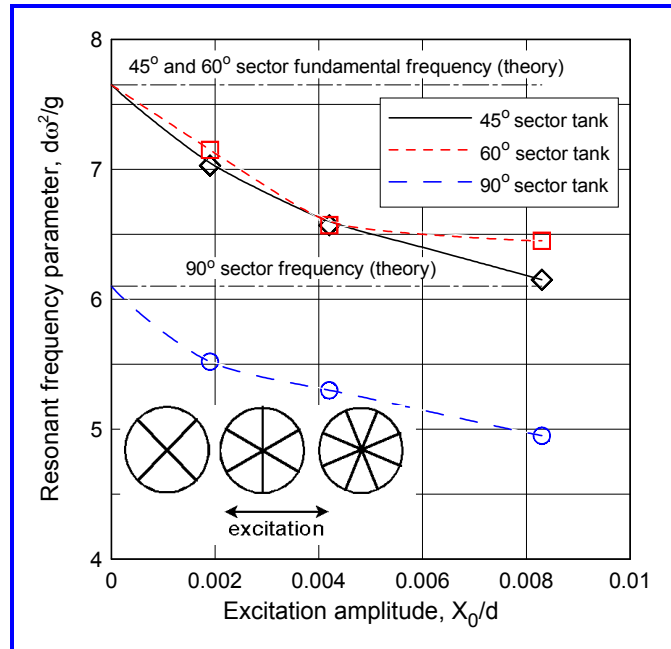


**Figure 5.1.** Effect of lateral excitation amplitude  $X_0$  on the lowest resonant frequency for sector tanks;  $d$  = tank diameter

The unexpectedly stringent requirements on the excitation amplitude for compartmented tanks were essentially due to the tank geometry. Continuity of the flow toward the center of the tank caused the wave amplitude at the center to be relatively high, since the liquid was “squeezed” into a corner. It will be shown in the Section 5.3 that the natural sloshing frequency is affected by wave amplitude. Hence, the lack of agreement between theory and experiment with respect to frequency for a compartmented tank was the result of the tank shape in magnifying an otherwise small wave amplitude into a nonlinear wave amplitude near the center of the tank.

Another remarkable finding for a compartmented tank is that holes in the compartment walls (used to reduce weight or increase damping) had a significant effect on the resonant frequency [ABRAMSON, ET AL, 1965, 1966]. When the composite Reynolds number  $Re = (dg^{0.5}D^{1.5})/(\nu X_0)$  defined in terms of the lateral excitation amplitude  $X_0$ , the tank diameter  $d$ , and the hole diameter  $D$  was less than about 10,000, the experimental natural frequencies corresponded to the natural frequencies of the individual compartments with solid walls. But when  $Re > 10,000$ , the experimental frequency

corresponded to the lower frequency of an uncompartmented cylindrical tank of the same diameter and liquid depth. The transition was not sharp, and slightly larger frequencies were measured near the transition. Apparently, for  $Re > 10,000$ , the holes were so large that the liquid sloshed back and forth into adjacent compartments as if the walls were not present. The slosh forces also displayed nonlinear characteristics.

**Spherical tanks.** Experiments with spherical tanks over a range of fill levels showed that the resonant frequency had nonlinear characteristics when the fill level was over 50% [ABRAMSON, ET AL, 1963, 1964]. This was again a result of tank shape, since for fill levels over 50%, the upward half of a slosh wave intersects a tank wall that was curved down towards it. The decreased area available to the wave promoted breaking waves. The effects of the nonlinearities for spherical tanks are not so pronounced, however, as they were for compartmented cylindrical tanks.

### 5.3 Theory of Large Amplitude Motions

It can be argued that any nonlinearities resulting from the tank shapes discussed in the previous section, are actually nonlinearities resulting from a finite amplitude of the slosh wave. Although this is undoubtedly true, the wave amplitude required to produce nonlinear effects is considerably smaller for those tank shapes than for cylinders and other common shapes. In any event, when the wave amplitude is large enough to cause nonlinear effects, the linearized theory discussed in Chapter 1 is not valid. Hence, in this section, the linear theory is extended to include finite wave amplitudes.

It is still valid to neglect viscous effects, so the nonlinear slosh theory can be derived from a velocity potential. Hence, the basic differential equation is still linear:

$$\nabla^2 \Phi = 0 \quad (5.1)$$

and the liquid velocities are still given by the spatial derivatives of the potential. All the nonlinearities enter the analysis through the boundary conditions. In the linear theory, these conditions are imposed at the undisturbed boundaries; in particular, the free surface conditions are imposed at the equilibrium location of the free surface. When finite wave amplitudes are considered, however, we have to impose the boundary conditions at the actual locations of the boundaries. *Figure 5.2* illustrates the differences between the linear and nonlinear boundaries for the case of a rectangular tank subjected to a transverse oscillation of amplitude  $X_0$ . The no-flow condition is now imposed at the displaced condition of the tank walls. The free surface conditions are now imposed on the actual wave surface location  $z = \delta(x, t)$ , although this location is unknown and must be determined as part of the solution.

Just as for the linear theory, we will begin by finding solutions for the case when the tank is not moving. Furthermore, surface tension effects will be neglected, and the effective gravity  $g$  is assumed to be directed downward along the tank axis. To develop

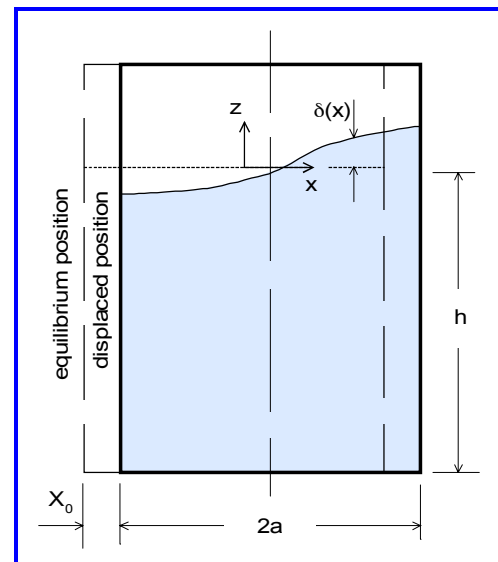


**Figure 5.2.** Locations of boundaries for nonlinear slosh analysis (rectangular tank)

the theory, we will focus on two dimensional waves in a rectangular tank similar to that shown in *Figure 5.2*.

With these assumptions, we have to consider only  $u$  velocities ( $x$  direction) and  $w$  velocities ( $z$  direction). The boundary conditions at the tank walls are:

$$\frac{\partial \Phi}{\partial x} = u = 0 \quad \text{for } x = \pm a \quad \frac{\partial \Phi}{\partial z} = w = 0 \quad \text{for } z = -h \quad (5.2)$$

For simplicity, the water depth is assumed to be much greater than the tank width, so the no-flow condition at the tank bottom is replaced by  $\partial \Phi / \partial z = w \rightarrow 0$  as  $h \rightarrow -\infty$ .

The nonlinear boundary conditions at the free surface are considerably more complicated than the linear theory boundary conditions. As before, the velocity of the wave perpendicular to the free surface has to be compatible with the liquid velocity at the free surface. This time, however, the condition is not applied to a flat surface so we have to include all the components of the liquid velocity, and the nonlinear boundary condition becomes:

$$\frac{\partial \delta}{\partial t} = \frac{\partial \Phi}{\partial z} - \frac{\partial \Phi}{\partial x} \frac{\partial \delta}{\partial x} \quad \text{for } z = \delta(x, t) \quad (5.3)$$

Likewise, the pressure at the free surface must be made equal to the gas pressure (the value of which can be absorbed into the definition of the potential). The nonlinear boundary condition that relates the pressure and wave motion at the free surface is:

$$\frac{\partial \Phi}{\partial t} = -g\delta - \frac{1}{2} \left[ \left( \frac{\partial \Phi}{\partial x} \right)^2 + \left( \frac{\partial \Phi}{\partial z} \right)^2 \right] \quad \text{for } z = \delta(x, t) \quad (5.4)$$

As was mentioned in the Section 5.1, these equations will be solved by the method of perturbations, which is also called the method of successive approximations. The discussion given below follows the development of PENNEY AND PRICE [1952], who formulated the analysis as part of a World War II effort to compute wave loads on floating breakwaters (called *Mulberry* harbors).

### Successive approximation solution

For this example, we will consider two-dimensional *symmetrical* waves; the same method could be used for antisymmetrical waves which are generally of the most interest for spacecraft. The symmetrical solution of Eq. (5.1) that satisfies Eqs. (5.2) is:

$$\Phi = \sum_{n=0}^{\infty} \alpha_n e^{n\pi z/a} \cos\left(\frac{n\pi x}{a}\right) \quad (5.5)$$

The  $n = 0$  term in this expression corresponds to the arbitrary time function in Bernoulli's equation and is needed only when calculating the pressure. When Eq. (5.5) is substituted into Eq. (5.4), the equation of the free surface is found (after some algebra) to be:

$$g\delta = \sum_{n=0}^{\infty} \dot{\alpha}_n e^{n\pi\delta/a} \cos\left(\frac{n\pi x}{a}\right) + \frac{1}{2} \left(\frac{\pi}{a}\right)^2 \sum_{n=1}^{\infty} \sum_{m=1}^{\infty} nm \alpha_n \alpha_m e^{(n+m)\pi\delta/a} \cos(m-n)\frac{\pi x}{a} \quad (5.6)$$

where the dot over  $\alpha_n$  indicates differentiation with respect to time. An equation of this form may be regarded as an implicit relation to solve for  $\delta$  in terms of  $x$ . Since the

coefficients are periodic functions of  $x$  it follows that  $\delta$  must also be periodic, but it does not necessarily follow that  $\delta$  is real for all real values of  $x$ . Hence, to ensure the existence of a continuous free surface, some theoretical limit must be imposed on the allowed values of the  $\alpha_n$  coefficients. This limit implies that the wave cannot exceed some maximum amplitude. Assuming that this condition (which at this point is not known) is satisfied, we can solve Eq. (5.6) by assuming a periodic solution for  $\delta$ :

$$\delta = \sum_{n=1}^{\infty} \beta_n \cos\left(\frac{n\pi x}{a}\right) \quad (5.7)$$

The  $\beta_n$  coefficients in Eq. (5.7) have to be computed in terms of the  $\alpha_n$  coefficients in Eq. (5.5).

Before working through the algebra of the solution, we will make the equations dimensionless by dividing lengths by  $a/\pi$  and time by  $(a/\pi g)^{0.5}$ . The dimensionless form of the  $\alpha_n$  coefficients is denoted by  $A_n$  and the dimensionless form of  $\beta_n$  by  $B_n$ . The method of solution begins by substituting the dimensionless forms of Eq. (5.5) and Eq. (5.7) into the free surface boundary conditions Eqs. (5.3) and (5.4), and collecting the coefficients multiplying each  $\cos(nx)$  term. The coefficient of each such term on the left and right hand sides of the equations must be separately equal, without regard to the other cosine terms. The algebraic labor is quite involved and involves expanding exponential terms into power series and using the sum and difference relations for products of cosines<sup>16</sup>. The coefficient of each cosine term is a function of all the  $A_n$  and  $B_n$ . If the approximation process is to converge, the magnitudes of  $A_n$  and  $B_n$  must decrease as  $n$  increases. Consequently, the number of terms in the coefficient of each cosine can be truncated after some finite number of terms. At this point it is assumed that  $A_n$  and  $B_n$  will decrease at least in proportion to a wave amplitude parameter  $\epsilon$  to the  $n^{\text{th}}$  power; we will show later that this assumption is correct. In the following summary, all the coefficients through fifth powers of  $\epsilon$  are derived, but the same process could be used to retain higher order terms.

The boundary condition Eq. (5.4) eventually yields the following series of ordinary coupled differential equations correct through fifth order terms.

$$0 = -2\dot{A}_0 + \dot{A}_1\left(B_1 + \frac{1}{2}B_1B_2 + \frac{1}{8}B_1^3\right) + \dot{A}_2\left(B_1^2 + 2B_2\right) - A_1^2\left(1 + B_1^2\right) - 6A_1A_2B_1 - 4B_2^2 \quad (5.8)$$

$$B_1 = \dot{A}_1\left(1 + \frac{3}{8}B_1^2 + \frac{1}{2}B_2 + \frac{1}{4}B_2^2 + \frac{1}{4}B_1^2B_2 + \frac{1}{4}B_1B_3 + \frac{5}{192}B_1^4\right) + \dot{A}_2B_1 - A_1^2\left(B_1 + B_1B_2 + \frac{1}{2}B_1^3\right) - 2A_1A_2 \quad (5.9a)$$

$$B_2 = \dot{A}_1\left(\frac{1}{2}B_1 + \frac{1}{2}B_1B_2 + \frac{1}{2}B_3 + \frac{1}{12}B_1^3\right) + \dot{A}_2\left(1 + B_1^2\right) + \frac{3}{2}\dot{A}_3B_1 - A_1^2\left(B_2 + \frac{1}{2}B_1^2\right) - 3A_1A_2B_1 - 3A_1A_3 \quad (5.9b)$$

$$B_3 = \dot{A}_1\left(\frac{1}{2}B_2 + \frac{1}{8}B_1^2 + \frac{5}{384}B_1^4 + \frac{1}{8}B_2^2 + \frac{3}{16}B_1^2B_2 + \frac{1}{2}B_1B_3 + \frac{1}{2}B_4\right) + \dot{A}_2B_1 + \dot{A}_3 - A_1^2\left(B_3 + B_1B_2 + \frac{1}{6}B_1^3\right) \quad (5.9c)$$

<sup>16</sup> For example,  $\exp\left[n \sum B_i \cos(mx)\right] = 1 + n \sum B_i \cos(mx) + 0.5n^2 \left(\sum B_i \cos(mx)\right)^2 + \dots$  and  $\cos(nx)\cos(mx) = 0.5\cos[(n-m)x] + 0.5\cos[(n+m)x]$ .

$$B_4 = \dot{A}_1 \left( \frac{1}{2} B_3 + \frac{1}{4} B_1 B_2 + \frac{1}{48} B_1^3 \right) + \dot{A}_2 \left( B_2 + \frac{1}{2} B_1^2 \right) + \frac{3}{2} \dot{A}_3 B_1 + \dot{A}_4 \quad (5.9d)$$

$$B_5 = \dot{A}_1 \left( \frac{1}{2} B_4 + \frac{1}{8} B_2^2 + \frac{1}{4} B_1 B_3 + \frac{1}{16} B_1^2 B_2 + \frac{1}{384} B_1^4 \right) + \dot{A}_5 \quad (5.9e)$$

Equation (5.8) is only needed to compute the arbitrary time function in the potential and will not be considered further here.

The boundary condition Eq. (5.3) yields the following series of differential equations:

$$\dot{B}_1 = -A_1 \left( 1 + \frac{1}{8} B_1^2 - \frac{1}{2} B_2 + \frac{1}{192} B_1^4 - \frac{1}{4} B_1 B_3 + \frac{1}{4} B_2^2 \right) - A_2 B_1 \quad (5.10a)$$

$$\dot{B}_2 = -A_1 \left( B_1 + \frac{1}{12} B_1^3 - B_3 \right) - 2A_2 \left( 1 + B_1^2 \right) - 3A_3 B_1 \quad (5.10b)$$

$$\dot{B}_3 = -A_1 \left( \frac{3}{8} B_1^2 + \frac{3}{2} B_2 + \frac{3}{128} B_1^4 + \frac{3}{16} B_1^2 B_2 - \frac{3}{8} B_2^2 - \frac{3}{2} B_4 \right) - 3A_2 B_1 - 3A_3 \quad (5.10c)$$

$$\dot{B}_4 = -A_1 \left( \frac{1}{12} B_1^3 + B_1 B_2 + 2B_3 \right) - A_2 \left( 2B_1^2 + 4B_2 \right) - 6A_3 B_1 - 4A_4 \quad (5.10d)$$

$$\dot{B}_5 = -A_1 \left( \frac{5}{384} B_1^4 + \frac{5}{16} B_1^2 B_2 + \frac{5}{8} B_2^2 + \frac{5}{4} B_1 B_3 + \frac{5}{2} B_4 \right) - 5A_4 \quad (5.10e)$$

**Linear approximation.** To determine how to proceed with the solution of these equations, we will first determine what they reduce to when the nonlinear terms are discarded. The linearized equations can be combined in pairs by differentiating, for example, Eq. (5.10a) and substituting Eq. (5.9a) into it, and similarly for all the other pairs. The result is:

$$\ddot{B}_n + nB_n = 0 \quad (5.11)$$

The solution of this equation is simply  $B_n = \varepsilon \sin(t\sqrt{n})$  or  $B_n = \varepsilon \cos(t\sqrt{n})$ . We will choose the sine solution. The solutions are all of the first order in the wave amplitude  $\varepsilon$ , which is the correct result and indicates that as the wave amplitude is made smaller, the wave shape approaches one of its natural modes. To pose a definite problem, we will require that the nonlinear solution reduces to the  $n = 1$  mode as the wave amplitude is made smaller. That is, we want to solve the problem in such a way that when all nonlinear terms are discarded in the solution, the wave is an oscillation of the form:

$$\Delta = \varepsilon \cos(x) \sin(t) \quad (5.12)$$

where  $\Delta$  is the dimensionless form of  $\delta$ . This assumption in effect eliminates all the linear solutions of Eqs. (5.9) and (5.10) except for the  $A_1$  and  $B_1$  solution. By examining the equations with the aid of Eq. (5.11), we find that the equations for  $A_n$  and  $B_n$  for  $n > 1$  involve no linear terms but only products; hence, these terms are nonlinear corrections to the  $n = 1$  wave shape and natural frequency.

**Second order approximation.** In the spirit of the successive approximation method, we will next examine the solution when second order terms are retained in the equations, assuming as indicated previously that  $A_n$  and  $B_n$  are proportional to  $\varepsilon^n$ . When the second order terms in Eqs. (5.9) and (5.10) are retained, the equations reduce to the following.

$$B_1 = \dot{A}_1 \quad \text{and} \quad \dot{B}_1 = -A_1 \quad (5.13a)$$

$$B_2 = \dot{A}_2 + \frac{1}{2} B_1 \dot{A}_1 \quad \text{and} \quad \dot{B}_2 = -2A_2 - B_1 A_1 \quad (5.13b)$$

$$B_n = \dot{A}_n \quad \text{and} \quad \dot{B}_n = -nA_n \quad \text{for } n > 2 \quad (5.13c)$$

From the first of these equations, we find that the original linear solution  $B_1 = \epsilon \sin(t)$  and  $A_1 = -\epsilon \cos(t)$  is also the second order solution for  $A_1$  and  $B_1$ ; that is, there are no second order corrections to  $A_1$  or  $B_1$ .

Combining Eqs. (5.13b) to eliminate  $B_2$  gives:

$$\ddot{A}_2 + 2A_2 = -\frac{1}{2}B_1\ddot{A}_1 - \frac{1}{2}\dot{B}_1\dot{A}_1 - B_1A_1 \quad (5.14a)$$

When the first order solutions for  $B_1$  and  $A_1$  are substituted into the right hand side of Eq. (5.14a), the result is found to be identically zero. The solution of Eq. (5.14a) is therefore  $A_2 = \epsilon \sin(t/2)$ , which, as we mentioned earlier, is discarded since it does not reduce to  $\epsilon \sin(t)$  when the amplitude  $\epsilon$  becomes small. Thus,  $A_2 = 0$  to the second order, and there is therefore no second order correction to the velocity potential. There is, however, a second order correction to the wave shape. From either of Eqs. (5.13b), we find:

$$B_2 = \frac{1}{2}B_1\dot{A}_1 \quad \text{or} \quad B_2 = \frac{1}{2}\epsilon^2 \sin^2 t = \frac{1}{4}\epsilon^2 [1 - \sin(2t)] \quad (5.14b)$$

Since  $B_2 > 0$ , there is a second order correction to the wave shape. The third set of equations, Eq. (5.13c), gives the solution  $A_n = \epsilon \sin(t/n)$ , but these are discarded since they do not reduce to the desired solution when  $\epsilon$  is small.

**Third order approximation.** By substituting the *second* order solutions into the *right hand* side of the set of equations and keeping terms through the third order, we find that the third order solution is determined by the following set of equations.

$$B_1 = \dot{A}_1 + \frac{5}{8}\dot{A}_1^3 - A_1^2\dot{A}_1 \quad \text{and} \quad \dot{B}_1 = -A_1 + \frac{1}{8}A_1\dot{A}_1^2 \quad (5.15a)$$

$$B_2 = \frac{1}{2}\dot{A}_1^2 \quad \text{and} \quad \dot{B}_2 = -A_1\dot{A}_1 \quad (5.15b)$$

$$B_3 = \frac{3}{8}\dot{A}_1^3 \quad \text{and} \quad \dot{B}_3 = -\frac{9}{8}A_1\dot{A}_1^2 \quad (5.15c)$$

$$B_n = \dot{A}_n \quad \text{and} \quad \dot{B}_n = -A_n \quad \text{for } n > 3 \quad (5.15d)$$

By combining the first set of equations, we get:

$$\ddot{A}_1 + A_1 = \frac{9}{8}A_1\dot{A}_1^2 + \ddot{A}_1A_1^2 - \frac{15}{8}\dot{A}_1^2\ddot{A}_1 \quad (5.16a)$$

The second order solution (i.e.,  $\ddot{A}_1 = -A_1$ ) can be used to evaluate the third order terms on the right hand side of this relation. This substitution gives:

$$\ddot{A}_1 + A_1 = 4A_1\dot{A}_1^2 - A_1^3 \quad (5.16b)$$

We want to find a solution for  $A_1$  that reduces to the linear solution  $\epsilon \cos(t)$  when second and third order terms are neglected. We therefore assume that  $A_1 = -\epsilon \cos(\sigma t) + \gamma$ , where  $\gamma$  is a function of the third order (since there is no second order correction to  $A_1$ ) and  $\sigma$  is a higher order frequency correction. Substituting this assumption into Eq. (5.16b) gives:

$$\begin{aligned} \sigma^2 \epsilon \cos(\sigma t) - \epsilon \cos(\sigma t) + \ddot{\gamma} + \gamma &= -4\epsilon^3 \sin^2(\sigma t) \cos(\sigma t) + \epsilon^3 \cos(\sigma t) \\ &= -\frac{1}{4}\epsilon^3 \cos(\sigma t) + \frac{5}{4}\epsilon^3 \cos(3\sigma t) \end{aligned} \quad (5.16b)$$

By equating coefficients of  $\cos(\sigma t)$  we find that:

$$\ddot{\gamma} + \gamma = \frac{5}{4}\epsilon^3 \cos(3\sigma t) \quad \text{or} \quad \gamma = -\frac{5}{32}\epsilon^3 \cos(3\sigma t) \quad (5.17a)$$

and

$$\sigma = \sqrt{1 - \frac{1}{4}\varepsilon^2} \quad (5.17b)$$

When the other pairs of Eq. (5.15) are solved, we find that all the  $A_n = 0$  for  $n > 1$  to the third order, although the  $B_n$  are not. Consequently, the third order solution for the velocity potential is:

$$A_1 = -\varepsilon \cos\left(\sqrt{1 - \frac{1}{4}\varepsilon^2} t\right) - \frac{5}{32}\varepsilon^3 \cos\left(3\sqrt{1 - \frac{1}{4}\varepsilon^2} t\right) \quad (5.18)$$

The coefficient  $B_1$  for the wave shape correct through the third order can be obtained from either of Eqs. (5.15a).

It should be noted that the natural frequency  $\sigma$  now depends on the wave amplitude and that it decreases (“softens”) as the wave amplitude increases. This conclusion agrees with the experimental observations discussed in Section 5.2.

**Higher order approximations.** The succeeding approximations are obtained by exactly the same process. For the fifth approximation, for example, the coefficients for the wave shape are given by:

$$B_1 = \left(\varepsilon + \frac{3}{32}\varepsilon^3 - \frac{137}{3072}\varepsilon^5\right)\sin\sigma t + \left(\frac{1}{16}\varepsilon^3 - \frac{11}{5276}\varepsilon^5\right)\sin 3\sigma t + \frac{163}{21504}\varepsilon^5 \sin 5\sigma t \quad (5.19a)$$

$$B_2 = \frac{1}{4}\varepsilon^2 + \frac{1}{15}\varepsilon^4 - \left(\frac{1}{4}\varepsilon^2 - \frac{95}{192}\varepsilon^4\right)\cos 2\sigma t - \frac{67}{1344}\varepsilon^4 \cos 4\sigma t \quad (5.19b)$$

$$B_3 = \left(\frac{9}{32}\varepsilon^3 - \frac{1}{256}\varepsilon^5\right)\sin\sigma t - \left(\frac{3}{32}\varepsilon^3 - \frac{2195}{14336}\varepsilon^5\right)\sin 3\sigma t - \frac{16365}{473088}\varepsilon^5 \sin 5\sigma t \quad (5.19c)$$

$$B_4 = \frac{1}{8}\varepsilon^4 - \frac{1}{6}\varepsilon^4 \cos 2\sigma t + \frac{1}{24}\varepsilon^4 \cos 4\sigma t \quad (5.19d)$$

$$B_5 = \frac{145}{768}\varepsilon^5 \sin\sigma t - \frac{515}{3072}\varepsilon^5 \sin 3\sigma t + \frac{85}{3072}\varepsilon^5 \sin 5\sigma t \quad (5.19e)$$

and the dimensionless frequency of the wave correct to the fifth order is:

$$\sigma = \sqrt{1 - \frac{1}{4}\varepsilon^2 - \frac{13}{128}\varepsilon^4} \quad (5.19f)$$

These relations show that the assumption that the higher order terms are at least as small as  $\varepsilon^n$  was correct. Furthermore, when Eqs. (5.19) are substituted into the dimensionless form of Eq. (5.7), we find that there is never a time when the surface is perfectly flat, the nearest to flat being a shape given by  $0.143\varepsilon^4 \cos(2x)$ , which occurs when  $\sigma t = n\pi$ .

As mentioned earlier, the maximum upward wave amplitude occurs when the wave is instantaneously at rest and the downward acceleration of the crest is equal to the gravitational acceleration (neglecting the effect of surface tension). By working through the algebra of the velocity potential, using values of  $A_n$  correct to the fifth order, we find that this condition corresponds to  $\sigma t = (n+0.5)\pi$  for  $n$  an even integer and the maximum allowed value of  $\varepsilon = 0.592$ . When  $n$  is an odd integer, the wave has its maximum downward deflection. Figure 5.3 shows these upward and downward wave profiles. The maximum nondimensional height of the crest is 0.885; since the nondimensional wave length is  $\lambda = 2\pi$ , the maximum wave height corresponds to  $0.141\lambda$  in dimensional terms. The deepest trough is 0.482, which corresponds to  $0.077\lambda$ . As can be seen, the upward wave is considerably more peaked than the flatter downward wave shape. In fact, in the limit, the crest makes a sharp angle of  $90^\circ$  rather than being slightly rounded as shown in

*Figure 5.3.* The maximum wave shape profiles agree satisfactorily with experimental measurements [TAYLOR, 1952].

#### Standing waves in tanks.

Nonlinear waves in tanks of rectangular and circular cross section have been analyzed by similar perturbation methods [TADJBAKSH AND KELLER, 1960; VERMA AND KELLER, 1962]. One interesting finding of these investigations is that when the liquid depth is shallow, the wave frequency *increases* with wave amplitude rather than decreasing as it does for greater depths; for a tank with a rectangular cross section, the critical depth corresponds to about 0.17 times the wave length.

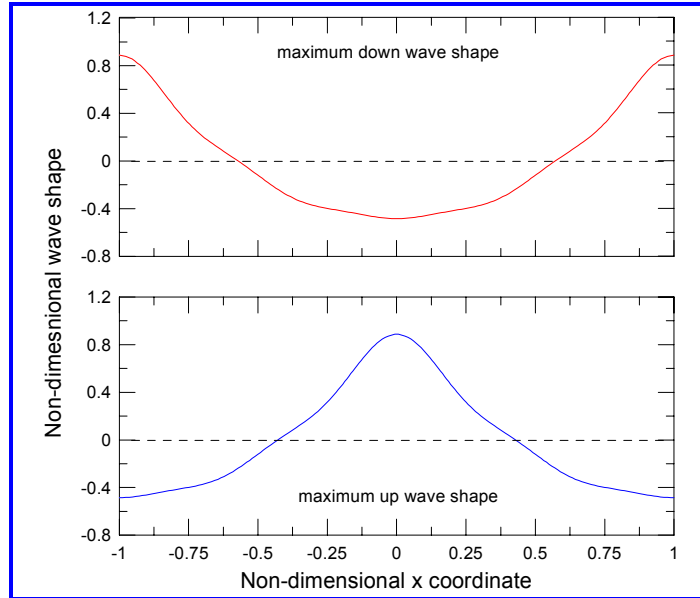


**Figure 5.3.** Profiles of maximum amplitude standing wave

**Forced motions.** The basic theory outlined above has been extended to include forced motions of a tank [e.g., BAUER, 1964 for a rectangular tank]. Because of the occurrence of terms in Eqs. (5.19) that vary at twice, three times, etc., the fundamental frequency, the forced motion theory demonstrates that it is possible to excite superharmonic resonances as well as motions at the fundamental frequency. The next section discusses another form of forced wave response that occurs for axisymmetric tanks.

## 5.4 Rotary Sloshing

Rotary sloshing in axisymmetric tanks was discussed in Section 3.6 from the standpoint of an equivalent conical pendulum model. From that discussion, it is recalled that if the frequency of the lateral oscillation of the tank is near the slosh natural frequency, there is a tendency for the up-and-down antisymmetric wave motion to lose stability. When the frequency is a little less than the slosh natural frequency, the nodal diameter of the antisymmetric wave begins to rotate at a nonsteady rate. This unstable swirling motion persists up to an excitation frequency a little above the natural frequency, where the antisymmetric wave mode can occur again. There is also a somewhat larger frequency range just above the natural frequency in which the nodal diameter can rotate stably at a constant rate. These kinds of nonlinear motions have been analyzed by the method of successive approximations, up through third order terms. The analysis is quite a bit more complicated than that discussed in Section 5.3 because the stability of the solution must also be investigated. The discussion below follows the analysis of HUTTON [1963].

The tank motion is treated by adding a velocity potential that “fits” the lateral motion of the tank to the general potential; in other words, the potential is of the form:

$$\Phi(r, \theta, z, t) = \dot{X}_o r \cos \theta + \phi(r, \theta, z, t) \quad (5.20)$$

This combined potential allows  $\phi$  to satisfy homogeneous boundary conditions at the tank walls and bottom:  $\partial\phi/\partial r = 0$  at  $r = R_o$  and  $\partial\phi/\partial z = 0$  at  $z = -h$ . It might be noted that we cannot make the further assumption that  $\phi$  varies as  $\cos\theta$ , as we did in Chapter 1, because when the nodal line rotates, the wave amplitude varies with  $\sin\theta$  as well as with  $\cos\theta$ .

As in Section 5.3, the amplitude of the  $n^{\text{th}}$  term in the successive approximation solution is taken to be proportional to a wave amplitude parameter to the  $n^{\text{th}}$  power. This fact is used to combine the two free surface boundary conditions [the cylindrical coordinate versions of Eqs. (5.3) and (5.4)] into a single boundary condition, given by:

$$G_1 + G_2 + G_3 = 0 \quad (5.21)$$

correct to the third order in the velocity potential. The terms  $G_1$ ,  $G_2$ , and  $G_3$  are complicated functions of the potential. For example,  $G_1$  and  $G_2$  are given by:

$$G_1 = \ddot{\phi} + g\phi_z + r\ddot{X}_o \cos\theta \quad (5.22a)$$

$$G_2 = 2\phi_r\dot{\phi}_r + \frac{2}{r^2}\phi_\theta\dot{\delta}_\theta + 2\phi_z\dot{\phi}_z + \ddot{X}_o\left(\phi_r \cos\theta - \frac{1}{r}\phi_\theta \sin\theta\right) - \frac{\ddot{\phi}_z + g\phi_{zz}}{g}(\dot{\phi} + r\ddot{X}_o \cos\theta) \quad (5.22b)$$

where the subscripts indicate differentiation with respect to the coordinates. The function  $G_3$  is composed of many terms all of which are of the third power in  $\phi$  and its derivatives or products of the second power of  $\phi$  and its derivatives with  $X_o$ . The various solutions of these equations are found for a tank motion that is given by  $X_o = \varepsilon \sin(\omega t)$ . The equations are made dimensionless just as in Section 5.3.

The linear solution of Eq. (5.21) is the same as that discussed in Chapter 1, but the nonlinear successive approximation solution of Eq. (5.21) requires a considerable amount of insight to find. The solution starts, like the method discussed in Section 5.3, by expressing  $\phi$  as a power series in the amplitude parameter  $\varepsilon$ :

$$\phi = \varepsilon[\psi_1 \cos \omega t + \zeta_1 \sin \omega t] + \varepsilon^2[\psi_0 + \psi_2 \cos 2\omega t + \zeta_2 \sin 2\omega t] + \varepsilon^3[\psi_3 \cos 3\omega t + \zeta_3 \sin 3\omega t] \quad (5.23)$$

The  $\psi_i$  and  $\zeta_i$  functions are solutions of Eq. (5.1). In particular,  $\psi_1$  and  $\zeta_1$  represent fundamental linear antisymmetric waves:

$$\psi_1 = [A_1(t)\cos\theta + B_1(t)\sin\theta]J_1(\lambda_{11})\frac{\cosh[\lambda_{11}(z+h)]}{\cosh(\lambda_{11}h)} \quad (5.24)$$

$$\zeta_1 = [C_1(t)\cos\theta + D_1(t)\sin\theta]J_1(\lambda_{11})\frac{\cosh[\lambda_{11}(z+h)]}{\cosh(\lambda_{11}h)}$$

The  $\psi_n$  and  $\zeta_n$  functions for  $n > 1$  involve sums of higher order symmetric and antisymmetric wave solutions. These functions are substituted into Eqs. (5.22) and the equations are solved by expanding them into a Fourier series and collecting the coefficients of  $\sin\omega t$ ,  $\cos\omega t$ , etc. terms. The process yields a set of first order, coupled, nonlinear differential equations in the generalized coordinates  $A_i(t)$ ,  $B_i(t)$ ,  $C_i(t)$ , and  $D_i(t)$ . The steady state harmonic solutions are found by considering only the four equations that involve  $A_1$ ,  $B_1$ ,  $C_1$ , and  $D_1$ . The steady state occurs when all the derivatives  $dA_i/dt$ ,  $dB_i/dt$ , etc. are equal to zero. There are two such solutions. The first one is a planar

solution that corresponds to the fundamental antisymmetric wave but with an amplitude  $A_1$  that depends on excitation frequency; the amplitude is the root of:

$$\left(\frac{A_1}{\varepsilon}\right)^3 + \nu K_1 \left(\frac{A_1}{\varepsilon}\right) + K_2 = 0 \quad (5.25a)$$

where  $K_1$  and  $K_2$  are constants that depend on tank shape and fill level. The other coefficients  $B_1$ ,  $C_1$ , and  $D_1$  are zero for this solution. The parameter  $\nu$  in Eq. (5.25a) is defined in terms of the linear natural frequency  $\omega_1$  of the fundamental antisymmetric slosh wave, the excitation frequency  $\omega$ , and the wave amplitude parameter  $\varepsilon$ :

$$\omega_1 = \omega \sqrt{1 - \nu \varepsilon^2} \quad (5.25b)$$

Note the similarity of Eq. (5.25b) to the corresponding natural frequency of an unforced standing wave given by Eq. (5.17b).

The second solution of the equations corresponds to a nonplanar motion in which the wave nodal line rotates around the tank axis. This motion has two non-zero generalized coordinates  $A_1$  and  $D_1$  that are the roots of:

$$\left(\frac{A_1}{\varepsilon}\right)^3 - K_3 \nu \left(\frac{A_1}{\varepsilon}\right) - K_4 = 0 \quad \text{and} \quad D_1 = \sqrt{A_1^2 + \frac{K_5}{A_1}} \quad (5.25c)$$

where  $K_3$ ,  $K_4$ , and  $K_5$  depend on the tank shape and fill level. The other two generalized coordinates  $B_1$  and  $C_1$  are zero. For this nonplanar motion there is a term in the potential, Eq. (5.23), that varies as  $\cos\theta\cos\omega t$  and a term that varies as  $\sin\theta\sin\omega t$ . These terms describe a nodal line that rotates around the tank axis. For both the planar and nonplanar motions, the parameter  $\nu$  specifies how close the excitation frequency is to the natural frequency.

Plots of the amplitude of the two steady state harmonic motions as a function of the frequency parameter  $\nu$ , are shown in Figure 5.4 for a specific value of tank diameter and fill level. The usual planar

wave motion can occur for any excitation frequency except near a small frequency band centered around the natural frequency. The width of this excluded band depends on the tank excitation amplitude  $\varepsilon$  (which is contained in the definition of the frequency parameter  $\nu$ ), and when  $\varepsilon$  is small, the actual range of excluded frequencies is very small. Non-planar rotary motion can occur for a range of frequencies that begins just slightly below the natural frequency and continues for a considerable extent above the natural frequency. In the range of frequencies where stable solutions of both planar and non-

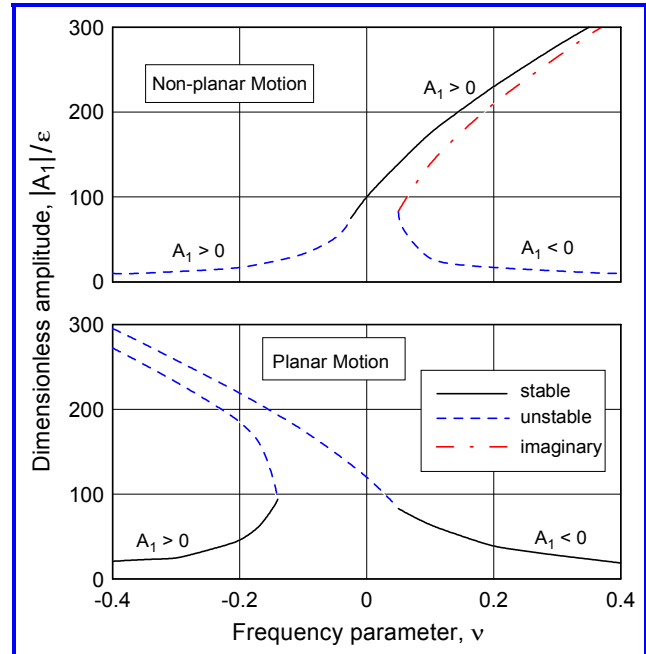


Figure 5.4. Planar and nonplanar slosh amplitude-frequency characteristics for a cylindrical tank

planar motion can occur, the observed motion depends on the initial conditions. Some pre-existing swirl or out-of-plane inclination of the free surface is required for the non-planar motion to occur, so the normal planar motion is usually observed in experiments.

There is a range of frequencies indicated in *Figure 5.4* where both types of harmonic motions are unstable. The most important of these regions is the one for which the excitation frequency is in the range just above the lower range for stable planar motions and just below the range for stable non-planar motions. In this range, the observed motion is an antisymmetric wave that has a to-and-fro rotational oscillation of its nodal line. In all other frequency ranges, a harmonic solution of one type or the other is stable. These regions of instability were found theoretically by superimposing a small disturbance  $\alpha_1 \exp(\beta t)$  on the corresponding steady state amplitudes  $A_1$  and  $D_1$  and then determining from the equations whether the amplitude of the disturbance increased with time (positive real part of  $\beta$ ) or decreased (negative real part of  $\beta$ ). Because of the non-linear coupling of the  $dA_1/dt$ ,  $dB_1/dt$ , etc., differential equations, all four of the original differential equations and all four amplitudes  $A_1$ ,  $B_1$ ,  $C_1$ , and  $D_1$  have to be included in the stability analysis.

In Section 3.6, the same regions of stability and instability were discussed by analogy to a conical pendulum. Although similar trends were observed, the frequency ranges for the various liquid motions and the analogous conical pendulum motions are not quite identical.

The prediction of two types of stable harmonic motion and the stability of these motions was a significant accomplishment at the time (circa 1960). Even with the computer power available now, it is not a simple exercise to predict unstable wave motions by CFD simulations. The planar and nonplanar (rotary) harmonic motion can both be investigated readily by starting the CFD simulation with a free surface that is inclined (for nonplanar motions) or is not inclined (for planar motions) to the direction of the lateral oscillation of the tank. The unstable or swirl motion is, however, more difficult to simulate and generally the simulation does not predict this type of motion; apparently, to do so requires a very careful treatment of the nonlinear interactions at the free surface.

## 5.5 Comments on the Successive Approximation Method

The analyses presented in Sections 5.3 and 5.4 are both special cases of the general successive approximation method. In general, the method involves the following kinds of analyses [MOISEYEV, 1958].

The nondimensional velocity potential  $\phi$  and the nondimensional wave shape  $\delta$  are expanded into a power series of a small parameter  $\varepsilon$ :

$$\phi = \varepsilon \sum_{n=0}^{\infty} \varepsilon^n \Phi_n \quad \delta = \sum_{n=1}^{\infty} \varepsilon^n \Delta_n \quad (5.26)$$

where  $\Phi_n$  are solutions of the governing differential equation, Eq. (5.1), and are generally taken to be the eigenfunctions of the corresponding linearized sloshing analysis. The  $\Delta_n$  are the free surface mode shapes for the appropriate  $\Phi_n$  of the linear analysis. Since the period or natural frequency of the nonlinear free oscillations is affected by the wave amplitude, it is also necessary to introduce a nondimensional time parameter that depends on the  $\varepsilon$  perturbation parameter:

$$\tau = \frac{t\omega_i}{1 + \sum_{n=1}^{\infty} \varepsilon^n H_n} \quad (5.27)$$

where  $\omega_i$  is the natural frequency of the mode for which nonlinear effects are to be investigated; the  $H_n$  must be determined as part of the solution, by methods similar to that described in Section 5.3.

The technique used to solve the equations to any order requires grouping the coefficients in the equations so that a set of first order equations, a set of second order equations, a set of third order equations, and so on, are derived. The solution of the first order equations is used to solve the second order set, the second order set is used to solve the third order set, etc. Details of the solution method depend on the problem (free or forced vibrations, etc.) but the solution is approached in every case by the method of finding successively better approximations.

## 5.6 References

- ABRAMSON, H. N., GARZA, L. R., AND KANA, D. D., 1962, *Some Notes on Liquid Sloshing in Compartmented Cylindrical Tanks*, **ARS J.**, **32**, pp. 978-980.
- ABRAMSON, H. N., CHU, W.-H., AND GARZA, L. R., 1963, *Liquid Sloshing in Spherical Tanks*, **AIAA J.**, **1**, 384-389.
- ABRAMSON, H. N., AND GARZA, L. R., 1965, *Some Measurements of Liquid Frequencies and Damping in Compartmented Cylindrical Tanks*, **AIAA J. Spacecraft and Rockets**, **2**, pp. 453-455.
- ABRAMSON, H. N., CHU, W.-H., AND KANA, D. D., 1966, *Some Studies of Nonlinear Lateral Sloshing in Rigid Containers*, **Trans. ASME, J. Applied Mechanics**, **33**, pp. 777-784.
- BAUER, H., 1964, *Nonlinear Propellant Sloshing in a Rectangular Container of Infinite Depth*, North American Aviation, Inc., S&ID Report SID 64-1593.
- BRASLOW, A. L., ed., 1968, *Propellant Slosh Loads*, NASA SP-8009,
- DEBNATH, L., 1997, **Nonlinear Water Waves**, Academic Press, New York.
- HUTTON, R., 1963, *An Investigation of Resonant, Nonlinear, Nonplanar Free Surface Oscillations*, NASA TN D-1870.
- MOISEYEV, N., 1958, *On the Theory of Nonlinear Vibrations of a Liquid of Finite Volume*, **Appl. Math. Mech. (PMM)**, **22**, pp. 860-870.
- PENNEY, W. G., AND PRICE, A. T., 1952, *Part II. Finite Periodic Stationary Waves in a Perfect Liquid*, **Phil. Trans. Royal Society (London)**, **244A**, pp. 254-284.
- STOKER, J. J., 1957, **Water Waves**, Interscience Publishers, New York.
- TADJBAKSH, I., AND KELLER, J., 1960, *Standing Waves of Finite Amplitude*, **J. Fluid Mechanics**, **8**, pp. 443-451.
- TAYLOR, G. I., 1952, *An Experimental Study of Standing Waves*, **Proc. Royal Society (London)**, **A218**, pp. 44-59.
- VAN DYKE, M., 1964, **Perturbation Methods in Fluid Mechanics**, Academic Press, New York,

## 5. NONLINEAR EFFECTS IN LATERAL SLOSHING

---

VERMA, G., AND KELLER, J., 1962, *Three-Dimensional Standing Waves of Finite Amplitude*, **Phys. Fluids**, **5**, pp. 52-56.

# LIQUID MOTIONS IN A SPINNING TANK

Most of the material in this chapter is not in NASA SP-106 and was newly written from the cited references.

## 6.1 Introduction

Spacecraft and rockets can be stabilized by spinning to make them gyroscopically stiff. Spinning also moderates the effects of orbital solar heating. But like a gyroscope, a rotating spacecraft precesses or nutates about its spin axis, as shown in *Figure 6.1*. The spin axis then does not coincide with the angular momentum vector, and the spacecraft appears to oscillate about its transverse  $x$  and  $y$  axes. This oscillation or *nutations* causes the liquids in the tanks to move relative to the tank. If the spacecraft spins about a major moment-of-inertia axis, the liquid motions tend to damp the nutation. But if it spins about a minor moment-of-inertia axis, which is common when the spacecraft is still attached to the upper stage booster, the liquid motions interact with the nutation to increase the coning amplitude  $\theta_c$  of the spacecraft nutation. For this case, the energy dissipated by the viscous liquid motion is an important measure of the seriousness of the interaction [GARG, et al, 1986]. The viscous energy dissipation is extracted from the spin kinetic energy of the spacecraft, but the dissipation does not lead to a gradually decreasing spin rate, as might be thought at first, but instead it leads to a gradually increasing nutation amplitude.

If the nutation growth is left unchecked, the spacecraft will eventually enter a “flat spin” around its major moment of inertia axis since this is the axis for which the kinetic energy is a minimum for a fixed amount of angular momentum [THOMSON, 1961]. Less catastrophic motions can prematurely deplete the propellants used for the guidance and control thrusters [e.g., MARTIN, 1971; SLABINSKI, 1978; POCHA, 1987]. Liquid-filled artillery shells are subject to the same kind of nutation instability, and for that reason liquid motions in a tank spinning about its own symmetry axis have been the subject of considerable investigation [e.g., STEWARTSON, 1959; STEWARTSON AND ROBERTS, 1963; KARPOV, 1965; GREENSPAN, 1969]. For many spacecraft, however, the tanks spin around an axis outside the tanks, so this extensive body of artillery-shell knowledge cannot be directly applied to spacecraft.

Possible types of liquid motions in a spinning tank include spin-up and spin-down, steady solid-body rotation, and oscillatory motions that occur after the spinning has persisted long enough for spin-up transients to have disappeared. In this chapter, we are concerned primarily with oscillatory, periodic motions superimposed on the liquid solid-body rotation, and we will not discuss spin-up phenomena. The energy dissipated by the

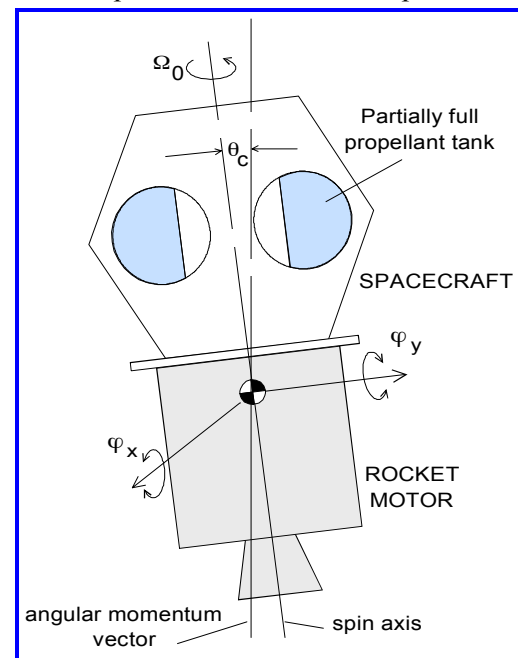


**Figure 6.1.** Spinning spacecraft and upper stage booster

oscillatory motions is extremely large when the nutation excites the liquid into resonance. For that reason, the natural frequencies of a liquid in a spinning tank are of much interest.

As a result of Coriolis effects, the characteristics of resonant liquid motions in a spinning tank can be quite different from the resonant motions in a non-spinning tank. The differences depend on whether a particular liquid natural frequency is less than or greater than twice the spin rate. In general, a liquid motion whose natural frequency is *greater* than twice the spin rate resembles the free-surface sloshing discussed in the previous chapters. A motion whose natural frequency is *less* than twice the spin rate, however, has no counterpart in a non-spinning tank. This motion does not resemble free-surface sloshing. In fact, the motion occurs throughout the liquid interior and is thus called an *internal* or *inertia* oscillation. Since the nutation frequency for spinning spacecraft is less than the spin rate, inertia oscillations are the more critical type of liquid motions for spacecraft stability.

Experimental verification of liquid natural frequency predictions and mode shapes is considerably more difficult for spinning tanks than it is for non-spinning tanks. The usual kind of experiment merely monitors the growth rate of the nutation amplitude  $\theta_c$ , from which the energy dissipation rate is inferred.

### Characterization of liquid motion regimes

The shape of the liquid free surface and the characteristics of liquid resonances are functions of several dimensionless ratios. Letting  $\Omega_0$  = spin rate,  $\omega_n$  = liquid natural frequency,  $g$  = gravity or an equivalent thrust-induced acceleration,  $\sigma$  = liquid surface tension,  $\rho$  = liquid density, and  $a$  = tank radius, we can derive three dimensionless ratios:

$$\frac{a\Omega_0^2}{g} = Fr_C = \text{centrifugal Froude number}$$

$$\frac{\rho a^3 \Omega_0^2}{\sigma} = Bo_C = \text{centrifugal Bond number}$$

$$\frac{\omega_n}{2\Omega_0} = \Omega^* = \text{frequency ratio}$$

The importance of the frequency ratio  $\Omega^*$  has already been implied above:  $\Omega^* = 1$  separates the regime of free-surface sloshing-like motions ( $\Omega^* > 1$ ) from the regime of inertia-oscillation like motions ( $\Omega^* < 1$ ). The two “centrifugal” dimensionless numbers determine whether the shape of the liquid surface depends on surface tension ( $Bo_C < 1$ ) and whether the motions are more “gravity” like than “centrifugal” like ( $Fr_C < 1$ ).

Nearly all the research on motions in a spinning tank has been for the conditions  $Fr_C \gg 1$  and  $Bo_C \gg 1$  since those are the common conditions for a liquid-filled shell ( $\Omega$  is very large) and for a spinning spacecraft ( $g$  is very small). For these conditions, the centrifugal acceleration pushes the liquid against the tank wall farthest from the spin axis, and the free surface shape forms part of a cylinder whose axis is the spin axis; if the spin axis is also the tank axis, the liquid forms a complete cylinder centered on the spin axis. For conditions when  $Fr_C \gg 1$  and  $Bo_C \ll 1$  (low gravity, very low spin rate), the free surface shape is dominated by surface tension and resembles the curved low- $g$  shapes discussed in Chapter 4; this combination of conditions can only occur in space. The regime for which  $Fr_C \ll 1$  and  $Bo_C \ll 1$ , is not common for any spacecraft

application; the free surface shape is practically independent of the spinning for these conditions, and the ordinary Bond number is a more relevant parameter.

The conditions for which  $Fr_c \ll 1$  and  $Bo_c \gg 1$  (slow spinning, large gravity, nearly flat free surface), are similar to the conditions that prevail in normal high-g sloshing, so the discussion of liquid motions starts with it.

## 6.2 Liquid Motions in a Slowly Spinning Axisymmetric Tank

When an axisymmetric tank in a gravitational field rotates around its symmetry axis so slowly that  $Fr_c \leq 1$  while at the same time  $Bo_c \gg 1$  (negligible surface tension), the free surface shape is paraboloidal, as shown in *Figure 6.2*. Even though these conditions are not common in spacecraft applications, the theory of liquid motions in a slowly spinning tank is more easily explained than for more realistic cases, so it will be reviewed here as an introduction to the subject.

The motion of the free surface of a liquid relative to an equilibrium state of uniform rotation about a vertical axis has been the subject of theoretical interest of hydrodynamicists for many years (i.e., the earth's oceans), although the motions have generally been analyzed on the basis of shallow water theory for which the theory is especially simple. The most striking feature of these analyses is that rotation induces a splitting of each liquid natural frequency into pairs. It has also been found that when the liquid depth is not shallow, the liquid oscillations do not necessarily decrease in amplitude exponentially with depth below the free surface, as it does for normal free surface sloshing [MILES, 1959].

Although the liquid motion in a spinning tank is not irrotational as it for normal sloshing, the basic theoretical equations are still fairly simple if the fluid velocities  $\mathbf{q}$  (a vector) are measured relative to the steady state rotation, and nonlinear products of the velocities are neglected (just as in Chapters 2 and 4). Euler's equations for an inviscid liquid in a rotating coordinate system when nonlinear terms are neglected reduce to:

$$\frac{\partial \mathbf{q}}{\partial t} + 2\boldsymbol{\Omega} \times \mathbf{q} + \boldsymbol{\Omega} \times \boldsymbol{\Omega} \times \mathbf{r} = -\nabla \left( \frac{p}{\rho} + gz \right) \quad (6.1)$$

where the spin axis is perpendicular to the radius vector  $\mathbf{r}$ . This equation is simplified further by introducing the acceleration potential  $\zeta$ :

$$\zeta = \frac{p}{\rho} - \frac{1}{2} \Omega_0^2 r^2 + gz \quad (6.2)$$

The  $\zeta$  potential specifies the pressure in excess of the steady state pressure caused by the centrifugal and gravitational force fields. The free surface shape is therefore defined by the condition  $\zeta = 0$  and  $p = 0$ . From Eq. (6.2) the shape is found to be a paraboloid:  $z - z_0 = 0.5(r\Omega_0)^2/g$  as indicated in *Figure 6.2*.

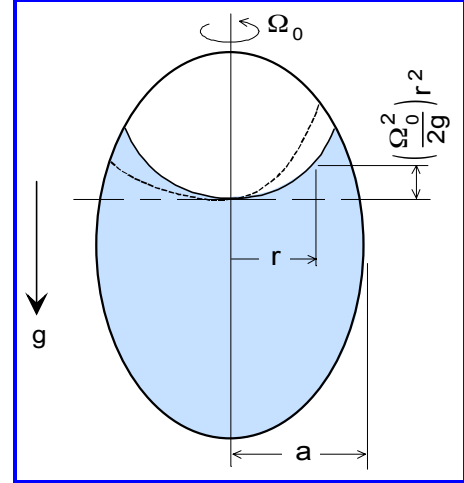


Figure 6.2. Free surface shape in a slowly spinning axisymmetric tank

The fluid motions are assumed to be harmonic in time with a frequency  $\omega$ ; hence the time derivative in Eq. (6.1) can be replaced by  $i\omega q(r,\theta,z)$  where now  $q$  is the spatial part of the velocity. With these definitions and assumptions, we can derive a differential equation for  $\zeta$  by taking the divergence of Eq. (6.1) twice and using the fact that the liquid is incompressible; this process gives:

$$\frac{1}{r} \frac{\partial}{\partial r} \left( r \frac{\partial \zeta}{\partial r} \right) + \frac{1}{r^2} \frac{\partial^2 \zeta}{\partial \theta^2} + \left[ 1 - \left( \frac{2\Omega_0}{\omega} \right)^2 \right] \frac{\partial^2 \zeta}{\partial z^2} = 0 \quad (6.3)$$

where  $\zeta$  is now defined as only the spatial part of the acceleration potential. The solutions of Eq. (6.3) must satisfy boundary conditions at the tank walls and bottom (velocity perpendicular to the wall is zero) and at the free surface. Before giving these conditions, the form of the differential equation needs to be discussed.

Unless the fluid motions do not depend on the  $z$  coordinate (one example, being shallow water), Eq. (6.3) is *elliptic* when  $\omega > 2\Omega_0$  and *hyperbolic* when  $\omega < 2\Omega_0$ . Since normal high-g and low-g sloshing theory is governed by an elliptic differential equation (i.e.,  $\Omega_0 = 0$ ), the solutions of Eq. (6.3) will resemble ordinary sloshing when  $\omega > 2\Omega_0$ . On the other hand, hyperbolic differential equations arise mostly in compressible flows, which admit the possibility of shock waves and other kinds of discontinuities. The solutions for  $\omega < 2\Omega_0$  thus should not be expected to resemble ordinary sloshing. Furthermore, there is no guarantee that the solutions of an hyperbolic differential equation can be made to satisfy boundary conditions for an elliptic differential equation, independently of any initial conditions from which the solution might arise.

### Cylindrical tank

The particular tank shape for which the various solutions is discussed below is a cylinder of radius  $a$  [MILES, 1959]. We will assume that the solutions depend on the angular coordinate  $\theta$  by trigonometric functions  $\exp(im\theta)$  [i.e., as  $\sin(m\theta)$  or  $\cos(m\theta)$ ] just as for normal sloshing;  $m = 1$  designates the fundamental antisymmetric mode sketched in Figure 6.2. With this assumption for the angular coordinate dependency, the acceleration potential can be written as  $\zeta = F(r,z)\exp(im\theta)$ , where as indicated  $F$  is a function that depends only on  $r$  and  $z$ . The radial velocity  $u$  is given in terms of the function  $F$  by  $u = (\partial F/\partial r) + (2\omega/\Omega_0)F/r$ , and there is a similar expression for the axial velocity  $w$ .

The boundary condition at the cylindrical tank wall is  $u = 0$  for  $r = a$ , and the condition at the tank bottom is  $w = 0$  for  $z = -h$ . The boundary conditions at the free surface have to be applied to a curved surface, so the same kind of mathematical difficulties occur as we found for low-g sloshing. To avoid these difficulties, we will assume that the rotation is slow enough that the free surface is practically flat or alternatively that the boundary conditions are imposed at the average surface location. In either case, the free surface boundary conditions reduce to  $\omega^2 F + g(\partial F/\partial z) = 0$  at  $z = 0$ .

A suitable general solution of the differential equation is  $F(r,z) = J_m(kr)\exp(\kappa z)$ , where  $k$  and  $\kappa$  are two parameters related by  $\kappa = -k/[1 - (2\Omega_0/\omega)^2]^{1/2}$  and  $J_m$  is a Bessel function. The parameter  $k$  is the eigenvalue of the problem and is determined by the boundary conditions. The mathematical details of determining  $k$ , etc., are not discussed here, but a summary of the results is given.

**Motions for  $\omega > 2\Omega_0$  (slosh modes).** Since Eq. (6.3) is elliptic for  $\omega > 2\Omega_0$ , its solutions describe motions that resemble ordinary sloshing; that is, the motions are concentrated near the free surface and the amplitude of the motion decreases with depth below the

surface. *Figure 6.3* shows the way the natural frequency of the  $m = 1$  fundamental antisymmetric mode varies with spin rate, for a tank having a liquid depth much greater than the tank diameter. The splitting of the normal sloshing mode into a higher and lower frequency pair is clearly shown in the figure.

As the spin rate is increased in *Figure 6.3*, a point is reached at which the lower of the two liquid natural frequencies becomes less than twice the spin rate, so for larger spin rates free-surface sloshing should not occur. The fact that sloshing motions are still indicated to exist for  $\omega < 2\Omega_0$  in *Figure 6.3* is a consequence of the approximations used in satisfying the free surface boundary condition. For the large centrifugal

accelerations and highly curved interfaces that occur when the spin rate is high, we cannot consider only the vertical component of the velocity in satisfying the free surface condition. By doing so, the axial motion is in effect suppressed, which means that the  $z$ -component of the differential equation Eq. (6.3) disappears, so it is elliptic even when  $\omega < 2\Omega_0$ . Thus the results shown in *Figure 6.3* if  $\omega < 2\Omega_0$  are not accurate.

Higher order antisymmetric modes and modes for which  $m > 1$  are not greatly affected by tank rotation. They are therefore not shown in *Figure 6.3*; some splitting of these modes is present but only to a small degree.

**Motions for  $\omega < 2\Omega_0$  (inertia oscillation modes)** The plots in *Figure 6.3* apply to a tank that has a liquid depth much greater than the tank diameter. For a tank of this shape, there are no true resonances for which the natural frequency is less than twice the spin rate. Apparently, inertia wave modes do not “fit” an infinitely deep tank. But when the liquid depth is finite, the theory shows that there are many inertia wave modes [MILES. 1959]. The liquid motion associated with these modes does not decay exponentially with depth below the free surface, as would a free surface sloshing mode, but persists all the way through the liquid volume. These are inertia modes and they can occur only for a spinning tank; free surface motions are not their most prominent feature. All the inertia modes are “squeezed” into the frequency range between  $\omega = 0$  and  $\omega = 2\Omega_0$ , a characteristic which again is quite different from slosh modes for which the higher order natural frequencies increase without limit. In fact, some of the  $m > 1$  inertia modes have lower natural frequencies than the  $m = 1$  inertia modes. For these reasons, the mode that creates the largest dynamics effects is not evident just from inspecting the natural frequencies. According to MCINTYRE AND TANNER [1987], modes with only a few *nodal* surfaces (an internal mathematical surface along which the velocity is zero) have the greatest potential for interacting with a spacecraft nutation. This observation means that for the critical modes, the motion is probably concentrated into an overall swirling or vortex motion that “fills” the liquid volume. This observation is the physical basis of the *homogeneous vortex* approximate analytical method described later.

**Forces and moments.** Although the force and moments can be computed from the general theory, it is not evident which inertia mode gives the largest forces and moments. But for the sloshing modes, a conventional mechanical model would give a reasonable estimate

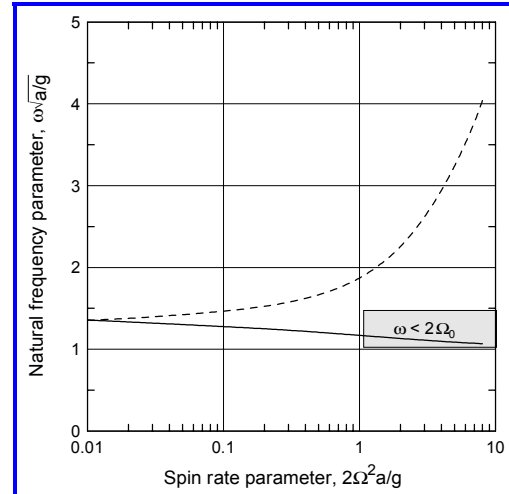


**Figure 6.3.** Natural frequency of fundamental antisymmetric slosh mode for a slowly spinning cylindrical tank in a gravitational field

of the forces and moments; the pendulum length would, however, have to be adjusted to make the pendulum natural frequency match the results shown in *Figure 6.3*, with an effective combined gravity equal to some average value, say  $(a\Omega_0^2/2 + g)^{0.5}$ . For most spacecraft applications, the forces and torques produced by free-surface sloshing are of less importance than the inertia mode forces and torque, since as was stated earlier, the nutation excitation frequency, which is less than the spin rate, tends to excite only the inertia modes.

**High spin rate results.** When the spin rate is large, the effects of gravity can be ignored and the liquid is disposed within the tank as an annular cylinder whose axis coincides with the spin axis and whose inner radius depends only on the fill fraction. A multiplicity of inertia waves are predicted for this axisymmetric configuration, many of which exert large disturbance torques on the tank [MILES AND TROESCH, 1961, DODGE, 1996].

### 6.3 Tanks off the Spin Axis – Exact Theory

Many spin-stabilized spacecraft contain tanks that are located off the spin axis. This configuration does not lend itself to mathematical treatment in any standard coordinate system. Hence, a numerical or some other approximate method is needed. Before discussing these methods, an idealized case is discussed, for which an exact analytical solution can be found, to illustrate the general characteristics of the liquid motions. The idealized configuration is shown in *Figure 6.4*. The tank is a sector of an annular cylindrical tank whose spin axis coincides with the cylinder axis. Gravity is neglected compared to the centrifugal acceleration ( $Frc \gg 1$ ), and the undisturbed liquid is in a state of steady rigid-body rotation. We might consider this tank to be an idealized off-spin-axis cylindrical tank having a diameter roughly equal to the distance between the radial walls. The figure shows a typical free surface wave.

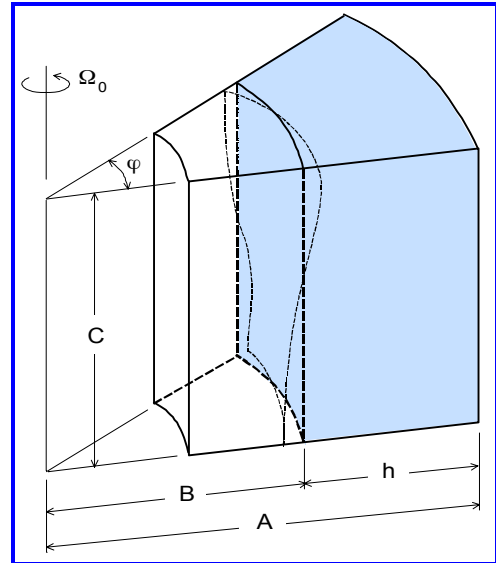


**Figure 6.4.** Rotating annular, sector cylindrical tank

As usual, the eigenvalues and eigenvectors of the problem are computed first [WEIHS AND DODGE, 1991]. By assuming an incompressible liquid and neglecting nonlinear products of the small oscillations superimposed on the steady rotation, the following equations of motion and boundary conditions are derived.

$$\frac{\partial u}{\partial t} - 2\Omega_0 v = -\frac{\partial p}{\rho \partial r} \quad r - \text{momentum} \quad (6.4a)$$

$$\frac{\partial v}{\partial t} + 2\Omega_0 u = -\frac{1}{r} \frac{\partial p}{\rho \partial \theta} \quad \theta - \text{momentum} \quad (6.4b)$$

$$\frac{\partial w}{\partial t} = -\frac{1}{\rho} \frac{\partial p}{\partial z} \quad z - \text{momentum} \quad (6.4c)$$

$$\frac{1}{r} \frac{\partial(ur)}{\partial r} + \frac{1}{r} \frac{\partial v}{\partial \theta} + \frac{\partial w}{\partial z} = 0 \quad \text{continuity} \quad (6.4d)$$

$$u = 0 \quad \text{at } r = B; \quad v = 0 \quad \text{at } \theta = \pm \phi/2; \quad w = 0 \quad \text{at } z = \pm C/2 \quad (6.4e)$$

$$\frac{\partial \delta}{\partial t} = u \quad \text{and} \quad p = -2\rho B \Omega_0^2 \delta \quad \text{at } r = B \quad (6.4f)$$

Here,  $\delta(r, \theta, t)$  is the radial amplitude of the standing wave on the free surface  $r = B$ . Since we are interested in oscillatory solutions, the velocities  $u$ ,  $v$ ,  $w$ , the free surface deflection  $\delta$ , and the pressure  $p$  are all assumed to vary as  $\exp[i(k\theta + lz + \omega t)]$ . For this type of solution, the boundary conditions at the walls and top and bottom surfaces require that:

$$k = \pm(2m + 1) \frac{\phi}{\pi} \quad m = 0, 1, 2, \dots \quad (6.5a)$$

$$l = \pm(2j + 1) \frac{\pi A}{C} \quad j = 0, 1, 2, \dots \quad (6.5b)$$

For oscillatory motions, the solution to Eqs. (6.4) reduces to a set of coupled ordinary differential equations in the  $r$  coordinate, which can be written, for example, as:

$$r^2 P'' + rP' + [r^2 l^2 (4\Omega_0^2 / \omega^2 - 1) - k^2] P = 0 \quad (6.6a)$$

$$U = -i [2k/r P + (\omega/\Omega_0) P'] / (4 - (\omega/\Omega_0)^2) \quad (6.6b)$$

where the primes indicate differentiation with respect to  $r$ . Here, the perturbation pressure  $p$  is written in dimensionless form as  $\rho \Omega_0^2 P(r) \exp[i(k\theta + lz + \omega t)]$ , the perturbation  $u$  velocity is written as  $A \Omega_0 U(r) \exp[i(k\theta + lz + \omega t)]$  and the  $v$  and  $w$  velocities are expressed in a similar form. The general solution for the pressure function  $P$  is in terms of Bessel functions; details are given in WEIHS AND DODGE, [1991]. It should be noticed that the character of the governing differential equation, Eq. (6.6a), depends on whether  $\omega$  is less than or greater than  $2\Omega_0$ .

**Two-dimensional motions.** For the case of an infinitely long tank ( $C \rightarrow 0$  in Figure 6.4), two-dimensional motions ( $l = 0$ ) are possible. For this case, the  $z$  dependence of the velocities and pressure disappears and the governing differential equation is elliptic. The motions are therefore all of the free surface sloshing type. If we let  $n = \omega/\Omega_0$ , the allowed values of  $n$  for these two dimensional motions are determined by the differential equations and boundary conditions; they turn out to be the roots of the following equation:

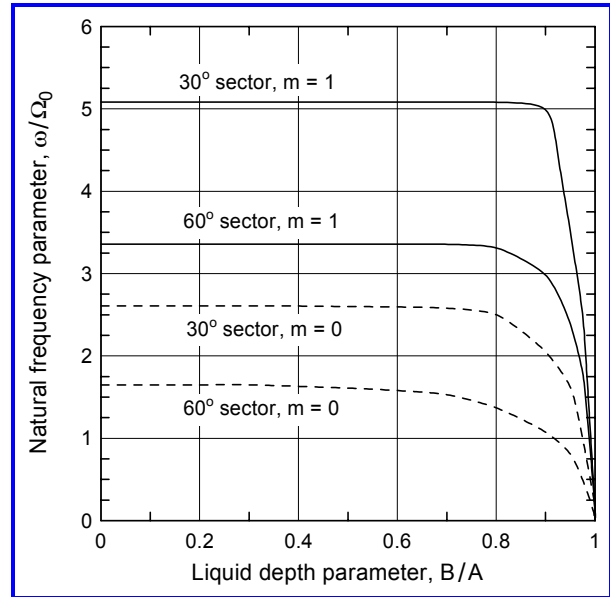


Figure 6.5. Slosh natural frequencies for a long ( $l = 0$ ) rotating annular sector cylindrical tank.

$$(n^2 - 2n + 2k)B^k + (n^2 + 2n - 2k)B^{-k} = 0 \quad (6.7)$$

The roots of this equation are plotted in *Figure 6.5* for the  $m = 0$  and the  $m = 1$  antisymmetric modes, for a tank with a sector angle  $\varphi$  of either  $30^\circ$  or  $60^\circ$ . For both tanks, the natural frequency decreases as the depth approaches zero ( $B/A \rightarrow 1$ ), just as for sloshing in a non-rotating tank. And just as for ordinary sloshing, the fundamental antisymmetric mode [in this case,  $m = 0$  because of the way  $k$  is defined in Eq. (6.5a)] has the lowest natural frequency.

### Three dimensional motions.

When the tank length is finite, sloshing modes and inertia modes both exist. The general solution for this case is too complicated for trends to be discerned easily. Therefore, results will be given for a few specific examples that display the general trends.

*Figure 6.6* shows some of the predicted slosh natural frequencies and the two highest natural frequency inertia modes for a  $30^\circ$  sector tank having a depth ratio  $B/A = 0.8$ , and some similar results for a tank having  $B/A = 0.5$ . The shaded area corresponds to the regime of free-surface sloshing; the symbolism  $(j,m)$  indicates that the curve is plotted for the indicated values of  $j$  and  $m$  in Eqs. (6.5a) and (6.5b). There are also higher harmonics for the inertia wave modes ( $\omega < 2\Omega_0$ ) but they are too densely packed to show clearly in the figure.

There is a small range of liquid heights for which two natural frequencies exist for some free-surface sloshing modes. It is interesting to note that many of the slosh modes tend to the limit  $\omega = 2\Omega_0$  as the tank height decreases (i.e., as  $A/C$  becomes larger). Also, when the radial liquid depth  $h = A - B$  decreases, the slosh frequency of a mode decreases, just as for normal sloshing. In contrast to normal sloshing, however, the mode disappears while the depth is still greater than zero.

Some investigators have modeled the sloshing responses in off-axis rotating tanks as if the tank were not rotating but had an effective radial gravity equal to the centrifugal acceleration at the free surface [ZEDD AND DODGE, 1984; GARG, ET AL, 1986; SLABINSKI, 1978]. Although from *Figure 6.6*, this approximation appears to be satisfactory for the  $m = 0$  antisymmetric modes for liquid depths  $B/A \lesssim 0.9$  and tank heights that are greater than about one third the tank radius, it fails to predict the disappearance of the  $m = 0$  modes when the liquid thickness is shallow in either the radial or axial direction.

The natural frequency of the highest frequency inertia wave mode increases slowly as the tank height decreases (i.e., as  $A/C$  becomes larger). For tanks with a bigger sector angle, the inertia wave frequencies tend to cluster around  $0.6\Omega_0$  to  $0.7\Omega_0$ , over a fairly wide range of liquid depth and tank height ratios, which indicates that this may be a particularly dangerous range of nutation excitation frequencies.

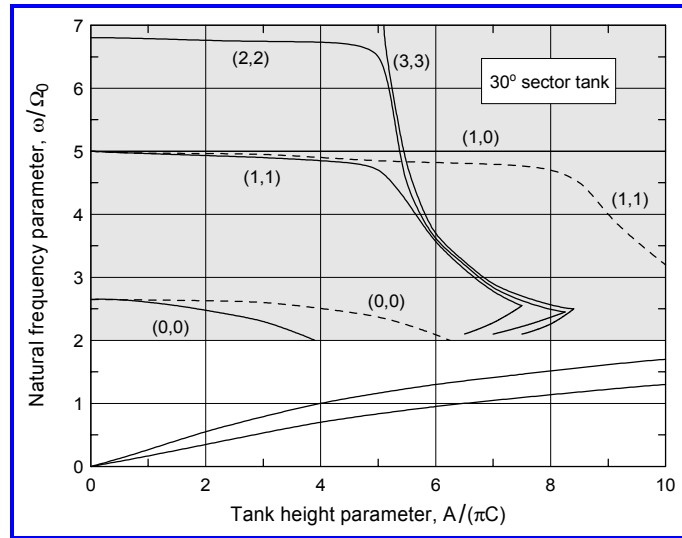


**Figure 6.6.** Slosh and inertia wave natural frequencies as a function of tank height. Solid lines are for  $B/A = 0.8$ , dashed lines are for  $B/A = 0.5$

**Forces and torques.** The forces and torques can be computed from the general theory. The sloshing forces and torques can in fact be approximated by an equivalent mechanical model as discussed above, so long as the radial or axial thickness of the liquid is not too small. It is not evident, however, which inertia wave mode gives the largest forces and torques since they all cluster rather closely in frequency space. Possibly a combination of modes would be excited by a given nutation frequency; the approximate theory discussed in the next section can be used to estimate these forces and torques.

## 6.4 Tanks Located off the Spin Axis – Approximate Theory

Many spacecraft tank shapes cannot be idealized as an annular sector cylindrical tank, for which the exact theory was described in the preceding section. Hence, an approximate analytical theory is needed. This section describes one such approximation, called the *homogeneous vortex model* [PFEIFFER, 1974; EL RAHEB AND WAGNER, 1981, DODGE, 1988]. The basic approximation is that all the details of the inertia waves in a spinning, off-axis tank can be replaced by a concentrated vortex. The theory predicts a single inertia mode, which presumably is the most important mode or combination of modes.

### Homogeneous vortex model

For the homogeneous vortex model, an unsteady velocity  $\mathbf{u}$  is superimposed on the steady solid-body rotation of the liquid, and  $\mathbf{u}$  is assumed to be composed primarily of concentrated vortices with whatever corrections are needed to make the vortex-like motion “fit” the tank shape. *Figure 6.7* shows the general configuration and the coordinate systems used in the analysis. An  $X, Y, Z$  system is fixed to and rotates with the spin axis, and an  $x, y, z$  system is fixed to the tank center, with the  $z$  axis parallel to the spin axis. We will usually let the  $Y$  axis point toward the tank center. The tank rotates around the spin axis at a steady rate  $\Omega_0$ . As usual, we will first predict the natural frequencies and modes.

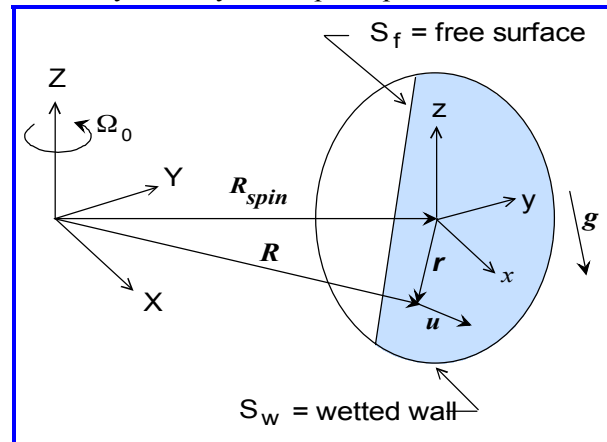


**Figure 6.7.** Coordinate systems for liquid oscillations in a tank rotating about an exterior axis

The homogeneous vortex assumption for the liquid velocity is expressed analytically as:

$$\mathbf{u} = \boldsymbol{\Omega} \times \mathbf{r} - \nabla \Phi - \nabla(\boldsymbol{\Omega} \cdot \boldsymbol{\psi}) \quad (6.8)$$

where the first term is the basic vortex motion, the second term is a velocity or scalar potential  $\Phi$  needed to allow free surface wave motions to exist, and the third term is a vector potential  $\boldsymbol{\psi}$  correction that makes the vortex motion fit the tank shape. In general, the vortex  $\boldsymbol{\Omega}$  is composed of the steady rotation  $\Omega_0$  and unsteady components  $\Omega_i = \Omega_x, \Omega_y, \Omega_z$  about each axis. The equations are linearized by assuming that  $\Omega_i$  and  $\Phi$  are small quantities, as are the products  $\Omega_i \psi_j$ . The linearized equations of motion are transformed by the vector curl operation to express them in terms of vorticity rather than velocities.

Then, the spatially varying quantities in the equations of motion are integrated over the liquid volume  $V$  to eliminate the spatial dependence of the vorticity. This integration is the point at which the analysis is simplified to the “homogeneous vortex” approximation. The final result for the vector equation of motion is:

$$\frac{d\mathbf{\Omega}}{dt} + \mathbf{\Omega}_0 \mathbf{k} \times \mathbf{\Omega} = -\frac{\Omega_0}{V} \iiint \frac{\partial}{\partial z} \nabla(\mathbf{\Omega} \cdot \boldsymbol{\Psi}) dV - \frac{\Omega_0}{V} \iiint \frac{\partial}{\partial z} (\nabla\Phi) dV \quad (6.9)$$

In addition to Eq. (6.9), the liquid motion must satisfy the requirement of incompressibility, which is the familiar Laplace equation imposed on both the  $\Phi$  and  $\boldsymbol{\Psi}$  potentials; this equation is:

$$\nabla^2 \Phi = 0 \quad \text{and} \quad \nabla^2 \psi_i \text{ for } i = x, y, z \quad \text{in the volume } V \quad (6.10)$$

Boundary conditions have to be considered to make the problem specific to a given tank shape. The conditions on the tank wall, as usual, state that the liquid velocity perpendicular to the wall must be zero; here this condition reduces to:

$$\mathbf{n} \cdot \nabla\Phi = 0 \quad \text{and} \quad (\mathbf{n} \cdot \nabla)\boldsymbol{\Psi} = -\mathbf{n} \times \mathbf{r} \quad \text{on the tank wall surfaces } S_w \quad (6.11)$$

where  $\mathbf{n}$  is the unit vector perpendicular to the walls. The boundary condition at the free surface is not, however, so straightforward to derive. The equations of motion in a rotating coordinate system have to be integrated to derive Bernoulli’s equation from which the unsteady pressure can be set equal to zero at the equilibrium free surface location. The equilibrium free surface shape itself is determined by the condition that the static pressure is constant (e.g., zero) on it, and the general radius to this surface is denoted by  $R_f$ . The deflection of the free surface relative to its equilibrium location is denoted by the vector  $\boldsymbol{\delta}(x, y, t)$ . With these definitions, the analytical expression for the pressure  $p = 0$  at the free surface reduces to the following expression:

$$\nabla \left[ -\frac{\partial(\Phi + \mathbf{\Omega} \cdot \boldsymbol{\Psi})}{\partial t} + (\mathbf{\Omega}_0 \mathbf{k} \times \mathbf{\Omega}_0 \mathbf{k} \times R_f + \mathbf{g}) \cdot \boldsymbol{\delta} \right] = -\frac{d\mathbf{\Omega}}{dt} \times \mathbf{r} - \mathbf{\Omega}_0 \mathbf{k} \times \mathbf{u} \quad (6.12a)$$

Even with the homogeneous vortex assumption, Eq. (6.12a) cannot be integrated rigorously. It is argued that the first term on the right hand side of Eq. (6.12a) only changes the phasing of the free surface motion relative to the homogeneous vortex, and the second term on the right does not change the energy of the motion, since it is normal to the velocity. Thus, these two terms are neglected, and the free surface pressure condition is then expressed as:

$$\frac{\partial\Phi}{\partial t} + \frac{d\mathbf{\Omega}}{dt} \cdot \boldsymbol{\Psi} = g_{eff} \boldsymbol{\delta} \quad \text{on the free surface } S_f \quad (6.12b)$$

where  $\boldsymbol{\delta}$  is now the free surface deflection normal to the curved equilibrium free surface and  $g_{eff}$  is the effective gravity at the free surface (a combination of centrifugal and gravitational accelerations); note that  $g_{eff}$  is constant in magnitude everywhere on this surface. Although the assumptions leading to Eq. (6.12b) might appear to be overly simplified, their consequences are not critical. As we observed in earlier sections, the natural frequencies of the free surface motions are higher than the natural frequencies of the internal, inertia wave motions. Thus, the two kinds of motions are nearly independent of each other, so even if the boundary condition at the free surface is an approximation, it should not significantly affect the more important inertia wave solution.

We also need a kinematic condition at the free surface. This condition is expressed as:

$$\frac{\partial \delta}{\partial t} = -\mathbf{n} \cdot \nabla \Phi \quad \text{and} \quad (\mathbf{n} \cdot \nabla) \boldsymbol{\psi} = -\mathbf{n} \times \mathbf{r} \quad \text{on the free surface } S_f \quad (6.13)$$

The first of Eqs. (6.13) and Eq. (6.12b) can be combined to give:

$$\frac{\partial^2 \Phi}{\partial t^2} + g_{eff} \mathbf{n} \cdot \nabla \Phi = -\frac{d^2 \boldsymbol{\Omega}}{dt^2} \cdot \boldsymbol{\psi} \quad \text{on the free surface } S_f \quad (6.14)$$

The general method of constructing a solution to these equations is first to set the right hand side of Eq. (6.14) equal to zero. This gives a standard eigenvalue problem for the potentials  $\Phi$  and  $\boldsymbol{\psi}_i$ . After the scalar potential eigenfunctions  $\phi_k$ ,  $k = 1, 2, 3, \dots$ , are obtained, the  $\Phi$  potential is expressed as a series of the eigenfunctions  $\phi_i$  with arbitrary expansion coefficients  $\lambda_k(t)$ . The full form of Eq. (6.14) is then used to determine the coupling between the  $\Phi$  motions and the  $\boldsymbol{\psi}_i$  motions. A typical Fourier expansion is sufficient for this purpose, such that the resulting equation for the  $k^{\text{th}}$  slosh mode is:

$$\frac{d^2 \lambda_k}{dt^2} + \omega_k^2 \lambda_k = -\frac{\iint (\boldsymbol{\psi} \cdot d^2 \boldsymbol{\Omega} / dt^2) \phi_k dS_f}{\iint \phi_k^2 dS_f} \quad k = 1, 2, 3, \dots \quad (6.15)$$

where  $\omega_k$  is the natural frequency of the mode. These equations relate the vorticity  $\boldsymbol{\Omega}_i$  for  $i = x, y, z$  to the slosh modal amplitudes  $\lambda_k$ . The spin rate and tank shape are related to  $\lambda_k$  and the  $\boldsymbol{\Omega}_i$  by Eq. (6.9).

The solution to the above set of equations can be found by purely analytical means only for some tank shapes. For most tank shapes, the solution has to be computed by finite difference computer codes or by other numerical methods. The general characteristics of the solutions are illustrated below for a tank shape for which an analytical solution can be found.

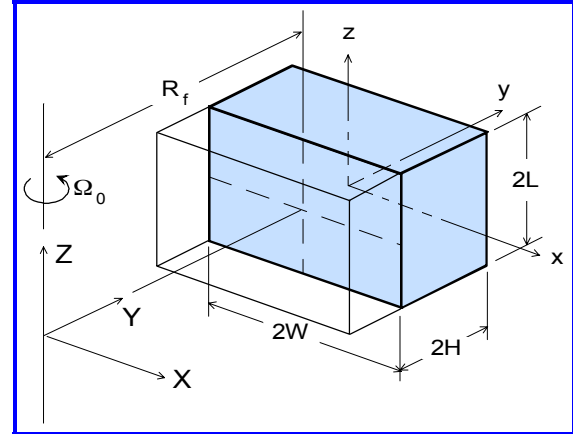


Figure 6.8. Tank and coordinate system for example of homogeneous vortex model

### Analytical/Numerical Example

As an analytical example of the homogeneous vortex model, a parallelepiped tank is considered. The tank and the coordinate systems are shown in Figure 6.8. The spin axis is aligned with the  $Z$  axis, and the free surface is located a distance  $R_f$  along the  $Y$  axis from the spin axis. The distance  $R_f$  is supposed to be large enough that the cylindrical shape of the free surface can be assumed to be effectively flat. The  $x, y, z$  coordinate system is located at the center of mass of the liquid and is fixed to the tank. For numerical results, we will set  $R_f = 8$ ,  $L = 2$ ,  $W = 1.5$ , and  $H = 1$ .

The solution for the vector potentials that satisfies Eq. (6.10) and the boundary conditions Eqs. (6.11) and (6.13) is:

$$\Psi_x = -yz + \sum_{n=1}^{\infty} \frac{4H^2 (-1)^{n+1}}{\pi^3 (n-1/2)^3} \sin[(n-1/2)(\pi y/H)] \frac{\sinh[(n-1/2)(\pi z/H)]}{\cosh[(n-1/2)(\pi L/H)]} \quad (6.16a)$$

$$\Psi_y = -xz + \sum_{n=1}^{\infty} \frac{4L^2 (-1)^{n+1}}{\pi^3 (n-1/2)^3} \sin[(n-1/2)(\pi z/L)] \frac{\sinh[(n-1/2)(\pi x/L)]}{\cosh[(n-1/2)(\pi W/L)]} \quad (6.16b)$$

$$\Psi_z = -xy + \sum_{n=1}^{\infty} \frac{4W^2 (-1)^{n+1}}{\pi^3 (n-1/2)^3} \sin[(n-1/2)(\pi x/W)] \frac{\sinh[(n-1/2)(\pi y/W)]}{\cosh[(n-1/2)(\pi H/W)]} \quad (6.16c)$$

The first few two-dimensional antisymmetric slosh waves along the  $z$  axis and the corresponding natural frequencies that satisfy Eq. (6.10) and boundary conditions Eq. (6.11) and Eq. (6.14) (with the right hand side set equal to zero) are:

$$\phi_{11} = \sin(\pi z/2L) \frac{\cosh[\pi(H-y)/2L]}{\cosh(\pi H/L)} \quad \omega_{11} = \Omega_0 \sqrt{(\pi R_f/2L) \tanh(\pi H/L)} \quad (6.17a)$$

$$\phi_{12} = \sin(3\pi z/2L) \frac{\cosh[3\pi(H-y)/2L]}{\cosh(3\pi H/L)} \quad \omega_{11} = \Omega_0 \sqrt{(3\pi R_f/2L) \tanh(3\pi H/L)} \quad (6.17b)$$

The first few two-dimensional antisymmetric slosh waves along the  $x$ -axis are:

$$\phi_{21} = \sin(\pi x/2W) \frac{\cosh[\pi(H-y)/2W]}{\cosh(\pi H/W)} \quad \omega_{11} = \Omega_0 \sqrt{(\pi R_f/2W) \tanh(\pi H/W)} \quad (6.17c)$$

$$\phi_{22} = \sin(3\pi x/2W) \frac{\cosh[3\pi(H-y)/2W]}{\cosh(3\pi H/W)} \quad \omega_{11} = \Omega_0 \sqrt{(3\pi R_f/2W) \tanh(3\pi H/W)} \quad (6.17d)$$

The lowest frequency three-dimensional antisymmetric slosh wave is described by:

$$\phi_{31} = \sin(\pi x/2W) \sin(\pi z/2L) \frac{\cosh\left[\pi\sqrt{1+(L/W)^2}(H-y)/2L\right]}{\cosh\left[\pi\sqrt{1+(L/W)^2}H/2L\right]} \quad (6.17e)$$

$$\omega_{311} = \Omega_0 \left[ (\pi R_f/2L) \sqrt{1+(L/W)^2} \tanh\left(\pi H \sqrt{1+(L/W)^2} / L\right) \right]$$

There are also symmetrical slosh waves that satisfy the boundary conditions.

When these  $\phi_i$  and  $\psi_i$  functions are inserted into Eq. (6.15) we find that the  $\phi_{11}$  slosh mode is coupled to the  $x$  component of the unsteady vorticity by:

$$\left(-\omega^2 + 5.762\Omega_0^2\right)\lambda_{11} = 1.0861\Omega_{x0}^2 \quad (6.18a)$$

where  $\omega$  is the frequency of the liquid motion and  $\Omega_{x0}$  is the amplitude of the  $\Omega_x$  vortex.

Likewise, the coupling equations for a few of the other slosh modes are:

$$\left(-\omega^2 + 18.847\Omega_0^2\right)\lambda_{12} = 0.0300\Omega_{x0}^2 \quad (6.18b)$$

$$\left(-\omega^2 + 10.361\Omega_0^2\right)\lambda_{31} = 0.5519\Omega_{y0}^2 \quad (6.18c)$$

$$\left(-\omega^2 + 20.627\Omega_0^2\right)\lambda_{32} = 0.1468\Omega_{y0}^2 \quad (6.19d)$$

$$\left(-\omega^2 + 25.906\Omega_0^2\right)\lambda_{33} = -0.1932\Omega_{y0}^2 \quad (6.19e)$$

As can be seen, the symmetry of this problem makes the coupling equations relatively simple, since no slosh mode is coupled to both the  $x$  and  $y$  components of the vorticity. Furthermore, none of the slosh modes is coupled to the  $z$  component of the vorticity.

With the functions for  $\phi_i$  and  $\psi_i$  given previously, the equations of motion, Eq. (6.9), reduce to:

$$-i\omega\Omega_{x0} - 0.791\Omega_0\Omega_{y0} = -0.126\Omega_0\lambda_{31} + 0.0646\Omega_0\lambda_{32} + 0.0515\Omega_0\lambda_{33} \quad (6.20a)$$

$$i\omega\Omega_{y0} + 0.541\Omega_0\Omega_{x0} = 0.126\Omega_0\lambda_{11} - 0.246\Omega_0\lambda_{12} \quad (6.20b)$$

All the components of the  $\Omega_{z0}$  equation are equal to zero, which means that there is no unsteady vorticity around the spin axis.

There is only root  $\omega_1$  of Eqs. (6.20) that is smaller than  $2\Omega_0$ , so presumably this root corresponds to inertia mode. The other roots  $\omega_i > 2\Omega_0$  correspond to free surface slosh modes. Since five slosh modes were retained, there are six natural frequencies:  $\omega_1 = 0.6634\Omega_0$ ;  $\omega_2 = 2.368\Omega_0$ ;  $\omega_3 = 3.2171\Omega_0$ ;  $\omega_4 = 4.342\Omega_0$ ;  $\omega_5 = 4.542\Omega_0$ ; and  $\omega_6 = 5.089\Omega_0$ . The slosh mode frequencies ( $i > 2$ ) are almost identical to the uncoupled slosh mode frequencies given by Eqs. (6.17). The inertia mode frequency  $\omega_1 = 0.6643\Omega_0$  is in the same numerical range as the inertia wave frequencies predicted by the exact theories discussed earlier.

For this numerical example, we first set  $\omega = \omega_1$  and give the vortex amplitude  $\Omega_{x0}$  a unit amplitude; we find that the amplitude of the  $y$ -component vortex  $\Omega_{y0}$  is 0.835, and the slosh mode amplitudes are  $\lambda_{11} = 0.098$ ;  $\lambda_{12} = 0.00076$ ;  $\lambda_{31} = 0.0245$ ;  $\lambda_{32} = 0.0032$ ; and  $\lambda_{33} = 0.0042$ . The relatively small magnitude of the slosh wave amplitudes proves that the  $\omega_1 = 0.6634\Omega_0$  mode is in fact an inertia mode. Conversely, when  $\omega = \omega_i$ ,  $i > 2$ , and the amplitude of one of the slosh modes is given a value of unity, the amplitudes of the unsteady vorticities are very small, indicating that these modes are in fact free surface modes with only a little inertia mode contribution.

### Axisymmetric tanks.

Other tank shapes can also be analyzed by the homogeneous vortex model, but the  $\phi_i$  and  $\psi_i$  potentials generally have to be found numerically. Figure 6.9 shows typical results for cylindrical and spherical tanks, as a function of tank fill level [CUTSHALL, et al, 1996]. The distance of the tank center from the spin axis was assumed to be 2.4 times the tank radius for these computations, but the results are reasonably insensitive to this assumption.

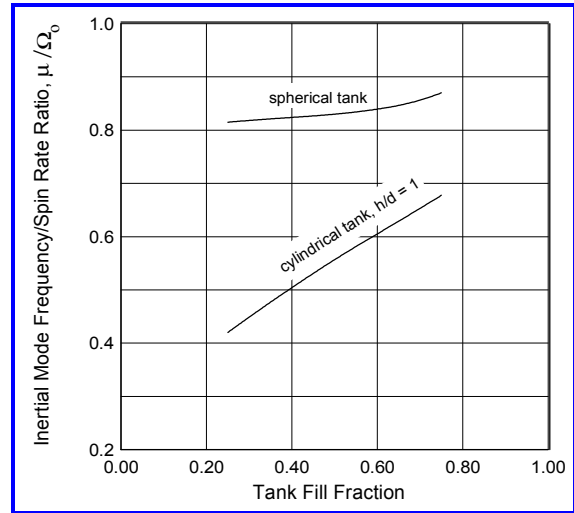


Figure 6.9. Inertia mode natural frequencies for cylindrical ( $h/d = 1$ ) and spherical tanks

### Forces and torques.

We will show later that an inertia wave mode does not exert a net force on a tank but only a net torque. To compute the torque,

the general tank configuration shown previously in *Figure 6.7* is assumed to have a nutation motion that is equivalent to a simple harmonic oscillation around the  $X$  and  $Y$  axes. The angular velocity of the nutation is  $\varphi_o$  and the frequency is  $\mu$ . For a nutation, the angular velocity around each axis (see *Figure 6.1*) is of the same magnitude but different in phase; hence:

$$\varphi = \varphi_o (\mathbf{i} - \mathbf{j}) e^{i\mu t} \quad (6.21)$$

The nutation causes the tank to oscillate laterally up and down and side to side as well as to oscillate angularly about the liquid center of mass. The angular motion of the tank excites both slosh modes and inertia modes, whereas the lateral motion excites only slosh modes. According to the homogeneous vortex model, the forces and moments of the slosh modes can be approximately analyzed just as for a non-spinning tank since the coupling between the slosh and inertia modes is negligible. Consequently, the slosh forces and torques will not be discussed here, and the coupling between the inertia modes and the slosh modes will be neglected.

For this unsteady rotation of the tank, the forced motion counterparts of Eq. (6.9) are:

$$i\mu\Omega_{xo} - W_{yx}\Omega_0\Omega_{yo} = -i\mu\varphi_o \quad (6.22a)$$

$$i\mu\Omega_{yo} + W_{xy}\Omega_0\Omega_{xo} = \mu\varphi_o \quad (6.22b)$$

where  $W_{xy}$  and  $W_{yx}$  are the integrals of  $\psi_i$  indicated in Eq. (6.9). In this approximation, the inertia wave natural frequency  $\omega_1$  is equal to  $(W_{xy}W_{yx})^{0.5}$ . The amplitudes of the homogeneous vortex can be found readily from Eqs. (6.22):

$$\Omega_{xo} = \left[ \frac{\mu^2 - W_{yx}\mu\Omega_0}{\omega_1^2 - \mu^2} \right] \varphi_o \quad \Omega_{yo} = -i \left[ \frac{\mu^2 - W_{xy}\mu\Omega_0}{\omega_1^2 - \mu^2} \right] \varphi_o \quad (6.23)$$

The vortex amplitudes become indefinitely large when the nutation frequency  $\mu$  is equal to the inertia mode frequency  $\omega_1$ . Just as was the case for the sloshing theory discussed in Chapter 1, this prediction of infinitely large motions is caused by the neglect of viscous effects. Damping can be introduced after-the-fact by a boundary layer analysis, just as for the sloshing analyses. (This topic is discussed in the Appendix to this chapter.)

There are, however, more serious conceptual physical difficulties with Eqs. (6.22) and (6.23) than just the absence of damping. These equations, which were derived by writing them in a rotating accelerating coordinate system, indicate that the amplitude of the vortex motion does not directly depend on the shape of the tank. This is clearly an approximation, because, for example, an unsteady rotation of a spherical tank about its own center would not cause any motion of an ideal, inviscid liquid; the tank would merely slide around the liquid. EL RAHEB AND WAGNER [1981] therefore argue that the terms retained on the right hand side of Eqs. (6.22a) should be neglected, and that the vortex motion is driven only by its coupling with the slosh modes [Eq. (6.18)]. The forcing of the slosh potential  $\Phi$  does in fact depend on the tank shape, as can be seen from Eqs. (6.11), so this would make the excitation of the inertia modes also depend on the tank shape. But the EL RAHEB AND WAGNER approach is not trouble-free, either, since for a tank shape such as a cylinder, an unsteady rotation of the tank is transmitted directly to the liquid. At this point, we just accept the fact that Eqs. (6.22) may sometimes lead to unrealistic amplitudes of the inertia mode for tank shapes such as a sphere, for which an unsteady rotation of the tank is not coupled strongly to the liquid. It

might be noted, however, that liquid motions in exactly those tank – for which the direction of the liquid pressure force acting on an element of the tank wall passes through the tank center – exert no net torque on the tank. Hence, the consequences for tanks for which Eqs. (6.22) are not particularly valid may not be particularly serious.

To compute the torque, an expression is needed to relate the liquid pressure to the tank motion. From the equations of motion expressed in a rotating coordinate system, this expression is found to be:

$$\frac{P}{\rho} = \dot{\Phi} + \dot{\boldsymbol{\Omega}} \cdot \boldsymbol{\psi} + (\mathbf{r} \times \mathbf{R}_s) \cdot \dot{\boldsymbol{\omega}} - (\boldsymbol{\omega} \times \mathbf{R}) \cdot (\Omega_0 \mathbf{k} \times \mathbf{R}) - \int [(\boldsymbol{\Omega} + \dot{\boldsymbol{\omega}}) \times \mathbf{r}] \cdot d\mathbf{r} - \int (2\Omega_0 \mathbf{k} \times \mathbf{u}) \cdot d\mathbf{r} \quad (6.24a)$$

where  $\mathbf{r}$  is the vector from the center of the tank to a point in the liquid,  $\mathbf{R}_s$  is the vector from the origin of the  $X, Y, Z$  coordinate system to the tank center, and  $\mathbf{R} = \mathbf{R}_s + \mathbf{r}$ . Since the interest is in the inertia wave mode, the free surface slosh potential  $\Phi$  is neglected as being coupled only very weakly to the inertia mode. Thus, after the integrals in this equation are evaluated, the required expression for the pressure on the tank walls is:

$$p_{wall}/\rho = \dot{\Omega}_x \psi_x + \dot{\Omega}_y \psi_y + 2\Omega_0 \Omega_x [xy n_z \cdot \mathbf{n}_y - xz(1 + \mathbf{n}_y \cdot \mathbf{n}_y)] + 2\Omega_0 \Omega_y [xy n_z \cdot \mathbf{n}_x - xz(1 + \mathbf{n}_x \cdot \mathbf{n}_x)] + \dot{\omega}_x (yZ_o - zY_o) + \dot{\omega}_y (zX - xZ_o) + \Omega_0 (z + Z_o) [\omega_x (x + X_o) + \omega_y (y + Y_o)] \quad (6.24b)$$

Here,  $X_o, Y_o, Z_o$  are the coordinates of the center of the tank, and  $\mathbf{n}_x, \mathbf{n}_y$ , and  $\mathbf{n}_z$  are the unit normal vectors at a point on the tank walls.

When the pressure is integrated over the tank walls, the net force is found not to contain any components that depend on the unsteady vorticity; that is, the inertia mode does not exert a net force on the tank, and the only force is a rigid-body like reaction. The torque exerted on the tank about the liquid center of mass is, however, not zero. By integrating the pressure over the tank walls, the unsteady torque is found to be::

$$M_x = \rho \left[ I_x \frac{d\Omega_x}{dt} + I_{xy} \Omega_0 \Omega_y \right] \quad M_y = \rho \left[ I_y \frac{d\Omega_y}{dt} - I_{yx} \Omega_0 \Omega_x \right] \quad (6.25)$$

where  $I_x, I_y, I_{xy}$ , and  $I_{yx}$  are volume integrals of  $\psi_x$  and  $\psi_y$ . There are also rigid-body like torques that are not included in Eqs. (6.25). The form of Eqs. (6.25) is the same as the torques produced by a precessing rigid body when the amplitude of the body's precession is proportional to the amplitudes of the inertia wave oscillation [DODGE, ET AL, 1994]. For a spherical tank,  $I_x, I_y, I_{xy}$ , and  $I_{yx}$  are all zero; this is a consequence of the fact that all the elemental pressure forces are directed through the center of the tank for a sphere.

For the parallelepiped tank example discussed previously, Eqs. (6.25) reduce to:

$$M_x = i\rho V (0.628i\mu\Omega_{x0} + 1.333\Omega_0\Omega_{y0}) e^{i\mu t} \quad M_y = \rho V (0.918i\mu\Omega_{y0} - 2.333\Omega_0\Omega_{x0}) e^{i\mu t} \quad (6.26)$$

where  $V$  is the liquid volume and  $\Omega_{x0}$  and  $\Omega_{y0}$  are given by Eqs. (6.23).

For a general case, the torque amplitudes from Eq. (6.25) are expressed in the form:

$$\frac{M_{x,y}}{m_{liq}\Omega_0\omega_o L^2} = \frac{A(\mu/\Omega_0) - B + C(\Omega_0/\mu)}{1 - (\omega/\mu)^2} \quad (6.27)$$

where the subscript  $x$  indicates the torque is exerted around the  $x$  axis and similarly for the subscript  $y$ . The parameter  $L$  is the characteristic dimension of the tank, which is the height of a cylindrical tank and the radius of a spherical tank. For the parallelepiped tank example, the  $x$ -torque parameters are  $A = 0.0785$ ,  $B = 0.229$ , and  $C = 0.090$ ; the  $y$ -torque parameters are  $A = 0.115$ ,  $B = 0.354$ , and  $C = 0.231$ . Figure 6.10 shows the values of the  $A$ ,  $B$ , and  $C$  parameters for a cylindrical tank located 2.4 tank radii from the spin axis, as a function of tank fill level [CUTSHALL, ET AL, 1996]. For the reasons discussed earlier,  $A$ ,  $B$ , and  $C$  are equal to zero for a spherical tank.

## 6.5 Energy Dissipation

### Nutation time constant

In Section 6.1, the effects of energy dissipation on the stability of spacecraft spinning around a minor moment-of-inertia axis were discussed briefly. Energy dissipation for such a spacecraft leads to an exponential growth of the nutation coning angle  $\theta_c$  that must be checked by the use of attitude control thrusters. Hence, it is important to know the *time constant*  $\tau$  of the nutation growth rate, defined by the relation  $\theta_c = \theta_{c0} \exp(t/\tau)$ . If the energy dissipation mechanism is considered to be a passive device, the time constant and the energy dissipation rate  $E$  are related by the *energy sink* model [THOMSON, 1961]; this model predicts the relation between  $E$ ,  $\theta_c$ , and  $\tau$  to be:

$$\tau = \frac{I_s \Omega_0 \mu \theta_c^2}{E} \quad (6.28)$$

where  $I_s$  is the moment of inertia about the spin axis and  $\mu$  is the nutation frequency. When the energy dissipation is large (e.g., a resonance of the liquid motion), the time constant is short, which implies that the nutation will grow rapidly if not checked.

For many mechanisms that dissipate energy, including small amplitude sloshing and inertia waves, the energy dissipation rate is proportional to the square of the nutation amplitude (i.e., the square of the nutation cone angle). For these conditions, as shown by Eq. (6.28), the time constant does not depend on the nutation amplitude  $\theta_c$ .

When the mass of the dissipative component is not small (e.g., liquid in large tanks), the energy dissipation mechanism is not necessarily passive, because the motion of the component itself may directly interact with the spacecraft motion. Part of the spacecraft rotational kinetic energy then oscillates back and forth with the dissipating component, and this can also lead to nutation growth even without energy dissipation. But even for non-passive dissipators, it is customary to define a nutation time constant.

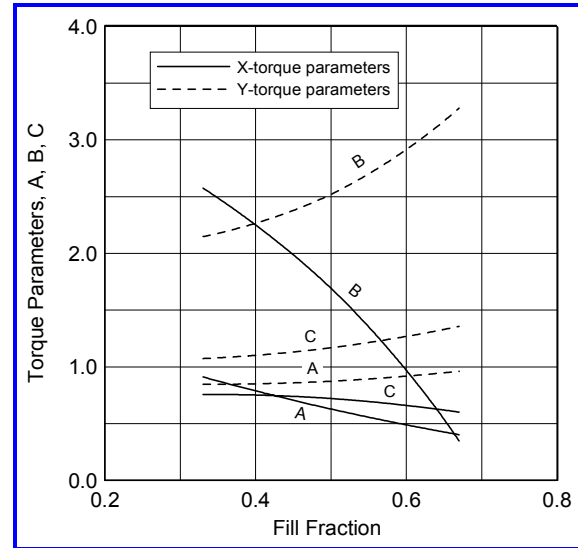


Figure 6.10. Inertia mode torque parameters for a cylindrical tank ( $h/d = 1$ )

## Experimental methods

Because of the critical effect of energy dissipation on the stability of a spinning spacecraft, it is usually a requirement to measure the nutation time constant or an equivalent parameter experimentally before the flight of any spacecraft that contains a significant quantity of liquid in its tanks. Several experimental methods can be used to determine the time constant, as discussed below.

**Air-bearing spin-table method.** In this method, a dynamically-scaled spacecraft model is mounted on a platform supported by an extremely low-friction air bearing and placed in a large vacuum chamber to minimize aerodynamic drag [PETERSON, 1976; NEER AND SALVATORE, 1972; MARCÉ AND ASSEMAT, 1980]. The platform is spun up by motors to the desired speed, and after a steady state is achieved, all restraints are removed and the spacecraft model is allowed to spin and nutate freely. The time history of the cone angle is monitored. The energy dissipation rate is inferred from Eq. (6.28). The dissipation rate is adjusted as necessary to compensate for any significant differences between the viscosity of the test liquid and the spacecraft liquid. Results from air-bearing tests have usually – but not always – been found to be reasonably well correlated with on-orbit data. The results are specific to the spacecraft in question.

**Free fall method.** In the free-fall method, a small scale model of the spacecraft is allowed to fall freely for a short period of time while spinning. The principal test measurement is the growth of the nutation cone angle. The free-fall method has generally supplanted the air-bearing spin table method since tests can be conducted more economically and without the need for a vacuum facility; in addition, the perturbing effects of gravity are removed so the test more nearly duplicates in-space conditions [HARRISON, GARG, AND FUROMOTO, 1983]. But because of the limitations imposed by available drop towers, the size of the spacecraft model used in a free fall test has to be quite small, and very high spin rates are required to accumulate enough nutation cycles to measure the cone angle growth in the time available. Hence, test conditions have to be determined by the principles of dynamic similarity, such that, for example, the Reynolds number of the liquid based on spin rate is the same for the model tank and the spacecraft tank. The scaling has been found to be reasonably successful for tanks without internal hardware or for tanks that contain only *rigid* baffles or other *rigid* (i.e., non-energy dissipating) hardware. If the time constant is judged to be too short, various kinds of baffles are inserted in the tank until an acceptable time constant is found empirically [POCHA, 1981]. Just as for the air bearing method, the test results are specific to the spacecraft in question.

**Forced motion spin-table method.** Both the air-bearing method and the free-fall method are ill suited for general investigations of liquid motions in spinning tanks. For example, to investigate liquid resonances parametrically, the nutation frequency has to be varied while the spin rate is held constant, and this is difficult for a freely nutating model since the only way the nutation rate can be changed is to change the mass distribution of the model spacecraft. Consequently, another method – called the forced-motion spin table method – has been developed to investigate general liquid motions. For this method, the spin table is driven by a set of electric motors whose rotation rate can be adjusted individually to cause the spinning table to execute a nutation-like motion [MARTIN, 1971; GARG, FUROMOTO, AND VANYO, 1984; GUIBERT, 1986; ZEDD AND DODGE, 1985; CHATO, ET AL, 1998]. The spin rate and nutation frequency can be varied independently from test to test by changing the speeds of the motors, and the cone angle can be varied by changing the tilt of the table relative to the spin motor axis. However, the nutation time constant obviously cannot be measured since the cone angle is not a function of time. Instead, the

## 6. LIQUID MOTIONS IN A SPINNING TANK

energy dissipation rate has to be measured from the electrical power consumption of the motors or inferred from liquid force and torque measurements. Since the tanks on the spin table are exposed to the perturbing effects of gravity, the spin rate also must be kept high to ensure that the centrifugal acceleration exerted on the tank is much larger than the gravitational acceleration. However, even with these limitations, the ease with which the parameters of the motion can be controlled makes this method ideal to investigate energy dissipation rate correlations as a function of tank shape, fill level, etc.

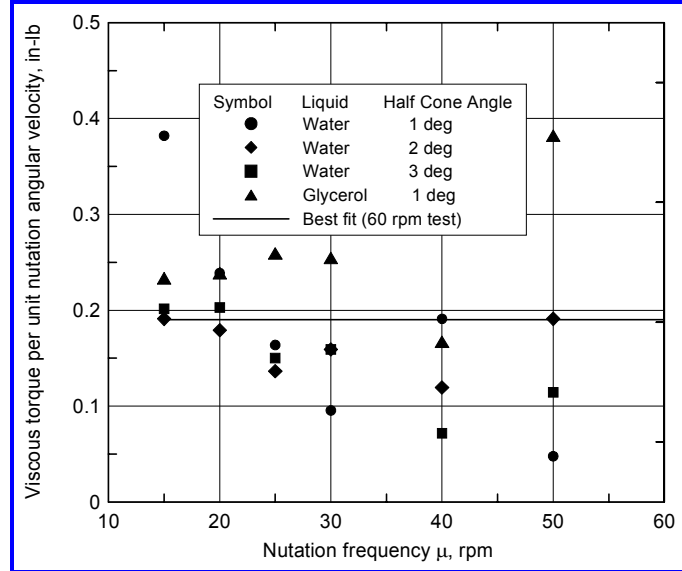


**Figure 6.11.** Viscous torque for 12-inch diameter spherical tank at  $\Omega = 60$  rpm; spin axis distance = 2.67 tank diameters

ZEDD AND DODGE [1984] used a forced-motion spin-table to measure the liquid forces and torques for a partially-full spherical tank one foot in diameter whose axis was 32 inches (2.67 tank diameters) from the spin axis. The load cell measurements were corrected to account for the rigid body torques of the tank itself, its mounting structure, and the equivalent frozen or rigidified liquid. The torque and force remaining after these rigid body torques were subtracted was assumed to be due to the motion of the liquid relative to the tank. *Figure 6.11* shows the torque results as a function of nutation frequency for a set of tests conducted at a spin rate of 60 rpm. Two different liquids were used: water and a water-glycerol mixture that had a viscosity ten times that of water. Three different values of the cone angle were tested. The nutation frequency was varied from nearly zero to nearly the spin rate. As can be seen, there is quite a bit of scatter in the data (especially for higher nutation frequencies, for which the nutation angular velocity approached zero for the particular mechanical arrangement of the spin table). Nonetheless, the best fit to the data shows that the torque per unit nutation angular velocity is roughly constant over the range of tested nutation frequencies, which is the expected result.

The energy dissipation rate was computed from the test results by integrating the product of the non-rigid body torque and the tank nutation rate (angular velocity) over one cycle of the motion. From all the tests conducted for spin rates from 20 rpm to 100 rpm, it was found that the energy dissipation rate was adequately correlated by:

$$E = 48.2\phi_0^2\rho d^5\Omega_0 F_W \sqrt{\frac{\nu}{\Omega_0 d^2}} \quad (6.29)$$

where  $\rho$  and  $\nu$  are the liquid density and kinematic viscosity,  $d$  is the tank diameter,  $F_W$  is the fraction of the tank wall that is wet by the liquid, and  $\phi_0$  is the nutation angular

velocity.<sup>17</sup> The energy dissipation rate  $E$  is proportional to the square root of the effective Reynolds number, just as it is for laminar flow. There was no evidence of inertia wave resonances in these tests, which was not unexpected for a spherical tank for reasons discussed previously.

A similar but considerably smaller spin table was used in a space experiment that investigated liquid motions in spinning tanks in zero-g [CHATO, ET AL, 1998]. The test tanks were spheres and cylinders having a diameter of 4.5 inch. For the spherical tanks with a spin rate of 20 rpm, a nutation angular velocity of 1 rpm, water as the test liquid, and fill levels of 33% and 67%, energy dissipation rates were inferred from the test torque data (by the method discussed above) to be in the range from 0.00005 to 0.0004 in-lb/sec. For these conditions, Eq. (6.29) predicts an energy dissipation rate of about 0.0005 in-lb/sec, which is of the same magnitude as the space experiment results.

Energy dissipation rates were also determined for the cylindrical tanks, which had a height-to-diameter ratio of  $h/d = 1$ . The computed energy dissipation rates for nutation frequencies that did not excite liquid resonances were somewhat smaller than for the spherical tanks. (Resonances were observed for cylindrical tanks.)

Figure 6.12 shows a different kind of forced-motion spin-table that measures the energy dissipation rate *directly*. This method is especially applicable to spherical tanks located on the spacecraft spin axis [VANYO, 1973; GARG, FUROMOTO, AND VANYO, 1984]. To measure the energy dissipation, a preliminary test has to be run without liquid in the tank to determine the electric power consumption required to overcome the bearing and aerodynamic frictional losses. For data tests when the tank contains liquid, the electrical power measured in excess of the frictional losses is the energy dissipation rate caused by liquid motions. Test results are correlated by expressions of the form:

$$E = Km_{liquid}\Omega_0^3 d^2 \theta_c^2 \left( \frac{\Omega_0}{\mu} \right) \sqrt{\frac{v}{\Omega_0 d^2}} \quad (6.30)$$

where  $m_{liquid}$  is the mass of liquid in the tank and  $K$  is a numerical parameter of order unity. This expression is equivalent in form to Eq. (6.29) since the nutation rate  $\phi_0$  in Eq. (6.29) is proportional to the product of the nutation frequency and the cone angle, and the nutation frequency  $\mu$  in Eq. (6.30) is proportional to the spin rate.

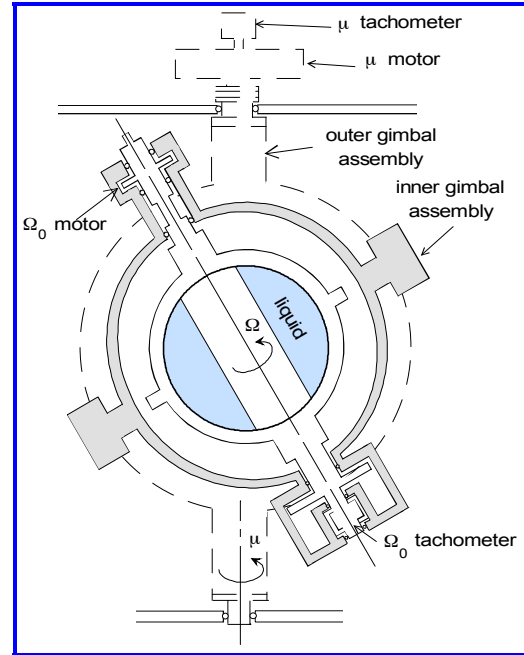


Figure 6.12. Apparatus for direct measurement of energy dissipation for on-axis tanks

<sup>17</sup> For a freely spinning body such as a axisymmetric spacecraft, the nutation rate is given by  $\phi_0 = \theta_c \Omega_0 (I_s/I_t)$  where  $I_s$  and  $I_t$  are the spin axis and transverse axis moments of inertia. For a forced motion spin table, the nutation angular velocity depends on the mechanical arrangement of the spin and nutation motors, but it is proportional to the cone angle.

### Analytical methods

Analytical methods of predicting energy dissipations are not as reliable as experimental methods because of the lack of an accurate analytical model of liquid motions in a spinning, nutating tank. Various kind of viscous boundary layer corrections to the homogeneous vortex model have been suggested [EBERT, 1984] and boundary layer corrections have also been employed with finite-element solutions of the complete equations of motion for an inviscid liquid [AGRAWAL, 1993; POHL, 1984]. Even the finite-element models are limited by the inability of a model of inviscid fluid motions to be coupled in an unambiguous way to the motions of the tank. A complete solution of the Navier-Stokes equations, including viscosity from the start, would seem to be required.

A relatively simple analytical method of estimating the energy dissipation rate is discussed in the Appendix to this chapter. It is based on a viscous boundary layer correction to the homogeneous vortex model, and it employs the analytical solution discussed earlier for a parallelepiped tank. To estimate the energy dissipation rate for another tank shape, an equivalent parallelepiped tank would have to be defined in terms of the volume, free surface area, and other relevant parameters of the actual tank.

## 6.6 Stability of a Rotating Interface in Zero-G

The stability of a static liquid-vapor interface in zero-g was discussed in detail in Section 4.4. The stability of the interface in a *rotating* tank is also of interest, especially with respect to the separation of the liquid and gas phases in the tank.

For the special case of zero Bond number, contact angle equal to zero, and an annular tank, the stability criterion for the interface was investigated by SEEBOLD AND REYNOLDS, [1965a, 1965b]. They found that the critical rotation rate  $\Omega_c$  is given by:

$$\Omega_c^2 = \frac{4\sigma}{\rho R_0^3} \left[ \frac{1}{(1 - R_i/R_0)^2} \right] \quad (6.31)$$

where  $R_0$  and  $R_i$  are the outer and inner radii of the annulus,  $\sigma$  is the liquid surface tension, and  $\rho$  is the liquid density. When the spin rate exceeds  $\Omega_c$ , the liquid is thrown to the outer walls of the tank. A general axisymmetric tank can be treated by setting  $R_i = 0$  in Eq. (6.31).

Equation (6.31) indicates that liquid in zero-g can be completely separated from the vapor in a large tank for very low rotation rates. For example, when  $R_0 = 1.5$  m and for typical liquid properties, a rotation rate of two revolutions per *hour* will produce complete separation of the liquid and gas in the tank (after a steady state rotation is achieved). Drop tower experiments have proved in fact that Eq. (6.31) is slightly conservative.

More general stability criteria have been examined by numerical solutions to the equations of motion [e.g., GANS AND LESLIE, 1987]. In addition, the stability of the basic inertia wave motion in rotating tanks has also been examined. It has been found that for excitation frequencies close to a liquid resonance, where large amplitude waves are excited, the inertia modes become unstable and exhibit many characteristics of chaotic behavior [MCEWAN, 1970; MANASSEH, 1992; TAN, 1994]. Unstable modes create exceptionally large energy dissipation rates. Hence, this is another reason why it is important to avoid liquid resonances in spinning spacecraft.

## 6.7 References

- AGRAWAL, B., 1993, *Dynamic Characteristics of Liquid Motion in Partially Filled Tanks of a Spinning Spacecraft*, **AIAA J. Guidance, Control, and Dynamics**, **16**, pp. 636-640.
- CHATO, D., DALTON, P., DODGE, F., AND GREEN, S., 1998, *Liquid Motion Experiment Flight Results*, AIAA Paper 98-3197, **34th AIAA/ASME/SAE/ASEE Joint Propulsion Conference**.
- CUTSHALL, W., DODGE, F., GREEN, S., AND UNRUH, J., 1996, *Modeling Low-G Liquid Motions in Spinning Spacecraft Tanks*, Final Report, SwRI Project 04-9769, January 1996.
- DODGE, F., UNRUH, J., GREEN, S., AND CRUSE, M., 1994, *A Mechanical Model of Liquid Inertia Waves for Use with Spinning Spacecraft*, **Fluid Transients 1994, ASME FED Vol. 198**, pp. 13-21.
- DODGE, F. T., 1996, *Dynamics of Partially Filled Tanks*, **Handbook of Fluid Dynamics and Fluid Machinery**, **3**, ed. J. A. Schetz and A. E. Fuhs, John Wiley and Sons, pp. 1793-1802, 1996.
- DODGE, F. T., 1988, *OUTREACH Definition Study: Liquid Motion in a Rotating Tank: Technical Requirements Document*, SwRI Project 04-2359, Contract NAS3-25358, October 1988.
- DODGE, F. T., and GREEN, S., 1999, *Modeling Liquid Motions in Spinning Spacecraft Tanks*, Final Report, SwRI Project 18-9946.
- EBERT, K., 1984, *Liquid Sloshing in Slowly Rotating Spacecraft*, **Proc. INTELSAT/ESA Symposium on Dynamic Effects of Liquids in Spacecraft Attitude Control**, Washington, D. C.
- EL-RAHEB, M., AND WAGNER, P., 1981, *Vibration of a Liquid with a Free Surface in a Spinning Spherical Tank*, **J. Sound and Vibration**, **76**, pp. 83-93.
- GANS, R., AND LESLIE, F., 1987, *Interface Stability in a Slowly Rotating Low-Gravity Tank*, **AIAA J. Spacecraft and Rockets**, **24**, pp. 232-235.
- GARG, S., FUROMOTO, N., AND VANYO, 1984, *Measurement of Energy Dissipation in Forced Precession Compared to Flight Data*, AIAA Paper 84-1841.
- GARG, S., FUROMOTO, N., AND VANYO, J., 1986, *Spacecraft Nutational Instability Prediction by Energy-Dissipation Measurements*, **AIAA J. Guidance, Control, and Dynamics**, **9**, pp. 357-362.
- GREENSPAN, H. 1969, **The Theory of Rotating Fluids**, Cambridge Univ. Press.
- GUIBERT, J., 1986, *Forced Motion on Spinning Test for Slosh-Moment Investigations*, ONERA Report T. P. 1986-82.
- HARRISON, J., GARG, S., AND FUROMOTO, N., 1983, *A Free Fall Technique to Measure Nutation Divergence, and Applications*, AIAA Paper 83-372.
- KARPOV, B., 1965, *Dynamics of Liquid-Filled Shell: Resonance and Effect of Viscosity*, Ballistic Research Laboratories Report No. 1279.

- MANASSEH, R., 1992, *Breakdown Regimes of Inertia Waves in a Precessing Cylinder*, **J. Fluid Mechanics**, **243**, pp. 261-296.
- MARCÉ, J., AND ASSEMAT, D., 1980, *SIMEP: Advanced Device for Measurement of the Energy Dissipation in Rotating Tanks*, **IAF Paper 80 E-238**.
- MARTIN, E., 1971, *Experimental Investigations on the Fuel Slosh of Dual-Spin Spacecraft*, **COMSAT Technical Review**, **1**, pp. 1-20.
- MCEWAN, A., 1970, *Inertia Oscillations in a Rotating Fluid Cylinder*, **J. Fluid Mechanics**, **40**, pp. 603-640.
- MCINTYRE, J., AND TANNER, T., 1987, *Fuel Slosh in a Spinning On-Axis Tank: An Eigenmode Approach*, **Space Communications & Broadcasting**, **5**, pp. 229-251.
- MILES, J., 1959, *Free Surface Oscillations in a Rotating Liquid*, **Physics of Fluids**, **2**, pp. 297-305.
- MILES, J., AND TROESCH, B., 1961, *Surface Oscillations of a Rotating Liquid*, **ASME J. Applied Mechanics**, **28**, pp. 491-496.
- NEER, J., AND SALVATORE, J., 1972, *Fuel Slosh Energy Dissipation on a Spinning Body*, Hughes Space and Communications Group Report SCG 20047R.
- PETERSON, R., 1976, *Air-Bearing Spin Facility for Measuring Energy Dissipation*, NASA TN D-8346.
- PFEIFFER, F., 1974, *Ein Näherungsverfahren für Flüssigkeitgefüllte Kreisel*, **Ingenieur-Archiv**, **43**, pp. 3306-316.
- POCHA, J., 1981, *An Experimental Investigation of Spacecraft Sloshing*, **Space Communication & Broadcasting**, **5**, pp. 323-332.
- POHL, A., 1984, *Dynamics Effects of Liquid in Spinning Spacecraft*, **Proc. INTELSAT/ESA Symposium on Dynamic Effects of Liquids in Spacecraft Attitude Control**, Washington, D. C.
- SEEBOLD, J., AND REYNOLDS, W., 1985a, *Configuration and Stability of a Rotating Axisymmetric Meniscus at Low G*, Stanford Univ., Dept. of Mech. Eng. Report LG-4.
- SEEBOLD, J., AND REYNOLDS, W., 1985b, *Shape and Stability of the Liquid-Gas Interface in a Rotating Cylindrical Tank at Low-G*, **AFOSR-LMSC Symposium on Fluid Mechanics and Heat Transfer Under Low Gravitational Conditions**, pp. 12-1 to 12-17.
- SLABINSKI, V., 1978, *COMSAT IV In-Orbit Liquid Slosh Tests and Problems in the Analysis of the Data*, **COMSAT Technical Review**, **8**, pp. 1-40.
- STEWARTSON, K., 1959, *On the Stability of a Spinning Top Containing Liquid*, **J. Fluid Mechanics**, **5**, pp. 577-592.
- STEWARTSON, K., AND ROBERTS, P., 1963, *On the Motion of a Liquid in a Spheroidal Cavity of a Precessing Rigid Body*, **J. Fluid Mechanics**, **17**, pp. 1-20.
- TAN, D., 1994, *Dynamics of a Spinning Spacecraft Containing Liquid Propellant*, **Aerospace Vehicle Dynamics and Control**, ed. M. V. Cook and M. J. Mycroft, Oxford Univ. Press, pp. 417-437.

- THOMSON, W. T., 1961, **Introduction to Space Dynamics**, John Wiley & Sons, New York.
- VANYO, J., 1973, *An Energy Assessment Method for Liquids in a Filled Precessing Spherical Cavity*, **ASME J. Applied Mechanics**, **38**, pp. 647-682.
- WEIHS, D., AND DODGE, F. T., 1991, *Liquid Motions in Nonaxisymmetric, Partially Filled Containers Rotating at Zero Gravity*, **AIAA J. Spacecraft and Rockets**, **28**, pp. 425-432.
- ZEDD, M., AND DODGE, F. T., 1984, *Energy Dissipation of Liquids in Nutating Spherical Tanks Measured by a Forced-Motion Spin Table*, AIAA Paper 84-1842-CP, **Proc., AIAA Guidance and Control Conference**, August 1984, pp. 73-83.
- ZEDD, M., AND DODGE, F. T., 1985, *Energy Dissipation of Liquids in Nutating Spherical Tanks Measured by a Forced-Motion Spin Table*, Naval Research Laboratory Report NRL 8932.

## Appendix. Analytical Energy Dissipation Estimate

The vector potential  $\boldsymbol{\psi}$  for a parallelepiped tank was discussed in Section 6.4 and was given analytically by Eqs. (6.16). These solutions are used here to estimate the energy dissipation. As was also explained in Section 6.4, only the  $\psi_x$  and  $\psi_z$  components of  $\boldsymbol{\psi}$  actually influence the liquid motions. Furthermore, free surface sloshing is neglected here as being a small correction to the vortex motion, so  $\boldsymbol{\Phi} = \mathbf{0}$ . The integrals on the right hand side of Eq. (6.9) can therefore be evaluated to give:

$$W_{yx} = \frac{2W}{V} [\psi_x(H, L) - \psi_x(-H, L) - \psi_x(H, -L) + \psi_x(-H, -L)] \quad (\text{A.1})$$

$$W_{xy} = \frac{2H}{V} [\psi_y(W, L) - \psi_y(-W, L) - \psi_y(W, -L) + \psi_y(-W, -L)] \quad (\text{A.2})$$

The natural frequency of the inertia wave mode is given in terms of these integrals by:

$$\omega_n = \Omega_0 \sqrt{(1 + W_{yx})(1 - W_{xy})} \quad (\text{A.3})$$

where  $\Omega_0$  is the tank rotation rate. The ratio of the amplitude of the  $y$ -axis vortex strength to the  $x$ -axis vortex strength is also given in terms of these integrals:

$$\Omega_{y0} = -\Omega_{x0} \left( \frac{\omega_n / \Omega_0}{1 - W_{xy}} \right) \quad (\text{A.4})$$

The magnitudes of the unsteady vortices will eventually be needed to compute the energy dissipation rate from the boundary layer correction to the homogeneous vortex model. In terms of a viscous damping coefficient  $\gamma$ , the amplitude of the  $x$ -component  $\Omega_{x0}$  of the homogeneous vortex is given by the expression:

$$\Omega_{x0} = \varphi_0 \frac{(\omega / \omega_n)^2 - W_{xy} (\Omega_0 \omega / \omega_n^2)}{\left\{ \left[ 1 - (\omega / \omega_n)^2 + (2\gamma \omega / \omega_n)^2 \right] \right\}^{0.5}} \quad (\text{A.5})$$

where  $\omega$  is the oscillation frequency (generally the nutation frequency) and  $\varphi_0$  is the amplitude of the unsteady angular velocity of the tank (usually,  $\omega \theta_c$  where  $\theta_c$  is the

rotation cone angle). This relation is a modification of Eq. (6.23) that incorporates viscous damping.

To damping coefficient  $\gamma$  can be computed, as shown by Eq. (2.2) in Chapter 2, by the ratio of the energy dissipation rate to the maximum energy of the inertia wave mode. Fortunately, this ratio can be computed without knowing in advance the actual amplitudes of the vortex motions  $\Omega_{xo}$  and  $\Omega_{yo}$ .

The maximum kinetic energy  $E$  of the inertia wave oscillation is computed by integrating the square of the liquid velocity over the liquid volume. (There is no potential energy contribution to the total energy.) The result is:

$$E = 0.5 \left( \frac{\Omega_{xo}}{\Omega_0} \right)^2 \rho V H^2 \Omega_0^2 \left[ \frac{4}{3} - 8 \frac{H}{L} \sum_{n=1}^{\infty} \frac{\tanh \left[ \pi \left( n - \frac{1}{2} \right) \frac{L}{H} \right]}{\pi^5 \left( n - \frac{1}{2} \right)^5} \right] \quad (\text{A.6})$$

where  $V$  is the liquid volume. The energy dissipation rate is computed from the viscous boundary layer correction model [DODGE AND GREEN, 1999]. The dissipation is given by:

$$\frac{dE}{dt} = \frac{\rho V H^2 \Omega_0^3}{16\sqrt{2}} \sqrt{\frac{\nu}{H^2 \Omega_0}} \left( \frac{\Omega_0}{\omega} \right)^{3/2} \left( \frac{\Omega_{xo}}{\Omega_0} \right)^2 F \quad (\text{A.7})$$

where  $\nu$  is the kinematic viscosity of the liquid and  $F$  is a function defined below. As can be seen, the  $\Omega_{xo}/\Omega_0$  ratio in both Eqs. (A.6) and (A.7) will cancel out when their ratio is formed.

The  $F$  function is given in terms of a set of other intermediate functions  $C_i$  by the expression:

$$\begin{aligned} I = & \frac{4HC_2}{L} + \left( \frac{\omega}{\Omega_0} \right)^2 \left[ \frac{1}{2} + \frac{H}{6W} + \frac{H}{L} (C_3 - 2C_5 + C_9) - \frac{H^2 C_1}{LW} \right] + \\ & 4 \left( \frac{\Omega_{yo}}{\Omega_{xo}} \right)^2 \left[ \frac{L}{H} + \frac{L^2}{HW} (C_8 - C_6) \right] + \\ & \left( \frac{\omega}{\Omega_0} \right)^2 \left( \frac{\Omega_{yo}}{\Omega_{xo}} \right)^2 \left[ \frac{L}{2H} + \frac{L^2}{6H^2} + \frac{L^2}{HW} (C_8 - 2C_6 + C_2) - \frac{L^3 C_4}{H^2 W} \right] + \\ & 8 \left( \frac{\omega}{\Omega_0} \right) \left( \frac{\Omega_{yo}}{\Omega_{xo}} \right) \left( \frac{2L}{W} C_7 - C_5 \right) \end{aligned} \quad (\text{A.8})$$

and the various  $C_i$  functions are defined as follows:

$$C_1 = \sum_{n=1}^{\infty} \frac{\tanh \left[ \pi \left( n - \frac{1}{2} \right) \frac{L}{H} \right]}{\pi^5 \left( n - \frac{1}{2} \right)^5} \quad (\text{A.9a})$$

$$C_2 = \sum_{n=1}^{\infty} \frac{\tanh^2 \left[ \pi \left( n - \frac{1}{2} \right) \frac{W}{L} \right]}{\pi^4 \left( n - \frac{1}{2} \right)^4} \quad (\text{A.9b})$$

$$C_3 = \sum_{n=1}^{\infty} \frac{\tanh^2 \left[ \pi \left( n - \frac{1}{2} \right) \frac{L}{H} \right]}{\pi^4 \left( n - \frac{1}{2} \right)^4} \quad (\text{A.9c})$$

$$C_4 = \sum_{n=1}^{\infty} \frac{\tanh \left[ \pi \left( n - \frac{1}{2} \right) \frac{W}{L} \right]}{\pi^5 \left( n - \frac{1}{2} \right)^5} \quad (\text{A.9d})$$

$$C_5 = \sum_{n=1}^{\infty} \frac{\tanh \left[ \pi \left( n - \frac{1}{2} \right) \frac{L}{H} \right]}{\pi^3 \left( n - \frac{1}{2} \right)^3} \quad (\text{A.9e})$$

$$C_6 = \sum_{n=1}^{\infty} \frac{\tanh \left[ \pi \left( n - \frac{1}{2} \right) \frac{W}{L} \right]}{\pi^3 \left( n - \frac{1}{2} \right)^3} \quad (\text{A.9f})$$

$$C_7 = \sum_{n=1}^{\infty} \sum_{m=1}^{\infty} \frac{\tanh \left[ \pi \left( n - \frac{1}{2} \right) \frac{L}{H} \right] \tanh \left[ \pi \left( m - \frac{1}{2} \right) \frac{W}{L} \right]}{\pi^6 \left( n - \frac{1}{2} \right)^3 \left( m - \frac{1}{2} \right)^3} \quad (\text{A.9g})$$

$$C_8 = \sum_{n=1}^{\infty} \sum_{n=1}^{\infty} \frac{\tanh \left[ \pi \left( n - \frac{1}{2} \right) \frac{W}{L} \right] + \tanh \left[ \pi \left( m - \frac{1}{2} \right) \frac{W}{L} \right]}{\pi^5 \left( n - \frac{1}{2} \right)^2 \left( m - \frac{1}{2} \right)^2 (n+m-1)} +$$

$$\sum_{n=1}^{\infty} \sum_{n=1}^{\infty} \frac{\tanh \left[ \pi \left( n - \frac{1}{2} \right) \frac{W}{L} \right] - \tanh \left[ \pi \left( m - \frac{1}{2} \right) \frac{W}{L} \right]}{\pi^5 \left( n - \frac{1}{2} \right)^2 \left( m - \frac{1}{2} \right)^2 (n-m)} \quad (\text{A.9h})$$

$$C_9 = \sum_{n=1}^{\infty} \sum_{n=1}^{\infty} \frac{\tanh \left[ \pi \left( n - \frac{1}{2} \right) \frac{L}{H} \right] + \tanh \left[ \pi \left( m - \frac{1}{2} \right) \frac{L}{H} \right]}{\pi^5 \left( n - \frac{1}{2} \right)^2 \left( m - \frac{1}{2} \right)^2 (n+m-1)} +$$

$$\sum_{n=1}^{\infty} \sum_{n=1}^{\infty} \frac{\tanh \left[ \pi \left( n - \frac{1}{2} \right) \frac{L}{H} \right] - \tanh \left[ \pi \left( m - \frac{1}{2} \right) \frac{L}{H} \right]}{\pi^5 \left( n - \frac{1}{2} \right)^2 \left( m - \frac{1}{2} \right)^2 (n-m)} \quad (\text{A.9i})$$

The damping coefficient is defined as:

$$\gamma = \frac{dE/dt}{2E\omega_n} \quad (\text{A.10})$$

and its value is calculable from Eqs. (A.3), (A.6) and (A.7).

After  $\gamma$  has been calculated, the magnitude of  $\Omega_{x0}$  can be computed from Eq. (A.5) for a given nutation frequency and nutation angular velocity; knowing  $\Omega_{x0}$ , the

## 6. LIQUID MOTIONS IN A SPINNING TANK

---

magnitude of  $\Omega_{y0}$  can be found from Eq. (A.4). With  $\Omega_{x0}$  and  $\Omega_{y0}$  known, the energy dissipation rate can be computed from Eq. (A.6).

# SPACECRAFT STABILITY AND CONTROL

This chapter is a very brief summary of Chapter 7 “Vehicle Stability and Control”. The original author was HELMUT F. BAUER of Georgia Institute of Technology.

## 7.1 Introduction

Since liquid propellants constitute the largest part of the total mass of many spacecraft and launch vehicles, the interaction of sloshing liquids with the trajectory of the flexible vehicle is important throughout the flight. The problems that need to be considered are how to assess the influence of this interaction on vehicle stability and control, and how to increase the stability by a proper choice of the control system and its gain values or by the adding of baffles to provide additional damping to the sloshing. These problems are discussed in this chapter by relatively simple, illustrative analyses using an example of a non-spinning launch vehicle during powered flight. The subject is covered in greater detail and generality in many textbooks [e.g., BLAKELOCK, 1991; SALI, 1997].

The analyses start by deriving the equations of motion for a vehicle that experiences small perturbations to its flight path. Then a control law is assumed and coupled to these equations. Finally, methods that can be used to solve the equations are discussed to the point at which it can be determined whether the perturbations to the trajectory increase with time (which represents an unstable flight) or decay with time (a stable flight).

## 7.2 Simplified Equations of Motion

*Figure 7.1* shows a schematic of a launch vehicle in flight and shows the coordinate systems used in the analyses. The  $X, Y$  system shown in the figure is a stationary inertial system, and the  $x, y$  system, which is fixed to the vehicle center of mass, accelerates with the vehicle. For simplicity, the motion of the vehicle is assumed to occur in the  $x, y$  plane. For the undisturbed trajectory, the  $X$  and  $x$  axes coincide with the vehicle axis; that is, the rotation  $\phi$  of the vehicle and the displacement  $y$  of the center of mass are equal to zero,

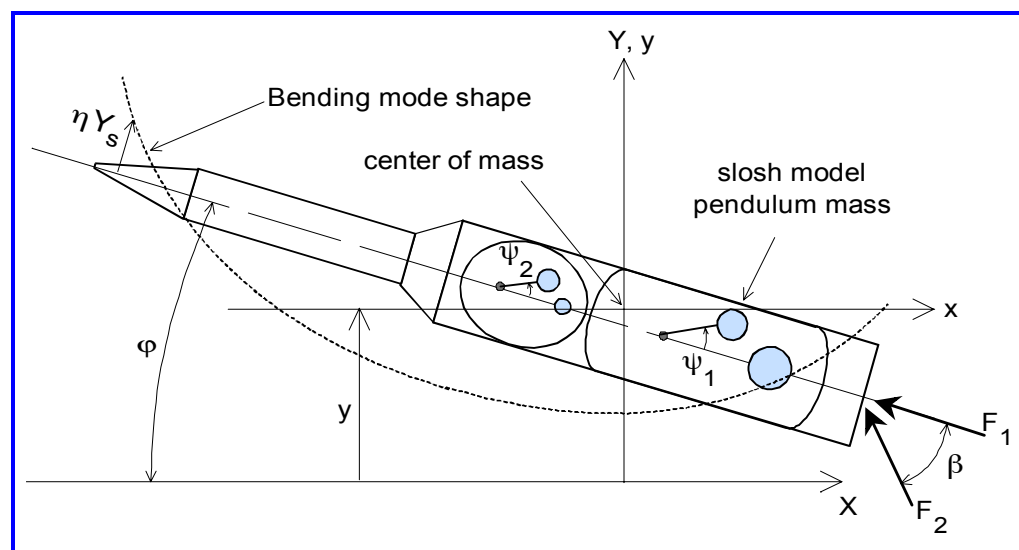


Figure 7.1. Coordinate systems for a space vehicle

and the flight path is aligned with the  $x$ -axis. The vehicle  $\phi, y$  displacements and the displacements of the slosh masses are assumed to be small, to allow the equations to be linearized with respect to them. The component of the acceleration of the  $x, y$  system along the flight path is created by the engine thrust. Aerodynamic effects are neglected, as are centrifugal and Coriolis forces resulting from rotations. Vehicle control is obtained by gimbaling (i.e., swiveling) the engine. Only a part  $F_2$  of the engine thrust can be gimbaled; the other part  $F_1$  remains aligned with the vehicle centerline.

In line with the simplified nature of this example, sloshing in the upper stages is neglected, and only the fundamental bending mode of the overall vehicle is considered. The shape of the bending mode is denoted by  $Y_v(x)$ , and it is normalized such that the deflection is unity at the engine swivel point; the actual amplitude of the mode is denoted by  $\eta$ . The vehicle translation is given by  $y$ . The deflections of the two slosh masses from the tank centerline are given by  $\psi_1$  and  $\psi_2$ , respectively. The small angle  $\beta$  specifies the angle of the gimbaled part of the force with respect to the tank centerline.

To derive the equations of motion for the stability and control analysis, we will employ the *Lagrange method* in the form [SYNGE AND GRIFFITH, 1959]:

$$\frac{d}{dt} \left( \frac{\partial KE}{\partial \dot{q}_i} \right) + \frac{\partial PE}{\partial q_i} + \frac{\partial D}{\partial \dot{q}_i} = Q_i \quad (7.1)$$

Here,  $KE$  and  $PE$  are the kinetic and potential energies of the system, and  $D$  is the damping or energy dissipation function. The generalized coordinates are represented by  $q_i$ . Each  $q_i$  is independent of the others, which means that, for example, the displacement of a point in the  $q_1$  direction does not change the value of the  $q_2, q_3, \dots$  coordinates of the point. The generalized coordinates for this problem are  $y, \phi, \psi_1, \psi_2$ , and  $\eta$ . The generalized forces  $Q_i$  are the external forces applied in the  $q_i$  directions. To use Eq. (7.1) we have to develop expressions for the various kinetic and potential energies, the rate of energy dissipation, and the generalized external forces.

The equation of motion for the vehicle in the flight path direction merely states that the thrust force  $F_1$  accelerates the vehicle along this path. This equation does not directly affect vehicle control. Hence, only the equations of motion for the perturbations of the vehicle flight path are considered, and these equations are written relative to the accelerating flight path.

**Kinetic energies.** The system kinetic energy is composed of the energy of the empty (rigid) space vehicle, the energy of the sloshing liquid propellants, and the energy associated with the vehicle structural deflections.

The translational velocity  $v$  and the angular velocity  $\omega$  of a point on the vehicle are the sum of translation, rotation, and bending displacements. They are given by:

$$v = \dot{y} - x\dot{\phi} + \dot{\eta}Y_v \quad \omega = \dot{\phi} - \dot{\eta}Y'_v \quad (7.2)$$

where superscript dots indicate differentiation with respect to time and superscript primes indicate differentiation with respect to  $x$ . These expressions have been linearized with respect to  $y, \phi$ , and  $\eta$ . The kinetic energy of the *empty vehicle* is thus:

$$KE_{ev} = \frac{1}{2} \int m_{ev} (\dot{y} - \dot{x}\phi + \dot{\eta}Y_v)^2 dx + \frac{1}{2} \int I_{ev} (\dot{\phi} - \dot{\eta}Y'_v)^2 dx \quad (7.3)$$

Here,  $m_{ev}$  is the mass of the empty vehicle per unit length and  $I_{ev}$  is the mass moment of inertia per unit length of the elemental segment  $dx$ . The integrations in Eq. (7.3) are performed over the entire length of the vehicle.

The kinetic energy of the *propellant* is obtained from a pendulum mechanical model. The sloshing masses move relative to the tank, so the kinetic energy of the liquid in the two propellant tanks is given by:

$$KE_l = \frac{1}{2} \sum_{j=1}^2 m_{0j} [\dot{y} - \dot{x}_{0j}\phi + \dot{\eta}Y_v(x_{0j})]^2 + \frac{1}{2} \sum_{j=1}^2 I_{0j} [\dot{\phi} - \dot{\eta}Y'_v(x_{0j})]^2 + \frac{1}{2} \sum_{j=1}^2 m_{sj} [\dot{y} - x_j\dot{\phi} + L_j\dot{\psi}_j + \dot{\eta}Y_v(x_j)]^2 \quad (7.4)$$

where  $x_{0j}$  is the location (relative to the loaded vehicle center of mass) of the  $j^{\text{th}}$  rigidly-attached mass  $m_{0j}$ ,  $x_j$  is the location of the pendulum hinge point for the  $j^{\text{th}}$  slosh mass  $m_{sj}$ ,  $L_j$  is the pendulum length for the  $j^{\text{th}}$  mode, and  $I_{0j}$  is the moment of inertia of the  $j^{\text{th}}$  rigid mass. The symbolism  $Y_v(x_{0j})$  indicates, as an example, that the bending deflection is evaluated at the  $x_{0j}$  location.

**Potential energies.** The potential energy is also composed of two parts, the empty vehicle and the propellant. The potential energy of the *empty vehicle* is itself composed of two parts, the elastic energy of deformation of the bending mode and the work done in raising the vehicle in the gravitational field. The elastic part of the structural potential energy is:

$$PE_{ev1} = \frac{1}{2} \int \eta^2 \frac{M^2}{EI} dx + \frac{1}{2} \int \eta^2 \frac{Q^2}{A_{sh}G} dx = \frac{1}{2} \omega_v^2 \eta^2 \left[ \int m_{ev} Y_v^2 dx + \int I_{ev} Y'_v dx \right] \quad (7.5a)$$

$M$  is the bending moment and  $Q$  the shear force acting on an elemental cross section;  $EI$  is the flexural stiffness,  $G$  is the shear modulus, and  $A_{sh}$  is the shear area of the cross section. The second form of the potential energy shown in Eq. (7.5a) involves the bending frequency  $\omega_v$ , available from a lateral bending analysis (likely, a finite element elastic computer code). With this form, the potential energy can be written compactly as:

$$PE_{ev1} = \frac{1}{2} \omega_v^2 \eta^2 M_B \quad (7.5b)$$

where  $M_B$  is the generalized bending mass of the vehicle structure, which is also available from the lateral bending analysis. The gravitational part of the empty vehicle potential energy is given by:

$$PE_{ev2} = \frac{1}{2} M_s g x_v \phi^2 \quad (7.5c)$$

where  $x_v$  is the coordinate of the center of mass of the empty vehicle.

The potential energy of the slosh is likewise composed of elastic-like energy stored in the pendulums and gravitational energy. The total potential energy is:

$$PE_l = \frac{1}{2} \sum_{j=1}^2 m_{sj} a L_j \psi_j^2 + g \phi^2 [m_{0j} x_{0j} + m_{sj} (x_j + L_j)] - \frac{1}{2} g \sum_{j=1}^2 m_{sj} L_j (\phi - \eta Y'_v) \quad (7.6)$$

where  $a$  is the vehicle acceleration along the flight path resulting from the thrust<sup>18</sup>.

**Energy dissipation functions.** Energy is dissipated by the damping of the structural bending motion and by the damping of the propellant motions.

Structural damping is generally considered to be proportional to the *amplitude* of the motion but in phase with the *velocity* of the motion. This conventional way of expressing structural damping leads to complex elements (i.e., terms with real and imaginary parts), that complicate the analysis considerably. Consequently, the damping is here assumed to be based on an equivalent viscous damping which is proportional to the amplitude of the bending mode velocity; this assumption is justified as long as the damping is small and only of importance when the excitation frequency is near the bending frequency. With this assumption, the dissipation function of the *empty vehicle* is:

$$D_{ev} = \frac{1}{2} \omega_v M_B \gamma_v \dot{\eta}^2 \quad (7.7)$$

Here,  $\gamma_v$  is the structural damping coefficient of the bending vibration, which generally has a value in the range of 0.001 to 0.05.

The dissipation function of the *propellant* motion is similarly:

$$D_l = \frac{1}{2} \sum_{j=1}^2 \gamma_{sj} \omega_j m_{sj} L_j^2 \dot{\psi}_j^2 = \frac{1}{2} \sum_{j=1}^2 \gamma_{sj} \left( \sqrt{\frac{a}{L_j}} \right) m_{sj} L_j^2 \dot{\psi}_j^2 \quad (7.8)$$

where  $\gamma_{sj}$  is the damping coefficient of the  $j^{\text{th}}$  slosh mode.

**Generalized forces.** The only external forces that act on the vehicle are the thrust forces:  $F_1$  which acts in the flight path direction, and  $F_2$  which is the part of the total thrust that can be swiveled and used for control; the total thrust is  $F = F_1 + F_2$  (which is not a vector sum). We have to compute how these forces act on the vehicle to cause an acceleration in each of the generalized coordinates.

The easiest way to do this is to compute the virtual work when each generalized force is given a virtual increment  $\delta q_i$ . The virtual work is defined as:

$$\delta W = \sum Q_i \delta q_i \quad (7.9)$$

Figure 7.2 shows the thrust forces. The stationary part of the force  $F_1$  acts along the tank axis, but the axis itself is deflected as a result of the elastic bending motion. The swiveled part of the force  $F_2$  is oriented at an angle  $\beta$  with respect to the thrust. The figure also shows the component of each

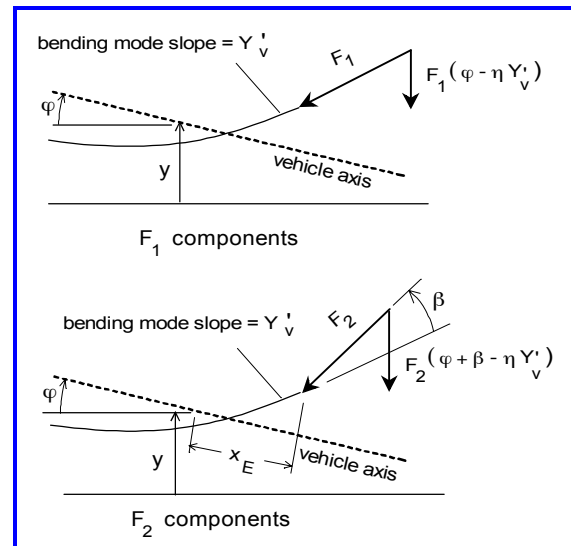


Figure 7.2. Generalized forces from thrust

<sup>18</sup> The elastic energy is easier to understand for a spring-mass model. The energy stored in a spring is  $0.5k_s(y_j)^2$  where  $y_j$  is the spring-mass deflection. But the spring constant  $k_s = m_j(\omega_j)^2$  and  $\omega_j = (a/L_j)^{0.5}$  for a pendulum; since  $y_j = L\psi_j$ , the pendulum elastic energy is  $0.5m_j g L (\psi_j)^2$ .

force that is aligned with the  $y$  motion of the vehicle center of mass.

The virtual work done by a virtual  $\delta y$  displacement is computed with the help of the relations shown in the figure; it is:

$$\begin{aligned}\delta W_y &= F_1 [\varphi - \eta Y'_v(x_E)] \delta y + F_2 [\varphi + \beta - \eta Y'_v(x_E)] \delta y \\ &= F [\varphi - \eta Y'_v(x_E)] \delta y + F_2 \beta \delta y\end{aligned}\quad (7.10a)$$

where  $x_E$  is the coordinate of the swivel point. Comparing this expression to Eq. (7.9) shows that the generalized force  $Q_y$  for the  $y$  displacement is:

$$Q_y = F [\varphi - \eta Y'_v(x_E)] + F_2 \beta \quad (7.10b)$$

The virtual work done by a virtual rotation  $\delta \varphi$  about the center of mass of the vehicle is computed similarly:

$$\begin{aligned}\delta W_\varphi &= \{x_E F_1 \eta Y'_v(x_E) - F_1 \eta Y_v(x_E)\} \delta \varphi - \{x_E F_2 [\beta - \eta Y'_v(x_E)] - F_2 \eta Y_v(x_E)\} \delta \varphi \\ &= F [x_E \eta Y'_v(x_E) - \eta Y_v(x_E)] \delta \varphi - (F_2 x_E \beta) \delta \varphi\end{aligned}\quad (7.11a)$$

(Because we are taking moments about the vehicle axis, there are no terms included in the work that depend on  $\varphi$ .) The generalized force  $Q_\varphi$  for the  $\varphi$  rotation is therefore:

$$Q_\varphi = F [x_E \eta Y'_v(x_E) - \eta Y_v(x_E)] - F_2 x_E \beta \quad (7.12b)$$

The virtual work done by a virtual bending displacement  $\delta \eta$  is found similarly. Since the thrust force is perpendicular to the bending motion, only the part of  $F_2$  that is proportional to the swivel angle does work. The generalized force is found to be:

$$Q_\eta = F_2 \beta Y_v(x_E) \quad (7.13)$$

The generalized force of the thrust with respect to the sloshing displacement is zero; that is,  $Q_\psi = 0$  for all  $\psi_j$ . Other external forces could also be considered if needed, such as aerodynamic forces from wind gusts.

**Generalized masses.** The vehicle mass  $m$ , moment of inertia  $I$ , and center of mass location, and the linear and angular momentum of the structural vibration have to satisfy the following definitions and constraints:

$$m = \int m_{ev} dx + \sum_{j=1}^2 (m_{0j} + m_{Sj}) \quad (7.14a)$$

$$I = \int (x^2 m_{ev} + I_{ev}) dx + \sum_{j=1}^2 [I_{0j} + x_{0j}^2 m_{0j} + (x_j + L_j)^2 m_{Sj}] \quad (7.14b)$$

$$\int x m_{ev} dx + \sum_{j=1}^2 [x_{0j} m_{0j} + (x_j + L_j) m_{Sj}] = 0 \quad (7.14c)$$

$$\int m_{ev} Y_v dx + \sum_{j=1}^2 [m_{0j} Y_v(x_{0j}) + m_{Sj} Y_v(x_j + L_j)] = 0 \quad (7.14d)$$

$$\sum_{j=1}^2 [x_{0j}m_{0j}Y_v(x_{0j}) + (x_j + L_j)m_{Sj}Y_v(x_j + L_j) + I_{0j}Y_v'(x_{0j})] + \int (xm_{ev}Y_v + I_{ev}Y_v')dx = 0 \quad (7.14e)$$

where the integrations are to be performed over the total vehicle length. Equation (7.14c) is the definition of the center of mass, and Eqs. (7.14d) and (7.14e) represent conservation of linear and angular momentum for the bending mode.

### Control law

The control system produces an angular deflection  $\beta$  of the swivel engine in accordance with signals sensed by accelerometers and gyroscopes mounted on the booster. The control equations cannot always be expressed as linear equations in terms of the translation and rotations sensed by these instruments, because nonlinear effects can be introduced from amplifier saturations, limited force and torque outputs of the devices that swivel the engine, and so forth. But in the spirit of this simplified treatment, the control equations are linearized nonetheless; this is acceptable when the control frequencies and the translation and rotation frequencies are small.

For this example, we will assume that a gyroscope is mounted at a location  $x_G$  on the vehicle axis and that it produces an angular signal  $\varphi_G$  proportional to the angular deflection at that point:

$$\varphi_G = \varphi - \eta Y_v'(x_G) \quad (7.15)$$

The time derivative of  $\varphi_G$  is available when needed from a differentiating network.

We will assume that the natural frequency of the control accelerometer is much higher than either the control frequency or the frequencies of the vehicle translation and rotation. The acceleration sensed by the accelerometer is then equal to the acceleration at the sensor:

$$A_A = \ddot{y} - x_A\ddot{\varphi} - g\varphi + \ddot{\eta}Y_v(x_A) + g\eta Y_v'(x_A) \quad (7.16)$$

where  $x_A$  is the location of the accelerometer relative to the center of mass.

A simple control law is assumed that relates the commanded swivel angle to the accelerometer and gyro signals:

$$\beta = a_0\varphi_G + a_1\dot{\varphi}_G + a_2A_A \quad (7.17)$$

This law and the equations of the gyro and the accelerometer are considerably simplified compared to actual control schemes used in practice [BAUER, 1963a; BLAKELOCK, 1991; SALL, 1997]. It is common, for example, to use a *rate* gyroscope that gives an output signal that is proportional to the angular velocity, and sometimes the damping of the accelerometer is important. Furthermore, the control law generally includes phase-lag coefficients to improve stability (i.e., the time derivatives of  $\beta$  are also controlled).

### Equations of motion

We can now derive the equations of motion of the vehicle from Eq. (7.1) by using the expressions for kinetic energy, potential energy, energy dissipation, and generalized force, and then simplifying by introducing the generalized mass relations, Eqs. (6.19).

**Translation.** The equation of motion for the translation of the vehicle center of mass is:

$$M\ddot{y} + \sum_{j=1}^2 m_{Sj} L_j \ddot{\Psi} = F\phi + F_2\beta - F\eta Y'_v(x_E) \quad (7.18)$$

**Pitching.** The equation of motion for the pitching of the vehicle about the center of mass is given by:

$$I\ddot{\phi} + \sum_{j=1}^2 (x_j + L_j) m_{Sj} L_j \ddot{\Psi}_j - g \sum_{j=1}^2 m_{Sj} \ddot{\Psi}_j = -x_E F_2 \beta + F [x_E \eta Y'_v(x_E) - \eta Y_v(x_E)] \quad (7.19)$$

**Propellant.** The equations of motion for the moving propellants is given by:

$$L_j \ddot{\Psi}_j + 2\gamma_j \sqrt{\frac{a}{L_j}} L_j \dot{\Psi}_j + \frac{a}{L_j} \Psi_j = -[\ddot{y} - (x_j + L_j) \ddot{\phi} + \ddot{\eta} Y_v(x_j + L_j)] + g[\phi - \eta Y'_v(x_j + L_j)] \quad j=1, 2 \quad (7.20)$$

**Bending.** The equation of motion for the structural bending vibration is:

$$M_B \ddot{\eta} + M_B g_v \omega_v \dot{\eta} + M_B \omega_v^2 \eta = F_2 Y_v(x_E) \beta - g \sum_{j=1}^2 m_{Pj} Y'_v(x_j + L_j) L_j \dot{\Psi}_j - \sum_{j=1}^2 m_{Sj} Y_v(x_j + L_j) L_j \ddot{\Psi}_j \quad (7.21)$$

where the generalized mass  $M_B$  of the bending vibration is given by:

$$M_B = \int [m_{ev} Y_v^2 + I_{ev} Y_v'^2] dx + \sum_{j=1}^2 [m_{0j} Y_v^2(x_{0j}) + I_{0j} Y_v'^2(x_{0j})] + m_{Sj} Y_v^2(x_j + L_j)$$

The solution of the equations of motion, Eqs. (7.18) – (7.21), and the control law, Eqs. (7.15) – (7.17), have to be investigated to determine whether the vehicle flight is stable and, if not, what must be done to make it stable.

## 7.2 Stability Analysis

Since all the equations of motion and the control law are linear with respect to the generalized coordinates, the solution obtained from the equations for each of the variables  $y$ ,  $\phi$ ,  $\eta$ ,  $\Psi_1$ , and  $\Psi_2$  is of the form  $\exp(st)$  where  $t$  is time and the frequency parameter  $s$  can have real and imaginary parts:  $s = \lambda + i\omega$ . If the real part of  $s$  is negative, any perturbations to the vehicle flight path caused by a gust of wind or a programmed change in the path will decay in time, and the flight path will be stable. Thus, the stability analysis reduces to determining the conditions for which  $\lambda$  is negative.

### Characteristic equation

When the assumed solution  $\exp(st)$  is substituted into the equations of motion, each equation reduces to an algebraic equation in the unknown complex frequency  $s$ . For example, the translation equation of motion, Eq. (7.18), becomes:

$$m y_0 s^2 + \sum_{j=1}^2 m_{Pj} L_j \psi_{0j} s^2 = F \phi_0 + F_2 \beta_0 - F Y'_v(x_E) \eta_0$$

where  $y_0$  is the amplitude of the translation motion,  $\psi_{0j}$  is the amplitude of the slosh mass motion, and so on. Although this equation does not contain a complex term, other equations of motion that include a first time derivative of a motion variable, such as Eq. (7.20), would result in complex (real and imaginary) terms.

All but one of the motion variables, say  $\phi_0$ , can be eliminated by combining the algebraic equations. This elimination process gives a single equation:

$$\left( \sum_{n=1}^N \alpha_n s^n \right) \phi_0 = 0 \tag{7.22}$$

where the total number of terms  $N$  is determined by the product of the number of equations and the highest time derivative in any equation. The  $\alpha_n$  are products and sums of products of the coefficients in the equations. The function inside the parenthesis is the *characteristic equation* of the motion. Since  $\phi_0$  is not zero in general, the characteristic equation must itself be zero. The values of  $s$  that make the characteristic equation zero are the roots or *zeroes* of the equation.

Optimization of the vehicle response is based upon the possibility of shifting these stability roots in the complex plane (the *root locus plane*) in such a fashion that they exhibit a larger negative real part. Figure 7.3 illustrates schematically how one root with a positive real part and one root with a negative real part move to more stable locations when a physical parameter of the system, such as an increase in the slosh damping, is changed. When the roots are all in the stable region, a disturbance to the vehicle flight is absorbed more rapidly. A convenient way to study the migration of the roots is by plotting them as continuous functions in this complex plane  $\lambda + i\omega$ . The effect of the change of any parameter can be obtained readily from these plots.

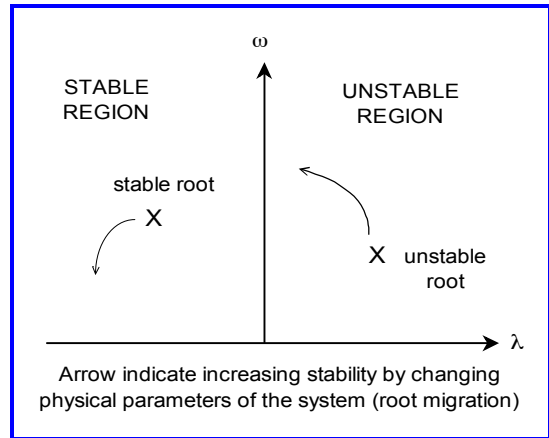


Figure 7.3. Root locus plane

For a real space vehicle, the characteristic equation is of a fairly high order; for the simple example given by Eqs. (7.15) – (7.21), the highest power  $N$  is eight, but more realistic cases would result in considerably higher powers. For a high order polynomial, the roots must generally be found by numerical means. For design purposes, it is usually sufficient to know whether the real parts of the roots are negative, thereby indicating stability, or positive. When a design parameter is considered as a variable, it is especially important to have a criterion for stability in terms of the roots. Criteria of this type are given by ROUTH [1877], HURWITZ [1895], and NYQUIST [1932], to mention a few classic examples. The Hurwitz method is fairly simple and will be illustrated here. Since the parameters depend on the total mass of the vehicle and the position of the center of mass,

the locations of the roots generally have to be found for the entire duration of the flight by solving the equations at a number of different times.

### Location of roots

A necessary and sufficient condition that all the roots of the characteristic equation

$$\sum_{n=1}^N \alpha_n s^n = 0 \quad (7.23)$$

have only negative real parts is that all the  $\alpha_n$  be positive and the values of all the determinants  $H_n$  be positive [HURWITZ, 1895]. The determinants  $H_n$  are defined as:

$$\begin{aligned} H_1 &= \alpha_1 \\ H_2 &= \begin{vmatrix} \alpha_1 & \alpha_3 \\ \alpha_0 & \alpha_2 \end{vmatrix} \\ H_3 &= \begin{vmatrix} \alpha_1 & \alpha_3 & \alpha_5 \\ \alpha_0 & \alpha_2 & \alpha_4 \\ 0 & \alpha_1 & \alpha_3 \end{vmatrix} \\ H_4 &= \begin{vmatrix} \alpha_1 & \alpha_3 & \alpha_5 & \alpha_7 \\ \alpha_0 & \alpha_2 & \alpha_4 & \alpha_6 \\ 0 & \alpha_1 & \alpha_3 & \alpha_5 \\ 0 & \alpha_0 & \alpha_2 & \alpha_4 \end{vmatrix} \end{aligned} \quad (7.24)$$

and so on up to  $H_N$ . Consequently, the flight stability of the vehicle can be adjusted by finding values for the  $\alpha_n$  (i.e., the coefficients in the differential equations) that give positive values for each and every  $H_n$ . How this is done is discussed in the next section.

## 7.3 Typical Conclusions of Stability Analyses

Many stability investigations have been conducted for large launch vehicles in which sloshing was a concern [for example, GEISLER, 1960; BAUER, 1961, 1963a, 1963b; HAYS AND SUMRALL, 1964]. Some conclusions from these studies are summarized below.

- The gyroscope should be located in a region where  $dY_v/dx > 0$ ; that is, it should be located behind the bending antinode.
- The accelerometer should be located forward of the instantaneous center of rotation and preferably forward of the center of mass.
- Additional slosh damping must be provided by the use of baffles for tanks in the aft portion of the vehicle because the stability boundary falls between the center of mass and the instantaneous center of rotation.

These conclusions have to be verified for each specific application because stability depends on a large number of factors, including control frequencies, slosh frequencies, amplifier gains, slosh and structural damping, etc. However, the guidelines do provide a starting point for such a more general investigation.

## 7.4 References

- BAUER, H., 1961, *Parametric Study of the Influence of Propellant Sloshing on the Stability of Space Crafts*, **J. Aerospace Sci.**, pp. 819-820.
- BAUER, H., 1963a, *Stability Boundaries of Liquid Propelled Space Vehicles with Sloshing*, **AIAA J.**, **1**, no. 7.
- BAUER, H., 1963b, *The Effects of Propellant Sloshing on the Stability of an Accelerometer Controlled Rigid Space Vehicle*, NASA TN D-1831.
- BLAKELOCK, J., 1991, **Automatic Control of Aircraft and Missiles**, Wiley-Interscience Publishers, New York.
- GEISSLER, E., 1960, *Problems in Attitude Stabilization of Large Guided Missiles*, **Aero-Space Engineering**, Oct., pp. 24-29.
- HAYS, P., AND SUMRALL, J., 1964, *Stability Analysis of SATURN SA-5 with Live S-IV Stage*, NASA TM X-53017.
- HURWITZ, A., 1895, *Über die Bedingungen unter welchen eine Gleichung nur Wurzeln mit negative reellen theilen besitzt*, **Mathematische Annalen**, **46**, pp. 273-284.
- NYQUIST, H., 1932, *Regeneration Theory*, **Bell System Technical Journal**, **11**, pp. 126-157.
- ROUTH, E., 1877, **A Treatise on the Stability of a Given Motion**, Macmillan Publishing Co., London.
- SALI, M., 1997, **Spacecraft Dynamics and Control: A Practical Engineering Approach**, Cambridge University Press, Cambridge.
- SYNGE, J., AND GRIFFITH, B., 1959, **Principles of Mechanics**, McGraw-Hill book Co., New York.

# NASA SP-106 REFERENCES BY CHAPTER

SP-106 was based on nearly all the relevant references in existence up through 1966. Not all of the references cited in SP-106 are cited in this revision. For the purposes of historical completeness, it is worthwhile to preserve the list of all the SP-106 references, even though many of them are company reports that are no longer easily available (some of the companies are no longer in existence!) and some of them are incomplete citations.

## 1. Introduction

by H. NORMAN ABRAMSON (SwRI)

- ABRAMSON, H. N., 1961, *Amazing Motions of Liquid Propellants*, **Astronautics**, **6**, pp. 35-37.
- ABRAMSON, H. N., 1961, *Liquid Dynamic Behavior in Rocket Propellant Tanks*, **Proc. ONR/AIA Symposium on Structural Dynamics of High Speed Flight**, pp. 287-318.
- ABRAMSON, H. N., 1963, *Dynamic Behavior of Liquids in Moving Containers*, **Applied Mechanics Reviews**, **16**, pp. 501-506.
- ABRAMSON, H. N., 1966, *Some Current Aspects of the Dynamic Behavior of Liquids in Rocket Propellant Tanks*, in **Applied Mechanics Surveys**, Spartan Books.
- ANON., 1961, *SATURN SA-1 Flight Evaluation*, NASA-MSFC Report MPR-SAT-WF-61-8.
- BARON, M. L., AND BLEICH, H., 1959, *The Dynamic Analysis of Empty and Partially Full Cylindrical Tanks. Part II – Analysis of Uplift and Structural Damage*, DASA Report 1123B.
- BISPLINGHOFF, R. L., AND MICHEL, D., 1963, *Some Structural Dynamic Problems of Space Vehicles*, **Japan Society of Aeronautical and Space Sciences**.
- BLAGOVESHCHENSKY, S. N., 1962, **Theory of Ship Motions**, Dover Books.
- CLOUGH, R. W., 1960, *Effects of Earthquakes on underwater Structures*, **Proc. Second World Conf. On Earthquake Engineering**, pp. 815-831.
- COOPER, R. M., 1960, *Dynamics of Liquids in Moving Containers*, **ARS J.**, **30**, pp. 725-729.
- GEISSLER, E. D., 1960, *Problems of Attitude Stabilization of Large Guided Missiles*, **Aerospace Engineering**, **19**, pp. 24-29 and 68-71.
- GLUCK, D. F., AND GILLE, J. P., 1965, *Fluid Mechanics of Zero-G Propellant Transfer in Spacecraft Propulsion Systems*, **Trans. ASME, J. Engineering for Industry**, pp. 1-7.
- GOLDSBOROUGH, G. R., 1930, *The Tidal Oscillations in an Elliptic Basin of Variable Depth*, **Proc. Royal Soc. (London)**, **A, 130**, pp. 157-167.
- GRAHAM, E. W., AND RODRIGUEZ, A. M., 1952, *The Characteristics of Fuel Motion Which Affect Airplane Dynamics*, **Trans, ASME, J. Applied Mechanics**, **19**, pp. 381-388.
- HOUSNER, G. W., *Dynamic Pressures on Accelerated Fluid Containers*, **Bull. Seis. Soc. Am.**, **47**, pp. 15-35.
- JACOBSEN, L. S., AND AYRE, R. S., 1951, *Hydrodynamic Experiments with Rigid Cylindrical Tanks Subjected to Seismic Motions*, **Bull. Seism. Soc. Am.**, **41**, pp. 313-346.
- LAMB, H., 1945, **Hydrodynamics**, 6th ed., Dover Books.
- MILES, J. W., 1959, *Free Surface Oscillations in a Rotating Liquid*, **Physics of Fluids**, **2**, pp. 297-305.
- MOISEYEV, N. N., MYSHKIS, A. D., AND PETROV, A. A., 1964, *On the Problems of Hydrodynamics in Cosmonautics*, **XVth International Astronautical Congress**.
- PENNEY, E. G., AND PRICE, A. T., 1952, *Some Gravity Wave Problems in the Motion of Perfect Fluids. Part II. Finite Periodic Stationary Gravity Waves in a Perfect Fluid*, **Phil. Trans. Royal Soc. (London)**, **A, 254**, pp. 254ff.
- SCOTT, W. E., *The Free Flight Stability of a Liquid Filled Spinning Shell*, BRL Reports 1120, 1135, and 1233.
- SEWALL, J. L., 1957, *An Experimental and Theoretical Study of the Effect of Fuel on Pitching-Translation Flutter*, NACA TN 4166.
- SLOANE, M. N., 1960, *The Dynamics of the Sloshing Phenomenon (a Literature Survey)*, Space Technology Laboratories Report GM-60-5111-5.

- STEWARTSON, K., 1959, *On the Stability of a Spinning Top Containing Liquid*, **J. Fluid Mechanics**, **5**, part 4.
- VANONI, V. A., AND CARR, J. H., 1951, *Harbor Surging*, **Proc. First Conf. On Coastal Engineering**, pp. 60-68.
- VASTA, J., GIDDINGS, A. J., TAPLIN, A., AND STILLWELL, J. J., 1961, *Roll Stabilization by Means of Passive Tanks*, **Trans. SNAME**, **69**, pp. 411-460.
- WERNER, P. W., AND SUNDQUIST, K. J., 1949, *Impulsive Hydrodynamics of Fluid Inside a Cylindrical Tank and of Fluid Surrounding a Cylindrical Pier*, **Bull. Seism. Soc. Am.**, **39**, pp. 189-204.
- WESTERGAARD, H. M., 1933, *Water Pressure on Dams During Earthquakes*, **Trans. ASCE**, **98**, pp. 189-204.
- WINCH, D. M., 1962, *An Investigation of the Liquid level at the Wall of a Spinning Tank*, NASA TN D-1536.

## 2. Lateral Sloshing in Moving Containers

by SANDOR SILVERMAN (SwRI) AND H. NORMAN ABRAMSON (SwRI)

- ABRAMSON, H. N., AND RANSLEBEN, G. E., Jr., 1960, *Simulation of Fuel Sloshing Characteristics in Missile Tanks by Use of Small Models*, **ARS J.**, **30**, pp. 503-612.
- ABRAMSON, H. N., AND RANSLEBEN, G. E., Jr., 1961, *Liquid Sloshing in Rigid Cylindrical Tanks Undergoing Pitching Motion*, SwRI Report 11, Contract DA-23-072-ORD-1251.
- ABRAMSON, H. N., AND RANSLEBEN, G. E., Jr., 1961, *Some Comparisons of Sloshing Behavior in Cylindrical Tanks with Flat and Conical Bottoms*, **ARS J.**, **31**, pp. 542-544.
- ABRAMSON, H. N., AND RANSLEBEN, G. E., Jr., 1961, *Wall Pressure Distributions During Sloshing in Rigid Tanks*, **ARS J.**, **31**, pp. 545-547.
- ABRAMSON, H. N., GARZA, L. R., AND KANA, D. D., 1962, *Liquid Sloshing in Compartmented Cylindrical Tank*, **ARS J.**, **32**, pp. 978-980.
- ABRAMSON, H. N., CHU, W.-H., AND GARZA, L. R., 1962, *Liquid Sloshing in a 45° Sector Compartmented Cylindrical Tanks*, SwRI Report No. 3, Contract NAS8-1555.
- ABRAMSON, H. N., CHU, W.-H., AND GARZA, L. R., 1962, *Liquid Sloshing in Spherical Tanks*, SwRI Report 2, Contract NAS8-1555.
- ABRAMSON, H. N., CHU, W.-H., AND GARZA, L. R., 1963, *Liquid Sloshing in Spherical Tanks*, **AIAA J.**, **1**, pp. 384-389.
- ABRAMSON, H. N., 1963, *Dynamic Behavior of Liquids in Moving Containers*, **Applied Mechanics Reviews**, **16**, pp. 501-506.
- ABRAMSON, H. N., AND GARZA, L. R., 1965, *Some Measurements of Liquid Frequencies and Damping in Compartmented Cylindrical Tanks*, **AIAA J. Spacecraft and Rockets**, **2**, pp. 453-455.
- ARMSTRONG, G. L., AND KACHIGAN, K., 1961, *Propellant Sloshing*, **Handbook of Astronautical Engineering**, pp. 14-14 to 14-27.
- BAUER, H. F., 1958, *Fluid Oscillations in a Circular Cylindrical Tank*, ABMA Report DA-TR-1-58.
- BAUER, H. F., 1958, *Fluid Oscillations of a Circular Cylindrical Tank Performing Lissajous Oscillations*, ABMA Report DA TR-2-58.
- BAUER, H. F., 1960, *Theory of the Fluid Oscillations in a Circular Cylindrical Tank Partially Filled with Liquid*, NASA TN D-557.
- BAUER, H. F., 1962, *Theory of Fluid Oscillations in Partially Filled Cylindrical Containers*, NASA-MSFC Report MTP-AERO-62-1.
- BAUER, H. F., 1962, *Theory of Liquid Sloshing in Compartmented Cylindrical Tanks due to Bending Excitation*, NASA-MSFC Report MTP-AERO-62-61.
- BAUER, H. F., 1963, *Liquid Sloshing in a Cylindrical Quarter Tank*, **AIAA J.**, **1**, pp. 2601-2606.
- BAUER, H. F., 1963, *Tables and Graphs of Zeros of Cross Product Bessel Functions*, NASA-MSFC Report MTP-AERO-63-50.
- BAUER, H. F., 1963, *Theory of Liquid Sloshing in Compartmented Cylindrical Tanks due to Bending Excitation*, **AIAA J.**, **1**, pp. 1590-1596.
- BAUER, H. F., 1964, *Fluid Oscillations in the Containers of a Space Vehicle and Their Influence Upon Stability*, NASA TR R-187.

- BAUER, H. F., 1964, *Theory of Liquid Sloshing in a 45° Sector Compartmented Cylindrical Tank*, **AIAA J.**, **2**, pp. 768-770.
- BUDIANSKY, B., 1960, *Sloshing of Liquids in Circular Canals and Spherical Tanks*, **J. Aerospace Sciences**, **27**, pp. 161-173.
- CHU, W. H., 1960, *Sloshing of Liquids in Cylindrical Tanks of Elliptical Cross Section*, **ARS J.**, **30**, pp. 360-363.
- CHU, W.-H., 1960, *Free Surface Condition for Sloshing Resulting from Pitching and Some Corrections*, **ARS J.**, **11**, pp. 1090-1094.
- CHU, W.-H., 1964, *Fuel Sloshing in a Spherical Tank Filled to an Arbitrary Depth*, **AIAA J.**, **2**, pp. 1972-1979.
- COOPER, R. M., 1960, *Dynamics of Liquids in Moving Containers*, **ARS J.**, **30**, pp. 725-729.
- DOKUCHAEV, L. V., 1964, *On the Solution of a Boundary Value Problem on the Sloshing of a Liquid in Conical Cavities*, **PMM**, **28**, pp. 151-154.
- EHRlich, L. W., RILEY, J. D., STRANGE, W. G., and TROESCH, B. A., 1961, *Finite-Difference Techniques for a Boundary Problem with an Eigenvalue in a Boundary Condition*, **J. Soc. Indust. Appl. Math.**, **9**, pp. 141-164.
- EIDE, D. G., 1964, *Preliminary Analysis of Variation of Pitch Motion in a Vehicle in a Space Environment due to Fuel Sloshing in a Rectangular Tank*, NASA TN D-2336.
- EULITZ, W. R., 1961, *Analysis and Control of Liquid Propellant Sloshing During Missile Flight*, NASA-MSFC Report VE-P-61-22.
- EULITZ, W. R., 1963, *Practical Consequences of Liquid Propellant SLOSH Characteristics Derived by Nomographic Methods*, NASA-MSFC Report VE-P-63-7.
- GRAHAM, E. W., AND RODRIGUEZ, A. M., 1951, *The Characteristics of Fuel Motion Which Affect Airplane Dynamics*, Douglas Aircraft Co. Report SM-14212.
- GRAHAM, E. W., AND RODRIGUEZ, A. M., 1952, *The Characteristics of Fuel Motion Which Affect Airplane Dynamics*, **Trans. ASME, J. Applied Mechanics**, **19**, pp. 381-388.
- KACHIGAN, K., 1955, *Forced Oscillations of a Fluid in a Cylindrical Tank*, Convair Astronautics Report ZU-7-046.
- LAMB, H., 1945, **Hydrodynamics**, 6th ed., Dover Books.
- LAWRENCE, H. R., WANG, C. J., AND REDDY, R. B., 1958, *Variational Solution of Fuel Sloshing Modes*, **Jet Propulsion**, **28**, pp. 729-736.
- LEONARD, H. W., AND WALTON, W. C., Jr., 1961, *An Investigation of the Natural Frequencies and Mode Shapes of Liquids in Oblate Spheroidal Tanks*, NASA TN D-904.
- LEVIN, E., 1963., *Oscillations of a Fluid in a Rectilinear Conical Container*, **AIAA J.**, **1**, p. 1447.
- LOMEN, D. O., 1965, *Digital Analysis of Liquid Propellant Sloshing in Mobile Tanks with Rotational Symmetry*, NASA CR-230.
- LOMEN, D. O., 1965, *Liquid Propellant Sloshing in Mobile Tanks with Rotational Symmetry*, NASA CR-222.
- MCCARTY, J. L., LEONARD, H. W., AND WALTON, W. C., Jr., 1960, *Experimental Investigation of the Natural Frequencies of Liquids in Toroidal Tanks*, NASA TN D-531.
- MCCARTY, J. L., AND STEPHENS, D. G., 1960, *Investigation of the Natural Frequencies of Fluids in Spherical and Cylindrical Tanks*, NASA TN D-252.
- MIKISHEV, G. N., AND DOROZHKIN, N. YA., 1961, *An Experimental Investigation of Free Oscillations of a Liquid in Containers*, **Izv. Akad. Nauk SSSR, Otd. Tekh. Nauk, Mekh. i Mashinostr.**, **4**, pp. 48-53.
- MILES, J. W., 1956, *On the Sloshing of Liquid in a Cylindrical Tank*, Ramo-Wooldridge Co. Report AM6-5.
- OKHOTSMKII, D. E., 1960, *Theory of the Motion of a Body with Cavities Filled with a Liquid*, NASA TT F-33.
- RATTAYA, J. V., 1965, *Sloshing of Liquids in Axisymmetric Ellipsoidal Tanks*, AIAA Paper 65-114.
- RAYLEIGH, J. W. S., 1945, **The Theory of Sound. Vol. II**, Dover Books.
- RILEY, J. D., AND TREMBATH, N. W., 1961, *Sloshing of Liquids in Spherical Tanks*, **J. Aerospace Sciences**, **28**, pp. 245-246.
- ROBERTS, J. R., BASURTO, E. R., AND CHEN, P. Y., 1966, *SLOSH Design Handbook I.*, NASA CR-406.

- SCHMITT, A. F., 1956, *Forced Oscillations of a Fluid in a Cylindrical Tank Undergoing both Translation and Rotation*, Convair Report ZU-7-069.
- STEPHENS, D. G., AND LEONARD, H. W., 1963, *The Coupled Dynamic Response of a Tank Partially Filled with a Liquid and Undergoing Free and Forced Planar Oscillations*, NASA TN D-1945.
- STOFAN, A. J., AND ARMSTEAD, A. L., 1962, *Analytical and Experimental Investigation of Forces and Frequencies Resulting from Liquid Sloshing in a Spherical Tank*, NASA TN D-1281.
- STOKER, J. J., 1957, **Water Waves**, Interscience Publishers.
- SUMNER, I. E., 1963, *Preliminary Experimental Investigation of Frequencies and Forces Resulting from Liquid Sloshing in Toroidal Tanks*, NASA TN D-1709.
- SUMNER, I. E., AND STOFAN, A. J., 1963, *An Experimental Investigation of the Viscous Damping of Liquid Sloshing in Spherical Tanks*, NASA TN D-1991.
- TROESCH, B. A., 1960, *Free Oscillations of a Fluid in a Container*, in **Boundary Problems in Differential Equations**, Univ. of Wisconsin Press.

### 3. Nonlinear Effects in Lateral Sloshing

by H. N. ABRAMSON (SwRI), WEN-HWA CHU (SwRI), AND FRANKLIN T. DODGE (SwRI)

- ABRAMSON, H. N., 1961, *Nonlinear Vibrations*, **Handbook of Shock and Vibration Control, Chapter 4**.
- ABRAMSON, H. N., CHU, W.-H., AND GARZA, L. R., 1962, *Liquid Sloshing in a 45° Sector Compartmented Cylindrical Tanks*, SwRI Report No. 3, Contract NAS8-1555.
- ABRAMSON, H. N., CHU, W.-H., GARZA, L. R., AND RANSLEBEN, G. E., Jr., 1962, *Some Studies of Liquid Rotation and Vortexing in Rocket Propellant Tanks*, NASA TN D-1212.
- ABRAMSON, H. N., CHU, W.-H., AND GARZA, L. R., 1963, *Liquid Sloshing in Spherical Tanks*, **AIAA J.**, **1**, pp. 384-389.
- ABRAMSON, H. N., AND GARZA, L. R., 1965, *Some Measurements of Liquid Frequencies and Damping in Compartmented Cylindrical Tanks*, **AIAA J. Spacecraft and Rockets**, **2**, pp. 453-455.
- ABRAMSON, H. N., CHU, W.-H., AND KANA, D. D., 1966, *Some Studies of Nonlinear Lateral Sloshing in Rigid Containers*, **Trans. ASME, J. Applied Mechanics**, **33**.
- BAUER, H. F., 1964, *Nonlinear Propellant Sloshing in a Rectangular Container of Infinite Length*, North American Aviation Co. Report SID 64-1593.
- BERLOT, R. R., 1959, *Production of Rotation in a Confined Liquid Through Translational Motion of the Boundaries*, **Trans. ASME, J. Applied Mechanics**, **26**, pp. 513-516.
- CHU, W.-H., 1964, *Fuel Sloshing in a Spherical Tank Filled to an Arbitrary Depth*, **AIAA J.**, **2**, pp. 1972-1979.
- DALZELL, J. F., CHU, W.-H., AND MODISETTE, J. E., 1964, *Studies of Ship Roll Stabilization Tanks*, SwRI Report No. 1, Contract NONR 3926 (00).
- FULTZ, D., 1962, *An Experimental Note on Finite Amplitude Standing Gravity Waves*, **J. Fluid Mechanics**, **13**, pp. 192-213.
- GAILLARD, P., 1963, *Theoretical and Experimental Research of Nonlinear Oscillations of Liquids in Containers and Channels of Constant Depth*, Publ. Sci. Tech. Minist. L'Air (France), No. 412.
- HUTTON, R. E., 1963, *An Investigation of Resonant, Nonlinear Nonplanar Free Surface Oscillations*, NASA TN D-1870.
- HUTTON, R. E., 1964, *Fluid Particle Motion During Rotary Sloshing*, **Trans. ASME, J. Applied Mechanics**, **31**, pp. 123-130.
- MILES, J. W., 1962, *Stability of Forced Oscillations of a Spherical Pendulum*, **Quart. Appl. Math.**, **20**, pp. 21-32.
- MOISEYEV, N. N., 1958, *On the Theory of Nonlinear Vibrations of a Liquid of Finite Volume*, **Appl. Math. Mech.**, **22**, pp. 860-870.
- NARIMANOV, G. S., 1957, *Concerning the Motion of a Container Partially Filled with a Liquid Taking into Account Large Motions of the Latter*, **Appl. Math. Mech.**, **21**.

- PENNEY, E. G., AND PRICE, A. T., 1952, *Some Gravity Wave Problems in the Motion of Perfect Fluids. Part II. Finite Periodic Stationary Gravity Waves in a Perfect Fluid*, **Phil. Trans. Royal Soc. (London)**, **A**, **254**, pp. 254ff.
- ROGGE, T. R., AND WEISS, H. J., 1965, *An Approximate Nonlinear Analysis of the Stability of Sloshing Modes Under Translational and Rotational Excitation*, NASA CR-220.
- STOKER, J. J., 1950, **Nonlinear Vibrations**, Interscience Publishers, 3rd Printing.
- TADJIBAKSHI, I., AND KELLER, J. B., 1960, *Standing Waves of Finite Amplitude*, **J. Fluid Mechanics**, **8**, pp. 443-451.
- TAYLOR, G. I., 1952, *An Experimental Study of Standing Waves*, **Proc. Royal Soc. (London)**, **A218**, pp. 44-59.
- VERMA, G. R., AND KELLER, J. B., 1962, *Three Dimensional Standing Surface Waves of Finite Amplitude*, **Phys. Fluids**, **5**, pp. 52-56.
- WEISS, H. J., AND ROGGE, T. R., 1965, *A Nonlinear Analysis for Sloshing Forces and Moments on a Cylindrical Tank*, NASA TN D-221.

#### 4. Damping of Liquid Motions and Lateral Sloshing

by SANDOR SILVERMAN (SwRI) AND H. NORMAN ABRAMSON (SwRI)

- ABRAMSON, H. N., AND RANSLEBEN, G. E., Jr., 1960, *Simulation of Fuel Sloshing Characteristics in Missile Tanks by Use of Small Models*, **ARS J.**, **30**, pp. 503-612.
- ABRAMSON, H. N., AND RANSLEBEN, G. E., Jr., 1961, *Some Studies of a Floating Lid Type Device for Suppression of Liquid Sloshing in Rigid Cylindrical Tanks*, SwRI Report No. 10, Contract DA-23-072-ORD-1251.
- ABRAMSON, H. N., AND RANSLEBEN, G. E., Jr., 1961, *Liquid Sloshing in Rigid Cylindrical Tanks Undergoing Pitching Motion*, SwRI Report No. 11, Contract DA-23-072-ORD-1251.
- ABRAMSON, H. N., CHU, W.-H., AND GARZA, L. R., 1962, *Liquid Sloshing in a 45° Sector Compartmented Cylindrical Tanks*, SwRI Report No. 3, Contract NAS8-1555.
- ABRAMSON, H. N., GARZA, L. R., AND KANA, D. D., 1962, *Liquid Sloshing in Compartmented Cylindrical Tanks*, **ARS J.**, **32**, pp. 978-980.
- ABRAMSON, H. N., CHU, W.-H., AND GARZA, L. R., 1963, *Liquid Sloshing in Spherical Tanks*, **AIAA J.**, **1**, pp. 384-389.
- ABRAMSON, H. N., AND GARZA, L. R., 1964, *Some Measurements of the Effects of Ring Baffles in Cylindrical Tanks*, **AIAA J. Spacecraft and Rockets**, **1**, pp. 560-562.
- ABRAMSON, H. N., AND GARZA, L. R., 1965, *Some Measurements of Liquid Frequencies and Damping in Compartmented Cylindrical Tanks*, **AIAA J. Spacecraft and Rockets**, **2**, pp. 453-455.
- ARMSTRONG, G. L., AND KACHIGAN, K., 1961, *Stability and Control*, **Handbook of Astronautical Engineering, Chapter 14**.
- BAUER, H. F., 1962, *The Damping Factor Provided by Flat Annular Ring Baffles for Free Fluid Surface Oscillations*, NASA-MSFC Report MTP-AERO-62-81.
- BAUER, H. F., 1964, *Fluid Oscillations in the Containers of a Space Vehicle and Their Influence Upon Stability*, NASA TR R-187.
- BISHOP, R. E. D., AND GLADWELL, G. M. L., 1963, *An Investigation into the Theory of Resonance Testing*, **Phil. Trans. Royal Soc. (London)**, **255A**, pp. 241-280.
- CASE, K. M., AND PARKINSON, W. C., 1957, *Damping of Surface Waves in an Incompressible Liquid*, **J. Fluid Mechanics**, **2**, pp. 172-184.
- COLE, H. A., AND GAMBUCCI, B. J., 1961, *Measured Two-Dimensional Damping Effectiveness of Fuel Sloshing Baffles Applied to Ring Baffles in Cylindrical Tanks*, NASA TN D-694.
- COLE, H. A., AND GAMBUCCI, B. J., 1961, *Tests of an Asymmetrical Baffle for Fuel-Sloshing Suppression*, NASA TN D-1036.
- EULITZ, W., 1958, *A Can-type Device Derived from Basic Slosh Studies*, ABMA Report DSD-TR-4-58.
- GARZA, L. R., 1963, *A Brief Comparison of Ring and Asymmetrical Baffle Characteristics*, NASA CR-51373.

- GARZA, L. R., 1964, *Measurements of Liquid Natural Frequencies and Damping in Compartmented Cylindrical Tanks*, SwRI Report No. 8, Contract NAS8-1555.
- GARZA, L. R., 1966, *Theoretical and Experimental Pressures and Forces on a Ring Baffle Under Sloshing Conditions*, **AIAA J. Spacecraft and Rockets**, **3**, pp. 276-278.
- GAUZY, H., *Measurement of Inertia and Structural Damping*, **Manual on Aeroelasticity, Vol. IV, Ch. 3**, NATO AGARD.
- GLADWELL, G. M. L., 1962, *A Refined Estimate of the Damping Coefficient*, **J. Royal Aeronautical Society**, **66**, p125.
- HOWELL, E., AND EHLER, F. G., 1956, *Experimental Investigation of the Influence of Mechanical Baffles on the Fundamental Sloshing Mode of Water in a Cylindrical Tank*, Space Technology Labs Report GM-TR-69.
- KEULEGAN, G. H., AND CARPENTER, L. H., 1956, *Forces on Cylinders and Plates in an Oscillating Fluid*, NBS Report 4821.
- LINDHOLM, U. S., KANA, D. D., CHU, W.-H., AND ABRAMSON, H. N., 1962, *Research in Liquid Dynamics in Missile Fuel Tanks*, SwRI Quarterly Report 7, Contract NASw-2.
- LIU, F. C., 1964, *Pressure on Baffle Rings due to Fuel Sloshing in a Cylindrical Tank*, NASA-MSFC Report R-AERO-4-64.
- MIKISHEV, G. N., AND DOROSHKIN, N. YA., 1961, *An Experimental Investigation of Free Oscillations of Liquid in Containers*, **Izv. Akad., Nauk SSSR, Otd. Tekn. Nauk, Mekh. i Mashinostr**, **4**, pp. 48-83.
- MILES, J. W., 1956, *On the Sloshing of Liquid in a Cylindrical Tank*, Ramo-Wooldridge Co. Report AM6-5.
- MILES, J. W., 1958, *Ring Damping of Free Surface Oscillations in a Circular Tank*, **Trans. ASME, J. Applied Mechanics**, **25**, pp. 274-276.
- MILES, J. W., 1961, *Note on the Damping of Free Surface Oscillations due to Drainage*, Aerospace Corp. Report TDR-930 (2270-20) TN-1.
- NELSON, R. H., Jr., 1960, *The Sloshing of a Fluid Draining from a Flexible Tank*, PhD Thesis, Massachusetts Institute of Technology.
- O'NEIL, J. P., 1960, *Final Report on an Experimental Investigation of Sloshing*, Space Technology Labs Report STL/TR-59-0000-09960.
- SCANLAN, R. H., AND ROSENBAUM, R., 1960, **Introduction to the Study of Aircraft Vibration and Flutter**, Macmillan Co., pp. 72-88.
- SILVEIRA, M. A., STEPHENS, D. G., AND LEONARD, H. W., 1961, *Damping of Liquid Oscillations in Cylindrical Tanks with Various Baffles*, NASA TN D-715.
- STEPHENS, D. G., 1966, *Flexible Baffles for Slosh Damping*, **AIAA J. Spacecraft and Rockets**, **3**, pp. 765-766.
- STEPHENS, D. G., LEONARD, H. W., AND SILVEIRA, M. A., 1961, *An Experimental Investigation of the Damping of Liquid Oscillations in an Oblate Spheroidal Tank with and without Baffles*, NASA TN D-808.
- STEPHENS, D. G., LEONARD, H. W., AND PERRY, T. W., 1962, *Investigation of the Damping of Liquids in Right Circular Cylindrical Tanks, Including the Effects of a Time-Variant Liquid Depth*, NASA TN D-1367.
- STOFAN, A. J., AND ARMSTEAD, A. L., 1962, *Analytical and Experimental Investigation of Forces and Frequencies Resulting from Liquid Sloshing in a Spherical Tank*, NASA TN D-1281.
- STOFAN, A. J., AND PAVLI, A. J., 1962, *Experimental Damping of Liquid Oscillations in a Spherical Tank by Positive-Expulsions Bags and Diaphragms*, NASA TN D-1311.
- STOFAN, A. J., AND SUMNER, I. E., 1963, *Experimental Investigation of the Slosh-Damping Effectiveness of Positive-Expulsion Bags and Diaphragms in Spherical Tanks*, NASA TN-D-1712.
- SUMNER, I. E., 1963, *Preliminary Experimental Investigation of Frequencies and Forces from Liquid Sloshing in Toroidal Tanks*, NASA TN D-1709.
- SUMNER, I. E., 1964, *Experimental Investigation of Slosh-Suppression Effectiveness of Annular-Ring Baffles in Spherical Tanks*, NASA TN D-2519.

SUMNER, I. E., AND STOFAN, A. J., 1963, *An Experimental Investigation of Viscous Damping of Liquid Sloshing in Spherical Tanks*, NASA TN D-1991.

## 5. Simulation and Experimental Techniques

I. **Simulation of Liquid Sloshing** by JOHN F. DALZELL (SwRI)

II. **Experimental Techniques and Apparatus** by GEORGE W. BROOKS (NASA-LaRC)

ABRAMSON, H. N., AND RANSLEBEN, G. E., Jr., 1960, *Simulation of Fuel Sloshing Characteristics in Missile Tanks by Use of Small Models*, **ARS J.**, **30**, pp. 503-612.

ABRAMSON, H. N., AND NEVILL, G. E., Jr., 1963, *Some Modern Developments in the Application of Scale Models in Dynamic Testing*, **ASME Colloquium on Use of Models and Scaling in Shock and Vibration**.

ABRAMSON, H. N., CHU, W.-H., AND KANA, D. D., 1966, *Some Studies of Nonlinear Lateral Sloshing in Rigid Containers*, **Trans. ASME, J. Applied Mechanics**, **33**.

BRIDGMAN, P. W., 1931, **Dimensional Analysis**, Yale Univ. Press

BROOKS, G. W., 1962, *Techniques for Simulation and Analysis of Shock and Vibration Environments of Space Flight Systems*, **ASME Colloquium on Experimental Techniques in Shock and Vibration**.

BROOKS, G. W., 1964, *Principles and Practices for Simulation of Structural Dynamics of Space Vehicles*, **VPI Conference on the Role of Simulation and Space Technology**.

BUCKINGHAM, E., 1915, *Model Experiments and the Forms of Empirical Equations*, **Trans. ASME**, **37**, p263.

COLE, H. A., AND GAMBUCCI, B. J., 1961, *Measured Two-Dimensional Damping Effectiveness of Fuel Sloshing Baffles Applied to Ring Baffles in Cylindrical Tanks*, NASA TN D-694.

DALZELL, J. F., AND GARZA, L. R., 1964, *An Exploratory Study of Simulation of Liquid Impact in Space Vehicle and Booster Tanks*, SwRI Report No. 9, Contract NAS8-1555.

DUNCAN, W. J., 1955, **Physical Similarity and Dimensional Analysis**, Edward Arnold & Co.

EPPERSON, T. B., BROWN, R. B., AND ABRAMSON, H. N., 1961, *Dynamic Loads Resulting from Fuel Motion in Missile Tanks*, **Proc. Fourth Symposium on Ballistic Missile and Space Technology**, pp. 313-327.

HARRIS, C. M., AND CREDE, C. E., 1961, **Shock and Vibration Handbook, Vol. I**, pp. 2-15.

HERR, R. W., AND CARDEN, H. D., 1963, *Support Systems and Excitation Techniques for Dynamics Models of Space Vehicle Structures*, **Proc. Symposium on Aeroelastic and Dynamics Modeling Technology**.

HOWELL, E., AND EHLER, F. G., 1956, *Experimental Investigation of the Influence of Mechanical Baffles on the Fundamental Sloshing Mode of Water in a Cylindrical Tank*, Space Technology Labs Report GM-TR-69.

HUTTON, R. E., 1964, *Fluid Particle Motion During Rotary Sloshing*, **Trans. ASME, J. Applied Mechanics**, **31**, pp. 123-130.

JASZLICS, I. J., AND MOROSOW, G., 1965, *Dynamic Testing of a 20% Scale Model of the TITAN III*, **Proc. AIAA Symposium on Structural Dynamics and Aeroelasticity**, pp. 477-485.

KEULEGAN, G. H., AND CARPENTER, L. H., 1956, *Forces on Cylinders and Plates in an Oscillating Fluid*, NBS Report 4821.

LEADBETTER, S. A., AND RANEY, J. P., 1965, *Some Analytical and Experimental Studies of the Dynamics of Launch Vehicles*, **Proc. AIAA Symposium on Structural Dynamics and Aeroelasticity**, pp. 523-527.

LEONARD, H. W., AND WALTON, W. C., Jr., 1961, *An Investigation of the Natural Frequencies and Mode Shapes of Liquids in Oblate Spheroidal Tanks*, NASA TN D-904.

LINDHOLM, U. S., KANA, D. D., AND ABRAMSON, H. N., 1962, *Breathing Vibrations of a Circular Cylindrical Shell with an Internal Liquid*, **J. Aerospace Sciences**, **29**, pp. 1052-1059.

- LINDHOLM, U. S., CHU, W.-H., KANA, D. D., AND ABRAMSON, H. N., 1963, *Bending Vibrations of a Circular Cylindrical Shell with an Internal Liquid Having a Free Surface*, **AIAA J.**, **1**, pp. 2092-2099.
- McCARTY, J. L., AND STEPHENS, D. G., 1960, *Investigation of the Natural Frequencies of Fluids in Spherical and Cylindrical Tanks*, NASA TN D-252.
- McCARTY, J. L., LEONARD, H. W., AND WALTON, W. C., Jr., 1960, *Experimental Investigation of the Natural Frequencies of Liquids in Toroidal Tanks*, NASA TN D-531.
- MILES, J. W., 1958, *Ring Damping of Free Surface Oscillations in a Circular Tank*, **Trans. ASME, J. Applied Mechanics**, **25**, pp. 274-276.
- MIXSON, J. S., AND HERR, R. W., 1962, *An Investigation of the Vibration Characteristics of Pressurized Thin-Walled Circular Cylinders Partially Filled with Liquid*, NASA TR R-145.
- MIXSON, J. S., CATHERINE, J. J., AND ARMAN, A., 1963, *Investigation of the Lateral Vibration Characteristics of a 1/5-Scale Model of SATURN SA-1*, NASA TN D-1593.
- MIXSON, J. S., AND CATHERINE, J. J., 1964, *Experimental Lateral Vibration Characteristics of a 1/5-Scale Model of SATURN SA-1 with an Eight-Cable Suspension System*, NASA TN D-2214.
- MIXSON, J. S., AND CATHERINE, J. J., 1964, *Comparison of Experimental Vibration Characteristics Obtained from a 1/5-Scale Model and from a Full-Scale SATURN SA-1*, NASA TN D-2215.
- MURPHY, G., 1950, **Similitude in Engineering**, The Ronald Press.
- RAYLEIGH, J. W. S., 1892, *Stability of Flow of Fluids and Investigations in Capillarity*, **Phil. Mag.**, **34**.
- ROUSE, H., 1959, **Advanced Mechanics of Fluids**, John Wiley & Sons.
- ROUSE, H., 1961, **Fluid Mechanics for Hydraulic Engineers**, Dover Books.
- RUNYAN, H. L., MORGAN, H. G., AND MIXSON, J. S., 1962, *Role of Dynamic Models in Launch Vehicle Development*, **ASME Colloquium on Experimental Techniques in Shock and Vibration.**
- SANDORFF, P. E., 1960, *Principles of Design of Dynamically Similar Models for Large Propellant Tanks*, NASA TN D-99.
- SILVEIRA, M. A., MAGLIERI, D. J. AND BROOKS, G. W., 1958, *Results of an Experimental Investigation of Small Viscous Dampers*, NACA TN 4257.
- SILVEIRA, M. A., STEPHENS, D. G., AND LEONARD, H. W., 1961, *Damping of Liquid Oscillations in Cylindrical Tanks with Various Baffles*, NASA TN D-715.
- STEPHENS, D. G., 1965, *Experimental Investigation of Liquid Impact in a Model Propellant Tank*, NASA TN D-2913.
- STEPHENS, D. G., LEONARD, H. W., AND SILVEIRA, M. A., 1961, *An Experimental Investigation of the Damping of Liquid Oscillations in an Oblate Spheroidal Tank with and without Baffles*, NASA TN D-808.
- STEPHENS, D. G., LEONARD, H. W., AND PERRY, T. W., 1962, *Investigation of the Damping of Liquids in Right Circular Cylindrical Tanks, Including the Effects of a Time-Variant Liquid Depth*, NASA TN D-1367.
- STEPHENS, D. G., AND LEONARD, H. W., 1963, *The Coupled Dynamic Response of a Tank Partially Filled with a Liquid and Undergoing Free and Forced Planar Oscillations*, NASA TN D-1945.
- STOFAN, A. J., AND ARMSTEAD, A. L., 1962, *Analytical and Experimental Investigation of Forces and Frequencies Resulting from Liquid Sloshing in a Spherical Tank*, NASA TN D-1281.
- STOFAN, A. J., AND PAVLI, A. J., 1962, *Experimental Damping of Liquid Oscillations in a Spherical Tank by Positive-Expulsions Bags and Diaphragms*, NASA TN D-1311.
- STOFAN, A. J., AND SUMNER, I. E., 1963, *Experimental Investigation of the Slosh-Damping Effectiveness of Positive-Expulsion Bags and Diaphragms in Spherical Tanks*, NASA TN-D-1712.
- SUMNER, I. E., 1963, *Preliminary Experimental Investigation of Frequencies and Forces from Liquid Sloshing in Toroidal Tanks*, NASA TN D-1709.
- SUMNER, I. E., AND STOFAN, A. J., 1963, *An Experimental Investigation of Viscous Damping of Liquid Sloshing in Spherical Tanks*, NASA TN D-1991.

- SUMNER, I. E., 1964, *Experimental Investigation of Slosh-Suppression Effectiveness of Annular-Ring Baffles in Spherical Tanks*, NASA TN D-2519.
- SUMNER, I. E., STOFAN, A. J., AND SHRAMO, D. J., 1964, *Experimental Sloshing Characteristics and a Mechanical Analogy of Liquid Sloshing in a Scale Model CENTAUR Liquid Oxygen Tank*, NASA TM X-999.
- VENNARD, J. K., 1961, **Elementary Fluid Mechanics, 4th ed.**, John Wiley & Sons.

## 6. Analytical Representation of Lateral Sloshing by Equivalent Mechanical Models

by FRANKLIN T. DODGE (SwRI)

- ABRAMSON, H. N., CHU, W.-H., AND RANSLEBEN, G. E., Jr., 1961, *Representation of Fuel Sloshing in Cylindrical Tanks by an Equivalent Mechanical Model*, **ARS J.**, **31**, pp. 1697-1705.
- ABRAMSON, H. N., CHU, W.-H., AND GARZA, L. R., 1962, *Liquid Sloshing in Spherical Tanks*, SwRI Report No. 2, Contract NAS8-1555.
- ABRAMSON, H. N., CHU, W.-H., AND KANA, D. D., 1966, *Some Studies of Nonlinear Lateral Sloshing in Rigid Containers*, **Trans. ASME, J. Applied Mech.**, **33**, no. 4.
- ARMSTRONG, G. L., AND KACHIGAN, K., 1961, *Propellant Sloshing*, **Handbook of Astronautical Engineering, Sections 14.14/15**, McGraw-Hill Book Co.
- BAUER, H. F., 1958, *Fluid Oscillation in a Cylindrical Tank with Damping*, ABMA Report DA-TR-4-58.
- BAUER, H. F., 1958, *The Moment of Inertia of a Liquid in a Circular Cylindrical Tank*, ABMA Report DA-TR-5-58.
- BAUER, H. F., 1962, *Mechanical Model of Fluid Oscillations in Cylindrical Tanks and Introduction of Damping*, NASA-MSFC Report MTP-AERO-62-16.
- BAUER, H. F., 1963, *Liquid Sloshing in a Cylindrical Quarter Tank*, **AIAA J.**, **1**, pp. 2601-2606.
- BAUER, H. F., 1964, *Fluid Oscillations in the Containers of a Space Vehicle and Their Influence on Stability*. NASA TR-R-187.
- BAUER, H. F., 1964, *Liquid Sloshing in a 45° Sector Compartmented Tank*, **AIAA J.**, **2**, pp. 768-770.
- BAUER, H. F., CLARK, C. D., AND WOODWARD, J. H., 1965, *Analytical Mechanical Model for the Description of the Rotary Propellant Sloshing Motion*, Georgia Institute of Technology, Engineering Experiment Station Final Report for Contract NAS8-11159.
- BERLOT, R. R., 1959, *Production of Rotation in a Confined Liquid Through Translational Motion at the Boundaries*, **Trans. ASME, J. Applied Mechanics**, **26**, pp. 513-516.
- DODGE, F. T., AND KANA, D. D., 1966, *Moment of Inertia and Damping of Liquids in Baffled Cylindrical Tanks*, **AIAA J. Spacecraft and Rockets**, **3**, pp. 153-155 (and discussion in same journal, **3**, pp. 957-959).
- FREED, L. E., 1957, *Stability of Motion of Conical Pendulums*, Report GM-45 3-437, Ramo Wooldridge Co.
- GRAHAM, E. W., AND RODRIGUEZ, A. M., 1951, *The Characteristics of Fuel Motion which Affect Airplane Dynamics*, Douglas Aircraft Report SM-14212.
- GRAHAM, E. W., AND RODRIGUEZ, A. M., 1952, *The Characteristics of Fuel Motion which Affect Airplane Dynamics*, **Trans. ASME, J. Applied Mechanics**, **19**, pp. 381-388.
- HARPER, J., 1958, *Propellant Sloshing in a Conical Tank Undergoing Arbitrary Forced Translational Motion*, Convair Report ZU-7-089.
- HOUSNER, G. W., 1957, *Dynamic Pressures on Accelerated Fluid Containers*, **Bulletin Seismological Society of America**, **47**, pp. 15-35.
- HOWELL, J. V., 1957, *Motion of Conical Pendulum*, Ramo-Wooldridge Report GM 42.4-4.
- KACHIGAN, K., 1955, *Forced Oscillations of a Fluid in a Cylindrical Tank*, Convair Report ZU-7-046.
- LOMEN, D. O., 1965, *Digital Analysis of Liquid Propellant Sloshing in Mobile Tanks with Rotational Symmetry*, NASA CR -230.

- LOMEN, D. O., 1965, *Liquid Propellant Sloshing in Mobile Tanks of Arbitrary Shape*, NASA CR-222.
- LUKENS, D. R., SCHMITT, A. F., AND BROUCEK, G. T., 1964, *Approximate Transfer Functions for Flexible-booster-and Autopilot Analysis*, Convair Report No. AE 61-0198 (Also, WADD TR-61-93).
- MILES, J. W., 1956, *On the Sloshing of Liquid in a Flexible Tank*, Ramo-Wooldridge Report GM TR-73.
- MILES, J. W., 1962, *Stability of Forced Oscillations of a Spherical Pendulum*, **Quart. Appl. Mech.**, **20**, pp. 21-32.
- OKHOTSIMSKII, D. E., 1960, *Theory of the Motion of a Body with Cavities Partially Filled with a Liquid*, NASA TT F-30.
- RATTAYA, J. V., 1965, *Sloshing of Liquids in Axisymmetric Ellipsoidal Tanks*, AIAA Paper 65-114.
- RUMYANTSEV, V. V., 1964, *Stability of Motion of Solid Bodies with Liquid Filled Cavities by Lyapunov's Methods*, **Advances in Applied Mechanics**, **8**, Academic Press.
- SCHMITT, A. F., 1956, *Forced Oscillations of a Fluid in a Cylindrical Tank Undergoing Both Translation and Rotation*, Convair Report ZU-7-069.
- SCHMITT, A. F., 1957, *Forced Oscillations of a Fluid in a Cylindrical Tank Oscillating a Carried Acceleration Field – A Correction*, Convair Report ZU-7-074.
- SCHY, A. A., 1951, *A Theoretical Analysis of the Effects of Fuel Motion on Airplane Dynamics*, NACA TN 2280.
- STEPHENS, D. G., AND LEONARD, H. W., 1963, *The Coupled Dynamic Response of a Tank Partially Filled with a Liquid and Undergoing Free and Forced Planar Oscillations*, NASA TN D-1945.
- SUMNER, I. E., 1965, *Experimentally Determined Pendulum Analogy of Liquid Sloshing in Spherical and Oblate-Spheroidal Tanks*, NASA TN D-2737.
- SUMNER, I. E., STOFAN, A., J., AND SHRAMO, D. J., 1964, *Experimental Sloshing Characteristics and a Mechanical Analogy of Liquid Sloshing in a Scale-Model CENTAUR Liquid Oxygen Tank*, NASA TM X-999.
- WARNER, R. W., AND CALDWELL, J. T., 1961, *Experimental Evaluation of Analytical Models for the Inertia and Natural Frequencies of Fuel sloshing in Circular Cylindrical Tanks*, NASA TN D-856.
- ZHUKOVSKII, N. E., 1936, *On the Motion of a Rigid Body Having Cavities Filled with a Homogeneous Liquid*, **Collected Works**, **3**.

## 7. Vehicle Stability and Control

by HELMUT F. BAUER (Georgia Institute of Technology and NASA-MSFC)

- BARTON, M., 1956, *Generalized Missile Dynamics Analysis*, Ramo-Wooldridge Corp. Report.
- BAUER, H. F., AND RHEINFURTH, M. H., 1960, *Flutter and Stability Analysis*, ABMA Report DA-TM-4-60.
- BAUER, H. F., 1961, *Dynamics of Liquid Propellant Vehicles*, **Proc. ONR/AIA Symposium on Structures and Dynamics of High Speed Flight**.
- BAUER, H. F., 1961, *Parametric Study of the Influence of Propellant Sloshing on the Stability of Space Crafts*, **J. Aerospace Sciences**, pp. 819-820.
- BAUER, H. F., 1961, *The Effects of Interaction of Structure, Control, and Propellant Sloshing upon the Stability of Large Space Vehicles*, NASA-MSFC Report MTP-AERO-83.
- BAUER, H. F., 1963, *Stability Boundaries of Liquid Propelled Space Vehicles with Sloshing*, **AIAA J.**, **1**.
- BAUER, H. F., 1963, *The Effects of Propellant Sloshing on the Stability of an Accelerometer Controlled Rigid Space Vehicle*, NASA TN D-1831.
- BAUER, H. F., 1963, *Wind Response of the SATURN LOR Vehicle*, NASA-MSFC Report MTP-AERO-63-19.
- BAUER, H. F., 1964, *Fluid Oscillations in the Containers of a Space Vehicle and Their Influence Upon Stability*, NASA TR-R-187.

- BRODETSKY, S., AND SMEAL, G., 1924, *On Graeffe's Method for Complex Roots of Algebraic Equations*, **Proc. Cambridge Phil. Soc.**, **22**, pp. 83-87.
- FULLER, A. T., 1957, *Stability Criteria for Linear Systems and Reliability Criteria for RC Networks*, **Proc. Cambridge Phil. Soc.**, **53**, pp. 878-896.
- GEISSLER, E. D., 1960, *Problems in Attitude Stabilization of Large Guided Missiles*, **Aero-Space Engineering**, Oct. issue, pp. 24-29.
- HAYS, P. J., AND SUMRALL, J. P., 1964, *Stability Analysis of SATURN SA-5 with Live S-IV Stage*, NASA TM X-53017.
- HEINRICH, K., AND KAUFMAN, F. H., 1956, *Sloshing Stability Criteria for Vehicles with One Free Fluid*, Ramo-Wooldridge Corp. Memo GM-45.3-45.
- HEIST, E. K., 1956, *Equations of Motion of Missile with Sloshing*, Ramo-Wooldridge Corp. Report GM-TM-146.
- HURWITZ, A., 1895, *Über die Bedingungen unter welchen eine Gleichung nur Wurzeln mit negative reellen Theilen besitzt*, **Mathematische Annalen**, **46**, pp. 273-284.
- LUKENS, D. R., SCHMITT, A. F., AND BROUCEK, G. T., 1961, *Approximate Transfer Function for Flexible-Booster-and-Auto-Pilot Analysis*, WFAFB Report WADD-TR-61-93.
- NYQUIST, H., 1932, *Regeneration Theory*, **Bell System Technical Journal**, **11**, pp. 126-147.
- RHEINFURTH, H. F., 1960, *Control Feedback Stability Analysis*, ABMA Report DA-TR-2-60.
- RHEINFURTH, M. H., 1961, *The Influence of Control Sensors on the Stability of Space Vehicles*, NASA-MSFC Report MTP-61-65.
- ROUTH, E. J., 1877, *A Treatise on the Stability of a Given Motion*, Macmillan Book Co., pp. 74-81.
- THORP, F. A., AND HUTCHINSON, R. C., 1959, *The Dynamics of Rocket-Powered Vehicles*, M.I.T Report R-206.
- ZURMÜHL, R., 1953, *Praktische Mathematik für Ingenieure und Physiker*, Springer Verlag.

## 8. Vertical Excitation of Propellant Tanks

by FRANKLIN T. DODGE (SwRI)

- BAIRD, M. H. I., 1963, *Resonant Bubbles in a Vertically Vibrating Liquid Column*, **Canadian J. Chemical Engineering**, **41**, pp. 52-55.
- BENJAMIN, T. B., AND URSELL, F., 1954, *The Stability of a Plane Free Surface of a Liquid in Vertical Periodic Motion*, **Proc. Royal Soc. (London)**, **A225**, pp. 505-515.
- BHUTA, P. G., AND KOVAL, L. R., 1964, *Coupled Oscillations of a Liquid with a Free Surface in a Tank Having a Free Bottom*, **Zeitschrift für angewandte Mathematik und Physik**, **15**, pp. 466-480.
- BHUTA, P. G., AND KOVAL, L. R., 1964, *Hydroelastic Solution of Sloshing of a Liquid In a Cylindrical Tank*, **J. Acoust. Soc. Am.**, **36**, pp. 2071-2079.
- BHUTA, P. G., AND YEH, G. C. K., 1965, *Liquid Sloshing due to a Time Dependent Discontinuous Boundary*, **Int. J. Mech. Sci.**, **7**, pp. 475-488.
- BLEICH, H. H., 1956, *Longitudinal Forced Vibrations of Cylindrical Fuel Tanks*, **Jet Propulsion**, **26**, pp. 109-111.
- BLEICH, H. H., 1956, *Effect of Vibrations on the Motion of Small Gas Bubbles in a Liquid*, **Jet Propulsion**, **26**, pp. 958-978.
- BLEICH, H. H., 1956, *Motions of Clusters of Gas Bubbles in Vibrated Vessels*, Ramo-Wooldridge Corp. Report GM-TR-27, Contract AF(600)-1190.
- BOLOTIN, V. V., 1956, *On Liquid Motion in a Vibrating Container*, **Prikladnaia Matematika in Mekhanika**, **20**, pp. 293-294.
- BUCHANAN, R. H., JAMESON, G., AND OEDJOE, D., 1962, *Cyclic Migration of Bubbles in Vertically Vibrating Liquid Columns*, **Industrial and Engineering Chemistry Fundamentals**, **41**, pp. 82-86.
- CHU, W.-H., 1965, *Subharmonic Oscillations in an Arbitrary Axisymmetric Tank Resulting from Axial Excitations*, SwRI Report No. 5, Contract NAS8-11045.

- DODGE, F. T., 1963, *A Review of Research Studies on Bubble Motions in Vertically Vibrating Tanks*, SwRI Report No. 11, Contract NAS8-11045.
- DODGE, F. T., KANA, D. D., AND ABRAMSON, H. N., 1965, *Liquid Surface Oscillations in Longitudinally Excited Rigid Cylindrical Containers*, **AIAA J.**, **3**, pp. 685-695.
- FARADAY, M., 1831, *On the Forms and States Assumed by Fluids in Contact with Vibrating Elastic Surfaces*, **Phil. Trans. Royal Soc. (London)**, **121**, pp. 319-340.
- FRITZ, C. G., AND PONDER, C. A., Jr., 1965, *Bubble Coalescence in a Longitudinally Vibrated Liquid Column*, **Proc. ASME Symposium on Cavitation in Fluid Machinery**, pp. 7-11.
- FULTZ, D., 1962, *An Experimental Note on Finite-Amplitude Standing Gravity Waves*, **J. Fluid Mechanics**, **13**, pp. 193-212.
- HUTTON, R. E., 1963, *An Investigation of Resonant, Nonlinear, Nonplanar Free-Surface Oscillations of a Fluid*, NASA TN D-1870.
- KANA, D. D., 1963, *Longitudinal Forced Vibration of Partially Filled Tanks*, SwRI Report No. 6, Contract NASw-146.
- KANA, D. D., 1963, *Vertical Oscillations of Partially Full Spherical Tanks*, SwRI Final Report, Contract NASw-146.
- KANA, D. D., 1966, *An Experimental Study of Liquid Surface Oscillations in Longitudinally Excited Compartmented Cylindrical and Spherical Tanks*, NASA CR-545.
- KANA, D. D., AND DODGE, F. T., 1966, *Bubble Behavior in Liquids Contained in Vertically Vibrated Tanks*, **AIAA J. spacecraft and Rockets**, **3**, pp. 760-763.
- LORD RAYLEIGH, 1883, *On Maintained Vibrations*, **Phil. Mag.**, **15**, 229-235.
- LORD RAYLEIGH, 1883, *On the Crispations of Fluid Resting Upon a Vibrating support*, **Phil. Mag.**, **16**, pp.50-58.
- LORD RAYLEIGH, 1887, *On the Maintenance of Vibrations by Forces of Double Frequency, and on the Propagation of Waves Through a Medium Endowed with a Periodic Structure*, **Phil. Mag.**, **24**, pp. 145-149.
- MACK, L. R., 1962, *Periodic, Finite-Amplitude Axisymmetric Gravity Waves*, **J. Geophys. Res.**, **67**, pp. 829-843.
- MATHIESSEN, L., 1868, *Akustische Versuche die Kleinsten Transversalwellen der Flüssigkeiten betreffend*, **Annalen der Physik**, **134**, pp.107-117.
- MATHIESSEN, L., 1870, *Über die Transversalschwingungen tönender tropfharer und elastischer Flüssigkeiten*, **Annalen der Physik**, **141**, pp. 275-393.
- MINNAERT, M., 1933, *On Musical Air Bubble and the Sounds of Running Water*, **Phil Mag., Series 7**, **16**, pp. 235-248.
- MOISEYEV, N. N., 1953, *The Problem of the Motion of a Rigid Body Containing Liquid Masses with Free Surfaces*, **Matem. Sbornik**, **32**, p. 32.
- MOISEYEV, N. N., 1964, **Introduction to the Theory of Oscillation of Liquid Containing Bodies**, Academic Press.
- PENNEY, W. G., AND PRICE, A. T., 1952, *Finite Periodic Standing Gravity Waves in a Perfect Liquid, II*, **Proc. Royal Soc. (London)**, **A244**, 254-284.
- SKALAK, R., AND YARYMOVYCH, M. I., 1962, *Forced Large Amplitude Surface Waves*, **Proc. Fourth U. S. National Cong. Applied Mechanics**, pp. 1411-1418.
- TADJIBAKSH, I., AND KELLER, J. B., 1960, *Standing Surface Waves of Finite Amplitude*, **J. Fluid Mechanics**, **8**, pp. 442-451.
- TAYLOR, G. I., 1950, *The Instability of Liquid Surfaces when Accelerated in a Direction Perpendicular to Their Planes, Part I*, **Proc. Royal Soc. (London)**, **A201**, pp. 192-196.
- TAYLOR, G. I., 1954, *An Experimental Study of Standing Waves*, **Proc. Royal Soc. (London)**, **A244**, pp. 44-59.
- VERMA, G. R., AND KELLER, J. B., 1962, *Three-Dimensional Standing Surface Waves of Finite Amplitude*, **Phys. Fluids**, **5**, pp. 52-56.
- YARYMOVYCH, M. I., 1959, *Forced Large Amplitude Surface Waves*, D. Eng. Sci. Thesis, Columbia University.

## 9. Interaction Between Liquid Propellants and the Elastic Container

by DANIEL D. KANA (SwRI)

- ARNOLD, R. N., AND WARBURTON, G. B., 1949, *Flexural Vibrations of the Walls of Thin Shells Having Freely Supported Ends*, **Proc. Royal Society (London)**, **A197**, pp. 238.
- ARNOLD, R. N., AND WARBURTON, G. B., 1953, *The Flexural Vibrations of Thin Cylinders*, **J. Proc. Inst. Mech. Eng. (London)**, **167**, pp. 62-74.
- BARON, M. L., AND BLEICH, H. H., 1959, *The Dynamic Analysis of Empty and Partially Full Cylindrical Tanks, Part I – Frequencies and Modes of Free Vibration and Transient Response by Mode Analysis*, Defense Atomic Support Agency Report DASA 1123A.
- BARON, M. L., AND BLEICH, H. H., 1959, *The Dynamic Analysis of Empty and Partially Full Cylindrical Tanks, Part II – Analysis of Uplift and Structural Damage*, Defense Atomic Support Agency Report DASA 1123B.
- BARON, M. L., AND SKALAK, R., 1962, *Free Vibrations of Fluid Filled Cylindrical Shells*, **ASCE J. Engr. Mech.**, **88**, No. EM3, Part I.
- BAUER, H. F., 1958, *Fluid Oscillations in a Circular Cylindrical Tank due to Bending of the Tank Wall*, ABMA Report DA-TR-3-58.
- BAUER, H. F., 1958, *Damped Fluid Oscillations in a Circular Cylindrical Tank due to Bending of the Tank Wall*, ABMA Report DA-TR-9-58.
- BAUER, H. F., 1961, *The Effects of Interaction of Structure, Control, and Propellant Sloshing upon the Stability of Large Space Vehicles*, NASA-MSFC Report MTP-AERO-83.
- BAUER, H. F., 1963, *Theory of Liquid sloshing in Compartmented Cylindrical Tanks due to Bending Excitation*, **AIAA J.**, **1**, pp. 1590-1596.
- BAUER, H. F., 1966, *Stability Boundaries of Liquid-Propellant Elastic Vehicles with Sloshing*, **AIAA J. spacecraft and Rockets**, **3**, pp. 240-246.
- BEAL, T. R., COALE, C. W., AND NAGANO, M., 1965, *Influence of Shell Inertia and Bending Stiffness on the Axisymmetric Modes of a Partially Filled Cylindrical Tank*, AIAA Paper 65-412.
- BERRY, J. G., AND REISSNER, E., 1958, *The Effect of an Internal Compressible Fluid Column on the Breathing Vibrations of a Thin Pressurized Cylindrical Shell*, **J. Aerospace Sci.**, **25**, pp. 228-294.
- BHUTA, P. G., AND KOVAL, L. R., 1964, *Coupled Oscillations of a Liquid with a Free Surface in a Tank Having a Flexible Bottom*, **Zeitschrift für angewandte Mathematik und Physik**, **15**, pp. 466-480.
- BHUTA, P. G., AND KOVAL, L. R., 1964, *Hydroelastic Solution of Sloshing of a Liquid In a Cylindrical Tank*, **J. Acoust. Soc. Am.**, **36**, pp. 2071-2079.
- BLEICH, H. H., 1956, *Longitudinal Forced Vibrations of Cylindrical Fuel Tanks*, **Jet Propulsion**, **26**, pp. 109-111.
- CHU, W.-H., 1963, *Breathing Vibrations of a Partially Filled Cylindrical Tank – Linear Theory*, **Trans. ASME, J. Applied Mech.**, **30**, pp. 532-536.
- CHU, W.-H., AND GONZALES, R., 1964, *Supplement to Breathing Vibrations of a Partially Filled Cylindrical Tank – Linear Theory*, **Trans. ASME, J. Applied Mech.**, **34**, pp. 722-723.
- CHU, W.-H., AND KANA, D. D., 1966, *A Theory for Nonlinear Transverse Vibrations of a Partially Filled Elastic Tank*, SwRI Final Report, Part I, Project 02-1748.
- FONTENOT, L. L., AND LIANIS, G., 1963, *The Free Vibrations of Thin Elastic Pressurized Cylindrical Shells Filled with a Perfect and Incompressible Liquid Having a Free Surface*, **International Symposium on Space Technology and Science**.
- FULLER, A. T., 1957, *Stability Criteria for Linear Systems and Reliability Criteria for RC Networks*, **Proc. Cambridge. Phil. Soc.**, **53**, pp. 878-896.
- FUNG, Y. C., SECHLER, E. E., AND KAPLAN, A., 1957, *On the Vibration of Thin Cylindrical Shells Under Internal Pressure*, **J. Aeron. Sci.**, **24**, pp. 650-660.
- GEISSLER, E. D., 1960, *Problems in Attitude Stabilization of Large Guided Missiles*, **Aero-Space Engineering**, Oct. issue, pp. 24-29.

- HU, W. C. L., 1964, *A Survey of the Literature on the Vibrations of Thin Shells*, SwRI Report 1, Contract NASr-94(06).
- HURWITZ, A., 1895, *Über die Bedingungen unter welchen eine Gleichung nur Wurzeln mit negative reellen Theilen besitzt*, **Mathematische Annalen**, **46**, pp. 273-284.
- HWANG, C., 1965, *Longitudinal Sloshing of Liquid in a Flexible Hemispherical Tank*, ASME Paper 65-APM-64.
- KANA, D. D., 1963, *Longitudinal Forced Vibration of Partially Filled Tanks*, SwRI Report 6, Contract NASw-146.
- KANA, D. D., LINDHOLM, U. S., AND ABRAMSON, H. N., 1966, *An Experimental Study of Liquid Instability in a Vibrating Elastic Tank*, **AIAA J. Spacecraft and Rockets**, **3**, pp. 1183-1188.
- LEROY, J., 1963, *Breathing Vibrations of Thin Cylinders Partially Full of Liquid*, **Comptes Rendus**, **257**, pp. 2607-2609.
- LINDHOLM, U. S., KANA, D. D., AND ABRAMSON, H. N., 1962, *Breathing Vibrations of a Circular Cylindrical Shell with an Internal Liquid*, **J. Aerospace Sci.**, **29**, pp. 1052-1059.
- LINDHOLM, U. S., CHU, W.-H., KANA, D. D., AND ABRAMSON, H. N., 1963, *Bending Vibrations of a Circular Cylindrical Shell Containing an Internal Liquid with a Free Surface*, **AIAA J.**, **1**, pp. 2092-2099.
- MILES, J. W., 1958, *On the Sloshing of Liquid in a Flexible Tank*, **Trans. ASME, J. Applied Mechanics**, pp. 277-283.
- MIXSON, J. S., AND HERR, R. W., 1962, *An Investigation of the Vibration Characteristics of Pressurized Thin-Walled Circular Cylinders Partially Filled with Liquid*, NASA TR R-145.
- NATUSHKIN, V. F., AND RAKHIMOV, I. S., 1964, *Oscillations of a Cylindrical Shell Partially Filled with a Fluid*, **Aviatsionnaia Tekhnika**, **17**, pp. 75-78.
- PALMER, J. H., AND ASHER, G. W., 1965, *Calculation of Axisymmetric Longitudinal Modes for Fluid-Elastic Tank-Ullage Gas System and Comparison with Model Test Results*, **Proc. AIAA Symposium on Structural Dynamics and Aeroelasticity**, pp. 189-193.
- RABINOVICH, B. I., 1959, *Concerning the Equations of Elastic Oscillations of Thin-Walled Bars Filled with a Liquid Having a Free Surface*, **Akad. Nauk. SSSR Izvestiya O. T. N. Mekhanika i Machinostrogenic**, **4**.
- RABINOVICH, B. I., 1964, *The Equations of the Transverse Vibrations of Liquid-Filled Shells*, NASA TT F-216.
- REISSNER, E., 1955, *On Transverse Vibrations of Thin Shallow Elastic Shells*, **Quart. Appl. Math.**, **13**, pp. 169-176.
- REISSNER, E., 1956, *Notes on Forced and Free Vibrations of Pressurized Cylindrical Shells which Contain a Heavy Liquid with a Free Surface*, TRW Space Technologies Laboratory Report GM-TR-87, AM No. 6-15.
- SALEME, E., AND LIBER, T., 1965, *Breathing Vibrations of Pressurized Partially Filled Tanks*, **AIAA J.**, **3**, pp. 132-136.
- SAMOILOV, E. A., AND PAVLOV, B. S., 1964, *Oscillations of a Hemispherical Shell Filled with a Fluid*, **Aviatsionnaia Tekhnika**, **17**, pp. 79-86.
- SHMAKOV, V. P., 1964, *The Equations of the Axially Symmetric Vibrations of a Liquid-Filled Cylindrical Shell*, NASA TT F-219.
- TIMOSHENKO, S., 1940, **Theory of Plates and Shells**, McGraw-Hill Book Co.
- TONG, P., AND FUNG, Y. C., 1964, *The Effect of Wall Elasticity and Surface Tension on the Forced Oscillations of a Liquid in a Cylindrical Container (Part I: Analysis)*, California Institute of Technology, Grad. Aero. Labs Report SM-64-40.
- YU, Y. Y., 1955, *Vibration of Thin Cylindrical Shells*, **Trans. ASME, J. Applied Mech.**, **22**, pp. 547-552.

## 10. Special Topics

- I. **Liquid Impact on Tank Bulkhead** by JOHN.F. DALZELL (SwRI)
- II. **Liquid Rotation an Vortexing During Draining** by FRANKLIN T. DODGE (SwRI)
- III. **Longitudinal Oscillations of Flight Vehicles** by DANIEL D. KANA (SwRI)

--, 1961, **Handbook of Astronautical Engineering**, McGraw Book Co.

ABRAMSON, H. N., CHU, W.-H., GARZA, L. R., AND RANSLEBEN, G. E., Jr., 1962, *Some Studies of Liquid Rotation and Vortexing in Rocket Propellant Tanks*, NASA TN D-1212.

BINNIE, A. M., AND HARRIS, D. P., 1950, *The Application of Boundary-Layer Theory to Swirling Liquid Flow Through a Nozzle*, **Quart. J. Mech. and Appl. Math.**, **3**, pp. 89-106.

BINNIE, A. M., HOOKINGS, G. A., AND KAMEL, M. Y. M., 1957, *The Flow of Swirling Water Through a Convergent-Divergent Nozzle*, **J. Fluid Mechanics**, **3**, pp. 281-274.

BRADY, W. F., POPE, M. D., AND PODE, L., 1962, *ABLESTAR Experimental Studies*, Space-General Report SGC 32R-19.

COKONIS, T. J., TOMASSONI, J. E., AND SEIFERTH, R. W., *Dome Impact Analysis – An Approximate Analysis*, Martin Co. Report TN LV-211.

DALZELL, J. F., AND GARZA, L. R., 1964, *An Exploratory Study of Simulation of Liquid Impact in Space Vehicles and Booster Tanks*, SwRI Report No. 6, Contract NAS8-1555.

DAVIS, W. F., LYNCH, T. F., AND MURRAY, T. R., 1964, *THOR 20-Cycle Longitudinal Oscillation Study*, **Shock and Vibration Bulletin**, **34**, pp. 177-196.

DERGARABEDIAN, P., 1960, *The Behavior of Vortex Motions in an Emptying Container*, **Proc. 13th Heat Transfer and Fluid Mechanics Institute**, pp. 47-61.

EIDE, D. G., 1964, *Preliminary Analysis of Variation of Pitch Motion of a Vehicle in a Space Environment due to Fuel Sloshing in a Rectangular Tank*, NASA TN D-2336.

EPPELSON, T. B., AND BROWN, R., 1957, *Dynamic Loads due to Fuel Motion in Fuel Tanks of Missiles*, SwRI Final Report, Contract DA-23-072-ORD-1062.

EPPELSON, T. B., BROWN, R., AND ABRAMSON, H. N., 1961, *Dynamic Loads Resulting from Fuel Motion in Missile Tanks*, **Proc. 4th Symposium on Ballistic Missile and Space Technology, Vol. II**, pp. 313-327.

GLUCK, D. F., AND GILLE, J. P., 1965, *Fluid Mechanics of Zero-G Propellant Transfer in Spacecraft Propulsion Systems*, **Trans. ASME, J. Eng. For Industry**, **87**, pp. 1-8.

HUTTON, R. E., 1964, *Fluid Particle Motion During Rotary Sloshing*, **Trans. ASME. J. Applied Mechanics**, **31**, pp. 123-130.

KAMEL, M. Y. M., 1964, *The Effect of Swirl on the Flow of Liquids Through Bottom Outlets*, ASME Paper 64-WA/FE-37.

KÜCHEMANN, D., 1965, *Report on the IUTAM Symposium on Concentrated Vortex Motions in Fluids*, **J. Fluid Mechanics**, **21**, pp. 1-20.

MCKENNA, K. J., WALKER, J. H., AND WINJE, R. A., 1965, *Engine-Airframe Coupling in Liquid rocket Systems*, **AIAA J. Spacecraft and Rockets**, **2**, pp. 254-256.

NOLTING, R. K., 1964, *Simulation of Orbital Mooring of GEMINI and AGENA Vehicles by Means of Dynamically Scaled Models*, **Proc. Symposium on Aeroelastic and Dynamics Modeling Technology**, USAF Report RTD-TDR-63-4197.

PINSON, L. D., 1963, *Propellant Dome Impact Analysis*, NASA Internal Memorandum.

PRANDTL, L., 1949, **Essentials of Fluid Dynamics**, Hafner.

RADOVICH, N. A., 1965, *Analytical Model for Missile Axial Oscillation Induced by Engine-Structure Coupling*, **Proc. AIAA Unmanned Spacecraft Meeting**.

ROSE, R. G., 1963, *Dynamics of the ATLAS – 5 cps Longitudinal Oscillation Following Launch as Related to the Tank Pressure Regulation System. Vol. I, Longitudinal Model Development*, General Dynamics/Astronautics Report.

ROSE, R. G., AND HARRIS, R., 1964, *Dynamic Analysis of Coupled Structural/Pneumatic System Longitudinal Oscillation for ATLAS Vehicles*, AIAA Paper 64-483.

- ROUSE, H., 1963, *On the Role of Eddies in Fluid Motion*, **American Scientist**, **51**, pp. 285-314.
- RUBIN, S., 1964, *Instability Model of Missile Longitudinal Oscillation Due to Propulsion Feedback*, Aerospace Corp. Report TOR-269(4126)-28.
- STEPHENS, D. G., 1965, *Experimental Investigations of Liquid Impact in a Model Propellant Tank*, NASA TN D-2913.
- WESKE, J. R., 1958, *ON the Origin and Mechanism of Vortex Motion at the Inlet of Intakes Placed Near a Flat Surface*, Univ. Maryland Tech Note BN-152, AFOSR TN-58 863.

## 11. Liquid Propellant Behavior at Low and Zero g

by WILLIAM C. REYNOLDS (Stanford Univ.) AND HUGH M. SATTERLEE (Lockheed Missiles and Space Co.)

- ADELBERG, M., 1965, *Boiling, Condensation and Convection in a Gravitational Field*, **AICHE National Meeting**.
- ANLIKER, M., AND BEAM, R. M., 1962, *On the Stability of Liquid Layers Spread Over Simple Curved Bodies*, **J. Aerospace Sci.**, **29**, p. 1196.
- ANLIKER, M., AND PI, W. S., 1963, *Effects of Geometry and Unidirectional Body Forces on the Stability of Liquid Layers*, Stanford Univ. Dept. of Aero. and Astro. Report SUDAER 150.
- BAILEY, T., VANDEKOPPEL, R., SKARTVEDT, G., AND JEFFERSON, J., 1963, *Cryogenic Propellant Stratification Analysis and Test Data Correlation*, **AIAA J.**, **1**, p. 1657.
- BELLMAN, R., AND PENNINGTON, R. H., 1954, *Effects of Surface Tension and Viscosity on Taylor Instability*, **Quart. J. Mech. Appl. Math.**, **12**, p.151.
- BHUTA, P. G., AND KOVAL, L. R., 1965, *Sloshing of a Liquid in a Draining or Filling Tank Under Variable G Conditions*, **Proc., AFOSR Symposium on Fluid Mechanics and Heat Transfer Under Low Gravitational Conditions**, pp. 10-1 to 10-24.
- BIKERMAN, J. J., 1958, **Surface Chemistry**, Academic Press.
- BLACKSHEAR, W. T., AND EIDE, D. G., 1964, *The Equilibrium Free Surface of a Contained Liquid Under Low Gravity and Centrifugal Forces*, NASA TN D-2471.
- BOND, W. N., AND NEWTON, D. A., *Bubbles, Drops, and Stokes Law*, **Phil. Mag.**, **5**, pp. 794-800.
- BRETHERTON, F. P., 1961, *The Motion of Long Bubbles in Tubes*, **J. Fluid Mechanics**, **10**, p. 166.
- CHANDRASEKHAR, S., 1961, **Hydrodynamic and Hydromagnetic Stability**, Clarendon Press.
- CLARK, J. A., AND BARAKAT, H. Z., 1964, *Transient, Laminar, Free-Convection Heat and Mass Transfer in Closed, Partially Filled, Liquid Containers*, Univ. Michigan Dept. of Mech. Eng. Report, Contract NAS8-825.
- CLODFELTER, R. G., 1963, *Fluid Mechanics and Tankage Design for Low Gravity Environments*, WPAFB Report ASD-TDR-63-506.
- CONCUS, P., 1963, *Capillary Stability in an Inverted Rectangular Tank*, **Symposium on Physical and Biological Phenomena in Weightlessness**, **14**.
- CONCUS, P., 1964, *Capillary Stability in an Inverted Rectangular Channel for Free Surfaces with Curvature of Changing Sign*, **AIAA J.**, **2**, p. 2229.
- CONCUS, P., CRANE, G. E., AND PERKO, L. M., 1965, *Inviscid Fluid Flow in an Accelerating Axisymmetric Container*, **Proc., AFOSR Symposium on Fluid Mechanics and Heat Transfer Under Low Gravitational Conditions**, pp. 3-1 to 3-20.
- DUPREZ, F., 1851, *Sur un Cas Particulier de L'équilibre de Liquides*, **Memoirs de L'Academie Royale de Sciences, de Lettres, et des Beau-Arts de Belgique**, **26**.
- DUPREZ, F., 1854, *Sur un Cas Particulier de L'équilibre de Liquides*, **Memoirs de L'Academie Royale de Sciences, de Lettres, et des Beau-Arts de Belgique**, **28**.
- EIDE, D. G., 1964, *Preliminary Investigation of Variation of Pitch Motion of a Vehicle in a Space Environment due to Fuel Sloshing in a Rectangular Tank*, NASA TN D-2336.
- ELLION, M. E., 1954, *A Study of the Mechanism of Boiling Heat Transfer*, Jet Propulsion Laboratory Memorandum No. 20-88.
- FLÜGGE, S. ed., 1960, **Handbuch der Physik**, Vol. X, Springer-Verlag.

- FUNG, F. W., 1965, *Dynamic Response of Liquids in Partially-Filled Containers Suddenly Experiencing Weightlessness*, **Proc., AFOSR Symposium on Fluid Mechanics and Heat Transfer Under Low Gravitational Conditions**, pp. 7-1 to 7-32.
- FUNK, E., AND WELCH, N. E., 1965, *Distributions of Noncondensable Gases in Liquids Under Low-g Conditions*, **Proc., AFOSR Symposium on Fluid Mechanics and Heat Transfer Under Low Gravitational Conditions**, pp. 5-1 to 5-19.
- GLUCK, D. F., AND GILLE, J. P., 1965, *Fluid Mechanics of Zero-g Propellant Transfer in Spacecraft Propulsion Systems*, **Trans. ASME, J. Engineering for Industry**, pp. 1-7.
- GLUCK, D. F., GILLE, J. P., SIMKIN, D. J., AND ZUKOSKI, E. E., 1965, *Distortion of the Liquid Surface During Tank Discharge Under Low G Conditions*, **AICHE National Meeting**, Houston, Texas.
- HERMANS, J. J., 1953, **Flow Properties of Disperse Systems**, Interscience Publishers.
- HOLLISTER, M. P., 1964, *Propellant Containment Utilizing Screen Mesh and Perforated Plate Surfaces*, Lockheed Missiles & Space Co. Report LMSC/A665481.
- HOLLISTER, M. P., AND SATTERLEE, H. M., 1965, *Low Gravity Liquid Reorientation*, **Proc., AFOSR Symposium on Fluid Mechanics and Heat Transfer Under Low Gravitational Conditions**, pp. 8-1 to 8-32.
- HRYCAK, P., AND HELGANS, R. E., Jr., 1964, *Equilibrium Temperature of Long Thin-Walled Cylinders in Space*, AICHE Preprint 17, 7th National Heat Transfer Conference.
- JAKOB, M., 1949, **Heat Transfer, Vol. 1**, ch. 29, John Wiley & Sons.
- KESHOCK, E. G., AND SIEGEL, R., 1964, *Forces Acting on Bubbles in Nucleate Boiling Under Normal and Reduced Gravity Conditions*, NASA TN D-2299.
- LAMB, H., 1945, **Hydrodynamics**, Dover Publ.
- LANDAU, L. D., AND LIFSCHITZ, E. M., 1960, **Electrodynamics of Continuous Media**, Pergamon Press, pp. 64 ff.
- LANE, W. R., AND GREEN, H. L., *The Mechanics of Drops and Bubbles*, **G. I. Taylor 70th Ann. Vol.**, Cambridge Univ. Press, pp. 162-215.
- LEE, S.-L., 1963, *Taylor Instability of a Liquid Film Around a Long, Horizontal, Circular Cylindrical Body in Still Air*, **Trans. ASME, J. Applied Mechanics**, **30**, pp. 443-447.
- LEVICH, V. G., 1962, **Physicochemical Hydrodynamics**, Prentice Hall.
- LEVY, A. M., CHIN, J. H., DONALDSON, J. O., GALLAGHER, L. W., HARPER, E. Y., HURD, S. E., AND SATTERLEE, H. M., 1964, *Analytical and Experimental Study of Liquid Orientation and Stratification in Standard and Reduced Gravity Fields*, Lockheed Missiles & Space Co. Report 2-05-64-1.
- MASICA, J. W., PETRASH, D. S., AND OTTO, E. W., 1964, *Hydrostatic Stability of the Liquid-Vapor Interface in a Gravitational Field*, NASA TN D-2267.
- MASICA, W. J., AND SALZMAN, J. A., 1965, *An Experimental Investigation of the Dynamic Behavior of the Liquid-Vapor Interface Under Adverse Low-Gravitational Conditions*, **Proc., AFOSR Symposium on Fluid Mechanics and Heat Transfer Under Low Gravitational Conditions**, pp. 2-1 to 2-18.
- MAXWELL, J. C., 1890, *Capillary Action*, **The Scientific Papers of James Clerk Maxwell, Vol. I**, Cambridge Univ. Press, p. 586.
- MCGINNES, H. D., 1961, *Capillary Pumping for Closed-Cycle Gas Systems*, **Research Summary 36-10, vol. 1, Jet Propulsion Laboratory**.
- MELCHER, J. R., 1963, **Field Coupled Surface Waves**, Chapter 2, MIT Press.
- MERTE, H., AND CLARK, J. A., 1962, *Boiling Heat Transfer Data for Liquid Nitrogen at Standard and Zero Gravity*, **Advances in Cryogenic Engineering**, **7**, Plenum Press.
- MILNE-THOMSON, L. M., 1960, **Theoretical Hydrodynamics**, Macmillan Co.
- NUSSEL, R. C., DERDUL, J. D., AND PETRASH, D. J., 1965, *Photographic Study of Propellant Outflow from a Cylindrical Tank During Weightlessness*, NASA TN D-2572.
- OTTO, E. W., 1964, *Static and Dynamic Behavior of the Liquid-Vapor Interface During Weightlessness*, NASA TM X-52016.
- PAYNTER, H. L., 1964, *Special Zero-Gravity Fluid Problems*, **Rocket Propellant and Pressurization Systems** (E. Ring, ed.), Prentice-Hall Book Co.

- PAYNTER, H. L., 1964, *Time for a Totally Wetting Liquid to Deform From a Gravity-Dominated to Nulled-Gravity Equilibrium State*, **AIAA J.**, **2**, p. 1627.
- PETRASH, D. A., AND OTTO, E. W., 1962, *Studies of the Liquid-Vapor Interface Configuration in Weightlessness*, **Proc. ARS Space Power Systems Conf.**
- PETRASH, D. A., ZAPPA, R. F., AND OTTO, E. W., 1962, *Experimental Study of the Effects of Weightlessness on the Configuration of Mercury and Alcohol in Spherical Tanks*, NASA TN D-1197.
- PETRASH, D. A., AND NELSON, T. M., 1963, *Effect of Surface Energy on the Liquid Vapor Interface During Weightlessness*, NASA TN D-1582.
- PETRASH, D. A., NUSSEL, R. C., AND OTTO, E. W., 1963, *Effect of the Acceleration Disturbances Encountered in the MA-7 Spacecraft on the Liquid-Vapor Interface in a Baffled Tank During Weightlessness*, NASA TN D-1577.
- PETRASH, D. A., AND OTTO, E. W., 1964, *Controlling the Liquid-Vapor Interface Under Weightless Conditions*, **Astronautics and Aeronautics**, **2**, p. 56.
- PORTER, R. N., AND STANFORD, H. B., 1965, *Positive Expulsion Devices Assure Smooth, Reliable Starts for Spacecraft in Zero-g Space*, **J. SAE**, pp. 70-77.
- RAYLEIGH, LORD, 1892, *On the Instability of Cylindrical Fluid Surfaces*, **Scientific Papers**, **Vol. 3**, Cambridge Univ. Press, p. 594.
- RAYLEIGH, LORD, 1920, *On the Theory of the Capillary Tube*, **Scientific Papers**, **Vol. VI**, Cambridge Univ. Press, p. 355.
- REID, W. H., 1960, *Oscillations of a Viscous Liquid Drop*, Brown Univ. Div. Of Appl. Mech. Report 32.
- REX, J., AND KNIGHT, B. A., 1964, *An Experimental Assessment of the Heat Transfer Properties of Propane in a Near-Zero Gravity Environment*, Ministry of Aviation (UK) Tech Note 39, ARC Document 26368.
- REYNOLDS, J. M., 1965, *Stability of an Electrically Supported Fluid Column*, **Phys. Fluids**, **8**, pp. 61-70.
- REYNOLDS, W. C., SAAD, M. A., AND SATTERLEE, H. M., 1964, *Capillary Hydrostatics and Hydrodynamics at Low-g*, Stanford University Dept. of Mech. Eng. Report LG-3.
- REYNOLDS, W. C., 1965, **Thermodynamics**, McGraw-Hill Book Co.
- SAAD, M. A., AND OLIVER, D., A., 1964, *Linearized Time-Dependent Free-Surface Flow in Rectangular and Cylindrical Tanks*, **Proc. 1964 Heat Transfer and Fluid Mechanics Institute**.
- SATTERLEE, H. M., AND REYNOLDS, W. C., 1964, *The Dynamics of the Free Liquid Surface in Cylindrical Containers Under Strong Capillary and Weak Gravity Conditions*, Stanford Univ. Dept. of Mech. Eng. Report LG-2.
- SATTERLEE, H. M., AND CHIN, J. L., 1965, *Meniscus Shape Under Reduced Gravity Conditions*, **Proc., AFOSR Symposium on Fluid Mechanics and Heat Transfer Under Low Gravitational Conditions**, pp. 13-1 to 13-24.
- SCHWARTZ, S. H., AND ADELBERG, M., 1965, *Some Thermal Aspects of a Contained Fluid in a Reduced-Gravity Environment*, **Proc., AFOSR Symposium on Fluid Mechanics and Heat Transfer Under Low Gravitational Conditions**, pp. 4-1 to 4-47.
- SCRIVEN, L. E., 1960, *Dynamics of a Fluid Interface*, **Chem. Eng. Sci.**, **12**, pp. 98-108.
- SCRIVEN, L. E., AND STERNLING, C. V., 1964, *On Cellular Convection Driven by Surface Tension Gradients: Effects of Mean Surface Tension and Surface Viscosity*, **J. Fluid Mechanics**, **19**, p. 321.
- SEEBOLD, J. G., AND REYNOLDS, W. C., 1965, *Configuration and Stability of a Rotating Axisymmetric Meniscus at Low G*, Stanford Univ. Dept. of Mech. Eng. Report LG-4.
- SEEBOLD, J. G., AND REYNOLDS, W. C., 1965, *Shape and Stability of the Liquid-Gas Interface in a Rotating Cylindrical Tank at Low-G*, **Proc., AFOSR Symposium on Fluid Mechanics and Heat Transfer Under Low Gravitational Conditions**, pp. 12-1 to 12-17.
- SHERLEY, J. E., 1963, *Nucleate Boiling Heat Transfer Data for Liquid Hydrogen at Standard and Zero Gravity*, **Advances in Cryogenic Engineering**, **8**, Plenum Press.

- SHULEIKIN, V. V., 1964, *Second Series of Ground-Level Experiments with Weightless Fluids*, **Soviet Physics-Doklady**, **8**, p. 1221.
- SIEGEL, R., 1961, *Transient Capillary Rise in Reduced and Zero Gravity Fields*, **Trans. ASME, J. Applied Mechanics**, **38**, p. 165.
- SIEGERT, C. E., PETRASH, D. A., AND OTTO, E. W., 1964, *Time Response of Liquid-Vapor Interface After Entering Weightlessness*, NASA TN D-2458.
- SMITH, J. M., CIMA, R. M., AND LI, Y.-S., 1965, *The Application of Hydrophilic and Hydrophobic Surfaces for Phase Separation in a Low-g Environment*, **Proc., AFOSR Symposium on Fluid Mechanics and Heat Transfer Under Low Gravitational Conditions**, pp. 16-1 to 16-20.
- SMITH, R., 1965, *Interfacial Stability of Liquid Layers on Elastic Surfaces*, **Proc., AFOSR Symposium on Fluid Mechanics and Heat Transfer Under Low Gravitational Conditions**, pp. 9-1 to 9-35.
- STEINLE, H. F., 1960, *An Experimental Study of Transition from Nucleate to Film Boiling Under Zero-Gravity Conditions*, **Proc. Heat Transfer and Fluid Mechanics Institute**, Stanford Univ. Press.
- SWALLEY, F. E., PLATT, G. K., AND HASTINGS, L. J., 1965, *SATURN V Low-Gravity Fluid Mechanics Problems and Their Investigation by Full-Scale Orbital Experiment*, **Proc., AFOSR Symposium on Fluid Mechanics and Heat Transfer Under Low Gravitational Conditions**, pp. 1-1 to 1-25.
- TONG, P., AND FUNG, Y. C., *The Effect of Wall Elasticity and Surface Tension on the Forced Oscillations of a Liquid in a Cylindrical Container*, **Proc., AFOSR Symposium on Fluid Mechanics and Heat Transfer Under Low Gravitational Conditions**, pp. 11-1 to 11-42.
- TREFETHEN, L., undated, *Surface Tension in Fluid Mechanics*, motion picture, Educational Services, Inc.
- UNTERBERG, W., AND CONGELIERE, J., 1962, *Zero Gravity Problems in Space Powerplants: A Status Survey*, **Am. Rocket Soc. J.**, **32**, pp. 862-872.
- USISKIN, C. M., AND SIEGEL, R., 1961, *An Experimental Study of Boiling in Reduced and Zero Gravity Fields*, **Trans. ASME, J. Heat Transfer**, **83**, pp. 243-251.
- WANG, N. P., 1962, *Study of Forces on Propellants due to Heat Transfer Influencing Propellant Temperatures in a Recovery-Type Vehicle*, Dynamic Science Corp. Report 2, Subcontract 28-2524.
- WEINBAUM, S., 1964, *Natural Convection in a Horizontal Circular Cylinder*, **J. Fluid Mechanics**, **18**, p. 409.
- WEINSTOCK, R., 1952, **Calculus of Variations**, McGraw-Hill Book Co.

## Appendix. Physical Properties of Selected Liquids

- ANON., 1949, *Physical Properties and Thermodynamic functions of Fuels, Oxidizers, and Products of Combustion. Parts I, II, III*, Battelle Memorial Institute Reports R-127, R-129, R-136.
- ANON., 1957, **Catalog of Industrial Safety Equipment**, Mine Safety Appliances Co., Catalog 7-B.
- ANON., 1960, **Handbook of Chemistry and Physics**, CRC Pub. Co.
- ANON., 1961, *Storable Liquid Propellants, Nitrogen Tetroxide/Aerozine-50*, Aerojet-General Corp. Report LRP 198, Rev. C.
- ANON., **Nitrogen Tetroxide**, Allied Chemical Co. Bulletin.
- ARMAND, H. (ed), 1954, **Best's Safety and Maintenance Directory of Safety, Maintenance, Fire Control, Hygiene, and First Aid Products and Equipment**, Alfred M. Best Co.
- BAMFORD, F., 1947, **Poisons, Their Isolation and Identification**, 2nd ed., J. & A. Churchill (London).
- BROOKS, V. J., AND JACOBS, M. B., 1958, **Poisons, Properties, Chemical Identification, Symptoms, and Emergency Treatment**, 2nd ed., D. Van Nostrand Co.
- ELKINS, H. B., 1959, **The Chemistry of Industrial Toxicology**, 2nd. Ed., John Wiley & Sons.
- FAIRHALL, L. T., 1957, **Industrial Toxicology**, 2nd ed., The Williams & Wilkins Co.
- JACOBS, M. B., 1949, **The Analytical Chemistry of Industrial Poisons, Hazards, and Solvents**, 2nd ed., Interscience Pub., Inc.

- LYERLY, G. A., AND PEPPER, H., 1964, *Summary Report – Studies of Interfacial Surface Energies*, NASA CR-54175.
- MASICA, J. W., PETRASH, D. S., AND OTTO, E. W., 1964, *Hydrostatic Stability of the Liquid-Vapor Interface in a Gravitational Field*, NASA TN D-2267.
- REYNOLDS, W. C., SAAD, M. A., AND SATTERLEE, H. M., 1964, *Capillary Hydrostatics and Hydrodynamics at Low-g*, Stanford University Dept. of Mech. Eng. Report LG-3.
- SANDORFF, P. E., 1960, *Principles of Design of Dynamically Similar Models for Large Propellant Tanks*, NASA TN D-99.
- SATTERLEE, H. M., AND REYNOLDS, W. C., 1964, *The Dynamics of the Free Liquid Surface in Cylindrical Containers Under Strong Capillary and Weak Gravity Conditions*, Stanford Univ. Dept. of Mech. Eng. Report LG-2.
- SAX, N. I., 1963, **Dangerous Properties of Industrial Materials**, 2nd ed., Reinhold Publishing Co.
- SCOTT, R. B., 1959, **Cryogenic Engineering**, D. Van Nostrand Co.
- SEVERNS, W. H., AND FELLOWS, J. R., 1958, **Air Conditioning and Refrigeration**, John Wiley & Sons, Inc.
- SILVERMAN, J., et al, 1961, *Liquid Propellants*, **Handbook of Astronautical Engineering**, McGraw-Hill Book Co.
- STEINLE, H., 1960, *An Experimental Study of the Transition from Nucleate to Film Boiling Under Zero-Gravity Conditions*, **13th Heat Transfer and Fluid Mechanics Institute**.
- SUMNER, I. E., 1963, *Preliminary Experimental Investigation of Frequencies and Forces Resulting from Liquid Sloshing in Toroidal Tanks*, NASA TN D-1709.

# TABLE A-1

## Physical properties of some propellants and model liquids

The numerical values in the following two tables were taken directly from NASA SP-106. The data correspond to room temperature except for cryogenics, for which they correspond to saturation temperature at one atmosphere. Contact angles are not listed since they depend on the tank wall material; for most liquids, the contact angle is nearly zero when the wall materials are those commonly used for scale model and propellant tanks, the notable exception being mercury.

### Common Propellants

Name	Boiling point, °C	Specific gravity	Kinematic viscosity, cm <sup>2</sup> /sec	Vapor pressure, atm.	Surface tension, dynes/cm
Aerozine	70	0.904	0.0101	0.161	30.3
Ethanol	78	0.79	0.0158	0.058	22.3
Hydrazine	113	1.008	0.0097	0.0136	63-75
Hydrogen	-253	0.071	0.00197	1.0	1.9
Hydrogen Peroxide	150	1.448	0.0087	< 0.007	80.4
Kerosene (RP-1)	≈ 220	0.806	0.0231	0.0014	23-32
Monomethylhydrazine	87	0.876	0.105	0.048	? (≈ 30)
Nitrogen Tetroxide	21	1.447	0.00292	0.95	27.4
Oxygen	-184	1.140	0.0017	1.0	13.2
Unsym-dimethylhydrazine	64	0.793	0.00695	0.162	24.4-27.7

### Model liquids

Name	Boiling point, °C	Specific gravity	Kinematic viscosity, cm <sup>2</sup> /sec	Vapor pressure, atm.	Surface tension, dynes/cm
Acetone	56	0.792	0.00417	0.24	23.7
Carbon Disulfide	46	1.26	0.00288	0.39	32.2
Ethyl Bromide	38	1.44	0.0027	0.51	24.2
Glycerol	290	1.26	12.0	<< 0.0001	63
Glycerol-H <sub>2</sub> O mixes	--	1.0-1.26	0.0.01 - 12.0	--	To 63.4
Methanol	64	0.792	0.00745	0.125	22.6
Methylene Chloride	40	1.34	0.0033	0.46	26.5
Methylene Bromide	98	2.46	0.005	0.053	≈ 25
Nitrogen	- 198	0.815	0.0021	1.0	≈ 25
Silicone Oil	High	0.76-0.90	0.0066-0.031	Low	≈ 25
Sucrose Solutions	≈ 100	1.1-1.29	0.017-0.43	Low	≈ 25-63
Water	100	0.998	0.0101	Low	to 73.4



# AUTHOR INDEX

Numbers refer to pages in which the references are cited.

## A

ABDALLA, 94  
ABRAMSON, 21, 28, 34, 35, 37, 38, 39, 50,  
55, 57, 118  
ADELBERG, 108  
AGRAWAL, 149  
ALBAYYARI, J., 109  
ANTAR, 80, 87  
ARMOUR, 102  
ARMSTEAD, 18, 28  
ASSEMAT, 146  
AYDELOTT, 108

## B

BABSKII, 80, 87  
BAILEY, 108  
BAIRD, 21  
BASS, 35  
BASSETT, 108  
BAUER, 13, 14, 18, 30, 33, 48, 50, 89, 92,  
125, 129, 165  
BENTZ, M., 109  
BERENYI, 94, 95  
BERLOT, 55, 57  
BHUTA, 94  
BIKERMAN, 67  
BINGHAM, 102  
BLAKELOCK, 157  
BLATT, 100, 102  
BLEVINS, 38  
BOWLES, 100, 102, 110  
BRAKKE, 76  
BRASLOW, 117  
BUDIANSKY, 16, 17  
BUGG, 34

## C

CADY, 109  
CANNON, 102  
CARNEY, 76  
CARPENTER, 31  
CHATO, 96, 110, 147, 148  
CHIN, 75  
CHU, 18, 28, 34, 37, 50, 55, 57, 118, 119  
CHRISTENSEN, 108

CIMA, 94  
CLARK, 92  
COLE, 29  
CONCUS, 77, 89, 91  
CONEY, 85, 91, 92  
CRANE, 89  
CRAWLEY, 92  
CROSS, 82  
CRUSE, 83, 91, 145  
CUTSHALL, 75, 143, 145

## D

DALTON, 147, 148  
DEAN, 68  
DEBNATH, 117  
DEBRECENI, 108  
DEBROCK, 99, 108  
DODGE, 21, 34, 35, 36, 37, 52, 54, 51, 58,  
65, 68, 76, 81, 83, 85, 89, 90, 92, 100,  
102, 108, 110, 136, 138, 139, 143,  
145, 147, 148, 153  
DOMINICK, 72, 96  
DOROZHKIN, 27, 28  
DOWDY, 99, 108  
DREYER, 107  
DRISCOLL, 72, 96

## E

EBERT, 149  
EHRlich, 18  
EIDEL, 18, 89  
ELLISON, 108  
EL RAHEB, 139, 144  
ENRIGHT, 58  
EULITZ, 35  
EVERSTINE, 22

## F

FEY, 51  
FISHER, 108  
FOX, D. W. 2  
FOX, D. J., 57  
FRANK, 108  
FREED, 56  
FUROMOTO, 138, 147, 149

**G**

GANS, 150  
 GAMBUCCI, 29  
 GARG, 138, 147, 149  
 GARZA, 34, 37, 38, 39, 52, 65, 68, 76, 85, 89,  
 90, 92, 118, 119  
 GEISSLER, 165  
 GLUCK, 95  
 GRAHAM, 5  
 GRAYSON, G., 93  
 GREEN, 58, 81, 83, 91, 143, 145, 147, 148,  
 153  
 GREENSPAN, 131  
 GRIFFITH, 158  
 GUIBERT, 147

**H**

HARPER, 108  
 HARRISON, 147  
 HASAN, M., 109  
 HAYS, 165  
 HISE, 99, 108  
 HOCHSTEIN, 81, 94  
 HONKONEN, 108  
 HURWITZ, 164  
 HUTTON, 55

**J**

JAEKLE, 99, 107, 108  
 JEFFERSON, 108

**K**

KAMEL, 95  
 KANA, 20, 21, 28, 36, 37, 54, 51, 55, 57, 188  
 KARPOV, 131  
 KELLER, 125  
 KEULEGAN, 31  
 KIKURA, 65  
 KNOLL, R., 109  
 KOMATSU, 92  
 KOPACHEVSKII, 80, 87  
 KOVAL, 94  
 KRAMER, 97  
 KUTTLER, 2

**L**

LABUS, 92  
 LAWRENCE, 18, 61  
 LAY, 108  
 LEONARD, 19, 27

LESLIE, 150  
 LEVY, 108  
 LI, 94  
 LIN, C., 109  
 LINDHOLM, 28  
 LOMEN, 60

**M**

MANASSEH, 150  
 MARCÉ, 146  
 MARTIN, E., 131, 147  
 MARTIN, J., 108  
 MASICA, 79, 81, 85, 89, 92, 93  
 MCCARTHY, 16, 19  
 MCEWAN, 150  
 MCINTYRE, 135  
 MERINO, 108  
 MICHAELS, 68  
 MIKISHEV, 27, 28  
 MILES, 21, 30, 56, 57, 133, 135, 136  
 MOISEYEV, 128  
 MUNKO, 108  
 MYSHKIS, 80, 87

**N**

NAVICKAS, 82  
 NEER, 146  
 NUOTIO-ANTAR, 80, 87  
 NUSSEL, 94  
 NYQUIST, 164

**O**

O'NEILL, 32  
 OKHOTSIMSKII, 43  
 OLSEN, 109  
 OTTO, 69

**P**

PARKINSON, 31  
 PATAG, 94  
 PAVLI, 36  
 PENNEY, 120  
 PERRY, 27  
 PETERSON, 99, 108, 146  
 PETRASH, 69  
 PFEIFFER, 139  
 PIETRZYK, 108  
 PITMAN, 54  
 POCHA, 131, 147  
 POHL, 149

POZRIKIDIS, 21  
PRICE, 120  
PUROHIT, 108

**R**

RANSLEBEN, 35, 36, 55, 118  
RATTAYA, 18  
REDDY, 18, 61  
REYNOLDS, 70, 74, 79, 85, 89, 90, 150  
RILEY, 17, 18  
ROBERTS, 131  
RODRIQUEZ, 20  
ROLLINS, 97  
ROSENBAUM, 26  
ROSS, 82  
ROUTH, 164

**S**

SAAD, 70, 74, 79  
SALI, 157  
SALVATORE, 146  
SALZMAN, 89, 91, 92, 93, 94  
SATTERLEE, 75, 85, 89, 90  
SAWADA, 65  
SCANLAN, 26  
SCHMIDT, 108  
SCHOLL, 34  
SCHUSTER, 108  
SCHWARTZ, 108  
SCHWIND, 34  
SCOTTI, 34  
SCRIVEN, 66  
SEEBOLD, 150  
SHRAMO, 51  
SIEGERT, 81  
SILVEIRA, 34, 37  
SKARTVEDT, 108  
SKOGH, 34  
SLABINSKI, 131, 138  
SLOBOZHANIN, 80, 87  
SMITH, 94  
SMOLKO, 108  
SNYDER, 92  
STEPHENS, 16, 27, 29, 34, 37, 79, 92  
STEWARTSON, 131  
STOFAN, 18, 28, 36, 51  
STOKER, 117  
STRANGE, 17  
SUMNER, 19, 28, 29, 34, 36, 51  
SUMRALL, 165

SYMONS, 95, 96, 102  
SYNGE, 158

**T**

TADJBAKSH, 125  
TAM, 108  
TAN, 150  
TANAHASHI, 65  
TANNER, 135  
TAYLOR, 125  
TEGART, 96, 102, 103, 108  
TELLEP, 108  
THOMSON, 131, 146  
TREMBATH, 18  
TROESCH, 18, 136  
TYUPTSOV, 80, 87

**U**

UNRUH, 51, 143, 145

**V**

VANDEKOPPEL, 108  
VANYO, 138, 147, 149  
VAN DYKE, Melissa., 107  
VAN DYKE, Milton 117  
VAN SCHOOR, 92  
VAN WINKLE, 82  
VERMA, 125

**W**

WAGNER, 139, 144  
WALTON, 19  
WANG, 18, 61  
WEIHS, 136  
WEISLOGEL, 82  
WOLLEN, 108  
WONG, 58  
WRIGHT, 103

**Y**

YARYMOVCH, 20  
YEH, 107  
YON, 21

**Z**

ZEDD, 138, 147  
ZHUKOVSKII, 43



# SUBJECT INDEX

## A

Analogy, mechanical; *see* mechanical model

## B

Baffles, flexible, 35  
flexibility parameter, 35  
period parameter, 35  
Baffles, ring, 30  
damping coefficient - cylindrical tank, 32  
design value of damping, 33  
effect of flexibility, 35  
effect on slosh frequency, 34  
general damping coefficient, 31  
holes - effect of, 35  
near a free surface, 32  
spherical or spheroidal tank, 34  
theory, 30

Bond number, 68

Bubbles

in low-g, 72

Bulkheads, perforated, 37  
damping, 37

## C

Capillary systems, 70  
capillary area, 71  
metastable configurations, 72  
minimum capillary area, 72  
non-isothermal, 72  
thermodynamics, 70  
CASSINI spacecraft  
mechanical model, 58  
Circular cylindrical tank  
damping by ring baffles, 32  
energy dissipation, 149  
inertia modes, 143  
inertia modes (slow spin rate), 135  
interface stability in zero-g, 77  
low-g sloshing, 89  
mechanical model, 48  
viscous damping, 28  
Configuration, preferred in low-g, 72  
Contact angle, 66  
Cylindrical tank - spherical dome  
viscous damping, 29

## D

Damping  
baffles - non-ring, 37  
circular cylindrical tank, 28

cylindrical tank with spherical dome, 29  
effect on slosh force and torque, 26  
experimental methods, 27  
floating lids, mats, and cans, 35  
low-g effects, 92  
membranes and diaphragms, 36  
perforated bulkheads, 37  
ring baffles, 30  
spherical tank, 29  
spheroidal tank - oblate, 30  
toroidal tank - horizontal, 30  
viscous, 28

Damping coefficient, 26

Damping ratio. *See* Damping coefficient

Drop tower, 65

Drops

in low-g, 72

## E

Energy dissipation, 146  
air-bearing spin table method, 146  
analytical approximation, 153  
analytical methods, 149  
cylindrical tank, 154  
experimental methods, 147  
forced-motion spin-table method, 148  
free-fall method, 148  
spherical tank, 149, 150

## F

Fluid management in low-g  
cryogenic fluids, 108  
drain vortex, 95  
fine mesh screens and perforated plates, 99  
galleries or channels, 105  
heat transfer with cryogenics, 108  
interaction of wicking and bubble point -  
cryogenics, 110  
liquid acquisition devices, 97  
liquid inflow to a tank, 95  
liquid management device - types, 197  
liquid settling and gas venting, 93  
partial communication devices, 98  
PMD designs (various), 98  
PMD/LAD design, 103  
pressure drop across screens, 102  
refillable devices, 98  
refillable trap or start basket, 103  
suction dip during outflow, 94  
tank filling and transfer - cryogenics, 109  
thermodynamic vent system, 109

total communication devices, 98  
 total control devices, 99  
 ullage bubble collapse - cryogenics, 111  
 vanes, 107  
 Froude number, 69

**G**

Gas-liquid separation; *see* spinning tank

**H**

Heat transfer  
   cryogenic fluids, 108  
 Hydrodynamics in low-g, 65, 69  
 Hydrostatics in low-g, 65, 69

**I**

Inertia mode (spinning tank)  
   cylindrical tank (slow spin rate), 135  
   cylindrical tank, 143  
   defined, 132  
   mode collapse, 150  
   spherical tank, 143  
 Interface configuration - non-axisymmetric  
   low-g, 75  
 Interface shape  
   low-g, 73  
 Interface stability  
   spinning tank, 150  
 Interface stability (zero-g)  
   annular interface, 79  
   cylindrical tank, 77  
   general criteria, 80  
   spherical tank, 79  
 Interfaces  
   stability in zero-g, 77

**L**

Liquid management; *see* fluid management in low-g  
 Logarithmic decrement, 26  
 Low-g response times, 69

**M**

Magnetic simulation of low-g, 65  
 Mechanical model  
   analytical derivation of parameters, 44  
   CASSINI spacecraft, 58  
   cylindrical tank, 48  
   equations of motion, 44  
   experimental derivation of parameters, 51  
   inclusion of damping, 49  
   large amplitude effects by CFD, 58  
   low-g sloshing, 88  
   nonlinear, 55  
   rectangular tank, 46  
   rotary slosh, 55

SKYLAB, 51  
 SLOSH code, 51  
 spherical tank, 48  
 spheroidal tank with bladder, 54  
 TDRS tanks, 54  
 Microgravity - defined, 65  
   *see* zero-g

**N**

Nutation, 131  
   angular velocity, 143  
   coning amplitude, 131  
 Nutation time constant, 146

**P**

Propellant management devices  
   cryogenic fluid failures, 111  
   design considerations, 103  
   effects of cryogenic fluids, 108  
   galleries and channels, 105  
   refillable trap or start basket, 103  
   vanes, 107

**R**

Rectangular tank  
   inertia modes, 140  
   mechanical model, 46  
 Reorientation; *see* Settling time in low-g

**S**

Screens, fine mesh  
   bubble point, 100  
   cross flow pressure drop, 102  
   design for fluid management, 99  
   geometric and flow data (table), 103  
   geometry, 100  
   wicking, 100  
 Settling time in low-g, 80  
 SLOSH code  
   mechanical model, 51  
   theory and equations, 60  
 Sloshing rotary  
   nonlinear theory, 125  
 Sloshing, lateral  
   analysis by finite element codes, 23  
   analysis by SLOSH code, 2  
   Bernoulli's equation, 3  
   boundary conditions, 3  
   circular cylindrical tank, 14  
   cylindrical tank - horizontal, 16  
   damping, 26  
   defined, 1  
   eigenfunctions, 6  
   eigenvalues, 6  
   fundamental antisymmetric mode, 2

- linear theory, 2
  - low-g effects, 85
  - mechanical model, 1
  - natural frequencies, 8
  - nonlinear effects, 121
  - rectangular tank - lateral motion, 9
  - rectangular tank - pitch motion, 11
  - rectangular tank - roll motion, 13
  - rectangular tank solution, 5
  - rotary, 58
  - sector-annular cylindrical tank, 15
  - slowly spinning tank, 133
  - spherical tank, 18
  - spheroidal tank, 18
  - toroidal tank, 19
  - velocity potential, 3
  - wave shapes, 8
  - Sloshing, longitudinal. *See* Sloshing, vertical
  - Sloshing, low-g
    - axisymmetric tank theory, 82
    - boundary conditions, 83
    - contact line effects, 88
    - cylindrical tank, 89
    - forces and torques, 87
    - lateral sloshing, 82
    - mechanical model, 89
    - spherical tank, 90
    - spheroidal tank, 93
    - viscous damping, 92
  - Sloshing, nonlinear
    - basic theory, 119
    - compartmented cylindrical tanks, 118
    - maximum wave amplitude estimate, 117
    - method of successive approximations, 120
    - rotary sloshing, 125
    - spherical tanks, 119
  - Sloshing, rotary, 56
    - conical pendulum - chaos effects, 58
    - mechanical model, 56
  - Sloshing, vertical, 21
    - subharmonic and superharmonic responses, 21
  - Spacecraft stability and control, 157
    - characteristic equation, 163
    - control law, 162
    - equations of motion, 157
    - guidelines, 165
    - Hurwitz criterion for stability, 164
    - stability analysis, 163
  - Spherical tank
    - damping by ring baffles, 34
    - energy dissipation, 148, 149
    - inertia modes, 143
    - interface stability in zero-g, 79
    - low-g sloshing, 90
    - mechanical model, 48
    - nonlinear lateral sloshing, 119
    - viscous damping, 29
  - Spheroidal tank
    - low-g sloshing, 91
    - viscous damping, 30
  - Spheroidal tanks
    - damping by ring baffles, 34
  - Spinning tank
    - cylindrical tank - inertia modes, 143
    - cylindrical tank (slow spin rate), 134
    - effect of energy dissipation, 131
    - energy dissipation, 146
    - flat spin, 131
    - forced tank motion (nutation), 143
    - forces and torques, 143
    - free surface modes, 135
    - homogeneous vortex model, 139
    - inertia modes, 132
    - inertia modes - rectangular tank, 140
    - inertia modes (slow spin rate), 135
    - interface stability, 150
    - liquid motion for slow spin rate, 133
    - liquid motion regimes, 132
    - liquid-vapor separation, 150
    - nutation, 131
    - nutation time constant, 147
    - off-axis tank (exact theory), 140
    - off-axis tank (approximate theory), 139
    - spherical tank - inertia modes, 143
  - Surface tension, 66
- T**
- Toroidal tank
    - damping, 30
- W**
- Weber number, 69
- Z**
- Zero-g
    - defined, 65
    - interface formation times, 81
    - interface shape, 73
    - Interface stability, 76
    - interface stability criteria, 80
    - multiple interfaces, 76
    - neutrally stable interface, 79
    - preferred configurations, 72
    - stability of annular interface, 79
    - stability of cylindrical tank interface, 78

